UNIVERSITY OF SOUTHAMPTON

HIGH-POWER CLADDING-PUMPED RAMAN AND ERBIUM-YTTERBIUM DOPED FIBRE SOURCES

by Christophe André Codemard

A thesis submitted for the degree of

DOCTOR OF PHILOSOPHY

OPTOELECTRONICS RESEARCH CENTRE

FACULTY OF ENGINEERING AND APPLIED SCIENCE

DEPARTMENT OF ELECTRONICS AND COMPUTER SCIENCE

FEBRUARY 2007

University of Southampton

ABSTRACT

FACULTY OF ENGINEERING AND APPLIED SCIENCE

OPTOELECTRONICS RESEARCH CENTRE

Doctor of Philosophy

HIGH-POWER CLADDING-PUMPED RAMAN AND ERBIUM-YTTERBIUM DOPED FIBRE SOURCES

by Christophe André Codemard

Raman fibres and rare-earth doped silica fibres have been investigated for many years as gain media for the amplification of optical signals in telecommunications thanks to their broad gain bandwidth. They are now widely used for that application. It is only recently that power scaling of fibre laser sources has taken place with the development of double-clad fibres and high-power laser diode pump sources. Cladding-pumped fibre lasers are now a rapidly expanding and emerging technology with a wide range of applications, where high-power and high-brightness laser sources are required. Nevertheless, so far, most high-power lasers have been based on highly efficient ytterbium-doped fibre, while progress to power-scale other rare-earth doped fibres and fibre Raman laser has been much more modest.

This thesis can be divided into two main themes. The first concerns the power-scaling and study of erbium-ytterbium doped fibre laser sources for optical amplification or as laser sources. The second theme concerns the development and study of high-power Raman fibre lasers and amplifiers based on the novel concept of a cladding-pumped Raman fibre. The themes are jointed in that the cladding-pumped Er:Yb doped lasers, developed in the first theme, are used as pump sources in this second part for the Raman devices. They are also jointed in that they both concern power-scaling of "eye-safe" sources at around 1.6 μm.

Firstly, in collaboration with co-workers, high-power, large core, erbium-ytterbium doped fibre laser sources are developed. Output powers in excess of 70 W are obtained. Good beam quality output is achieved thanks to a tapered fibre section. The taper is compatible with standard single-mode fibre which enabled the realization of tuneable fibre lasers free from bulk external grating. The laser's tuning characteristics are investigated in the C- and L-band range. Subsequently, a master-oscillator power-amplifier (MOPA) based on large core Er:Yb doped fibres is developed for the generation of high-energy pulses. The details of the MOPA are studied and presented. With careful design considerations, pulses free from non-linear effects, with energy up to 1 mJ and peak powers up to 6.6 kW, with narrow spectral linewidth, are obtained at 1535 nm.

Secondly, using a double-clad fibre, consisting of raised index, germanium doped, core and inner cladding, with a pure silica outer cladding, a high-power CW single mode Raman fibre laser, pumped by a multi-mode erbium-ytterbium doped fibre laser, is demonstrated for the first time. The laser slope efficiency is 67% and the output power is in excess of 10 W. An experimental and theoretical study of the laser is performed. Then, the pulse amplification in a cladding-pumped Raman fibre is studied in a single pass amplifier configuration. The effects on the laser performance of the pump and Stokes seed powers, fibre length and four-wave mixing are presented. The Stokes's small-signal gain can be as high as 50 dB. Using this configuration, 700 ns long pulses are amplified up to 10 μJ which shows that, potentially, optical pulses could be amplified to much higher energy. Finally, these results together, let predict that, soon, cladding-pumped Raman fibre could be used as direct brightness converter.

List of Contents

List of Figures

List of Tables

List of Abbreviation

AOM	Accousto-Optic Modulator
ASE	Amplified Spontaneous Emission
CW or cw	Continuous Wave
DC	Direct Current
DCF	Double Clad Fibre
DCRF	Double Clad Raman Fibre
DCRFA	Double Clad Raman Fibre Amplifier
DCRFL	Double Clad Raman Fibre Laser
DFB	Distributed Feed-Back
EDFA	Erbium Doped Fibre Amplifier
EOM	Electro-Optic Modulator
ESA	Excited State Absorption
EYDF	Erbium-Ytterbium (co-)Doped Fibre
EYDFA	Erbium-Ytterbium (co-)Doped Fibre Amplifier
EYDFL	Erbium-Ytterbium (co-)Doped Fibre laser
FOD	Fast Optical Discharge
FWHM	Full Width at Half Maximum
FWM	Four Wave Mixing
GVD	Group Velocity Dispersion
HF	Holey fibre
HNLF	Highly non-linear fibre
HR	High Reflection
HT	High Transmission
JAC	Jacketed Air-Clad (fibre)
QCE	Quantum Conversion Efficiency
LIDAR	LIght Detection And Ranging
LP	Linearly Polarized (mode)
LMA	Large Mode Area
MCVD	Modified Chemical Vapour Deposition
MFD	Mode Field Diameter
MO	Master Oscillator
MOPA	Master Oscillator – Power Amplifier
NA	Numerical Aperture
OC	Output Coupler
OPA	Optical Parametric Amplifier
ORC	Optoelectronics Research Centre
PDG	Polarisation Dependent Gain
PC	Polarisation Controller
PCE	Power Conversion Efficiency
PIQ	Pair Induced Quenching
RE	Rare Earth
RF	Radio Frequency
RFA	Raman Fibre Amplifier
RIP	Refractive Index Profile
SBS	Stimulated Brillouin Scattering
SHG	Second Harmonic Generation
SMF	Single Mode Fibre
SRS	Stimulated Raman Scattering
TF	Tuneable Filter
THG	Third Harmonic Generation

TLS	Tuneable Laser Source
VOA	Variable Optical Attenuator
WDM	Wavelength Division Multiplexing

Thesis Contributions

The work presented in this thesis has been carried out by the author while in candidature for a research degree at this University. The work on high-power continuous-wave erbium-ytterbium doped fibre laser has been realised in collaboration with others colleagues from the High Power Fibre Lasers group, which is reflected in the authors lists of the relevant publications. The other experiments have been realised solely by the author. The work on pulsed erbium-ytterbium fibre lasers has been realised using fibre made under contract by Qinetiq.

Acknowledgements

During my research years at the ORC of the University of Southampton I have had the chance to meet, discuss, argue and work with numerous people from different backgrounds on some exciting aspects of optics. I should like to take this opportunity to thank them all for sharing their knowledge and their contributions.

Firstly, I would like to think my wife, Catherine, who supported and encouraged me during the past four years. I am also very grateful to Dr Anatoly Grudinin and Dr Shaif-Ul Alam who somehow manage to incite me to start this adventure at the ORC. I would like to thank my supervisor Dr Johan Nilsson for his supervision and for giving me confidence. For his excellent optical fibres and our numerous discussions on novel fibre lasers, I am grateful to Dr. J.K. Sahu. All my thanks go to past and present members of the High Power Fibre Laser and Silica group with whom I have worked, including, Dr. C. Alegria for his encouragements and good tips, Dr. Y. Jeong for the demonstration of his handling of high-power fibre lasers, Daniel Soh for his questions, Pascal Dupriez for his friendship, Carl Farell, Jaesun Kim and Dr. S. E. Yoo for their help in various situations and for sharing an office with me. I would like also to thank Dr. M. Ibsen for his gratings. I am also indebted to Dr. K. Gallo and Dr. C. Corbari for their insights into non-linear optics.

In addition, I would like to acknowledge Dr. E. Tarbox for her proof reading, and Simon Butler, Timothy McIntyre and Chris Nash for their practical help in the lab. Also, I would like to thank the great Eve Smith who organised most of this PhD.

Finally I am particularly grateful to the EPSRC which funded my PhD.

To my wife, Catherine and my son, Joseph.

PART I: BACKGROUND

Chapter 1 Overview

This chapter presents the motives and contents of this thesis. Section 1.1 introduces, historically, fibre lasers, describes some of their properties and advantages, and presents their fields of applications. Then, section 1.2 exposes the motivations to study erbium-ytterbium doped fibre and Raman fibre lasers. After that, in section 1.3, the thesis objectives are stated and the achievements are given. Finally, section 1.4 shows the organization of the thesis and gives an overview of its contents.

1.1 Fibre laser sources

1.1.1 History

The first laser was made in 1960 by T. Maiman [1] at the Hughes Research Laboratory. It was a ruby rod emitting at 694 nm pumped by a flash lamp. Only three years after the birth of the laser, the first fibre laser was demonstrated with erbium and neodymium doped glass lasers by Snitzer and Koester [2 - 4]. The first fibre laser consisted of a coiled neodymium-doped fibre transversely pumped by a flash lamp. The fibre laser emitted around 1060 nm with a multi-mode output. However, progress was slow during the next two decades, due to the difficulties in manufacturing high-quality, low-loss fibres and because the only viable pump sources were flash lamps, which necessitate transverse pumping. Fibre lasers are not well suited to transverse pumping. Still, during this period, the first longitudinally pumped fibre laser, pumped by a laser diode, was demonstrated by Stone and Burrus [5]. Meanwhile non-linear effects such as Raman scattering, Brillouin scattering and four-wave mixing in single-mode silica fibre were extensively studied [6, 7]. The break-through in the fabrication of rare-earth doped silica fibre came in 1985 thanks to the development of solution doping as a way to incorporate rare earths into preforms fabricated through modified chemical vapour deposition (MCVD) by Poole, Payne and Fermann [8] at the University of Southampton. Later, Mears, Reekie, Poole, and Payne demonstrated a Nd-doped silica singlemode fibre laser [9] followed by the first erbium doped-fibre amplifier (EDFA) [10]. Since then fibre lasers made with various rare-earth dopants including Nd, Er, Yb, Tm, Pr, Ho, and Sm have been investigated. In addition to silica, new types of glass hosts called soft glasses (e.g. fluoride and chalcogenide glasses) have also been developed [11]. However, it is the EDFA for optical telecommunications which catalyses

telecom research, resulting in the development of novel pump laser diodes and optical components. The first laser-diode pumped optical fibre amplifier [12] was demonstrated in 1988 by Snitzer et al. and in 1992 the first commercial EDFA was produced. In addition, fibre Raman amplification was developed to complement EDFAs and to extend the reach of optical signals in long-haul transmission. Meanwhile, practical Fibre Bragg Grating (FBG) [13] and Distributed FeedBack (DFB) fibre lasers [14] were also developed.

In parallel, with a few years' delay, high-power fibre amplifier and laser development started with the invention of the double-clad fibre [12, 15] in 1988 and thanks to the progress made in high-power multi-mode laser diodes. Nowadays, diode-stacks and other pump sources based on a large number of multi-mode emitters can produce several kW of output power. These have enabled the emergence of high-brightness kW-class fibre lasers [16 - 18] operating at around 1080 nm. Rare-earth doped fibres can also be operated to generate or amplify light pulses. Recently, record energy-levels from a fibre amplifier have been demonstrated [19] with extremely high-peak powers and high brightness output. The progress and developments are steady and commercial products are becoming more and more available, thus making fibre laser sources strong contenders to conventional "bulk" (non-waveguiding) solid state lasers.

1.1.2 Properties and advantages

Optical fibres which form the gain medium of fibre lasers, are primarily optical waveguides which transport energy in the form of electromagnetic radiation. Most fibres are made of silica glass, which is transparent in the visible and near infrared wavelength spectra. Conventionally, light is guided by a core with a higher refractive index than the surroundings through total internal reflection. A schematic of an optical fibre is shown in figure 1.1. The shape of the fibre refractive index profile and the refractive index difference allow a certain number of modes to be sustained in the fibre core and/or in the different surrounding layers of optical material. A main attraction of an optical fibre laser source is the ability to control the fibre modality through the refractive index profile and obtain a diffraction limited output, as required by many applications.

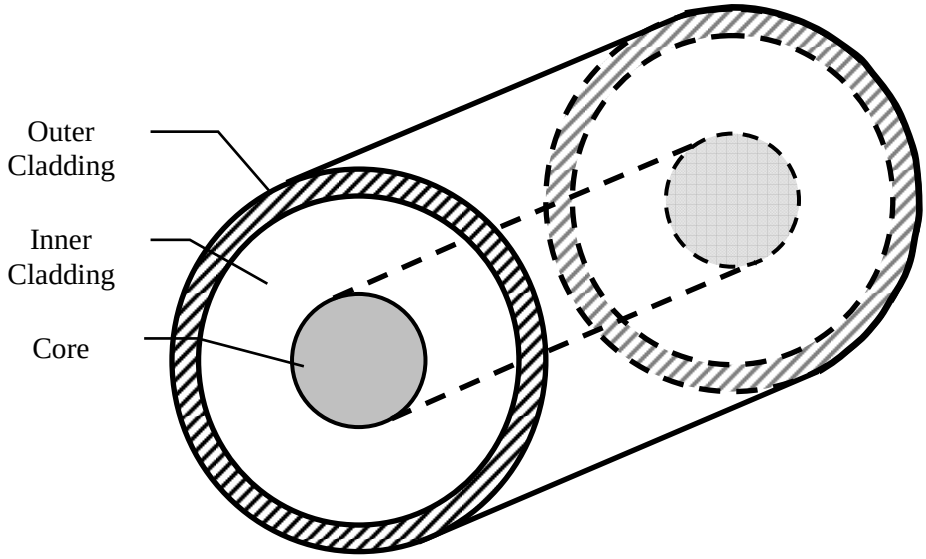

Figure 1.1: Schematic of an optical fibre. Typically, the core diameter is ~ 10 μm while the inner-cladding diameter varies between 80 – 400 μm.

Glass fibres can be doped with laser-active elements to obtain optical amplification through stimulated emission, e.g., from rare-earth ions. Rare-earth (RE) elements are the most common active dopant elements used for optical amplification in optical fibre. The dopant is generally situated in the fibre core or in close proximity in order to interact with both the exciting optical light-wave, called "pump", and the optical light-wave to be amplified, called "signal", transported in the fibre core. The operating wavelengths of rare-earth doped fibres are limited to the specific radiative transitions of the rare-earth ions. Some emission bands of RE-doped silica are shown in figure 1.2.

However, also fibres that do not contain any laser-active dopants and would normally be passive, can amplify through non-linear scattering which occurs in all fibres. Thus, also passive fibres can become "active", i.e., amplifying, when optically pumped at the power levels required for processes such as stimulated Raman scattering. In such a case, the optical pump beam interacts with the material of the optical fibre to create gain through a non-linear interaction. Thus energy is transferred from the pump beam to a signal beam. As for rare-earth doped fibre, the amplification process is normally accompanied by a wavelength change. The composition of the fibre is important. For example, germanium-doping is often used to enhance stimulated Raman scattering.

The silica fibre benefits from a remarkably low material loss, as shown in figure 1.2, and even when loss-increasing rare-earth dopants are used the losses can be as low as a few dB/km. Therefore optical fibres form an ideal amplification medium with a tight beam

confinement, a low background loss and long length. Consequently, the threshold of non-linear and actively doped fibre lasers can be reduced to a few mW.

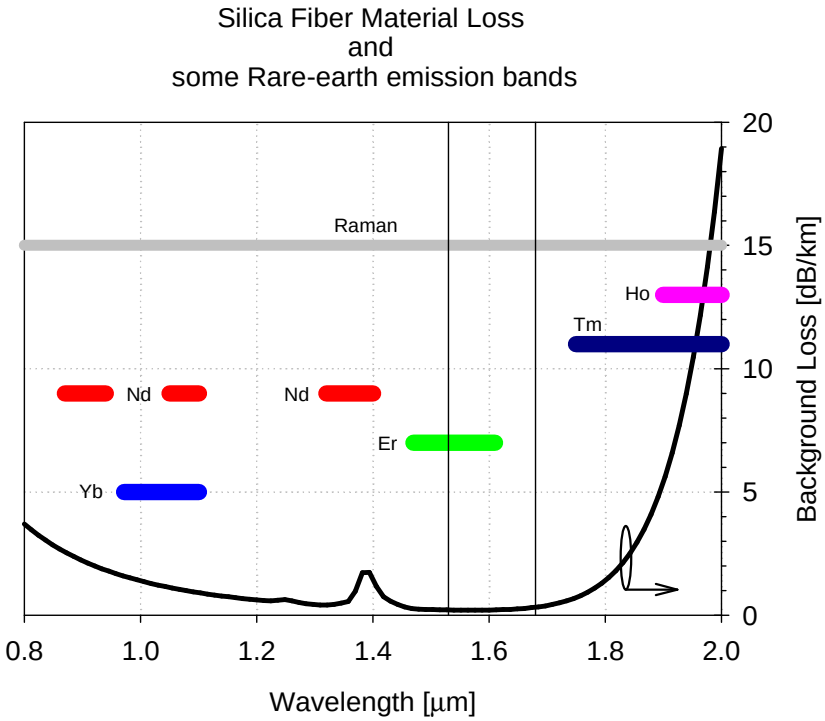

Figure 1.2: Silica background loss and emission bands of some rare-earth dopants in the 0.8 - 2.0 μm wavelength range.

Fibre laser sources differ from other type of lasers by their geometrical and mechanical properties. Practical optical fibres are generally made from glass, often silica, which can be readily fabricated in extremely long lengths with a precisely controlled geometry. The diameter of optical fibres varies from a few microns to around a millimetre in diameter, where it effectively becomes a solid glass rod. So-called nano-fibres can be fabricated with sub-micron diameter. Most commonly, the fibre diameter lies in the range between 80 µm to 700 µm. Such fibres are relatively easy to work with, and can be coiled with sub-metre or even cm-scale diameters. Therefore even kilometre-long fibres can be compactly packaged into small-footprint devices.

Furthermore silica based fibres are excellent candidates for high power operation thanks to the high damage threshold of silica and their good thermal properties. Although silica glass is not a very good thermal conductor, this is compensated by the long length and the small transverse dimension of the fibre which allow for easy thermal management [20 - 22]. Still, active fibre cooling is used in commercial product to insure long term performance across a certain temperature range.

Finally, silica fibres can be fusion spliced with very low losses which eliminates alignment problems. Consequently, a fibre laser system can maintain a diffraction-limited beam quality (maximum brightness at a given power level) independent of variables like system age or environmental changes. Also, wavelength reflectors or filters can be integrated directly into the fibre by either writing fibre Bragg gratings or by appropriate waveguide design. For example, guiding can be completely suppressed for certain wavelength ranges, allowing for strong distributed filtering throughout the fibre. Polarisation effects which are intrinsically very small can be enhanced by fibre design if required. Thus fibre devices can easily be made compact and robust with integrated functionality and so present unique advantages that enable a large number of applications.

1.1.3 Applications

Applications for fibre lasers and amplifiers fall into two main categories: industrial applications and scientific applications. Industrial applications can be divided into several categories. The first and principal application is in telecommunications, for amplification of optical signals, thanks to the broad and high gain available in for example erbium doped fibre amplifiers and Raman amplifiers. These amplifiers operate in the low loss region of the silica fibre (also called third window) which extends from 1450 to 1650 nm. Recently, it has been proposed to use high-power fibre lasers for free-space inter-satellite [23] or even inter-planetary telecommunications. The second industrial application is in heavy industries where high-power fibres are becoming a competitive alternative to solid-state lasers for drilling, cutting or soldering [16]. In addition fibre lasers are used or considered for defensc and aerospace applications such as remote missile defence and remote sensing and range-finding, including LIDAR. An emerging area of potential applications for fibre lasers is in display technology where fibre lasers are used for high-power visible sources.

The second category is scientific applications. Fibre lasers have multiple applications in medicine such as for microsurgery, dentistry and optical coherence tomography which requires broadband sources. Other scientific applications and research areas include sensing, atom cooling, interferometry, spectroscopy and non-linear optical conversion.

1.2 Motivations

1.2.1 Erbium-ytterbium co-doped fibre laser sources

Power-scaling of fibre laser sources has started only recently with the development and improvement of double-clad fibres and the power increase from diode pump sources. Cladding-pumped fibre lasers and amplifiers have attracted a tremendous interest due to their capability to deliver high output power with good beam quality. Lately, fibre lasers and amplifiers have demonstrated, in cw operation, up to several kW of output power with single-mode output beam [17 - 18] and tens of kilowatts with multi-mode output while, in the pulsed regime, MW peak power [19, 24] and multi-mJ [25] energy have been achieved. The growth and development of fibre lasers have made the most of the improvements in fibre design and fabrication in conjunction with the availability of reliable pump diode sources. Therefore, fibre lasers are now used in cutting [26], engraving and soldering. However, these results and these lasers are mainly obtained in the 1 – 1.1 μm wavelength range with highly efficient ytterbium-doped fibre sources [27]. These are superbly well suited to power scaling, thanks to factors such as a broad absorption band, simple energy level diagram with only two levels, resilience to concentration quenching, small quantum defect, and more. Since these fibres emit at wavelengths of 1 – 1.1 μm, they can be used as plug-in substitutes for Nd:YAG lasers at 1064 nm in a large number of systems. However, other rare earths emit at other wavelengths that are better suited to meet the needs of other applications. At the beginning of my thesis project, power-scaling at those wavelengths had been quite modest in comparison.

Fibre lasers in the 1530 – 1670 nm wavelength range, in the so-called “eye-safe”[1] spectral range, are also very attractive because of good atmospheric transmission and the existence of well-established and reliable components developed for optical fibre communications which facilitate the realization of sophisticated high-power systems. There is, especially for narrow linewidth laser, considerable interest in numerous applications which require sources operating in this specific part of the spectra, for example, in the domains of defense and aerospace, from remote sensing to range-finding [28], free-space communications [29] to name a few. “Eye-safe” narrow linewidth laser are also used for scientific research (e.g. non-linear optical conversion) and in medical science (e.g. laser surgery [30] and imaging). In

[1] Radiation at wavelengths longer than 1400 nm is strongly absorbed by tissue so it does not penetrate the through the eye and does not cause retinal damage. Hence the term "eye-safe", even though it is far from safe for the eye even at a power level of a watt. In reality none of the lasers I have worked with is anywhere near eye-safe. Still, scattered light is also a concern, and a much higher level of scattering can be accepted from “eye-safe” lasers.

addition, these lasers are of interest for materials processing, in particular for work that for some reason cannot be completely enclosed. Depending on the applications these lasers can be operated in the continuous-wave or pulsed regime but most often high power and narrow linewidth output are required.

Power scaling of erbium doped fibres at 1.5 – 1.6 μm relies on the double-clad fibre structure to allow for the injection of high power pump light together with ytterbium co-doping [31] to enhance the pump absorption. The pump absorption is otherwise too low in cladding-pumped Er-doped fibres, because of the modest maximum permissible Er-concentration and because of the low peak absorption cross-section of Er^{3+}.

Indeed, in 2003, the maximum output power in the short wavelength range of the erbium emission band, called the "C-band", was reported by Nilsson et al. [32]. Even though this was a cladding-pumped erbium-ytterbium fibre laser, it was limited to 16.8 W of output power in a free-running double ended configuration. A 6.7 W tuneable fibre laser with a linewidth of 0.25 nm was also demonstrated. In the long wavelength range or "L-band", Laroche et al. [33] developed a cladding-pumped Er:Yb co-doped tuneable fibre laser pumped at 940 nm by two beam-shaped diodes to achieve up to 29 W of output power with a broader linewidth of 0.6 nm. The laser was tuneable from 1561 nm to 1627 nm using an external bulk grating. The output beam was not diffraction limited (M^2 = 2.9). In both cases, the laser cavity was built using free space optics which result in bulky setups. Therefore there is a clear need to reach higher output power from EYDF laser and to improve the laser brightness, preferably using all-fibre configurations to keep the benefits of fibre lasers: compactness and small form factor.

Another interesting feature of rare-earth doped fibres is their ability to generate or amplify light pulses to high energy levels. In previous work, 0.5 mJ pulses [34] have been obtained from a large core erbium-doped ytterbium free multi-mode fibre amplifier. As discussed previously, the power and energy scaling of (Yb-free) erbium doped fibre is difficult. Therefore, efforts have been concentrated on erbium-ytterbium doped fibres which can be more easily power scaled. However, high energy extraction from EYDF had limited success. For example, 0.1 mJ pulses were obtained from a Q-switched erbium-ytterbium doped fibre laser [35]. Here, the energy stored was constrained by the small cross-sectional area of a fibre core close to that of a standard single-mode core. The energy available for extraction (energy stored in the gain medium) is defined by the number of excited ions in the active medium. There is an upper limit for the ion concentration in silica because of the clustering of the rare-earth ions. Furthermore, the output from [35] was not narrow linewidth, which restrains the application range of this type of source.

The energy stored can be increased by augmenting the number of ions by expanding the fibre doped area [36]. In addition, a large core mitigates non-linearities which can broaden the linewidth. At the beginning of my thesis work, a first encouraging result was demonstrated by the HPFL group at the ORC. Large core EYDFs were used, successfully, to amplify 100 ns long, 20 kHz spectrally wide, pulses to 0.29 mJ [28]. Consequently, this result, in combination with the in-house fibre facilities of the ORC, incited me to further investigate energy scaling of narrow linewidth EYDF lasers with good output beam quality. To meet the requirements to generate high energy pulses, large core EYDFs would be used in conjunction with a taper fibre section to improve the laser brightness.

1.2.2 Cladding-pumped Raman fibre laser sources

High-power rare-earth doped fibres are restricted by their wavelength coverage (see fig. 1.2) while Raman fibre lasers are much more wavelength-agile. Traditionally, these have been core-pumped single-mode devices with a relatively small core. Until recently, the lack of singlemode high-power pump sources had limited the power of Raman lasers to a few watts. While Raman scattering in multi-mode fibres has been the subject of early studies [37, 38], the recent availability of high power fibre laser sources and of low loss fibres present a unique opportunity to explore and study the beam-clean up properties of SRS [39, 40]. Due to the fact that SRS is a nearly instantaneous inelastic scattering process that is not phase-matched, the instantaneous pump intensity defines the actual instantaneous gain profile for the Stokes wave. In conventional multi-mode fibre, the transverse pump distribution that typically results with most laser pump sources results in gain preferentially for the lower-order modes at the Stokes wavelength. This results in brightness enhancement. Brightness enhancement through SRS in multi-mode fibre has seen a revived interest in the last few years [41 - 44] and recently Nilsson, Jang et al. from the ORC demonstrated a cladding-pumped Raman source [45]. However this concept still remains unexplored territory in the continuous-wave and, in particular, in the pulsed regime.

Single-mode, high energy pulses are required in many applications. These pulses can be produced by rare-earth doped fibre devices, often in an amplifying, so-called MOPA configuration. High-power MOPAs take advantage of the high gain and high efficiency offered simultaneosuly by rare-earth doped optical fibres. In a MOPA, the light from a low power oscillator, known as a “seed laser”, is amplified to high powers in one or several amplifiers. In case of a pulsed MOPA, the energy from the oscillator is often below a nanojoule, and high-gain amplification is then required to reach high output pulse energies. However, in practice, in conventional rare-earth doped fibre amplifiers, the gain is limited to 25 - 30 dB because ASE

and ultimately spurious lasing leads to large losses of power at high gain. In addition, limits on gain also limit the energy that can be stored and extracted with RE-doped fibre amplifiers. Already small amounts of stored energy lead to a high gain because of the tight confinement of fibre amplifiers. Thus several amplification stages are required to amplify a nanojoule seed pulse to high energies, but this lead to a complex system of cascaded amplifiers [34]. In order to reduce the propagation and amplification of the ASE in the MOPA, the different stages are isolated using optical isolators, spectral filters, and / or time gating elements. These additional components lead to extra losses which must be compensated for. One solution to this problem is to use a large doped core fibre, where the gain is reduced and the energy stored is increased. The small signal gain G_0 (in linear units) and extractable energy E_{ext} are related by the saturation fluence ε_{sat} and the doped area A by this expression [46]:

$$E_{ext} = \varepsilon_{sat} A \ln\left(G_0\right) \tag{1.1}$$

In addition, large core fibre benefits from an increased damage threshold [47], which is particularly critical for the generation of high energies in short pulses, i.e., high peak powers [19]. Typically, for pulse durations shorter than 10 ns, damage limits the energy that can be extracted, whereas for pulses longer than 100 ns the limit is set by the stored energy.

However, as the core becomes larger in these fibres, it also becomes multi-moded and the signal beam quality is degraded. The highest energy reported from a single-mode or good beam quality rare-earth doped fibre has been in low NA[2] (~ 0.05 - 0.08) Yb-doped fibres [46, 47, [48]. The low NA improves the beam quality in large-core fibres and reduces the number of guided modes in which ASE builds up. Furthermore, the high efficiency of Yb-doped fibres and the low losses it implies also facilitates high-energy pulse generation. In addition, the saturation fluence is relatively large in YDFs at 1060 – 1100 nm. Other systems are more challenging to energy-scale; for example, Yb doped fibres at 980 nm [49], Nd-doped fibres at 930 nm [50], and Er:Yb co-doped fibre at 1550 nm [51]. There are various reasons for this. For example, the saturation fluence ε_{sat} is very low for Yb-doped fibres at 980 nm, while Nd-doped fibres at 930 nm utilise spectral waveguide filters that require relatively small cores.

[2] The NA (Numerical aperture) of the fibre is the sine of the maximum angle (or acceptance angle) of an incident beam with respect to the fibre axis, so that the transmitted beam is guided in the core. (The underlying assumption is that the incident beam comes from air, i.e., from a region with n = 1.) The NA is determined by the refractive index difference between the fibre core and cladding so that the light propagates with the critical angle for total internal reflection.

An alternative to rare-earth doped fibre amplifiers is to use non-linear processes to amplify the pulse seed to higher energy. Scattering and parametric processes have already demonstrated the capability to achieve extremely high gain, e.g., more than 60 dB for a fibre optical parametric amplifier (OPA) [52]. Stimulated Raman scattering (SRS), is another possibility, with the attraction that it is a phenomenon which does not require phase-matching. This is in contrast with, for example, optical parametric amplification, which is based on the FWM process.

However, because Raman amplification is a weak non-linear effect, high pump power and / or long, low-loss fibre with tight beam confinement, e.g., single-mode fibre, are required. Still, [45] demonstrates that with sufficient power, multi-mode and double-clad fibres can be used for Raman amplification. In the pulsed regime, high peak powers simplify non-linear conversion while the cw regime requires high power cw pump sources. In addition, the novel approach of cladding-pumped fibre Raman devices has the benefit of generating an output light with a better beam quality than that of the pump. This phenomenon is called the “beam clean-up” effect [43]. Of great interest is that this brightness enhancement is possible even in the pulsed regime. The SRS process does not store energy in the optical medium, but relies on a nearly instantaneous energy exchange, of the order of few femtoseconds, involving optical phonons. The nearly instantaneous response is attractive for brightness enhancement of pulses.

To further illustrate the differences between RE-doped and Raman fibres, Table 1.1 summarises and compares their properties.

	RE doped fibre	Raman fibre
Wavelength	Limited to the emission range of the active ions [53].	Wavelength-agile operation depends on the pump wavelength, the material phonon energy and the background loss [54].
Power scaling	Depends on the active media and the pump power availability. Thermal management can be an issue [21].	Other non-linear effects and cascaded Raman scattering can limit the maximum power obtainable at a given wavelength.
Energy	Energy stored in active ions [53].	Fast energy transfer involving optical phonons.
System dynamics	Slow dynamic gain depending on relevant time constants of the dopants as well as the photon flux density (intensity) [53].	Instantaneous gain.
Pulsed mode operation	CW pump and pulsed signal.	- CW signal and pulsed pump - CW pump and pulsed signal - Synchronised pulsed signal and pump [45]
Architecture	Multiple stages are required for high gain, because of ASE [34].	Single-stage possible for high gain [55].
Pulse shape	Pulse distortion due to energy saturation and ASE.	Clean pulses are possible, if pump pulses are clean.
Linewidth	Can be single-frequency because the device can be very short, e.g., [56].	Stimulated Brillouin scattering makes it very difficult to operate with single-frequency because of the much lower threshold than SRS. Narrow-linewidth operation is possible but then FWM (in CW or pulsed regime) and SPM (in pulsed regime) can also be present and increase the output linewidth.

Table 1.1: Properties of rare-earth doped and Raman fibres

The concept of cladding-pumped Raman fibre laser represents an appealing solution to transform multi-mode light into either in CW or pulsed single mode laser output. This is possible thanks to the unique properties of SRS: beam clean-up and fast energy transfer. Such a laser source benefit from the wavelength flexibility of Raman process. Furthermore, there are no restrictions on the type of pump light sources as long as they are bright enough. This new field would seem to provide much potential for pioneering and exciting research.

1.3 Objectives and achievements

In the previous section, the need for higher power and higher energy eye-safe fibre laser sources was identified. In this thesis, I propose two approaches to power and energy scale fibre lasers operating in this wavelength range. Both approaches rely on the brightness conversion process which takes place in cladding-pumped fibre.

The first approach is based on large core erbium-ytterbium doped fibres. Here, the objective is to demonstrate that power and energy scaling of narrow linewidth EYDF laser is possible. So far the power and energy of EYDF lasers has remained deceptively low by comparison to ytterbium doped fibre laser. Furthermore this work is confined to narrow-linewidth laser sources that have a large application range. Consequently, using large core EYDF and tapered fibre section, I have, with the help of others, demonstrated the highest power [57 - 58] and energy [28, 51, 59] from any erbium-ytterbium sources, and any source in the 1.5 – 1.6 μm spectral range, at that time.

The second approach is completely new and largely unknown, and, therefore, is more challenging. I propose to realise the power scaling of Raman fibre laser using a double clad fibre. This direct brightness enhancement through stimulated Raman scatting is possible thanks to the special properties of SRS. Here, the first objective is to establish some theoretical foundation to understand the working principles and the behaviour of DCRF laser. The second objective is the demonstration and study of a high power CW cladding-pumped Raman fibre in the “eye-safe” spectral range using a high power EYDF laser as pump sources. This objective has been fulfilled and the first continuous-wave high power DCRF fibre laser with a single mode output compatible with standard SMF has been demonstrated [60 - 61]. The power levels obtained were also amongst the highest reported from a Raman fibre laser. The last objective is to investigate the potential and possibly to demonstrate high energy pulses from a DCRF source. The potential has been put in evidence with a high gain in single-stage configuration [55] and the demonstration of the generation of 10 μJ pulses. Still, the full capability of cladding-pumped Raman fibre laser still remains to be investigated.

1.4 Outline

This thesis is divided into three related, but distinctive, sections. The first section comprises two chapters. This first, current, chapter introduces fibre lasers and their properties, and presents the motivations, objectives and achievements of this thesis. The second chapter gives an overview of the background theory. Firstly, the laser beam quality and brightness are

defined. Secondly, the general properties of cladding-pumped double-clad fibres are presented. Thirdly, a comprehensive view of the modal properties of optical fibres is given. Finally, non-linear effects are introduced with an emphasis on Raman scattering.

The second section contains the work on power-scaling and the study of erbium-ytterbium doped fibre laser sources. Chapter 3 contains background information specific to erbium-ytterbium doped fibre and pulsed rare-earth doped fibre amplifier. In addition the details of the fibres, used in this thesis, are presented. In Chapter 4, C- and L-band tuneable, high power, continuous-wave EYDF laser sources are described. Both lasers include a tapered fibre section to control the output beam quality. The characteristics of the lasers are also discussed. Next, Chapter 5 contains the work on pulsed erbium-ytterbium doped fibre lasers. High-energy pulses with narrow spectral linewidth have been obtained from a MOPA based on large core EYDF. Challenges and limitations on energy scaling in erbium-ytterbium doped fibre are discussed.

The third section concerns the development and study of high-power Raman fibre lasers and amplifiers based on the novel concept of a cladding-pumped Raman fibre. This section also contains three chapters. Fibre laser sources developed previously are being used as intermediate pump sources to create Raman gain in an undoped double-clad fibre. Firstly, Chapter 6 presents the principles and theory of continuous-wave and pulsed cladding-pumped Raman fibre laser sources. Then, in Chapter 7, an experimental and numerical study of high-power continuous-wave single-mode Raman fibre laser is presented. Next, in Chapter 8, a high gain pulse amplification operation is demonstrated in a single-pass configuration. In addition, the potential to reach high-energy pulse in a double-clad Raman fibre amplifier is discussed and illustrated with some experimental results. Limitations due to other competing non-linear effects are examined and alternatives to overcome these are considered.

Finally, Chapter 9 summarises the main results and achievements of this thesis and describes possible areas for further research. The thesis concludes with two appendices. Appendix I treats the modeling of stimulated Raman scattering in multi-mode fibres with an example of a computer program. Finally, Appendix II contains a list of the publications arising from my work during my Ph.D. studies at the ORC.

1.5 References

[1] T. H. Maiman, "Stimulated optical radiation in ruby masers", Nature **187**, 493 (1960).

[2] E. Snitzer, "Proposed fiber cavities for optical lasers", J. Appl. Phys. **32**, 36-39 (1961).

[3] E. Snitzer, "Optical maser action of Nd^{3+} in a barium crown glass", Phys. Rev. Lett. **7**, 444-446 (1961).

[4] C. J. Koester, and E. Snitzer, "Amplification in a fiber laser", Appl. Opt. **3**, 1182-1186 (1964).

[5] J. Stone, and C. A. Burrus, "Neodymium-Doped Silica Lasers in End-Pumped Fiber Geometry", Appl. Phys. Lett. **23**(7), 388-389 (1973).

[6] R. Y. Chiao, C. H. Townes, and B. P. Stoicheff, "Stimulated Brillouin Scattering and Coherent Generation of Intense Hypersonic Waves", Phys. Rev. Lett. **12**(21), 592-595 (1964).

[7] R. H. Stolen, "Nonlinear properties of optical fibers" in *Optical Fiber Telecommunications*, (S. E. Miller and A. G. Chynoweth, Eds. New York: Academic, 1974).

[8] S. B. Poole, D. N. Payne., and M. E. Fermann, "Fabrication of low loss optical fibres containing rare-earth ions", Electron. Lett. **21**, 737-738 (1985).

[9] R. J. Mears, L. Reekie, S. B. Poole, and D. N. Payne, "Neodymium-doped silica single-mode fibre laser", Electron. Lett. **21**, 738-740 (1985).

[10] R. J. Mears, L. Reekie, S. B. Poole, and D. N. Payne, "Low-Threshold Tunable-Cw and Q-Switched Fiber Laser Operating at 1.55 μm", Electron. Lett. **22**(3), 159-160 (1986).

[11] J. E. Townsend, S. B. Poole, and D. N. Payne, "Solution-doping technique for fabrication of rare-earth-doped optical fibres", Electron. Lett. **23**, 329 (1987).

[12] E. Snitzer, H. Po, F. Hakimi, R. Tumminelli, and B. C. McCollum, "Double-clad, offset core Nd fiber laser", in *Proc. Opt. Fiber Sensors*, New Orleans, 1988, post-deadline paper PD5.

[13] K. O. Hill, B. Malo, F. Bilodeau, D. C. Johnson, and J. Albert, "Bragg gratings fabricated in monomode photosensitive optical fiber by UV exposure through a phase mask", Appl. Phys. Lett. **62**, 1035 (1993).

[14] J. T. Kringlebotn, J. L. Archambault, L. Reekie, and D. N. Payne, "$Er^{3+}Yb^{3+}$ Codoped Fiber Distributed-Feedback Laser", Opt. Lett. **19**(24), 2101 (1994).

[15] J. D. Kafka, "Laser diode pumped fibre laser with pump cavity", US patent 4,829,529 (1989).

[16] Information available from IPG Photonics: http://www.ipgphotonics.com and SPI Lasers: http://www.spilasers.com.

[17] A. Liem, J. Limpert, H. Zellmer, A. Tünnermann, V. Reichel, K. Mörl, S. Jetschke, S. Unger, H. -R. Müller, J. Kirchhof, T. Sandrock, A. Harschak, "1.3 kW Yb-doped fiber laser

with excellent beam quality", in *Proc. Conference on Lasers and Electro-Optics (CLEO)*, San Francisco, US, 2004, postdeadline paper CPDD2.

[18] Y. Jeong, J. K. Sahu, D. N. Payne, and J. Nilsson "Ytterbium-doped large-core fiber laser with 1.36 kW continuous-wave output power", Opt. Express **12**(25), 6088 (2004).

[19] M. Y. Cheng, Y. C. Chang, A. Galvanauskas, P. Mamidipudi, R. Changkakoti, and P. Gatchell, "High-energy and high-peak-power nanosecond pulse generation with beam quality control in 200-μm core highly multimode Yb-doped fiber amplifiers", Opt. Lett. **30**(4), 358 (2005).

[20] K. I. Ueda, "High power fiber lasers", in *Proc. Pacific Rim Conference on Lasers and Electro-Optics (CLEO)*, Chiba, 2001.

[21] L. Zenteno, "High power double clad fibre lasers", J. Lightwave Technol. **11**(9), 1435-1447, (1993).

[22] D. C. Brown and H. J. Hoffman, "Thermal, stress, and thermo-optic effects in high average power double-clad silica fiber lasers", IEEE J. Quantum Electron. **37**(2), 207 (2001).

[23] J. Koroshetz, E. Schneider, I. T. McKinnie, D. Smith, J. Unternahrer, W. A. Clarkson, J. Nilsson, J. Sahu, P. Jander, A. Carter, K. Tankala, J. Farroni, and G. Duchak, "High power eye-safe fiber transmitter for free space optical communications", (IEEE, Big Sky, MT, USA, 2004), pp. 1730-1735.

[24] C. D. Brooks and F. Di Teodoro, "1-mJ energy, 1-MW peak-power, 10-W average power, spectrally narrow, diffraction-limited pulses from a photonic-crystal fiber amplifier", Opt. Express **13** (22), 8999 (2005).

[25] B. C. Dickinson, S. D. Jackson, and T. A. King, "10 mJ total output from a gain-switched Tm-doped fibre laser", Opt. Comm. **182**(1-3), 199-203 (2000).

[26] M. L. Stock, H. Endert, R. Patel, " "Time-tailored" laser pulses: a new approach for laser micromachining and microfabrication processing", Proc. SPIE **4984,** 202 (2003).

[27] Y. Jeong, J. K. Sahu, S. Baek, C.Alegria, D. B. S. Soh, C. Codemard, V. Philippov, D. J. Richardson, D. N.Payne, and J. Nilsson, "Ytterbium-doped double-clad large-core fiber lasers with kW-level continuous-wave output power", in *Proc. Conference on Lasers and Electro-Optics (CLEO)*, San Francisco, US, 2004.

[28] V. Philippov, C. Codemard, Y. Jeong, C. Alegria, J. K. Sahu, J. Nilsson, and G. N. Pearson, "High-energy in-fiber pulse amplification for coherent lidar applications", Opt. Lett. **29**, 2590-2592 (2004).

[29] V. P. Gapontsev, "High power fiber lasers and amplifiers for high-speed free-space and satellite optical communication", Technical Digest of 'Photonics WEST98', LASE'98, (San Jose, USA, 1998).

[30] K. Kincade, "Optoelectronic Applications: Biophotonics - Fiber lasers find opportunities in medical applications", Laser Focus World, September 2005.

[31] G. G. Vienne, J. E. Caplen, L. Dong, J. D. Minelly, J. Nilsson, and D. N. Payne, "Fabrication and characterization of Yb^{3+}:Er^{3+} phosphosilicate fibers for lasers", IEEE J. Lightwave Technol. **16**(11), 1990-2001, (1998).

[32] J. Nilsson, S. -U. Alam, J. A. Alvarez-Chavez, P. W. Turner, W. A. Clarkson, A. B. Grudinin, "High-power and tunable operation of erbium-ytterbium Co-doped cladding-pumped fiber lasers", IEEE J. Quantum Electron. **39**(8), 987 (2003).

[33] M. Laroche, W. A. Clarkson, J. K. Sahu, J. Nilsson, Y. Jeong, "High power cladding-pumped tunable Er-Yb fiber laser", in *Proc. Conference on Lasers and Electro-Optics (CLEO)*, Baltimore US, 2003, paper CWO5.

[34] B. Desthieux, R. I. Laming, D. N. Payne, "111 kW (0.5 mJ) pulse amplification at 1.5μm using a gated cascade of three erbium-doped fiber amplifiers", Appl. Phys. Lett. **63**(5), 586 (1993).

[35] S. Alams, P. W. Turner, A. B. Grudinin, and J. Nilsson, "High energy, high repetition rate, tunable Er-Yb-codoped Q-switched fibre laser", in *Proc. Conference on Lasers and Electro-Optics (CLEO)*, Baltimore, US, 2001.

[36] C. C. Renaud, H. L. Offerhaus, J. A. Alvarez-Chavez, J. Nilsson, W. A. Clarkson, P. W. Turner, D. J. Richardson, A. B. Grudinin, "Characteristics of Q-switched cladding-pumped ytterbium-doped fiber lasers with different high-energy fiber designs", IEEE J. Quantum Electron. **37**(2), 199 (2001).

[37] K. X. Liu, and E. Garmire, "Role of Stimulated Four-Photon Mixing and Efficient Stokes Generation of Stimulated Raman-Scattering in Excimer-Laser-Pumped UV Multimode Fibers", Opt. Lett. **16**(3), 174-176 (1991).

[38] K. S. Chiang, "Stimulated Raman scattering in a multimode optical fiber: evolution of modes in Stokes waves", Opt. Lett. **17**(5), 352-354 (1992).

[39] R. S. F. Chang, R. H. Lehmberg, M. T. Duignan, and N. Djeu, "Raman Beam Cleanup of a Severely Aberrated Pump Laser", IEEE J. Quantum Electron. **21**(5), 477-487 (1985).

[40] J. Reintjes, R. H. Lehmberg, R. S. F. Chang, M. T. Duignan, and G. Calame, "Beam Cleanup with Stimulated Raman-Scattering in the Intensity-Averaging Regime", J. Opt. Soc. Am. B-Opt. Phys. **3**(10), 1408-1427 (1986).

[41] J. T. Murray, W. L. Austin, and R. C. Powell, "Intracavity Raman conversion and Raman beam cleanup", Opt. Mater. **11**(4), 353-371 (1999).

[42] T. H. Russell, Ph.D. Thesis, *Laser Intensity scaling through stimulated scattering in optical fibers,* (Air Force Institut of Technology Wright-Patterson, December 2001).

[43] T. H. Russell, S. M. Willis, M. B. Crookston, and W. B. Roh, "Stimulated Raman scattering in multi-mode fibers and its application to beam cleanup and combining", J. Nonlinear Opt. Phys. Mater. **11**(3), 303-316 (2002).

[44] R. Rice, "Multimode raman fiber amplifier and method", US patent no. 6,353,087 (2002).

[45] J. N. Jang, J. K. Sahu, R. Selvas, J. Nilsson, D. C. Hanna , A. B. Grudinin, "Raman amplification and pulsed lasing in cladding-pumped germanosilicate fiber", in Optical Amplifiers and Their Applications, J. Nagel, S. Namiki, and L. Spekman,ed(s), (Optical Society of America, Washington, D.C., 2002).

[46] J. Limpert, S. Hoffer, A. Liem, H. Zellmer, A. Tunnermann, S. Knoke, and H. Voelckel, "100-W average-powerg high-energy nanosecond fiber amplifier", Appl. Phys. B **75**(4-5), 477 (2002).

[47] A. Tünnermann, T. Schreiber, F. Röser, A. Liem, S. Höfer, H. Zellmer, S. Nolte and J. Limpert, "The renaissance and bright future of fibre lasers", J. Phys. B. **38** (9), 681 (2005).

[48] Y. Jeong, J. K. Sahu, M. Laroche, W. A. Clarkson, K. Furusawa, D. J. Richardson, J. Nilsson, "120-W Q-switched cladding-pumped Yb-doped fibre laser", in *Proc. Conference on Lasers and Electro-Optics/Europe (CLEO/Europe),* Munich, 2003, paper CL5-4.

[49] R. Selvas, J. K. Sahu, J. Nilsson, S. U. Alam, A. B. Grudinin, "Q-switched 980nm Yb-doped fiber laser", in *Proc. Conference on Lasers and Electro-Optics (CLEO),* Long Beach, California, 2002, paper CThR6.

[50] J. Kim, P. Dupriez, D. B. S. Soh, J. K. Sahu, J. Nilsson, D. N. Payne, "Nd:Al-doped depressed clad hollow fiber laser at 930 nm", in *Proc. Advanced Solid-State Photonics (ASSP),* Vienna, 2005.

[51] V. N. Philippov, J. K. Sahu, C. A. Codemard, W. A. Clarkson, J. N. Jang, J. Nilsson, and G. N. Pearson, "All-fiber 1.15-mJ pulsed eye-safe optical source", Proc. SPIE **5335**, 1-7 (2004).

[52] K. K. Y. Wong, K. Shimizu, K. Uesaka, G. Kalogerakis, M. E. Marhic and L. G. Kazovsky, "Continuous-Wave Fiber Optical Parametric Amplifier With 60-dB Gain Using a Novel Two-Segment Design", IEEE Photon. Technol. Lett. **15**(12), 1707 (2003).

[53] M. J. F. Digonnet, *Rare-Earth Doped Fiber Lasers and Amplifiers*, (2nd Ed., New York: Marcel Dekker, 2001).

[54] R. H. Stolen, E. P. Ippen, "Raman oscillation in glass optical waveguide", Appl. Phys. Lett. **20**(2), 62-64, (1972).

[55] C. Codemard, J. K. Sahu, and J. Nilsson, "Cladding-pumped Raman fiber amplifier for high-gain high-energy single-stage amplification", in *Proc. Optical Fiber Communication Conference (OFC)*, Anaheim, USA, 2005, paper OTuF5.

[56] C. Alegria, Y. Jeong, C. Codemard, J. K. Sahu, J. A. Alvarez-Chavez, L. Fu, M. Ibsen, J. Nilsson, "83 W single-frequency narrow-linewidth MOPA using large-core erbium-ytterbium co-coped fiber", IEEE Photon. Technol. Lett. **16**(8), 1825 (2004).

[57] Y. Jeong, C. Alegria, J. K. Sahu, L. Fu, M. Ibsen, C. Codemard, M. R. Mokhtar, J. Nilsson, "A 43W C-band tunable narrow-linewidth erbium-ytterbium co-doped large-core fiber laser", IEEE Photon. Technol. Lett. **16**(3), 756 (2004).

[58] J. K. Sahu, Y. Jeong, C. Codemard, J. Nilsson, M. R. Mokhtar, M. Ibsen, D. J. Richardson, D. N. Payne, "Tunable narrow linewidth high power erbium:ytterbium co-doped fiber laser", in *Proc. Conference on Lasers and Electro-Optics (CLEO)*, San Francisco, US, 2004, paper CMK.

[59] C. Codemard, C. Farrell, V. N. Philippov, P. Dupriez, J. K. Sahu, and J. Nilsson, "1 mJ narrow-linewidth pulsed fiber MOPA source at 1535 nm", in *Proc. Conference on Lasers and Electro-Optics (CLEO)*, Munich, Germany, 2005, paper CJ3-3.

[60] C. A. Codemard, P. Dupriez, Y. Jeong, J. K. Sahu, M. Ibsen, and J. Nilsson, "High-power continuous-wave cladding-pumped Raman fiber laser", Opt. Lett. **31**(15), 2290 (2006).

[61] C. A. Codemard, P. Dupriez, Y. Jeong, J.K. Sahu, M.Ibsen, J. Nilsson, "High power cladding-pumped Raman fiber laser with true single-mode output at 1660 nm", in *Proc. Optical Fiber Communication Conference (OFC)*, Anaheim, USA, 2006, paper OThJ2.

Chapter 2 Background

This chapter is divided into several sections that present an overview of theory and information required to understand the later chapters. Firstly, section 2.1 presents the notion of brightness and its relation to the beam quality in the case of a fibre laser source. Then, in section 2.2, the principle of cladding-pumping and double-clad fibres for high-power, high-brightness output is introduced. Thereafter, the fibre waveguide theory, that describes the properties of electro-magnetic fields in an optical fibre, is briefly presented in section 2.3. This helps in the understanding of non-linear effects in multi-mode fibre. Finally, section 2.4 introduces some of the non-linear effects that arise from the propagating high intensity optical field in optical fibre, with a particular attention for Raman scattering.

2.1 Beam quality and brightness

Laser sources with high beam quality enable tight focusing of a beam, for example, in laser material processing, printing, marking, cutting and drilling, as well as long working distances and low divergence beams, such as in LIDAR or frequency conversion. These laser sources are generally optically pumped lasers which then, normally, generate laser beams of much higher brightness than the pump beam; although the output power is lower the beam quality is much higher. Furthermore compared to alternative pumping schemes, optical pumping has the advantage that its primary requirement is high optical quality, but that will necessarily be fulfilled by any laser gain medium. By contrast, other pumping schemes such as electrical injection place many additional requirements on the gain medium, which are often difficult to combine with high-power, high-brightness operation.

Fibre lasers based on double-clad fibres which convert light from multi-mode semiconductor pump source into diffraction limited output beam are examples of lasers that can be optically pumped by high-power, low-brightness beams. Consequently they can be seen as brightness converters. In fact, due to recent developments, fibre lasers are among the brightest laser sources in existance, as figures 2.1 and 2.2 show.

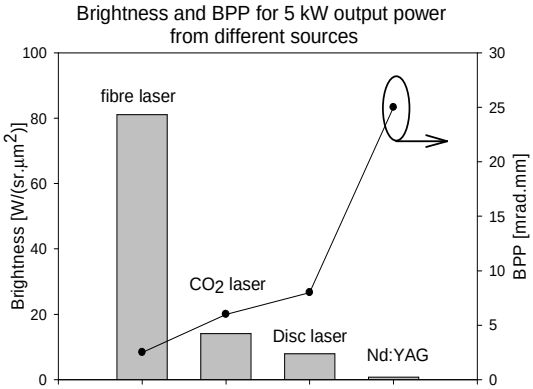

Figure 2.1: Comparison of the brightness and beam parameter product from different laser sources.

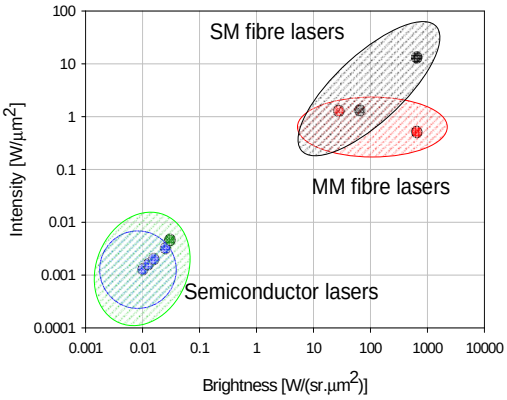

Figure 2.2: Comparison of the brightness from commercially available semiconductor and fibre laser sources

Due to confusion between beam quality and brightness, it is convenient to remind oneself of the definitions of these. Indeed the term high-brightness indicates either a high power output and/or a high beam quality. The brightness is also called the radiance and is defined as the amount of light that passes through or is emitted from a particular area, and falls within a given solid angle in a specified direction. Brightness is expressed in W/(sr.m^2).

Therefore, in the small angle approximation, in an optical fibre, the brightness B can be expressed as [1]:

$$B = \frac{P}{\Omega A} \approx \frac{P}{NA^2 \pi A} \tag{2.1}$$

where B is the fibre brightness, P is the emitted power from an area of size A in a solid-angle Ω (in the far-field), and NA is the fibre numerical aperture. B is expressed in W/(sr.m^2). Hence a high brightness fibre laser is one with a low optical divergence from a small emitting core and with a high power output, whose performance approaches that of an idealised beam.

The beam quality of a laser source is described by the beam propagation factor M^2 which can be expressed as [2]:

$$M^2 = \frac{D_0 \Theta}{4\lambda / \pi} \tag{2.2}$$

where D_0 is the diameter of the focal point (i.e. waist diameter), Θ is the full angle in the far field of the light emerging through the focal point and λ is the wavelength of the optical radiation.

Note that normally, the beam forms a waist at the fibre end. Hence, the in-fibre beam diameter can be used for D_0.

The M^2 factor is related to the minimum spot size, which can be achieved at a certain wavelength with a certain aperture and numerical aperure. However, it is independent of the power. Practically, the M^2 factor can be measured according to ISO standard 11146 [3] by a fitting procedure from the measured evolution of the second order moment of the beam radius along the propagation direction. In the case of fibre lasers, a diffraction-limited beam can be obtained when the laser operates uniquely on the lowest order mode of the fibre core. However, even with a single-mode fibre, the M^2-value depends on the refractive index profile of the core. A diffraction limited beam has a M^2 factor which is unity. A single-mode step-index fibre typically has an M^2-value of 1.05, which still can be considered to be diffraction-limited. Conveniently, the beam propagation factor is linked to the source's brightness by:

$$B = \frac{P}{\left(M^2 \lambda\right)^2} \tag{2.3}$$

where P is the power emitted from the laser, M^2 is the beam propagation factor and λ is the wavelength of the optical radiation.

Finally, there is another common term, which is used to quantify the beam quality of a laser source, called the "beam parameter product" or BPP. It is defined as:

$$BPP = M^2 \frac{\lambda}{\pi} = \frac{D_0 \Theta}{4} \tag{2.4}$$

Other definitions may exclude the factor of 1/4. In contrast to the M^2-parameter, the BPP directly tells us how tightly a beam can be focused (at a certain numerical aperture), without any explicit dependence on the wavelength.

2.2 Double-clad fibres

2.2.1 Principles

The breaktrough RE-doped fibres realised in the mid-1980s were single- or few-moded devices that were pumped in the core. They generally relied on single-mode pumping, which limited their scope for brightness-enhancement. Their potential for power-scaling was also limited, since suitable single-mode pump-laser diodes are still limited in power to the watt-level. To overcome these limitations we would like to break the constraint of single-mode pumping

and to allow greater amounts of pump power to be coupled into the fibre, while at the same time retain a diffraction-limited output beam. A solution was proposed in 1989 by Po et al. [4] which consisted of a fibre whose cladding is surrounded by a lower index outer cladding which then forms a waveguide, outside of the primary core waveguide. The pump light can be introduced into the inner cladding and can propagate along the fibre, interacting with the rare-earth doped core as shown in figure 2.3. Such a fibre is called a double-clad fibre [5]. Since the core is often single-moded, a diffraction-limited output is obtained even with high-power multi-mode pumping.

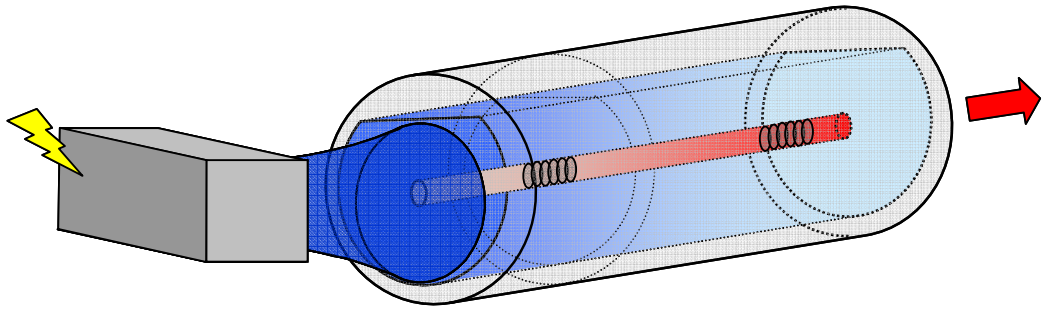

Figure 2.3: Working principle of a double-clad fibre laser. The pump light (in blue) from a laser diode propagates in the inner cladding of the double clad fibre, while lasing (in red) occurs in the core in a cavity formed by two embedded fibre gratings.

In order to maximize the amount of pump power that can be launched, the second cladding must have a refractive index as low as possible, to yield an NA of the inner cladding that is as high as possible. The inner cladding can also have a significantly larger area than the core. Consequently, with a typical value for silica face damage of about 10 W/μm^2 at around 980 nm, more than 1.256 MW could theoretically be launched into a 400 μm diameter circular fibre. Unfortunately, although a larger inner-cladding enables more pump power to be coupled into the fibre structure, as long as the core design is fixed with a fixed RE-ion concentration, the pump absorption decreases as the interaction between the pump and the core is reduced (the overlaps between the modes of the inner cladding and the core decrease). Nonetheless this can be compensated with a longer fibre length, up to limits set by background loss and non-linearities. In addition, the pump power coupled into the fibre can be further increased with spectral and spatial multiplexing of multi-mode pump sources such as laser diodes stacks, diode bars or multiple single laser emitters. Therefore, from the development of the double-clad fibre, a new class of high power high-brightness laser sources emerged: the fibre laser.

2.2.2 Cladding designs

Double-clad fibres have a secondary lower index, outer, cladding. There are three types of outer cladding. Firstly, the cladding can be composed of a low-index glass. For example, fluorine doped silica yields a numerical aperture of typically about 0.2 to 0.3 for a pure-silica inner cladding. Such double-clad fibres are also called all-glass double-clad fibres. Advantages include a high thermal resilience and low propagation loss. It is based on well-known technology used for the fabrication of large-core fibres, but then with a large pure-silica core surrounded by a fluorosilicate cladding. The double-clad fibre design would introduce a (primary) RE-doped core into the pure-silica core of such a fibre. Secondly, the outer cladding can consist of a polymer or polymer-like coating, e.g., a fluoro-acrylate or a silicone. In this case, the NA (relative to a pure-silica inner cladding) can become 0.4 – 0.5. This is the most commonly used approach because the fabrication is straightforward and the cladding can be easily removed and the fibre easily cleaved. Figure 2.5 shows a cleaved end-face of D-shaped double-clad fibre which was coated with a low index polymer. Finally, the secondary cladding can consist of air holes in a silica fibre as shown in figure 2.4, such fibres being known as all-glass air-clad fibre (also Jacketed Air-Clad fibre). The numerical aperture depends on the structure. Values approaching unity have been reported [6], but are difficult to realise and to work with in practice. Typical values are lower, e.g., about 0.6 [7]. This is much higher than the other fibre designs due to the high refractive index contrast between silica and air. Still JAC fibres are challenging to fabricate and to handle and, therefore, are only occasionally used.

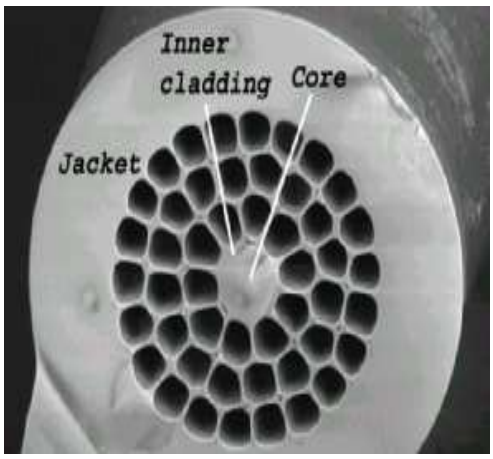

Figure 2.4: Jacketed Air-Clad fibre whose outer cladding is formed by air-holes (here, the inner-cladding diameter is ~ 30μm) [7].

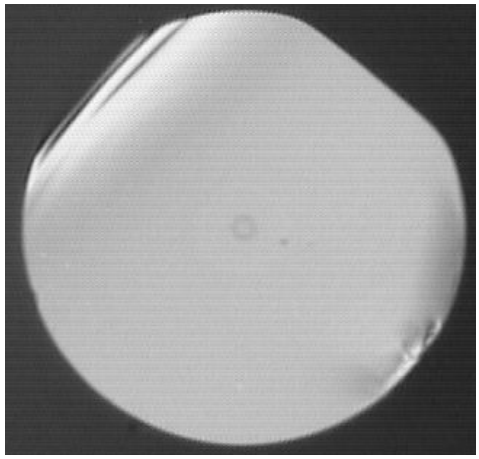

Figure 2.5: D-shape double-clad fibre with a low-index polymer outer cladding.

Another important aspect of the cladding design is its shape, which influences the interaction between the pump light and the doped core [8 - 11]. For example, in fibres with circular symmetry, there are skew modes, which never overlap with the core. In a step-index structure, these correspond to higher-order Bessel functions, which vanish in the centre. Only J_0 is non-zero in the centre, and the corresponding modes will see a high absorption. In contrast, the pump power contained in skew modes cannot interact efficiently with a core in the centre of the fibre. A large part of it is simply lost, without contributing to the amplification process. In the case of circular fibre, bending the fibre can induce some pump mode mixing. Thus, for example, pump power can be transferred into the J_0-modes and prevent these from being depleted. Therefore bending is commonly used to increase the pump absorption in circularly symmetric fibres. A more robust and repeatable alternative is to use cladding designs that do not support skew modes [12, 13] as shown in figure 2.6. For example, fibres with a rectangular inner cladding have shown an increased pump absorption over circularly symmetric fibres [14 - 16]. An off-centre core is another way of breaking the symmetry of circular fibres.

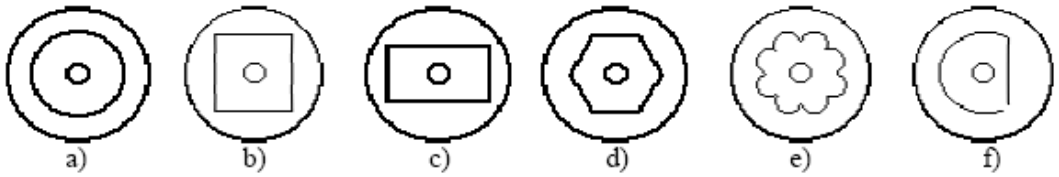

Figure 2.6: Common shapes of the inner cladding of double-clad fibres: a) circular, b) square, c) rectangular, d) hexagonal, e) flower shape, f) D-shape [17].

2.2.3 Light injection methods

The injection of the pump light into the inner-cladding of the DCF can be achieved through various means, partly depending on the fibre geometry. The choice of the injection method is important as it, together with the pump brightness, determines the maximum permissible pump power, which can be coupled into a DCF. In many cases, this determines the performance that can be reached with a high-power fibre laser. The pump injection methods can be divided in two groups according to the location of the injection point along the double-clad fibre: end-pumping and side-pumping. There are also hybrid schemes, in which the pump power is first launched into a passive fibre through its sides. The pump power is, then launched into the active fibre through its end, by splicing the passive fibre to the active one.

The simplest method is to launch the pump directly into the inner cladding of the active fibre through one or both of the fibre ends using free-space coupling optics. Free-space end-pumping is easy to implement in an experimental set-up and the launch efficiency is generally good (e.g., 80%) if the beam quality of the pump source is sufficiently high. An additional advantage of free-space end-pumping is that the pump power can be scaled using diode bars or diode stacks whilst maintaining a high launch efficiency. Sometimes, free-space end-pumping is the only practical brightness-preserving solution when the source and fibre NA are very different, for example, in the case of high-NA, small inner-cladding fibres such as jacketed air clad fibres which have down to 30 μm inner cladding diameters [7]. However, the launch optics require precise and stable alignment. Furthermore, the fibre ends are not accessible for splicing which means that the signal has to be accessed with free space optics (at least with double-ended pumping). However, in commercial products all-fibre pumping schemes are preferred as it reduces or replaces a number of bulk optic components, enabling the construction of monolithic fibre laser sources in which the light propagates within the fibre. For example, fused components and fibre splices cannot be misaligned (although they can still suffer from excess accumulated heat in some cases).

Therefore, tapered fibre bundles (TFB) with signal feed-through [18, 19], which are only recently becoming commercially available, are commonly used in fibre laser. A tapered fibre bundle combines a fibre with a signal-guiding core and a number of pump fibres into a single double-clad fibre, guiding both the signal in its core and the pump in the inner cladding. Typically, the common double-clad fibre is not RE-doped, but is spliced to an active double-clad fibre. However, with a passive TFB that is spliced to the end of an active fibre, this effectively becomes an end-pumping method. As such, the maximum number of injection points is limited to the two fibre ends. In addition, in high power applications, the high pump power intensity at the injection points can lead to thermal loading at the fibre ends and special cooling arrangements must be then implemented to reduce fibre damage.

The second group of injection methods utilise some coupling mechanism that takes place on or along the side of the double-clad fibre. The notch coupling invented by Goldberg et al. [20] consists of a V-shaped groove cut into the fibre inner-cladding which is used to reflect the pump. V-groove side pumping allows for multiple injection points along the fibre with a typical launch efficiency of 75% [21]. However, the power scaling ability is poor because the number of V-grooves increases with power and the output power of laser diodes chips remains quite limited. Other side pumping methods consist of injecting the pump light through a side fibre in optical contact with the inner-cladding [22, 23]. This co-linear coupling is basically a long coupler, extended over the whole fibre where the pump and signal fibre are independently free and share a common low index cladding. This coupling mechanism is less prone to high

thermal loading because the pump power is slowly distributed to the active fibre inner-cladding [24]. Another side coupling method is the fused taper side-coupling invented by Samartsev et al. [25]. Little is really known about the power handling capability of this method, but in its design it is quite similar to the tapered fibre bundle and should have comparable power handling capability.

2.3 Fibre modes

To understand the properties of an optical fibre for the propagation of an optical wave, it is necessary to consider the optical fibre modes. An optical field can be described as the superposition of guided modes and radiation modes. Fibre modes describe how the electromagnetic field $(\mathbf{E},\mathbf{H})$ (where $\mathbf{E}$, $\mathbf{H}$ are the electric and magnetic fields, respectively) is distributed transversely in the waveguide and how the light propagates along the fibre. Many aspects of light propagation in optical fibres is best described in terms of modes. Therefore, they are important to understand the behaviour of cladding-pumped devices. In order to determine the properties of these modes, generally, the theory of electromagnetic wave propagation in a linear medium is considered. Thus, like all electromagnetic phenomena, the optical field is governed by Maxwell's equations and associated boundary conditions. Because derivations are rather lengthy and tedious and because the equations are well known and presented in numerous textbooks, e.g. [26], they are not shown here in detail. Broadly, from Maxwell's equations and after some considerations regarding the physical properties of the propagating medium (for example, the medium is non-magnetic), and some mathematical manipulation [26], Maxwell's equations can be converted into the wave equation which is also called Helmholtz's equation. This equation is used to describe the properties of optical waves in a waveguide. The optical waves, which can propagate in the waveguide, are discrete solution of the wave equation and are referred to as modes of the waveguide. The modal properties of optical fibre depend on the fibre geometry, the material refractive index and the wavelength of operation.

2.3.1 Helmholtz equation

When a medium where the optical field is propagating is non-magnetic, Maxwell's equations can be converted [26] into the wave equation (2.5) for the electric field $\mathbf{E}$ (and similarly for the magnetic field $\mathbf{H}$). .

$$\nabla\times\nabla\times\mathbf{E}=-\frac{1}{c^2}\frac{\partial^2\mathbf{E}}{\partial t^2}-\mu_0\frac{\partial^2\mathbf{P}}{\partial t^2} \tag{2.5}$$

where $\mathbf{E}$ is the electric field vector, $\mathbf{P}$ is the induced polarisation from the electric dipoles, c is the velocity of light in the vacuum, μ_0 is the vacuum permeability and is related to the speed of light by $\mu_0\varepsilon_0=\frac{1}{c^2}$ where ε_0 is the vacuum permittivity.

This relation is valid in the electric-dipole approximation with a local medium response. The wave equation can be further simplified by the relation $\nabla\times\nabla\times\mathbf{E}=\nabla\left(\nabla\cdot\mathbf{E}\right)-\nabla^2\mathbf{E}$ where $\nabla\cdot\mathbf{D}=\varepsilon\nabla\cdot\mathbf{E}=0$ and ε represents the medium dielectric constant. In addition, if the optical loss of the fibre is small (i.e. $\varepsilon\approx n^2$), then (2.5) can be written as:

$$\nabla^2\mathbf{E}+\nabla\left[\mathbf{E}\frac{\nabla n^2}{n^2}\right]=\frac{n^2}{c^2}\frac{\partial^2\mathbf{E}}{\partial t^2} \tag{2.6}$$

where n is the refractive index distribution of the optical waveguide medium, and c is the velocity of light in vacuum. The term ∇n^2 can be neglected if the relative change of the refractive index is small over the distance of one wavelength [27] (that is the case in a real optical fibre). Thus, by expressing the field in the frequency domain by a Fourier transform (i.e. $\tilde{\mathbf{E}}\left(\mathbf{r},\omega_0\right)=\int_{-\infty}^{\infty}\mathbf{E}\left(\mathbf{r},t\right)\mathrm{e}^{-i\omega_0 t}\,dt$), equation (2.6) can be reduced to the well-known homogeneous wave equation (also called the Helmholtz equation):

$$\nabla^2\tilde{\mathbf{E}}\left(\mathbf{r},\omega\right)+n^2\left(\mathbf{r},\omega\right)\frac{\omega^2}{c^2}\tilde{\mathbf{E}}\left(\mathbf{r},\omega\right)=0 \tag{2.7}$$

Here $\tilde{\mathbf{E}}$ is the electric-field vector in the frequency domain and is linked to $\mathbf{E}$ by a Fourier transform, $\mathbf{r}$ is the position vector and ω is the angular frequency.

Assuming the slowly varying envelope approximation [26] and a circularly symmetric structure like an optical fibre, the electric field can be written as a function of independent variables in (2.8).

$$\tilde{E}\left(\mathbf{r},\omega\right)=\tilde{A}\left(z,\omega-\omega_0\right)F\left(r\right)\exp\left(\pm im\phi\right)\exp\left(i\beta_0 z\right) \tag{2.8}$$

where F is the transverse field distribution which only depends on the radial position r, the angular dependence is given by $\exp\left(\pm im\phi\right)$ where m is an integer, $\tilde{A}$ is the amplitude of the

field that varies along the z-axis of the fibre and the term $\exp(i\beta_0 z)$ contains the phase modulation during the propagation with β_0 the propagation constant.

By inserting equation (2.8) into equation (2.7), the variables F and $\tilde{A}$ can be separated into two distinct equations:

$$\left[\frac{d^2}{dr^2}+\frac{1}{r}\frac{d}{dr}+\left\{k_0{}^2 n^2(r)-\tilde{\beta}^2(\nu,l)-\frac{m^2}{r^2}\right\}\right]F(\nu,r)=0 \tag{2.9}$$

$$2i\beta_0\frac{\partial\tilde{A}}{\partial z}+\left(\tilde{\beta}^2-\beta_0{}^2\right)\tilde{A}=0 \tag{2.10}$$

where $n(r)$ is the radial refractive index distribution, ν is the radial mode number, m is the azimuthal mode number, k_0 is given by $k_0=\frac{\omega}{c}=\frac{2\pi}{\lambda}$, and $\tilde{\beta}$ is the eigenvalue of (2.9). Equation (2.9) defines the transverse field distribution while equation (2.10) describes the field amplitude variation during its propagation in the waveguide.

In a step-index fibre, the general solution of (2.9) is given by Bessel functions of the first and of the second kind. There are several solutions for each integer value of m, which, in order to have a physical meaning, must decay exponentially for large value of r, away from the waveguiding region. Therefore, the fibre modes are designated by the numbers (m,ν) to which correspond a unique value $\tilde{\beta}$. These numbers are used to designate Linearly Polarized (LP) fibre modes, ignoring the degenerate modes originating from the polarization orientation of the modes [28].

Equation (2.10) can be expanded to the non-linear Schrödinger equation when the Kerr non-linearity is included. This equation is discussed further in section 2.4.1.

Generally, a fibre optical waveguide consists of a cylindrically symmetric core region surrounded by a low index cladding region to form a waveguide and guide the light along the core as in figure 2.7. The eigenequation (2.9) must be solved for the given refractive index profile (RIP) to find the propagation constants of the various LP modes guided by the structure.

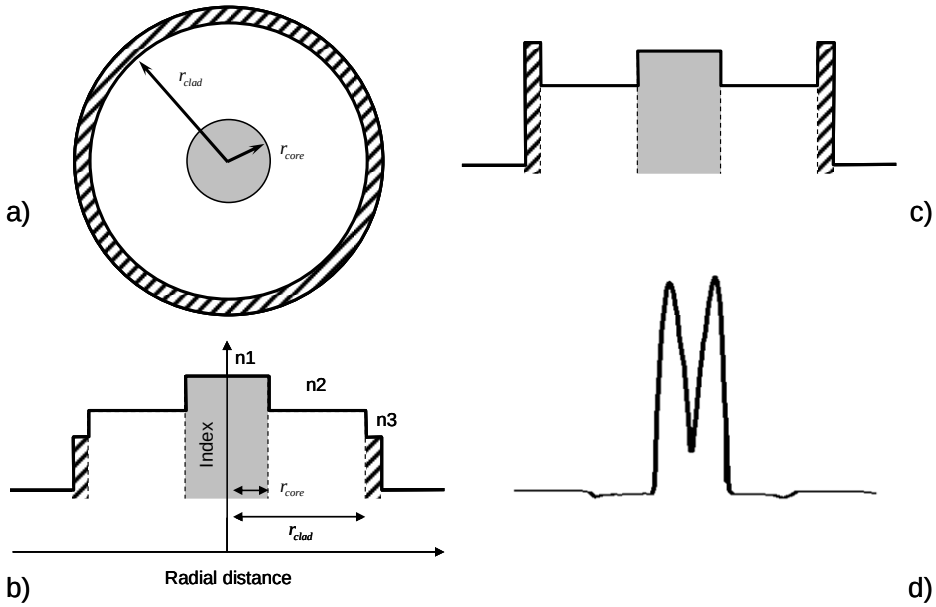

Figure 2.7: Optical fibre waveguiding structure: a) fibre cross-section b) typical double-clad fibre RIP c) multi-mode fibre RIP with high index coating and d) Measured RIP of the core F402-LF122 manufactured at the ORC

In the case of an arbitrary index profile, several numerical methods in the literature [29 - 31] are discussed to solve equation (2.9). Depending on their values of β_0 [32], the modes are either predominantly propagating in the core region and are core modes, or they propagate (predominantly) in the cladding region and are called radiation modes. In the case of single mode fibre, the radiation modes extend into the cladding region and into the jacket, which is generally absorbing. Hence, this category of mode tends to disappear quickly in single mode fibre but not in double clad fibre because of the outer low refractive index region. In fact, in that case the modes in the inner cladding are also guided modes.

2.3.2 Modal excitation

When an optical fibre is illuminated with an incoming light beam, certain modes are excited according to the spot size, offset and tilt (with respect to the optical axis of the fibre) of the illuminating light beam. Hence, the incident power is distributed among these excited modes. This can be used to selectively or preferentially excite low order modes in large-core multi-mode fibre, e.g., the fundamental mode of a multi-mode fibre [33]. Therefore, it is important, in order to model accurately any multi-mode system, to know the modal power decomposition at the light injection point. Theoretical modal power decomposition can be determined from a knowledge of the incident light beam properties. Several methods exist, for

example, the mode matching method, the plane wave expansion [34] and the direct phase vector matching method [35]. It is also possible to determine experimentally the modal excitation of optical fibre, but, so far, it is rather difficult to measure it in device-length fibre and it is practically cumbersome [36].

Based on the mode matching method, the modal decomposition coefficient $\eta_{m,n}$, for an incident input field F_i into a supported mode $F_{m,n}$ (where m and n are the azimutal and the radial mode numbers), is calculated using the following well-know overlap expression [37]:

$$\eta_{m,n} = \frac{\int_{-\infty}^{\infty}\int_{-\infty}^{\infty} F_i(x,y).F_{m,n}(x,y)\,dxdy}{\sqrt{\left(\int_{-\infty}^{\infty}\int_{-\infty}^{\infty}\left|F_i(x,y)\right|^2 dxdy\right)\left(\int_{-\infty}^{\infty}\int_{-\infty}^{\infty}\left|F_{m,n}(x,y)\right|^2 dxdy\right)}} \tag{2.11}$$

where $F_i(x,y)$ is the input field, $F_{m,n}(x,y)$ is the modal field. This is the method used in this work to calculate the modal excitation of multi-mode fibre such as the double-clad fibre used for Raman amplification.

The same principle of modal excitation is used to determine the butt-joint splice loss, between, for example, the fundamental mode losses of two fibres. The splicing loss for two fibres with mismatched fundamental-mode diameters and a lateral displacement d is given by [38]:

$$L_{splice\_dB} = -10Log_{10}\left(\frac{4}{\left[\left(\frac{w_1}{w_2}\right)+\left(\frac{w_2}{w_1}\right)\right]^2}\exp\left(-2\frac{d^2}{w_1^{\,2}+w_2^{\,2}}\right)\right) \tag{2.12}$$

where w_1 and w_2 are the mode field diameters of the first and second fibre, respectively.

2.3.3 Mode coupling

Mode coupling occurs in multi-mode optical fibre when the waveguiding properties of the fibre are perturbed, for example, through macro-bending [32] or core deformation [39]. Mode coupling can be undesirable when the fibre modal integrity must be preserved, for example, in the case of single mode operation of a multi-mode fibre [33]. On the contrary, in some cases, strong mode coupling and mode mixing is a useful feature, for example in rare-

earth doped double-clad fibre where strong coupling of pump modes increases the pump absorption. In this work, mode coupling is important for the cladding-pumped Raman fibre [40].

Let us consider an optical field E which travels down a fibre. The field can be constructed as a superposition of mode fields, F_i, which are supported by this fibre and associated with the propagation constants β_i. Equation (2.13) [41 - 43] expresses such a superposition of modes of amplitudes A_i.

$$E(x,y,z) = \sum_{i=1}^{N} A_i(z) F_i(x,y;\beta(z)) \exp\left(i\int_0^z \beta_i(z)\,dz \right) \tag{2.13}$$

If the fibre is translationally invariant, there is no mode coupling but mode beating occurs. In that case, the modes fields, F_i, and the propagation constant β_i can be calculated by solving equation (2.9). Otherwise, the modes and the propagation constants at every point z evolve and the F_i's and the propagation constants β_i become a function of z. These modes are known as local modes.

Assuming the weak guidance approximation [43], coupling equations can be used to describe the modal power transfer which can be reduced to tracking the evolution of the modal amplitudes $A_i(z)$ [41 - 43]. Equation (2.14) governs the evolution of the amplitudes along the propagation axis (the z-axis).

$$\frac{dA_i(z)}{dz} - i\beta_i(z)A_i(z) = i\sum_{j=1}^{N} C_{ij}(z)A_j(z) \tag{2.14}$$

where the C_{ij} are the mode coupling coefficients between the i^{th} and j^{th} modes. The value of the mode coupling coefficients C_{ij} depends on the type of perturbation. In the absence of any perturbation the amplitude A_i oscillates along the propagation axis such as $A_i(z) = \tilde{A}_i.e^{i\beta_i z}$. If the fibre perturbation is small and oscillates around an average value then the mode coupling coefficient is given by equation (2.15) where the transverse dependence is omitted for simplicity [43].

$$C_{ij}(z) = \frac{k}{2n_{ref}} \int_{S_\infty} \left(n^2(z) - \bar{n}^2\right) F_i(\beta_i) F_j(\beta_j)\,dS \tag{2.15}$$

where k is the amplitude of the wave vector defined in section 2.3.1, n_{ref} is a representative reference index i.e. typically the core refractive index, and S_∞ represents the infinite cross-

section at a given position. The β_j's represent the propagation constants of the modes of the unperturbed waveguide.

If the waveguide perturbation is significant, e.g., in the case of a strong taper, the concept of local modes must be used and the coupling coefficient is now given by:

$$C_{ij}(z) = \frac{k}{2n_{ref}} \frac{1}{\beta_i(z) - \beta_j(z)} \int_{S_\infty} \frac{\partial n^2(z)}{\partial z} F_i(\beta_i) F_j(\beta_j) dS \tag{2.16}$$

where the local mode fields F_i's are functions of the position z through a local $\beta_i(z)$ [43].

2.4 Raman scattering and non-linear effects in optical fibres

2.4.1 Introduction to non-linear effects

Optical fibre shows a non-linear response to intense optical fields which give rise to effects such as harmonic generation, beam self-focusing, Kerr effect [44] and stimulated scattering processes. This non-linear response originates from several effects, including the oscillation of nuclei and the anharmonic motion of bound electrons under the influence of an applied field. In general, when a propagating electric field $\mathbf{E}$ exists in a material, a polarization density $\mathbf{P}$ is induced which may be expressed as a power series in the field [26]:

$$\mathbf{P} = \varepsilon_0 \left(\chi^{(1)}.\mathbf{E} + \chi^{(2)}.\mathbf{E}.\mathbf{E} + \chi^{(3)}.\mathbf{E}.\mathbf{E}.\mathbf{E} + \ldots \right) \tag{2.17}$$

where ε_0 is the vacuum permittivity and $\chi^{(j)}\ (j = 1, 2, \ldots)$ is the medium's j^{th} order susceptibility represented by a tensor of rank j+1. The linear susceptibility $\chi^{(1)}$ is the dominant contribution of the polarization. The linear susceptibility results in a refractive index n and an attenuation coefficient α. The second order susceptibility $\chi^{(2)}$ is responsible for non-linear effects such as second harmonic generation and sum-frequency generation. In an isotropic material such as a silica fibre, this phenomenon arises from a lack of inversion symmetry of the medium. However it is extremely weak and in practice vanishes. Therefore, the lowest-order non-linear effects in optical fibre originate from the third order susceptibility $\chi^{(3)}$. This is responsible for phenomena such as third-harmonic generation, four-wave mixing, the intensity dependence of the refractive index (Kerr effect) and non-linear inelastic scattering. The $\chi^{(3)}$ processes can be separated in two distinct classes of scattering effects. Elastic scattering effects do not exchange energy with the medium by definition. These effects are phase matched and

arise from the electronic response of the medium. The second class concerns scattering processes that are inelastic in that part of the optical field energy is transferred to the non-linear medium. These effects are non-phased matched and are induced by the nuclear or the electrostrictive response of the medium. These are the three main processes that commonly contribute to $\chi^{(3)}$ depending on the light – medium interaction.

$$\chi^{(3)} = \chi^{(3)}_{Electronic} + \chi^{(3)}_{nuclear} + \chi^{(3)}_{electrostriction} \tag{2.18}$$

The electronic contribution results from the non-parabolic nature of the electronic energy wells. It has a minimum response time of order 10^{-16} s, while the nuclear contribution arises from optical-field-induced changes in motions of the nuclei and has a response time of order 10^{-12} s. The electrostrictive contribution results from electric-field induced strains and responds in 10^{-8} s.

In order to simplify some equations it is useful to introduce the non-linear intensity dependent refractive index n_2 that collects up the $\chi^{(3)}$ effects

$$n = n_0 + n_2 I = n_0 + \left(n_2^{real} + n_2^{img}\right) I \tag{2.19}$$

where I is the light intensity, n_0 is the material refractive index, n_2 is the non-linear contribution i.e. perturbation to n_0. The real part of the non-linear refractive index, n_2, which corresponds to the electronic response, is found to vary in the range 2.2 - 3.9 10^{-20} $m^2.W^{-1}$ for silica fibre. The variation in the value of n_2 is explained by the different dopants used in the fibre core and cladding, such as GeO_2 and Al_2O_3. The imaginary part of the non-linear refractive index n_2^{img} is related to the non-linear scattering processes.

For a better understanding of non-linear phenomena in optical fibres, it is necessary to consider the theory of electromagnetic wave propagation in dispersive non-linear media. Like all electromagnetic phenomena, the propagation of optical fields in an optical fibre is governed by Maxwell's equations (2.5) where the polarization $\mathbf{P}$ is replaced by $\mathbf{P} = \mathbf{P}_{Linear} + \mathbf{P}_{NL}$. If we consider only the third order susceptibility, the non-linear contribution becomes:

$$\mathbf{P}_{NL}(\mathbf{r},t) = \varepsilon_0 \chi^{(3)} \vdots \mathbf{E}(\mathbf{r},t)\mathbf{E}(\mathbf{r},t)\mathbf{E}(\mathbf{r},t) \tag{2.20}$$

And, after insertion of (2.20) into (2.5), the inhomogeneous wave equation (2.21) is obtained:

$$\nabla \times \nabla \times \mathbf{E} - \frac{1}{c^2}\frac{\partial^2 \mathbf{E}}{\partial t^2} = \mu_0 \frac{\partial^2 \mathbf{P}_L}{\partial t^2} + \mu_0 \frac{\partial^2 \mathbf{P}_{NL}}{\partial t^2} \tag{2.21}$$

The total electric field $\mathbf{E}$ can be represented as a superposition of one or several monochromatic waves in one or several modes:

$$\mathbf{E}(\mathbf{r},t)=\sum_{i=1}^{N}E_i\cos(\omega_i t-\beta_i z) \tag{2.22}$$

Then the non-linear contribution to the polarization becomes:

$$\mathbf{P}_{NL}(\mathbf{r},t)=\varepsilon_0\chi^{(3)}\sum_{i=1}^{N}\sum_{j=1}^{N}\sum_{k=1}^{N}E_i\cos(\omega_i t-\beta_i z)E_j\cos(\omega_j t-\beta_j z)E_k\cos(\omega_k t-\beta_k z) \tag{2.23}$$

where i, j and k represent the index of various modes considered with ω and β their respective optical frequency and propagation constant.

The same process as in Section 2.3.1 can be used to solve the scalar wave equation (2.21). A new amplitude equation called the non-linear Schrodinger equation (NLSE) [26] describes the various non-linear effects:

$$\frac{\partial A(z,t)}{\partial z}-\frac{i}{2}\left[\left(\frac{d^2k}{d\omega}\right)_{\omega_0}+\frac{1}{k(\omega_0)}\left(\frac{dk}{d\omega}\right)^2_{\omega_0}\right]\frac{\partial^2 A(\mathbf{r},t)}{\partial z}=-i\frac{3k_0}{8n_0}\chi^{(3)}\left|A(z,t)\right|^2A(z,t) \tag{2.24}$$

In practice, the power is a more convenient representation than the amplitude of the electric field because it can be directly measured. The power P is related to the amplitude A by $P=AA^*\int_S FF^*dS$, with F being the field distribution over the cross-section S. Once, the equation (2.24) is integrated over the cross-section S, the equations of the evolution of stimulated Raman scattering are derived (2.26) - (2.27). In that case, effective areas [45] are introduced and are defined as:

$$A_{eff}^{i,j,k,l}=\frac{\sqrt{\int_S|F_i|^2dS\int_S|F_j|^2dS\int_S|F_k|^2dS\int_S|F_l|^2dS}}{\int_S F_iF_jF_kF_ldS} \tag{2.25}$$

where $F(x,y)$ is the optical mode field distribution over the transverse area S of the optical fibre and i,j,k and l are indices which represent the various fibres modes involved in the non-linear process. The overlap integral, $\int_S F_iF_jF_kF_ldS$, arising from integration over the waveguide mode-fields can differ depending on the specific modes involved. This overlap integral is non-zero for processes like Raman scattering which deals with two distinct modes ($i=j$ and $k=l$

in equation (2.25)) or for combinations of modes with the proper symmetry in processes, like four-wave mixing, which involve four distinct fibre modes.

2.4.2 Raman scattering

2.4.2.1 Introduction

As seen in the previous section, the optical medium can give rise to an electronic and nuclear non-linear response under the incidence of a high intensity beam. The interaction of optical photons with phonons (vibrational state) results in the scattering of the pump photons called Stokes wave. The spontaneous scattering occurs by the optical phonon vibrational modes of the medium determined by the temperature of the medium. The intensity of the scattered wave is strongly dependent on the angle of scattering and the optical power density in the material. However, in silica fibre, a fraction of the scattered light generated by the spontaneous scattering is captured by the waveguiding core, resulting in the transfer of energy from the pump wave to the Stokes wave [46]. Because of the capture effect, the Stokes wave light is emitted in the forward and backward direction of the waveguide. This phenomenon is called the Raman effect. The Stokes wave is frequency down shifted with respect to the pump wave, by an amount determined by the optical phonon of the medium [47]. Fused silica and other fused silica doped glasses, like GeO_2 and P_2O_5, exhibit a broad Raman gain spectra, as shown in [47], due to the amorphous nature of the glass. In silica fibre, the peak gain frequency shift is about 13 THz from the pump frequency and the gain bandwidth is 10 THz. It is noteworthy that the Raman shift is independent of the pump wavelength but its intensity scales inversely with the pump wavelength.

In the case of low-loss optical fibre and an intense pump wave, the scattered radiation can propagate with the pump wave over long distances. Under these circumstances, it is possible for the Stokes wave to continue to interact efficiently with the pump wave and, therefore, to grows exponentially with much of the pump energy being transferred to the Stokes wave. Alternatively, the Stokes wave can be seeded to force the energy transfer from the pump wave. This is referred as Stimulated Raman Scattering (SRS).

2.4.2.2 Theory of Raman scattering in optical fibre

Signal amplification by SRS, in the CW and quasi-CW regime, in a single mode fibre for the pump and the Stokes wave, can be expressed by the following equations:

$$\frac{dP_p}{dz} = -\frac{\omega_p}{\omega_s}\frac{g_R}{A_{eff}}P_pP_s - \alpha_p P_p \tag{2.26}$$

$$\frac{dP_s}{dz} = \frac{g_R}{A_{eff}}P_sP_p - \alpha_s P_s \tag{2.27}$$

where P_p and P_s are the power of the pump and Stokes optical waves oscillating at the frequencies ω_p and ω_s, respectively. A_{eff} is the effective area for a two wave interaction as defined in (2.25) and g_R is the Raman gain coefficient of the optical fibre. α_p and α_s represent the pump and signal background loss during fibre propagation.

If the solution for the pump evolution is substituted in (2.27), the signal can be solved and takes the form:

$$P_s(z) = P_s(0)\exp\left(\frac{g_R}{K}\frac{1}{A_{eff}}\int_0^z P_p(u)\,du - \alpha_s z\right) = P_s(0)\exp\left(\frac{g_R}{K}\frac{P_p(0)}{A_{eff}}L_{eff}(z) - \alpha_s z\right) \tag{2.28}$$

where $P_s(0)$ and $P_p(0)$ are the Stokes wave and the pump power at the signal injection point, respectively, $P_p(z)$ is the pump power at the distance z from the injection point, K is a factor which depends on the polarization state of the pump and signal, L_{eff} is the pump effective length, and α_s is the Stokes wave background loss. K takes the value 1 if the pump and signal waves are polarization matched or 2 if both are depolarised. If the pump and signal are orthogonally polarized, K becomes large as the Raman interaction between crossed polarizations is weak.

As the pump wave propagates along the fibre, its power decreases because of attenuation and non-linear interaction. Thus, the effective length is defined by [26]:

$$L_{eff} = \frac{\int_0^z P_p(u)du}{P_p(0)} = \frac{1}{P_p(0)}\int_0^z P_p(0)\,\mathrm{e}^{-\alpha_p u}du = \frac{1-e^{-\alpha_p z}}{\alpha_p} \tag{2.29}$$

with α_p the background loss of the pump in m^{-1}. The maximum effective length is when the non-linear interaction is weak. In that case the pump is only attenuated by the background loss. If the background α_p grows, the effective length tends toward a finite value of $1/\alpha_p$ while in the absence of background loss, L_{eff} approximates z, i.e., the actual length of the fibre.

From (2.28), the small-signal gain for the first Stokes, neglecting the signal background loss, is expressed as [48]:

$$G_{linear}^{SRS} = \exp\left(\frac{g_R}{A_{eff}} P_p(0) L_{eff}\right) \tag{2.30}$$

It is related to the gain in decibel by the expression: $G_{dB}^{SRS} = 4.34 ln\left(G_{linear}^{SRS}\right)$. For example, at 1 μm, the Raman gain coefficient is $g_R \approx 10^{-13}$ m/W. Thus the gain, per unit length and unit area, becomes $G_{dB}^{SRS} \approx 0.43\,\text{dB.}\mu\text{m}^2/(\text{W.m})$. Therefore, high Raman gain can be achieved with high pump power, long effective lengths, small effective area and high SRS gain coefficient.

2.4.2.3 Numerical modeling

It is possible to expand (2.26) and (2.27) in order to obtain a more realistic model of the SRS phenomenon. A large number of wavelengths can be encompassed using multiple wavelength bins. In that case, a more complex propagation equation of the optical power present in the fibre can be considered:

$$\begin{aligned}
\pm\frac{dP_i^{\pm}}{dz} &= -\alpha(\nu_i) P_i^{\pm} && \text{(a)}\\
&+ P_i^{\pm} \sum_j^{\nu_j>\nu_i} \frac{g_{eff}(\nu_j,\nu_i)}{A_{eff}(\nu_j,\nu_i)} \left(P_j^{+} + P_j^{-}\right)\Delta\nu && \text{(b)}\\
&+ 2\sum_j^{\nu_j>\nu_i} \frac{g_{eff}(\nu_j,\nu_i)}{A_{eff}(\nu_j,\nu_i)} \left(P_j^{+} + P_j^{-}\right)\Delta\nu.h\nu_i \left(1 + \frac{1}{\exp\left(\frac{h(\nu_j-\nu_i)}{k_B T}\right)-1}\right) && \text{(c)}\\
&- P_i^{\pm} \sum_j^{\nu_j<\nu_i} \frac{\nu_i}{\nu_j} \frac{g_{eff}(\nu_i,\nu_j)}{A_{eff}(\nu_i,\nu_j)} \left(P_j^{+} + P_j^{-}\right)\Delta\nu && \text{(d)}
\end{aligned} \tag{2.31}$$

where index i refers to the signal considered at the power P_i while j is the index of any other signals. $\alpha(\nu_i)$ is the background loss at the frequency, ν_i. The sign $\pm$ indicates the propagation direction with $+$ for forward and $-$ for backward. $A_{eff}(\nu_j,\nu_i)$ is the effective area between the mode at the frequency ν_i and ν_j respectively. $\Delta\nu$ is the optical bandwidth of the wavelength bin considered, $g_{eff}(\nu_j,\nu_i)$ is the effect Raman gain coefficient for a wavelength

shift $|\nu_i - \nu_j|$, h is the Planck's constant, k_B is the Boltzman's constant and T is the absolute temperature of the fibre in Kelvin.

The term (a) represents the propagation loss of the signal. The terms (b) and (c) represent the stimulated energy transfer from higher frequency signals and the spontaneous generation of signal due to the thermal noise. The term (d) represents the energy transfer of the signal to lower frequency optical signals. The signal acts as a pump for the longer wavelength signals, which can become amplified by SRS into higher order Stokes.

The set of equations (2.31) can be numerically integrated using well-established methods such as Runge-Kutta, to model the CW or quasi-CW behaviour of the various signals propagating along the fibre.

2.4.2.4 Critical power and threshold

The critical power is a useful criterion to estimate the pump power or fibre length at which the SRS becomes significant. This is the case when designing a Raman amplifier or when one wants to avoid SRS, for example, in a high-power rare-earth doped fibre amplifier. The Raman critical power is defined as the input pump power at which the Stokes power, when unseeded, becomes equal to the pump power at the fibre output. The critical pump power can be expressed as follows [48].

In case of forward SRS:

$$P_{critical}^{p} = 16\frac{A_{eff}K}{g_R L_{eff}} \tag{2.32}$$

In case of backward SRS:

$$P_{critical}^{p} = 20\frac{A_{eff}K}{g_R L_{eff}} \tag{2.33}$$

where A_{eff} is the fibre mode effective area, K is a factor which takes into account the pump and signal states of polarization (for polarized light $K=1$ and for un-polarized light $K=2$), g_R is the SRS gain factor, and L_{eff} is the effective interaction length defined in (2.29).

In the case of a Raman fibre laser, it is also useful to determine the pump power or fibre length required to reach the lasing threshold. The threshold corresponds to the point where the SRS gain compensate the cavity loss, and, in a simple Fabry-Perot, is given by [49]:

$$P_{threshold}^{p} = \frac{\alpha_p A_{eff}}{g_R}\left[\frac{\alpha_s L - \frac{1}{2}\ln\left(R_1 R_2\right)}{1-\exp\left(-\alpha_p L\right)}\right] = \frac{A_{eff}}{g_R L_{eff}}\left[\alpha_s L - \frac{1}{2}\ln\left(R_1 R_2\right)\right] \tag{2.34}$$

where L is the fibre cavity length and R_1, R_2 are the mirrors reflectivity that forms the cavity, and the other terms already defined.

2.4.3 Overview of other non-linear effects

In this section, not all the non-linear effects are reviewed (e.g. modulation effects); only the most relevant effects to the content of this thesis are presented.

2.4.3.1 Stimulated Brillouin scattering

When an intense light beam propagates in optical fibre, a non-linearity can arise from the interaction between the propagating light waves (photons) and the acoustic waves (phonons) in the fibre core. A fraction of the light wave travelling through the medium is scattered by the acoustic noise originating from the thermal noise. This phenomenon is called Spontaneous Brillouin Scattering. The scattered light interferes with the forward propagating light to create a power-induced index modulation of the propagation medium through the Kerr effect. The index modulation acts a grating that scatters the incoming light through Bragg reflection. This phenomenon is called electrostriction. Due to electrostriction, periodical compression zones moving at a speed given by the optical frequency difference are induced in the material. If this speed corresponds to the speed of sound in the material at this frequency, an acoustic wave is created. This acoustic wave in turn reinforces the scattering process. The scattered light is downshifted in frequency, because of the Doppler shift associated with the grating moving at the acoustic velocity. In that case, the scattering process is referred to as Stimulated Brillouin Scattering (SBS). The SBS phenomenon takes place in a very narrow bandwidth of about 20 MHz in case of an optical wavelength of 1.55 μm in silica fibre.

The Stokes intensity is found to grow exponentially in the backward direction. The impact of SBS can be estimated at low power level by the concept of critical power. The critical power of SBS, defined in [48], corresponds to the power where the Stokes wave at the fibre input becomes equal to the pump power at the fibre output. The SBS critical power is defined, under the nondepletion assumption and assuming a Lorentzian gain shape, as [50]:

$$P_{critical}^{p} = 21\frac{A_{eff} K}{g_B L_{eff}}\frac{\Delta\nu_p + \Delta\nu_B}{\Delta\nu_B} \tag{2.35}$$

where A_{eff} is the fibre mode effective area, K is a factor which takes into account the polarization of the pump (for polarized light $K=1$ and for un-polarized light $K=2$), g_B is the SBS gain factor, L_{eff} is the effective interaction length defined as for SRS by (2.29), and $\Delta\nu_p$ and $\Delta\nu_B$ are the Lorentztian linewidths of the pump and of the SBS gain, respectively. The value of the factor 21 may change with the fibre length as discussed in [51], but it remains that (2.35) gives an indication of the threshold. When $\Delta\nu_B >> \Delta\nu_p$ equation (2.35) reduces to the well-know critical power definition as [48]:

$$P^{p}_{critical} = 21\frac{A_{eff}K}{g_B L_{eff}} \tag{2.36}$$

The peak value of g_B is nearly independent of the pump wavelength and the typical parameter value for fused silica is $g_B \approx 5.10^{-11}$ m/W. This value is nearly three orders of magnitude larger than the SRS gain coefficient.

2.4.3.2 Four-wave mixing

Four-wave mixing (FWM) (also called four-photon mixing) involve four optical waves interacting through the electronic response of the third-order susceptibility. It generally occurs when two or more light beams with different propagation constants propagate through an optical fibre with a high intensity. When the light beams are phase matched, additional light components are generated by transferring some optical power from the pumps waves into the anti-Stokes and Stokes wave. In fact two pump photons are annihilated with the simultaneous creation of an anti-Stokes and a Stokes photon. The anti-Stokes wave has a higher frequency than the pump frequencies while the Stokes has a lower frequency. The phase matching (conservation of momentum) requirement, in an optical fibre, is given by [52]:

$$\beta_1 + \beta_2 = \beta_a + \beta_s \tag{2.37}$$

where β_1 and β_2 are the propagation constants for pump 1 and 2 while β_a and β_s are the ones for the anti-Stokes and Stokes waves, respectively. Furthermore, the frequencies must also be matched, i.e., $\omega_1 + \omega_2 - \omega_a - \omega_s = 0$ (conversation of energy).

If only the pump lightwave is incident in the fibre, with the frequencies and propagation constant phase-matched, the Stokes and the anti-Stokes waves can be generated from noise and

then amplified by the parametric process. The parametric gain in a single-mode fibre is expressed as:

$$g = \sqrt{\left(2\gamma\sqrt{P_1 P_2}\right)^2 - \left(\frac{\kappa}{2}\right)^2} \tag{2.38}$$

where γ is the (averaged) non-linear parameter, P_1 and P_2 are the incident pump powers and κ is the net phase mismatch. The parametric gain is maximum when the phase matching is satisfied, i.e. $\kappa = 0$.

The non-linear parameter, γ, is defined by:

$$\gamma = \frac{n_2^{elec}\omega_0}{cA_{eff}} \tag{2.39}$$

where n_2^{elec} is the electronic contribution to the non-linear refractive index, ω_0 is the pump frequency and A_{eff} is effective area of the photon distribution interacting in the process.

The net phase mismatch can be expressed as:

$$\kappa = \Delta k + 2\gamma P_0 \tag{2.40}$$

where Δk is the phase mismatched defined by $\Delta k = \beta_1 + \beta_2 - \beta_a - \beta_s$. This represents the contribution of the dispersion due to the waveguiding and to the material. The term $2\gamma P_0$ represents the non-linear contribution to the phase mismatch where P_0 is the total launched pump power (i.e. $P_0 = P_1 + P_2$).

2.5 References

[1] O. Svelto, *Principles of Lasers*, (4th Ed., Springer, (trans. David Hanna), 1998).

[2] A. E. Siegman, "How to (maybe) measure laser beam quality", in Diode Pumped Solid State Lasers: Applications and Issues, M. W. Dowley, Ed. : Optical Society of America, 1998, vol. 17, OSA Trends in Optics and Photonics Series, pp. 184-199.

[3] ISO Standard 11146

[4] H. Po et al., "Double-clad high brightness Nd fiber laser pumped by GaAs phased array", in *Proc. Optical Fiber Communication Conference (OFC)*, Houston, USA, 1989, Post-deadline paper PD07. See also U.S. Patent 4815079.

[5] L. Zenteno, "High power double clad fibre lasers", J. Lightwave Technol. **11**(9), 1435-1447 (1993).

[6] T. A. Birks, "Reducing losses in photonic crystal fibres", in *Proc. Optical Fiber Communication Conference (OFC)*, Anaheim, CA, USA, 2006, paper OFC7.

[7] J. K. Sahu, C. C. Renaud, K. Furusawa, R Selvas, J. A. Alvarez-Chavez, D. J. Richardson, and J. Nilsson, "Jacketed air clad cladding pumped ytterbium doped fibre laser with wide tuning range", Electron. Lett. **38**, 1116-1117 (2001).

[8] D. Kouznetsov, J. V. Moloney, and E. M. Wright, "Efficiency of pump absorption in double-clad fibre amplifiers. I. Fibre with circular symmetry", J. Opt. Soc. Am. B-Opt. Phys. **18**(6), 743 (2001).

[9] D. Kouznetsov and J. V. Moloney, "Efficiency of pump absorption in double-clad fibre amplifiers. II. Broken circular symmetry", J. Opt. Soc. Am. B-Opt. Phys. **19**(6), 1259 (2002).

[10] D. Kouznetsov and J. V. Moloney, "Efficiency of pump absorption in double-clad fibre amplifiers. III. Calculation of modes", J. Opt. Soc. Am. B-Opt. Phys. **19**(6), 1304 (2002).

[11] L. Philippe, V. Doya, R. Philippe, P. Dominique, M. Fabrice, and L. Olivier, "Experimental study of pump power absorption along rare-earth- doped double clad optical fibres", Opt. Commun. **218**(4-6), 249 (2003).

[12] V. Doya, O. Legrand, and F. Mortessagne, "Optimized absorption in a chaotic double-clad fibre amplifier", Opt. Lett. **26**(12), 872 (2001).

[13] P. Leproux, S. Février, "Modeling and optimization of double-clad fibre amplifiers using chaotic propagation of the pump", Opt. Fibre Technol. **7**(4), 324 (2001).

[14] S. Bedö, W. Lüthy and H. P. Weber, "The effective absorption coefficient in double-clad fibres", Opt. Commun. **99**(5-6), 331 (1993).

[15] A. Liu, K. Ueda, "The absorption characteristics of circular, offset, and rectangular double-clad fibers", Opt. Commun. **132**(5-6) 511 (1996).

[16] A. P. Liu and K. Ueda, "The absorption characteristics of rare earth doped circular double-clad fibres", Opt. Rev. **3**(4), 276 (1996).

[17] P. Even, D. Pureur, "High power double clad fiber lasers: a review", Proc. SPIE **4638** (2002).

[18] DiGiovanni et al., "Tapered fiber bundles for coupling light into and out of cladding-pumped fiber devices", US patent 5,864,644.

[19] Fidric et al., "Optical couplers for multimode fiber", US patent 6,434,302.

[20] Goldberg et al., "Method and apparatus for side pumping an optical fiber", US patent 5,854,865 and "Angle selective side-pumping of fiber amplifiers and lasers", US patent 6,529,657.

[21] L. Goldberg, B. Cole, and E. Snitzer, "V-groove side-pumped 1.5 μm fibre amplifier", Electron. Lett. **33**(25), 2127 (1997).

[22] MacCormack et al., "Side coupled pumping of double clad fiber gain media", US patent 6,434,295.

[23] A. B. Grudinin et al., "Multi-fibre arrangements for high power fibre lasers and amplifiers", US patent 6,826,335.

[24] S. U. Alam, "Low cost multi-port reconfigurable erbium doped cladding pumped fibre amplifier", in *Proc. European Conference on Optical Communication (ECOC)*, Munich, Germany, 2000.

[25] G. Samartsev, et al., "Coupling arrangement between a multi-mode light source and an optical fiber trough an intermediate optical fiber length", US patent US 5,999,673.

[26] G. P. Agrawal, *Nonlinear Fiber Optics*, (2nd Ed., Academic Press Inc, San Diego CA, 1995).

[27] D. Marcuse, *Light Transmission Optics* (Van Nostrand-Reinhold, New-York, 1972).

[28] D. Gloge, "Weakly guiding fibers", Appl. Opt. **10**, 2252 (1971).

[29] M. R. Shenoy, K. Thygarajan and A. K. Ghatak, "Numerical Analysis of optical Fibres using Matrix Approach", J. Lightwave Technol. **6**(8), 1285 (1988).

[30] K. Morishita, "Numerical analysis of pulse broadening in graded index optical fibers", IEEE Trans. Microwave Theory Tech. **MTT-29**, 348-352 (1981).

[31] A. C. Boucouvalas and G. Georgiou, "External refractive-index response of tapered coaxial couplers", Opt. Lett. **11**, 257 (1986).

[32] R. Olshansky, "Propagation in glass optical waveguide", Rev. Mod. Phys. **51**(2), 341-369 (1979).

[33] M. E. Fermann, D. J. Harter, "Single-mode Amplifiers and Compressors based on Multi-Mode Fibers", US patent 5,818,630.

[34] J. -T. Horng and D. C. Chang, "Coupling an elliptical Gaussian beam into a multimode step-index fiber", Appl. Opt. **22**, 3887- (1983).

[35] K. -Y. Lee and W. -S. Wang, "Ray-optics analysis of the coupling efficiency from a Gaussian beam to a rectangular multimode embedded strip waveguide", Fiber Integrated Opt. **13**, 321-330 (1994).

[36] D. B. S. Soh, J. Nilsson, S. Baek, C. Codemard, Y. C. Jeong, and V. Philippov, "Modal power decomposition of beam intensity profiles into linearly polarized modes of multimode optical fibers", J. Opt. Soc. Am. A **21**(7), 1241 (2004).

[37] Technical documentation of FiberCad 1.5, Optiwave® corporation.

[38] M. Ohashi, N. Kuwaki, N. Uesugi, "Suitable definition of mode filed diameter in view of splice loss evulation", J. Lightwave Technol. **LT-5**(12), 1687 (1987).

[39] D. Marcuse, *Theory of dielectric waveguide* (Academic Press, San Diego, CA, 1991).

[40] F. Capasso, P. Di Porto, "Coupled-mode theory of Raman amplification in lossless optical fibers", J. Appl. Phys., **47**(4), 1472 (1976).

[41] A. Snyder, "Coupled-Mode Theory for Optical fibers", J. Opt. Soc. Am. A **62**(11), (1972).

[42] P. D. McIntyre, A. Snyder, "Power transfer between optical fibres", J. Opt. Soc. Am. A **63**(12), 1518 (1973).

[43] A. W Snyder and J. D. Love**,** *Optical Waveguide Theory*, (Chapman & Hall, London, 1983).

[44] Y. R. Shen, *Principles of Nonlinear Optics* (Wiley, New York, 1984).

[45] P. V. Mamyshev and S. V. Chernikov, "Ultrashort-pulse propagation in optical fibers", Opt. Lett. **15**(19), 1076 (1990).

[46] R. H. Stolen, C. Lee, and R. K. Jain, "Development of the Stimulated Raman-Spectrum in Single-Mode Silica Fibers", J. Opt. Soc. Am. B **1**(4), 652 (1984).

[47] F. L. Galeneer, J. C. Mikkelsen, R. H. Geils, and W. J. Mosby, "The relative Raman cross section of vitreous SiO_2, GeO_2, B_2O_3, and P_2O_5", Appl. Phys Lett. **32**(1), 34-36 (1978).

[48] R. G. Smith, "Optical power handling capacity of low-loss optical fibers as determined by stimulated Raman and Brillouin scattering", Appl. Opt. **11**(11), 2489–2494 (1972).

[49] J. Auyeung and A. Yariv, "Theory of a Cw Fiber Raman Oscillator", J. Opt. Soc. Am. **68**(10), 1383 (1978).

[50] Y. Aoki, K. Tajima and I. Mito, "Input Power Limits of Single-Mode Optical Fibers due to Stimulated Brillouin Scattering in Optical Communication Systems", J. Lightwave Technol. **6**(5), 710 (1998).

[51] S. Le Floch and P. Cambon, "Theoretical evaluation of the Brillouin threshold and the steady-state Brillouin equations in standard single-mode optical fibers", J. Opt. Soc. Am. A **20**(6), 1132 (2003).

[52] R. H. Stolen and J. E. Bjorkholm, "Parametric Amplification and Frequency Conversion in Optical Fibres", IEEE J. Quantum Electron. **18**(7), 1062 (1982).

PART II: ERBIUM-YTTERBIUM DOPED CLADDING-PUMPED FIBRE LASERS

Chapter 3 Principles of erbium-ytterbium doped fibre laser

This chapter presents the fundamentals of cladding-pumped erbium-ytterbium doped fibre (EYDF) and of pulsed rare-earth doped fibre. Section 3.1 presents the motives for co-doping erbium doped fibre with ytterbium ions to power scale laser output power from erbium ions. Then, section 3.2 presents background information on the fabrication and characterization of EYDF as well with some typical characteristic values. Subsequently, the details of erbium-ytterbium co-doped fibres used in this work are given in section 3.3. Thereafter, the properties of pulsed rare-earth doped fibre are introduced with details specific to EYDF. Finally, section 3.5 summarises this chapter

3.1 Introduction

Originally, co-doping, also called sensitisation, was invented [1] to improve the often undesirably low pump absorption of rare-earth doped fibre. In a double-clad fibre, because of the low brightness of the pump source and the maximum ion concentration permissible in silica fibre, it leads to a low pump absorption. Sensitisation also reduces the threshold, which is particularly important in systems with significant ground-state absorption. In co-doped fibres, the pump radiation is absorbed by the sensitizer ions, which then become excited. These ions then transfer their energy nonradiatively to a (quasi-) resonant energy level of the acceptor ions, which in turn, emit photons on a lower energy transition, at a longer wavelength. The best example is erbium doped fibre sensitized with ytterbium ions. Such fibres have been widely used in high power double clad lasers and amplifiers emitting at wavelengths around 1550 nm. Because of the poor absorption of Er-doped fibres (without Yb co-doping), it is difficult to use cladding-pumping to power-scale them. Core-pumping of EDFs at 980 nm or 1480 nm works quite well, but the output power is limited by the pump power available from single-mode diodes. By contrast, EYDF can be pumped in the broad ytterbium absorption band (~910 – 980 nm) by high power, low-brightness, multi-mode laser diode sources in double-clad fibre configurations. Therefore, co-doping or sensitisation by ytterbium ions in a double-clad fibre structure, is the current approach to power scaling erbium doped fibre laser sources operation in the 1.5 – 1.6 μm wavelength range.

3.2 Background on erbium-ytterbium doped silica fibre

3.2.1 Fabrication

Erbium-ytterbium doped fibres are commonly fabricated using the modified chemical vapour deposition (MCVD) process and the solution doping technique, which was adapted by J. E. Townsend at Southampton University [2]. In this process, the soot deposition and the sintering phase are separated, which improves the homogeneity of the fibre core doping. A soot layer is processed on the inside of a quartz tube, called a preform, using the MCVD technology to form a porous frit. The perform is then soaked in a solution containing a solvent and the dopants such as chlorides, for example, $ErCl_3$, $YbCl_3$, $AlCl_3$. In order to achieve a uniform doping, the preform is dried evenly to avoid any uneven dopant build-up under gravitational force. The preform is dehydrated on the lathe to densify the frit and lock the solute in the glass by vaporising the solvent. The dopant chlorides are left in the glass. The preform temperature is increased so that the chlorides become oxidised and the dopant oxides are consolidated into the silica glass. Then, the glass is sintered. Finally, the preform is collapsed under heat treatment into a solid core rod. The deposited soot layer forms the core while the silica tube forms the inner cladding. The rod can be "sleeved" with a pure silica glass tube to make the cladding thicker, or etched to make the cladding thinner.

Currently, phosphorous based glass is considered to be the best host for Yb-sensitised Er-doped fibre because of the high RE-solubility and the low occurrence of energy back transfer from Er^{3+} to Yb^{3+} [26, 3]. Consequently, the most efficient silica-based Er:Yb co-doped fibre devices have used a phosphorous doped glass matrix [4]. This host is often referred to as phosphosilicate. However, the high volatility of phosphorous during the collapse process limits its incorporation into the fibre core. As a result of the phosphorous volatility, a central dip in the refractive index profile is quite common in EYDF.

Furthermore, the control of the dopant concentration with the solution doping process, which depends on solute concentration, soot density, and dehydration conditions, can be quite challenging in practice. The concentrations of the various dopants are found to vary along the preform [5], and the lasing performance will vary accordingly from section to section.

Finally, erbium-ytterbium co-doped phosphosilicate fibres not only benefit from a high pump absorption, but also from a higher than usual permissible Er-concentration. This is a result of the high solubility of rare earths in phosphosilicate, as well as of the low probability of Er clustering: RE-ions are prone to form clusters, but because the Yb-concentration is much higher than the Er-concentration, the Er-ions are more likely to form clusters with Yb-ions than with

other Er-ions, as the Yb- and Er-ions are essentially chemically equivalent. While clusters with several Er-ions are expected to be detrimental, clusters with an Er-ion and one or several Yb-ions may even enhance the performance.

3.2.2 Spectroscopy

Rare-earths, including erbium (atomic number: 68) and ytterbium (atomic number: 70) all belong to the lanthanides group. The lanthanides are characterised by the progressive filling of the 4*f* electronic shell. Because the electrons are shielded from the outer perturbation, the radiative transitions occur within energy levels between an inner orbital of the electronic shell. These transitions are comparatively host independent. Lanthanides are generally trivalent when oxidised in the glass matrix, e.g. Yb^{3+} and Er^{3+}. The energy level corresponding to the electronic layer is annotated according to the Russell-Saunders scheme or LS coupling. An ion energy level is represented by the L, S and J triplet ($^{2S+1}L_J$), where L is the angular orbital momentum, S the angular spin momentum and J is the total angular momentum. The conventional energy-level diagram of an erbium-ytterbium co-doped system is shown in figure 3.1.

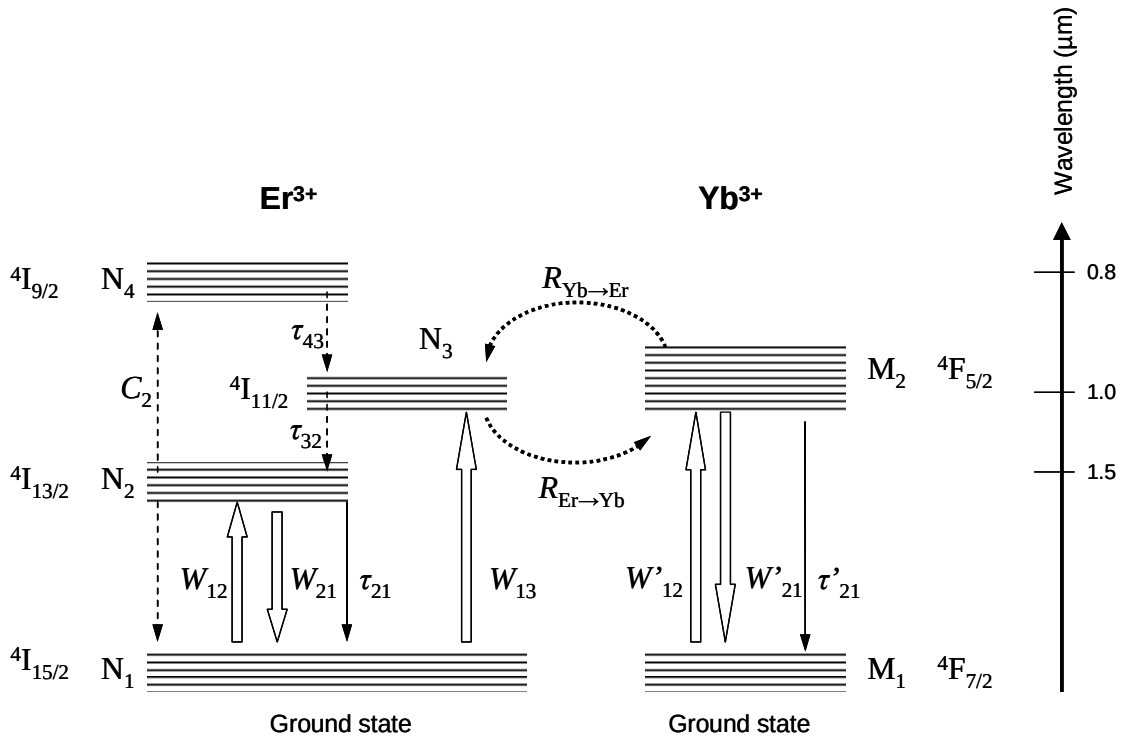

Figure 3.1: Energy level diagram for the Er:Yb co-doped system (from [6])

In figure 3.1, N_1, N_2, N_3 and N_4 are the erbium populations of the $^4I_{15/2,}$ $^4I_{13/2}$, $^4I_{11/2}$ and $^4I_{9/2}$ Stark's split energy levels, respectively, while M_1 and M_2 are the population for the $^2F_{7/2}$ and $^2F_{5/2}$ energy level of Yb. The large arrows correspond to absorption and stimulated emission transitions with rate W_{ij} and W_{ji}, respectively between the ith and jth energy level. The solid line arrows correspond to the spontaneous emission rate (fluorescence decay) from the excited level to the ground state level, while the dashed line arrows correspond to non-radiative decay from upper levels into intermediate energy levels. The lifetime of the ith energy level decaying to the jth energy level is denoted τ_{ij} for the erbium ion and $\tau_{21}^{'}$ for the ytterbium ion. The homogeneous upconversion process for two particles, from $^4I_{13/2}$ to $^4I_{9/2}$ that can occur for two excited Er-ions is also shown, represented with a thicker dashed line. The cooperative upconversion is an energy transfer process between two excited Er ions, in close proximity in the $^4I_{13/2}$ level, that interact to promote one of the Er ions into the $^4I_{9/2}$ state and de-excites nonradiatively the other in the $^4I_{15/2}$ ground state. This process decreases the $^4I_{13/2}$ population proportionally to the term $-C_2N_2^{\,2}$ and reduces the gain available for amplification and the available stored energy [7]. The dependence of the upconversion parameter C_2 on the concentration in EYDF is discussed further in [8 - 9].

Finally, the energy transfer between iso-energetic level $^4I_{11/2}$ and $^4F_{5/2}$ is represented by dotted arrows and the transfer rate are $R_{Yb\to Er}$ and $R_{Er\to Yb}$. It is normally assumed that both coefficients are equal. Generally, they are different as they are given by overlap integrals of different emission and absorption spectra. However, because the dominant Yb absorption and emission peaks are quite sharp and nearly overlap with the Er-peak, the rates will be similar if not equal. A previous study [10] found that $R_{Yb\to Er}$ is strongly dependent on the ytterbium concentration and that the coefficient can be roughly approximated by a linear relation in the 10^{26} – 10^{27} ions/m^3 range. The Yb→Er energy transfer increases the population of the $^4I_{13/2}$ energy level by $R_{Yb\to Er}N_1M_2$, while the Er→Yb transfer decreases the $^4I_{11/2}$ population and indirectly the $^4I_{13/2}$ population by $R_{Er\to Yb}N_3M_1$. This back-transfer process is usually neglected because it requires a significant population of the short-lived $^4I_{11/2}$-level to become significant.

Using the population rate equations, EYDF lasers sources can be modelled and several publications [6, 8, 11 - 13] cover this subject. The model can be made as complex as required to encompass for example, the effect of cross-relaxation [14 - 16], or to include the upconversion processes of the erbium ions [14].

3.2.3 Characterisations

3.2.3.1 Absorption and concentration

The measurement of the absorption of light propagating in the core and inner cladding by the dopant ions in a double-clad fibre is very important as it can help to determine the dopant concentration and the length of fibre required for a given pump absorption. The dopant absorption in a double-clad fibre depends not only on the ion concentration, but also on the fibre geometry. Furthermore, different cladding-modes experience different absorption, so the measured absorption depends on the excited modes. Furthermore, the absorption does not follow Beer's law (i.e., it is non-exponential). Thus the absorption depends on the measurement set-up, and can be difficult to perform in an accurate and relevant manner. Typically, the absorption spectrum is measured with a low-power broadband light source that is transmitted through a given length of fibre and a detection system, e.g., an optical spectrum analyser (OSA) [17]. A cut back method is generally used to remove the uncertainty in the light launch condition. The inner-cladding can be over-filled to create a reproducible well-defined measurement condition to further reduce the uncertainty. Still, there are generally fewer uncertainties with core absorption measurements. These are, therefore, often better for exact determination of dopant concentration. However, in the case of EYDF, the absorption by the ytterbium ions is so large that the core absorption is difficult to measure. Instead, the inner-cladding absorption is measured by injection of light into the fibre inner-cladding, taking care that all the transmitted light is collected by an OSA. From the cladding and doped region dimensions it is possible to estimate the core absorption [18]. Typical core absorptions of EYDFs are in the range 1000 – 2000 dB/m at 975 nm. Therefore, even with large cladding the absorption is significant, in the range of 1-5 dB/m with these fibres. The absorption by the erbium ions is best measured in the 1550 nm wavelength range because the absorption at 980 nm from the Yb^{3+} ions dominates the Er-absorption at this wavelength. In addition, because of the large concentration difference between the Yb^{3+} and the Er^{3+} ions, the absorption from the Erbium is preferably measured through a direct core absorption measurement. From the absorption data, it is possible to either calculate the dopant concentration knowing the dopant cross-section [17], or simply by using a look-up table which accounts for dopant cross-sections, molecular weights, and densities as necessary [2].

3.2.3.2 Cross-section

In order to model doped fibre laser sources reasonably well it is important to accurately determine the fibre absorption and emission (fluorescence) cross-section. Several methods, not detailed here, are used to experimentally obtain the cross-section [19 - 22].

In the case of Er:Yb doped fibre, reported cross-sections vary a lot, depending on the fibre composition [23] (and undoubtedly also as a result of measurement inaccuracies). For example, the absorption cross-section for the 977 nm peak from the Yb^{3+} ions, has been measured in the range 0.9 to 2.8 10^{-24} m^2. The cross-section of one of the EYDFs, F195-LF59, used in this thesis, is shown in figure 3.2.

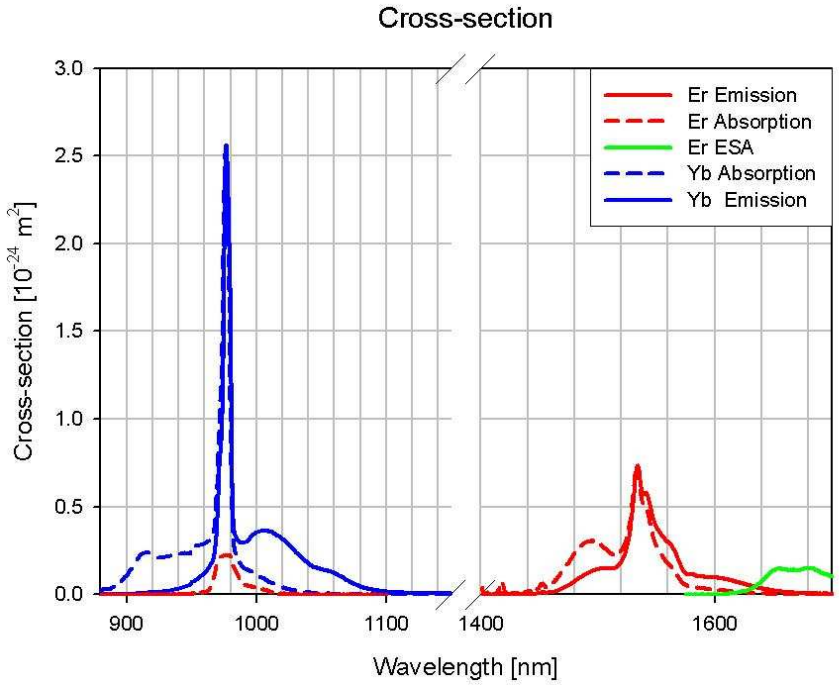

Figure 3.2: Er and Yb cross-section of F195-LF59
(measured by M. Laroche)

3.2.3.3 Lifetime

The lifetime of the excited states of ions is given by the decay of spontaneous emission, which can be measured with a pulsed pump source and fast detector [17, 24]. Continuous-wave excitation is possible as well, and this often leads to some differences in the excitation conditions. In any case, when turned off, the pump source must decay more rapidly than the spontaneous emission of interest. While the lifetime of metastable states of rare earths is long enough for this to be simple, other states as well as rapid initial effects can exhibit much shorter time constants and are therefore more difficult to measure. Furthermore, the pump should be switched off during a period several times longer than the lifetime of any involved energy levels, so that all excited ions return to the ground state. In addition, the energy of the pump pulse must be sufficient to excite a sufficient fraction of ions in order to have a clear measurement trace. The accuracy of the measurement depends on the speed and dynamic range

of the detection system. However, amplified spontaneous emission and reabsorption must be avoided, by making sure that the fibre is sufficiently short and / or that the fraction of excited ions is small. Typically, the pump power level is varied to verify that the fluorescence decay is free from fast decay caused by ASE, for example. A fast decay can also be caused by upconversion processes or quenched ions [25]. Finally, the fluorescence light must be filtered to remove any pump or any emissions from other transitions. In the case of some EYDFs used in this work, the erbium lifetime has been measured using the excitation of the $^4I_{9/2}$ energy level by a 808 nm pulsed laser diode.

3.2.3.4 Signal background loss

The signal background loss of Er:Yb co-doped fibre is generally significantly higher than that of Yb- or Er- doped fibre because of the high concentration required for an efficient energy transfer. Figure 3.3 shows the background loss of commercial EYDF from different fibre manufacturers as a function of the core erbium absorption (i.e. concentration), and also, for comparison, the background loss of erbium-doped ytterbium-free fibres.

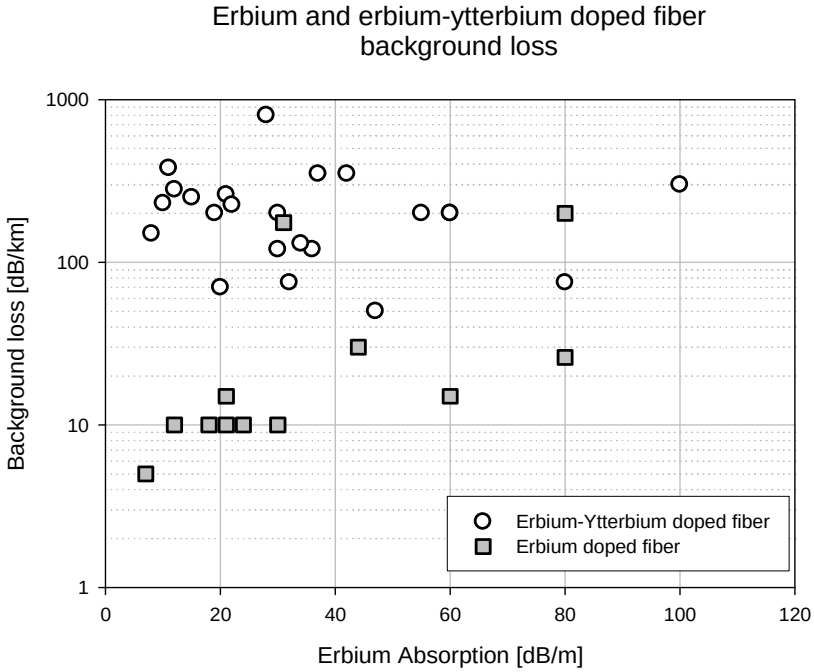

Figure 3.3: EDF and EYDF background loss at 1.3 μm
(Data from various commercial doped fibre. Manufacturers: INO and Coreactive)

The background loss of EYDF is typically in the 100 – 200 dB/km range and seems to be relatively invariant with respect to the erbium concentration. By contrast, in erbium-doped Yb-

free fibre, the background loss increases with the erbium concentration, as one would expect. This difference is explained by the large number of Yb ions in the glass as required for efficient fibre. Typically, the Yb ion concentration is 10 to 20 times larger than that of the Er ions. Therefore, the Yb ions contribute more significantly to the background loss than the Er ions. Furthermore, EYDFs are also heavily doped with phosphorous, and this can well contribute to the background loss. Obviously, the relatively high background loss restricts the maximum useable length of EYDF but this is compensated for a much higher pump absorption which enables the use of relatively short cladding-pumped fibres.

3.3 Fibre characteristics

As discussed previously, EYDF fabricated with the MCVD technique tends to have a central dip in the fibre refractive index profile before of the phosphorous evaporation during the fabrication. Some of the Er:Yb co-doped fibre preforms used in this thesis suffer from such a dip. The fibre preform refractive index profiles are shown in figure 3.4. Note, however, that the refractive index can vary significantly along the preform (and fibre).

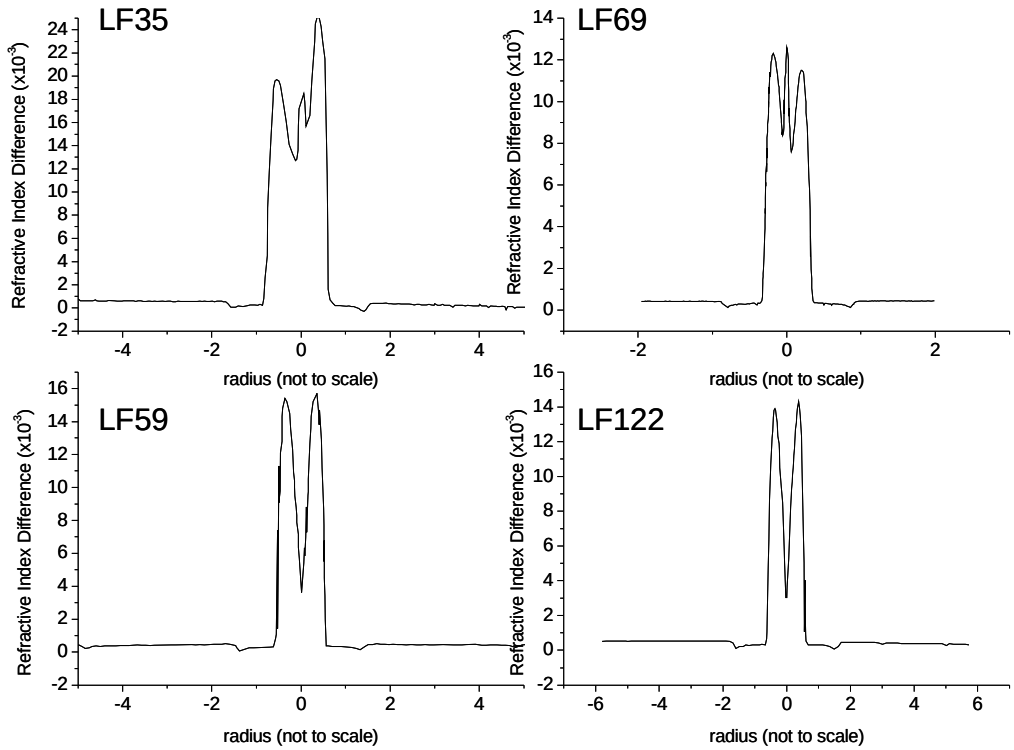

Figure 3.4: Refractive index of EYDF preforms of fibres used in this thesis.

Such fibres have predominantly ring-shaped modes, including even the fundamental mode. The fundamental mode will not be diffraction-limited when its shape differs strongly from that of a gaussian beam. To circumvent this problem it is possible to dope the fibre with aluminium, which is less prone to evaporation than the phosphorous during the collapse phase. This reduces the central dip so that a more Gaussian-like fundamental mode can be obtained. Fibre F225-LF69 is such an example. The central dip would be less of a problem if these fibres could be manufactured with a low numerical aperture. However, the high phosphorous- and ytterbium-concentrations increase the refractive index, already EYDFs with moderately large cores are multi-mode with a typical numerical aperture of about 0.2. Consequently, it is important to eliminate the central dip, and even then, special measures have to be taken to enable large-core fibres to operate in the fundamental mode.

In addition to the refractive index profile, a number of other criteria must be considered in order to achieve high performance from the EYDF. Firstly, the ytterbium concentration needs to be high enough to efficiently absorb the pump power in a double-clad fibre. Therefore, the Yb concentration is typically between 10000 and 30000 ppm. Secondly, the erbium-concentration needs to be high enough to be able to create a sufficient gain per unit length somewhere in the 1.53 - 1.62 μm wavelength region. The Er concentration is typically from 1000 to 3500 ppm. Finally, the overall composition must be well balanced such that the pump energy can be efficiently transferred from Yb^{3+} to Er^{3+} while avoiding the creation of high gain at 1 μm and excessive upconversion. Also, the signal background loss must be kept low. Our fibres were quite typical with background loss about 200 dB/km at 1300 nm.

A widely accepted rule of thumb is that the best erbium:ytterbium concentration ratio is 1:20. This is based on the work of J. Townsend which shows that this ratio gives the lowest lasing threshold in Er:Yb Al_2O_3 co-doped fibre [2]. However, the most efficient EYDF characterised by the HPFL group, e.g. [4], had a erbium:ytterbium ratio of between 1:8 and 1:15. With typical erbium concentration of 2000 – 3000 ppm, this corresponds to a core absorption of roughly 2000 dB/m at 975 nm for Yb ions and a core absorption at 1535 nm in the 50 – 100 dB/m range by the erbium ions. The concentration and absorption, as well as other characteristics of the fibres used in this thesis, are given in Table 3.1.

Fibre designation	Core diameter (μm)	Cladding diameter (μm)	Absorption at 976 nm (dB/m) clad.	Absorption at 1535 nm (dB/m) core	[Er] (ppm)	[Yb] (ppm)	Core area (μm^2)	E_{sat} at 1535 nm (μJ)	E_{sat} at 1565 nm (μJ)	Threshold [2]		Where used (Chapter)
										SRS ($W.m^{-1}$)	SBS ($W.m^{-1}$)	
F196-LF59	35	400/375 [1]	4.5	86 – 101	3000-3500	18000	710	64.2	227	163600	164	4, 7
F225-LF69	25	400/375 [1]	2.5	45 - 50	2300-2500	18000	628	56.8	201	144700	144	4
F260-LF35	50	400/375 [1]	18.3 - 20.3	29 – 34	1000-1200	20000-25000	1500	135.7	480	345600	345	5, 8
F402-LF122	27	180 [1]	25.7	57	2500	20000-25000	572	52	183	131800	131	5
F546-LF218	90	510 [1]	10	48	2200	7000 - 12000	6360	575	2035	1465500	1465	5

Table 3.1: Characteristics of Erbium-Ytterbium doped fibres used in this work.

Notes:

[1] – D-shaped cladding

[2] – Threshold estimatation based on a 50 dB gain

3.4 Pulse amplification in erbium-ytterbium doped fibre

This section is focused on high-energy pulse amplification, meaning that the energy extracted from the amplifier by a single pulse is sufficiently high to alter the gain in the fibre.

3.4.1 Saturation energy

An important parameter for a doped fibre is the intrinsic saturation energy which corresponds to the energy that halves the absorption or gain, per unit length locally in a fibre. The intrinsic saturation energy of a doped fibre is given by (3.1).

$$E_{sat}^{s} = \frac{h\nu_s}{\left(\sigma_e^s + \sigma_a^s\right)} \frac{A_{core}}{\Gamma_s} \tag{3.1}$$

where $h\nu_s$ is the energy of a signal photon and σ_e^s and σ_a^s are the emission and absorption cross-section at the signal wavelength, respectively, while A_{core} is the doped core area and Γ_s is the signal overlap with the doped area. Generally, Γ_s is equal to or less than unity and in this work it will be assumed to be unity unless stated otherwise. The (intrinsic) saturation energy is the same irrespective of the state of the fibre, i.e., if it is pumped or un-pumped and there may or may not be signals or ASE present. Furthermore, it can be assessed at any wavelength, including the pump wavelength. The pump saturation energy of a double-clad fibre is quite large, because of the low value of the overlap between the pump and doped area.

Note that a saturation energy can be defined similarly also for an extended fibre, but this will have a different dependence of the fibre parameters and will depend on the gain or absorption of the fibre.

3.4.2 Frantz and Nodvik's model

The well-known model of Frantz and Nodvik [27], initially developed for bulk solid state amplifiers, can be used to predict the output energy also for fibre amplifiers according to (3.2).

$$E_{out} = E_{sat} \ln\left(G_0\left[\exp\left(E_{in}/E_{sat}\right)-1\right]+1\right) \tag{3.2}$$

where E_{in}, E_{out} and E_{sat} are the input, the output and the saturation energies, respectively, and G_0 is the linear gain in the fibre immediately before the pulse enters the input of the fibre amplifier. Once the input pulse is launched into an amplifier, it extracts energy, whereby the

energy stored in the form of an inverted gain medium, is reduced and the gain compresses. Then, once the pulse exits the fibre, the pump re-excites the ions until the initial gain is reached again (in case of stable pulsed operation). The energy storage and gain depend on the geometric and fibre parameters, and also on factors such as the efficiency and background loss of the fibre. Equation (3.2) neglects any excess loss mechanisms such as background loss and excited state absorption. Note that equation (3.2) is valid only if the inequality, $E_{sat} >> E_{in}\exp(G_0)$, is not satisfied, which is the case generally.

If the incident number of photon is sufficiently large, i.e. $E_{in} > E_{sat}$, equation (3.2) can be approximated by:

$$E_{out} = E_{in} + E_{sat}\ln(G_0) \tag{3.3}$$

3.4.3 Extractable energy

Assuming the doped fibre is in a steady state when a pulse enters and perturbs the fibre inversion, the energy stored before the pulse is given by:

$$E_{stored} = h\nu_s A_{core}\int_0^L n_2(z)dz \tag{3.4}$$

where the integral term represents the sum of all the ions in the excited state and can be rewritten as: $\int_0^L n_2(z)dz = LN_0^{Er}\overline{n_2}$. In that case $\overline{n_2}$ is the averaged ratio of excited ions and N_0^{Er} is the total number of erbium ions present in the fibre of length L. It is here assumed that all excited ions are in the upper laser level (level 2).

Energy can be extracted from the stored energy in the fibre only as long as the dopants provide a net positive gain [28], i.e. down to the point where the amplifier becomes transparent ($G_E^{lin} = 1$). From (3.2), the linear energy gain, G_E^{lin}, can written as:

$$G_E^{lin} = \frac{E_{out}}{E_{in}} = \frac{E_{sat}}{E_{in}}\ln\left(G_0\left[\exp\left(E_{in}/E_{sat}\right)-1\right]+1\right) \tag{3.5}$$

Thus, the energy extractable is given by (3.6).

$$E_{Extractable} = E_{out} - E_{in} = E_{in}\left(G_E^{lin}-1\right) \tag{3.6}$$

Using equation (3.3) into (3.6) yields:

$$E_{Extractable} = E_{sat} \ln\left(G_0\right) \tag{3.7}$$

Using the average inversion model [17], the linear small-signal gain is given by (3.8).

$$G_0^{lin} = \exp\left(\Gamma_s N_o^{Er} L\left(\left(\sigma_e^{Er} + \sigma_a^{Er}\right)\overline{n_2} - \left(\sigma_a^{Er}\right)\right)\right) \tag{3.8}$$

In an erbium-ytterbium doped fibre the small-signal gain per unit length per ppm, according to the average inversion, using the cross-sections given in figure 3.2, is shown in figure 3.5.

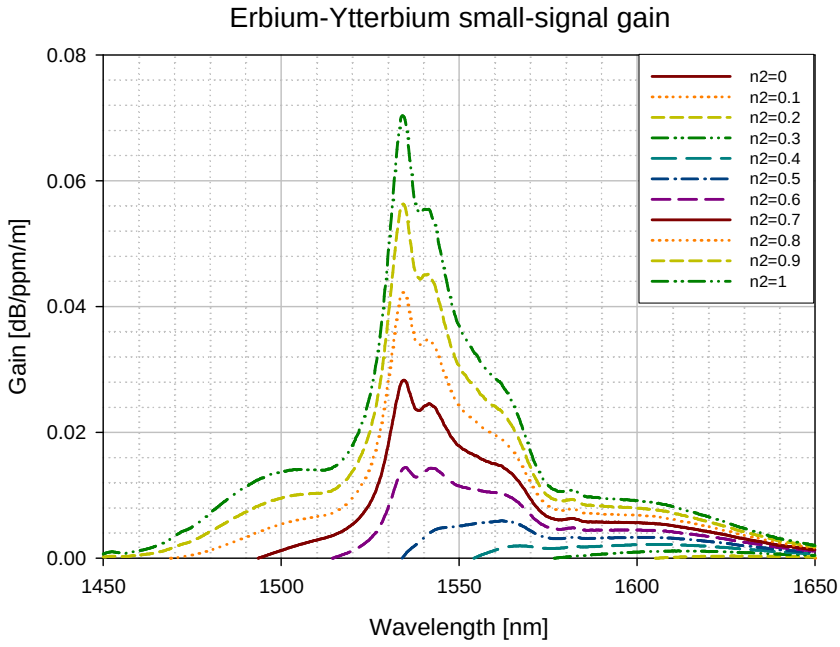

Figure 3.5: Net small-signal gain as function of the average fibre inversion, n_2

Thus, using (3.7) and (3.8) [29], the extractable energy becomes:

$$E_{Extractable} = \frac{h\nu_s}{\left(\sigma_e^s + \sigma_a^s\right)} A_{core} L N_0^{Er} \left(\left(\sigma_e^{Er} + \sigma_a^{Er}\right)\overline{n_2} - \left(\sigma_a^{Er}\right)\right) \tag{3.9}$$

where ν_s is the signal wavelength, σ_e^{Er} and σ_a^{Er} are the erbium emission and absorption cross-sections respectively, A_{core} is the doped area, L is the amplifier length, N_0^{Er} is the Er-concentration (ions per unit volume), and $\overline{n_2}$ is the fraction of excited ions.

The energy extraction possible from an erbium-ytterbium doped fibre according to Eq. (3.9) is given in figure 3.6. This has a strong wavelength dependence because the bleaching

level is wavelength-dependent. At wavelengths beyond 1610 nm, excited-state absorption (ESA) reduces the extractable energy.

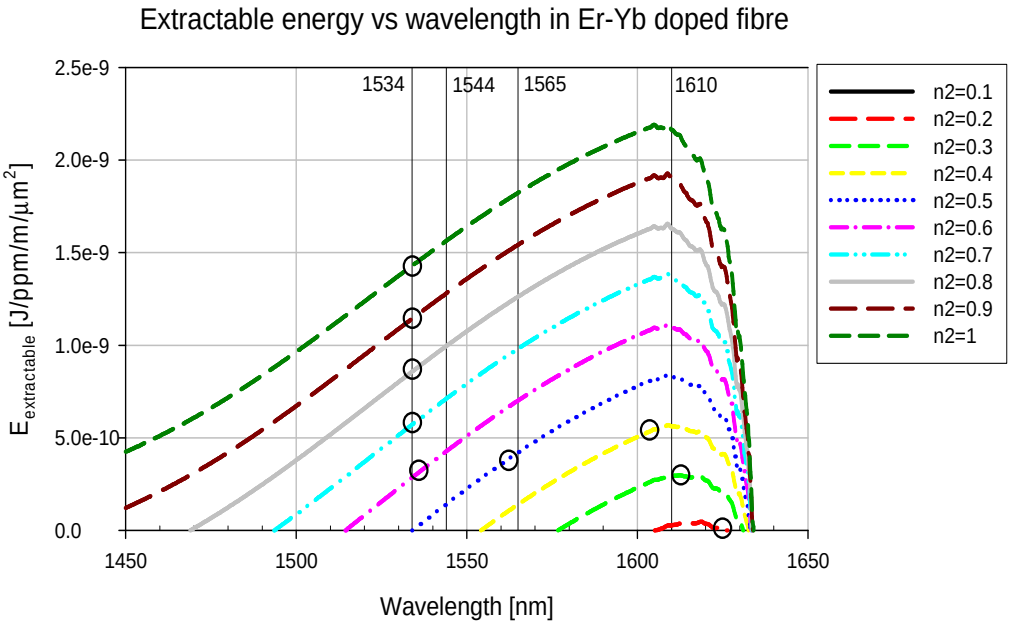

Figure 3.6: Extractable energy and optimum gain (indicated by the symbol, ○) according to the average population inversion and the wavelength.

In figure 3.6, the best extractable energy is always at 1600 – 1620 nm. From (3.7), a high small-signal gain helps in actually extracting the energy, i.e., in "saturating" the energy extraction. The small-signal gain of EYDFs normally peaks at 1544 or 1565 nm, although it can also peak at around 1535 nm for short fibres and at longer wavelengths for long fibres. The optimum gain, marked in figure 3.6, corresponds to the highest small-signal gain in the wavelength range for a given inversion.

Note that the extractable energy can be limited by factors such as ASE and spurious lasing. In the high gain regime, the stored energy is limited by self-saturation from ASE (from the erbium ions). In self-saturation, the number of ions, in the excited state, is clamped and any increase of the pump power produces more ASE, and only increases the stored energy (i.e. number of ions in the excited state) by a small fraction. In optical fibre, ASE is dependent on the fibre core NA, diameter, core refractive index and wavelength, which determine the fraction of spontaneous light captured by the core modes [17]. Importantly, in EYDF, ASE can occur from the Er and from the Yb ions. The ytterbium ions, which have a much higher dopant concentration then erbium ions, are also susceptible to ASE and spurious lasing [30].

3.5 Summary

In this chapter, a brief overview of the fabrication and features of cladding-pumped erbium-ytterbium doped fibre is presented. Subsequently, the characteristics of the EYDFs fabricated at the ORC and used in this thesis are presented. These EYDFs have generally a large core and their typical erbium concentration is around 2000 ppm while the ytterbium concentration is about 20 000 ppm.

Then the last section of this chapter is focused on the background theory of pulse amplification. The Frantz and Nodvik's model is applied to erbium-ytterbium doped fibre to determine the maximum extractable energy from EYDF depending on the wavelength operation.

3.6 References

[1] R. F. Woodcock, "Laser Material Comprised of Erbium and Ytterbium Doped Glass Core and Neodymium Doped Glass Sensitizer Element", US patent 3,590,004.

[2] J. E. Townsend, Ph.D. Thesis, *The development of optical fibres doped with rare-earth ions*, (University of Southampton, 1990).

[3] G. G. Vienne, J. E. Caplen, L. Dong, J. D. Minelly, J. Nilsson, and D. N. Payne, "Fabrication and characterization of Yb^{3+}:Er^{3+} phosphosilicate fibers for lasers", J. Lightwave Technol. **16**(11), 1990-2001 (1998).

[4] J. Nilsson, S. -U. Alam, J. A. Alvarez-Chavez, P. W. Turner, W. A. Clarkson, A. B. Grudinin, "High-power and tunable operation of erbium-ytterbium Co-doped cladding-pumped fiber lasers", IEEE J. Quantum Electron. **39**(8), 987-994 (2003).

[5] ORC Internal document by V. Philippov.

[6] E. Yahel and A. Hardy, "Efficiency optimization of high-power, Er^{3+}–Yb^{3+}-codoped fiber amplifiers for wavelength-division-multiplexing applications", J. Opt. Soc. Am. B **20**(6), 1189 (2003).

[7] B. C. Hwang, S. B. Jiang, T. Luo, J. Watson, G. Sorbello and N. Peyghambarian, "Cooperative upconversion and energy transfer of new high Er^{3+}- and Yb^{3+}-Er^{3+}-doped phosphate glasses", J. Opt. Soc. Am. B **17**(5), 833 (2000).

[8] M. Federighi and F. Di Pasquale, "The effect of pair-induced Energy transfer on the performance of silica waveguide amplifiers with high Er-Yb concentrations", IEEE Photon. Technol. Lett. **7**(3), 303 (1995).

[9] M. Karasek, "Optimum design of Er^{3+}-Yb^{3+} codoped fibres for large-signal high-pump power applications", IEEE J. Quantum Electron. **33**(10), 1699 (1997).

[10] C. Lester, A. Bjarklev, T. Rasmussen, and P. G. Dinesen, "Modeling of Yb^{3+}-sensitized Er^{3+}-doped silica waveguide amplifiers", J. Lightwave Technol. **13**(5), 740–743 (1995).

[11] P. R. Morkel, "Modelling erbium/ytterbium-doped fibre amplifiers", in Optical Amplifiers and Their Applications Technical Digest, 1992 (Optical Society of America, Washington, D. C., 1992), vol. 17, pp. 206-209.

[12] E. Desurvire, D. Bayart, B. Desthieux, S. Bigo, *Erbium-doped fiber amplifiers: Device and System Developments*, (John Wiley & Sons, New York, 2002).

[13] J. Nilsson, P. Scheer, and B. Jaskorzynska, "Modeling and optimization of short Yb^{3+}-sensitized Er^{3+}-doped fiber amplifiers", IEEE Photon. Technol. Lett. **6**(3), 383-385 (1994).

[14] F. Song, G. Y. Zhang, M. R. Shang, H. Tan, J. Yang, and F. Z. Meng, "Three-photon phenomena in the upconversion luminescence of erbium-ytterbium-codoped phosphate glass", Appl. Phys. Lett. **79**(12), 1748 (2001).

[15] P. Blixt, J. Nilsson, T. Carlnäs, and B. Jaskorzynska, "Concentration dependent up-conversion in Er^{3+}-doped fiber amplifiers: experiments and modeling", IEEE Photon. Technol. Lett. **3**(11), 996-998 (1991).

[16] E. Delevaque, T. Georges, M. Monerie, P. Lamouler, and J. -F. Bayon, "Modeling of pair-induced quenching in erbium-doped silicate fibers", IEEE Photon. Technol. Lett., **5**(1), 73-75 (1993).

[17] E. Desurvire, *Erbium-doped fiber amplifiers: principles and applications*, (John Wiley & Sons, New York, 1994).

[18] L. Zenteno, "High power double clad fibre lasers", J. Lightwave Technol. **11**(9), 1435-1447 (1993).

[19] W. L. Barnes, R. I. Laming, E. J. Tarbox, and P. R. Morkel, "Absorption and Emission Cross-Section of Er^{3+} Doped Silica Fibers", IEEE J. Quantum Electron. **27**(4), 1004 (1991).

[20] W. J. Miniscalco and R. S. Quimby, "General procedure for the analysis of Er^{3+} cross sections", Opt. Lett. **16**(4), 258–260 (1991).

[21] M. J. F. Digonnet, E. Murphy-Chutorian, and D. G. Falquier, "Fundamental limitations of the McCumber Relation Applied to Er-doped Silica and other Amorphous-Host lasers", IEEE J. Quantum Electron. **38**(12), 1629–1637 (2002).

[22] H. Zech, "Measurement Technique for the Quotient of Cross Sections $\sigma_e(\lambda_s)$ $\sigma_a(\lambda_s)$ of Erbium-Doped Fibers", IEEE Photon. Technol. Lett. **7**(9), 986–988 (1995).

[23] G. C. Valley, "Modeling Cladding-Pumped Er/Yb Fiber Amplifiers", Opt. Fiber Technol. **7**(1)**,** 21-44 (2001).

[24] ORC internal document by J Nilsson, Spectroscopic_measurements_7 (2004).

[25] R. Wu, J. D. Myers, M. J. Myers, C. Rapp, "Fluorescence lifetime and 980nm pump energy transfer dynamics in erbium and ytterbium co-doped phosphate laser glasses", Proc. SPIE **4968**, 11 (2003).

[26] J. E. Tonwnsend, W. L. Barnes, K. P. Jedrzejewski, S. G. Grubb, "Yb^{3+} sensitised Er^{3+}-doped optical fibre in silica host with very high transfer efficiency", Electron. Lett. **27**(21), 1958-1959 (1991).

[27] L. M. Frantz and J. S. Nodvik, "Theory of pulse propagation in a laser amplifier", J. Appl. Phys. **34**, 2346–2349 (1963).

[28] A. E. Siegmann, *Lasers*, (7^{th} edition, University Science Books, Sausalito, 1986).

[29] C. C. Renaud, H. L. Offerhaus, J. A. Alvarez-Chavez, J. Nilsson, W. A. Clarkson, P. W. Turner, D. J. Richardson, and A. B. Grudinin, "Characteristics of Q-switched cladding-pumped ytterbium-doped fiber lasers with different high-energy fiber designs", IEEE J. Quantum Electron. **37**(2), 199 (2001).

[30] J. K. Sahu, Y. Jeong, D. J. Richardson, J. Nilsson, "A 103 W erbium–ytterbium co-doped large-core fiber laser", Opt. Commun. **227**(1-3), 159 (2003).

Chapter 4 Continuous-wave erbium-ytterbium doped fibre lasers

This chapter treats of the power scaling of double-clad erbium-ytterbium co-doped fibre in the continuous-wave regime. Firstly, section 4.1 introduces and reviews CW erbium-ytterbium doped fibre laser. Then, section 4.2 describes the requirements for single-mode operation of large core fibres with an emphasis on fibre taper as the means to select low order mode. Section 4.3 presents C and L-band continuous-wave tuneable fibre lasers based on large-core fibre and tapered fibre section. Then the lasers characteristics are shown and discussed in section 4.4. Finally, section 4.5 summarises the results and findings of this chapter.

4.1 Introduction

As discussed in Chapter 1, continuous-wave, widely tuneable and narrow-linewidth laser systems are of great interest in the “eye-safe” wavelength range. Cladding pumped EYDF lasers should be able to reach much higher power than reported in the literature [1 - 4] while maintaining good output beam quality and good spectral properties, i.e. a narrow spectral line. However, the power-scaling of narrow-linewidth sources is difficult because of the modest efficiency of EYDF (typically around 30 - 40%) and because of the limitations associated with non-linear effects. In particular, a relatively long fibre with a small core diameter (typically <10 μm) leads to a low threshold power for stimulated Raman scattering (SRS), which degrades the laser performance and can limit the maximum output power achievable [5]. Furthermore, when working with single-frequency lasers (typically with a linewidth narrower than 50 MHz), stimulated Brillouin scattering is the dominant non-linear effect. Therefore, for power-scaling, a careful design of the laser system is required in order to suppress the effect of SRS or SBS, for example, by using a large-core fibre and a short device length. However, special precautions must be taken to avoid the degradation of the beam quality with such large core fibres.

4.2 Single mode excitation

4.2.1 Single mode operation and mode selection

In some case, it is convenient to use large-core fibre either to increase the energy stored for the pulsed operation of rare-earth doped fibre or simply to avoid non-linear effect through the reduction of the core light intensity. However, high, even diffraction-limited, beam quality is desired in most high power, high brightness laser systems. Therefore, single mode fibres with large mode area have been developed [6]. Typically, the size of the mode field is increased by reducing the effective numerical aperture of the core either by special fibre refractive index profile designs [7] or by simply reducing the NA of a step index fibre [8]. In 1998, Broderick and co-workers [6] demonstrated that a large mode area (LMA) fibre was able to produce a robust single-mode output while the mode effective area was increased several times over that of a standard single-mode fibre. However, there is a practical limit to how complex the refractive index profile can be designed and to how low the fibre NA can be (typically NA ~ 0.06 - 0.08) before the core stops guiding the signal light without significant losses into the cladding.

Furthermore, e.g., for erbium-ytterbium doped fibre (EYDF), it is not easy to reduce the core NA without a special refractive index profile, such as raised inner-cladding, because efficiency requirements imposes constraints on the dopant. Thus, single mode operation of multi-mode fibre with relatively large cores is required for some applications. This can be achieved by using a distributed modal loss [9] or by using a discrete discriminating loss element such as a taper which removes any higher order modes [10] or by selective modal excitation [11]. In this section, different methods that are generally applied to EYDF are reviewed.

4.2.1.1 Distributed modal losses

The simplest way to select the fundamental mode in a multi-mode fibre is to coil the fibre such as to create a distributed and selective modal bend loss. In 2000, Koplow demonstrated a single mode output amplifier from a multi-mode coiled double clad fibre [9]. The core diameter was 25 μm and the V-number[3] was 7.4 thus the fibre was supporting a large number of modes. By coiling the fibre, significant loss was induced to all modes except for the

[3] The V number is a parameter which determines the number of modes supported by the fibre. It is defined as: $V=2\pi/\lambda.a.NA$, where λ is the vacuum wavelength, a is the radius of the fibre core, and NA is the numerical aperture. For V values below 2.405, a fibre is single-mode. Above, this value the fibre is multi-mode.

fundamental mode, LP_{01}. Therefore, the output of the multi-mode amplifier was single-moded. This method can be applied to both fibre lasers and fibre amplifiers. More recently, in 2001, the fundamental-mode operation of a fibre with 2000 μm^2 core area was achieved with the coiling technique [12].

However, for this method to be efficient, which is an over-riding requirement at high powers, the loss for the fundamental mode must be low. This requires that the effective refractive index of the modes must be well separated. When the modes are tightly spaced tighter coiling is required to discriminate the fundamental mode from the other modes. In order to illustrate this, the bend loss for a step index fibre with a 0.2 NA, operating at 1060 nm, coiled with 30 mm radius, is shown in figure 4.1 as a function of the V-number. The estimate of the losses induced by the bending of a fibre can be calculated using the formulae given in [13] for step index fibre and in [14] in case of an arbitrary fibre refractive index profile. In any case, the bend loss is calculated by evaluating the amount of power traveling outside the core.

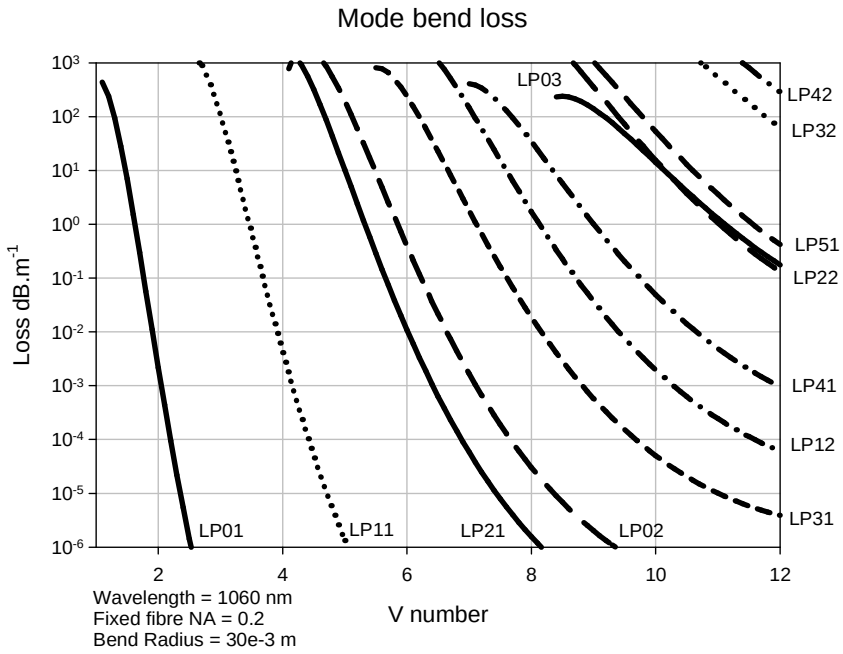

Figure 4.1: Modal bend loss estimation versus the V-number of a step index core fibre (NA = 0.2). The bend radius is fixed at 30 mm.

When the fibre has a V-number of 10, in figure 4.1, the four lowest order modes, LP_{01}, LP_{11}, LP_{21} and LP_{02}, respectively, are well guided for this given bend radius. A tighter bend radius is therefore required to discriminate the fundamental mode from the other modes. However, there is a limit, below which the bend radius becomes impractical. This is an even

greater concern when the fibre has a large cladding diameter in order to accept more pump power like the EYDF used in this work.

4.2.1.2 Discrete mode selection

The alternative approach is to use a discrete mode-selective element, which removes or prevents the propagation of higher order modes in the fibre while maintaining a low transmission loss for the fundamental mode. For example a pin hole placed after a multi-mode laser will act as spatial filter and can be used to select some lower order modes, but this will considerably reduce the laser efficiency. Alternatively, the mode filter can be placed within the laser cavity. For example, in [10], a tapered fibre section placed inside a fibre laser cavity shows a M^2 improvement from 2.4 to 1.9 while the output power is reduced by 19%. Thus, the laser brightness improved by 2.4 times.

Single mode operation of an amplifier can be achieved using selective mode excitation as demonstrated by M. E. Ferman [11]. A light source is imaged onto the input fibre facet such that the image has a maximum overlap with the fundamental mode of the fibre. The modal excitation is determined by equation (2.11). In practice, a set of lenses is used to launch the light from a diffraction limited source into the multi-mode core. The diffraction limited source has a gaussian transverse mode profile which can, with appropriate imaging optics, be matched in size to the fundamental mode of the multi-mode fibre. If the image is centred on the core (and does not propagate at an angle), only circularly symmetric modes are excited.

A more robust way of selective mode excitation is to use a tapered fibre section to progressively adapt the size of the mode field diameter while at the same time ensuring that mode-coupling does not occur [11]. The taper can support a single mode in one end and then increase in core size to the required diameter. Ideally, the taper can be used for connecting two mismatched fibres to each other, without any intermediate free-space propagation. This approach removes any uncertainty from optical misalignment and allows for all-fibre beam propagation as well as easier integration and small form device. However, it is very important that the loss of the taper is minimised and therefore the taper must be adiabatic for the fundamental mode [15].

Another requirement for single mode operation with discrete mode selection is that the fundamental mode must not couple power into higher order modes, as it propagates down the fibre. Mode-coupling degrades the output beam quality and reduces the laser brightness. Typically, mode coupling arises from perturbation of the core-cladding interface. For example,

these perturbations can be induced by microbends from the fibre fabrication process. Then, the mode coupling coefficient can be approximated by [16]:

$$\eta \approx \frac{1}{1+(\pi.\Delta n_{eff} / \kappa.\lambda)^2} \tag{4.1}$$

where κ is the perturbation amplitude due to index and microbend fluctuations and Δn_{eff} is the difference in effective indices between the different modes at the wavelength λ. Thus a large Δn_{eff} is desirable for low level mode coupling (e.g. Δn_{eff} $>10^{-4}$). However as the fibre's effective area increases, Δn_{eff} decreases as the modes become closer [11] and mode coupling cannot be avoided. Thus, large core are fibres become more sensitive to index perturbations in the core and tighter control of the fibre fabrication is required. Because the amplitude of the core perturbation is dependent on the cladding diameter, larger diameter fibres are less susceptible to core perturbation and to mode coupling (with a fixed core size) [11]. Therefore, it should be possible to use larger diameter core EYDF, with for example an outer diameter of 400 μm, and still achieve good beam quality from a multi-mode core as demonstrated in [17].

4.2.2 Taper for single mode operation

In some of the experimental work presented in this thesis, fibre tapers are used to ensure single mode or low order mode operation of high power large core fibre laser sources. The tapers losses for the fundamental mode must be kept to a minimum in order to insure a good optical performance but most importantly to avoid excess heat being dumped into the tapered fibre section. The role of the taper is to select the operating laser mode and to suppress any higher order modes while managing any waste heating resulting from this modal loss. To minimise mode coupling in the taper, the taper must be free from imperfections, which can locally couple modes together and excite higher order modes. In addition the taper should reflect as little as possible of the higher order modes back into the large diameter core.

Thus, the taper must gently adapt the size of the fundamental mode during the transition, i.e. an adiabatic taper. Otherwise, some power will be radiated into the (inner) cladding. From there, it may be absorbed by a high index material or it may couple back into the core, e.g., in the waist region of another taper. The taper loss is minimised when the taper is slowly varying according to the adiabatic criterion defined as [18]:

$$\left|\frac{dr}{dz}\right| \leq \frac{r(\beta_1 - \beta_2)}{2\pi} \tag{4.2}$$

where β_1 and β_2 are the local propagation constants in the transition of the fundamental mode (LP_{01}) and the closest mode (typically LP_{11}) and r is the core radius which varies along the taper. When this criterion, which defines an angle, is achieved the loss is minimal and essentially no power is coupled between the modes. Consequently, the closer the two modes are, the smaller is the angle and the longer the taper must be.

It is possible in the case of a linear taper to approximate the taper length required in order to have only the fundamental mode present. The number of LP modes present in the large core fibre can be approximated by $N_{\text{modes}} \approx \frac{V^2}{2}$ where V is the V-number defined by $V = \frac{2\pi}{\lambda}.NA.r$. Under the assumption that the modes are equally distributed in the core, their effective index spacing is $\Delta_{neff} = \frac{n_{core} - n_{clad}}{N_{\text{modes}}}$. Thus the taper angle Ω becomes: $\Omega = r.\frac{\Delta_{neff}}{\lambda}$, where r is the radius of the large core fibre and λ is the operating wavelength. Ideally, the taper defines a single mode when the radius reaches a value where the V-number is 2.405. The largest core radius for single mode operation is given by $r_{final} = \frac{2.405}{\frac{2\pi}{\lambda} NA}$. Therefore the minimum taper length for an adiabatic taper can be calculated as:

$$L_{taper} = \frac{\left(r - r_{final}\right)}{\Omega} = \frac{\left(r - \frac{2.405}{\frac{2\pi}{\lambda} NA}\right)}{r.\frac{\Delta_{neff}}{\lambda}} \tag{4.3}$$

For example, a fibre with a core of 0.22 NA, 15 μm radius operating at 1.550 μm, requires a linear taper of about 6.8 mm long to be adiabatic and single mode.

Even though the modes are not evenly distributed in a step-index core, the expression is still a reasonable estimate of the required taper length.

In practice, the taper waist region is spliced to a single mode fibre. Although, this fibre is singlemoded, it can have a different mode field diameter (MFD) than the waist region. Thus, the waist diameter must be tailored to minimise the splice loss between the dissimilar MFDs. The final dimension core radius can be determined by matching both fibres MFD using the following expression for the MFD [19] valid when $V < 8$:

$$2w_0 = 2a_{core}\left(0.65 + \frac{1.619}{V^{1.5}} + \frac{2.879}{V^6}\right) \tag{4.4}$$

There are other parameters, which can contribute to the performance of the taper such as the smoothness of the surface of the taper. A smooth surface helps to avoid any mode coupling in the transition region. Finally, an important use of tapers is to connect readily available standard sized fibre components with large-core fibres to form practical all-fibre high-power solutions.

4.2.3 Taper fabrication

The taper fabrication generally consists of heating a silica fibre to the softening point and then stretching the fibre to taper it. The first tapers made by myself, were fabricated using a standard splicer (Ericsson FSU-995). At first, the fibre is heated by an electrical arc, between two electrodes, then a displacement of the fibre holders stretch the fibre. However, the splicer did not allow for a good control of the taper shape and length, and only fibre with a diameter less than 350 μm could be tapered adequately with this machine. In figure 4.2, a taper manufactured using the Ericsson splicer is shown. The left hand side is the waist section which is then spliced into single-mode fibre, while the right hand side is the transition region from the large-diameter fibre to the waist.

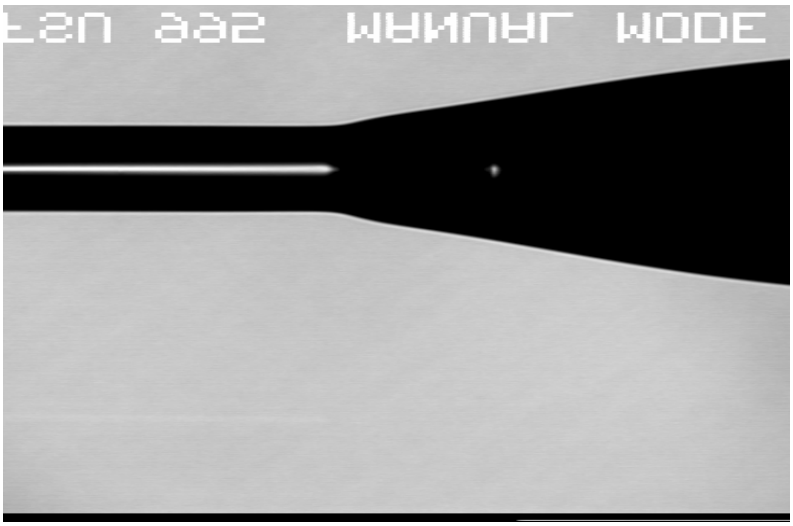

Figure 4.2: Large core fibre tapered and spliced to a single mode fibre using an Ericsson splicer. The total length is about 5 mm

Therefore, a commercial industrial-grade splicing machine with tapering facility from Vytran (LDS-1250) was used to fabricate the taper sections. Here, the heating element consisted of a tungsten filament, which could reaches temperature as high as 3000 °C. In contrast to other

existing method, e.g. moving flame [20], the filament is set at a fixed position while the fibre is feed through the furnace at a differential rate between the left and right fibre holders. The transfer rate is determined by the glass volume, the filament temperature and the desired taper shape. This method gives a good control of the shape and dimension while also giving a good uniformity of the taper shape. In general the tapers were deliberately made about 1 cm long to reduce the core loss. Thus, the typical total loss from the single mode fibre to the large-core fibre (including the splice loss in the waist region and the taper loss) was measured in the region of 0.3 to 0.5 dB with an 1.3 μm laser source.

4.3 CW tuneable laser set-up

Narrow-band tuneable lasers are useful in their own right. Equally important for my work is that wavelength tuning provides important additional information about the laser, which helps to better understand them. For high-power high-brightness operation, it is necessary to use a large core and a mode-selector such as a taper, as discussed in the previous sections.

4.3.1 C-band laser

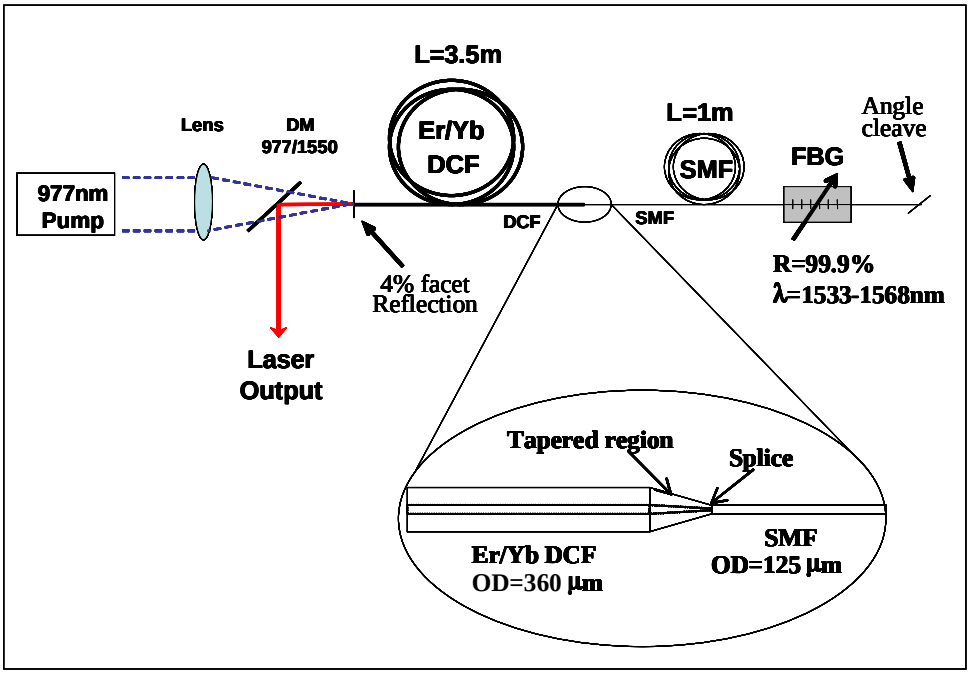

Figure 4.3: Experimental setup of tuneable EYDFL.

The experimental setup for the C-band tuneable laser is shown in figure 4.3. The laser consists of a cladding pumped large core Er:Yb doped fibre (F196-LF59). The inner-cladding is

D-shaped in order to increase the pump absorption. The inner-cladding diameters for the long and short sections are 400 μm and 360 μm, respectively. The phosphosilicate core is co-doped with Er and Yb. It has a diameter of 35 μm, with a numerical aperture of 0.22. The core refractive index profile is shown in figure 3.4. Finally, the fibre is coated with a low refractive index polymer which provides the outer cladding for the double-clad structure with an NA of 0.48. The fibre has a pump absorption of about 4.5 dB/m at the pump wavelength of 975 nm and the total fibre length is L = 3.5 m. The fibre length is such that the total pump absorption is about 15 dB, such as to protect the opposite fibre end. The pump is launched into the inner-cladding through the free fibre end, so that the laser is counter pumped with respect to the laser output. The laser cavity is formed by the 4% Fresnel reflection of the perpendicularly cleaved fibre end facet at the pump injection point and by a 99.9% reflectivity fibre Bragg grating in the other end. The grating is written in a standard single mode fibre, which is spliced to the doped fibre.

In order to achieve the best matching of the fundamental-mode between the single-mode fibre and the large core doped fibre, the latter is tapered to a suitable diameter [21, 22]. The single mode fibre is 1 m long and high-index coated. The purpose of this section of fibre is to eliminate any higher order modes propagating in the laser and therefore to achieve an improved beam quality. Higher order modes are radiated out from the core in the taper and then stripped away (and partially absorbed) by the high index gel which covers the taper. The mode stripping arrangement is such that it takes place along a certain length to distribute the heat generated by the remaining unabsorbed pump and the radiated higher-order signal modes. The taper is cooled to prevent any damage from leaking high power light. The estimated unabsorbed pump power is only a few watts. No thermal damage was observed in the SMF section or the taper, even with 140 W of launched pump power.

The grating was manufactured in-house by Dr M. Ibsen and packaged in a way so that it can be tuned from 1533 to 1578 nm based on a grating compression technique [23]. The grating fibre is terminated by an angle-cleave to avoid any reflection which could lead to spurious lasing at other wavelengths, e.g. at 1.1 μm by the Yb ions.

The EYDF is pumped by a diode stack based source at 977 nm. A dichroic mirror (DM) with high reflectivity at ~1.5 μm is used to separate the pump radiation at 977 nm from the output of the tuneable laser around 1550 nm. A second DM with a high reflectivity at ~1.1 μm is also inserted between the pump and launch end to filter out any laser emissions at 1.1 μm which, due to the excitation of Yb ions, might have damaged the pump. Finally, the pump launch end of the fibre is held in a water-cooled metallic V-groove that is designed to prevent

thermal damage to the fibre coating by any non-guided pump power or by the heat generated in the laser cycle itself.

4.3.2 L-band laser

A setup similar to the previous one (fig. 4.3) is used for an L-band tuneable laser. Here, the EYDF (F225-LF69) is 10 m long and has a phosphosilicate core of 25 μm diameter with NA of 0.22, surrounded by a D-shaped pure silica inner-cladding with a 400 μm diameter. The fibre is coated with a low refractive index polymer that provides an inner-cladding NA of 0.48. In this case the fibre has a small-signal inner-cladding absorption of ~ 2.5 dB/m at the pump wavelength of 975 nm. The cavity design is identical to that of the short-wavelength laser. A fibre taper connects and mode matches a single mode fibre with a HR FBG written in it. A diode-stack based pump source, operating at 975 nm, is launched into the EYDF through a simple combination of lenses. The laser output is taken from the pump launch end via a dichroic mirror, HR at ~ 1.5 – 1.6 μm.

4.4 Laser characteristics

4.4.1 C-band laser

The incorporation of a fibre Bragg grating in the laser cavity provides a wavelength selective feedback into the cavity, thus restricting the laser operation to the bandwidth of the grating. The grating reflection spectrum is shown in figure 4.4 (dashed line). It has bandwidth of 0.7 nm (FWHM). In comparison, the laser radiation (solid line) is much narrower with a linewidth of only 160 pm, due to the normal linewidth narrowing that occurs in a laser with its multiple pass amplification. The experimental results for the laser linewidth, shown in figure 3.8, were measured at an output power of 20 W with an optical spectrum analyzer (ANDO AQ6315) with a 50 pm resolution bandwidth.

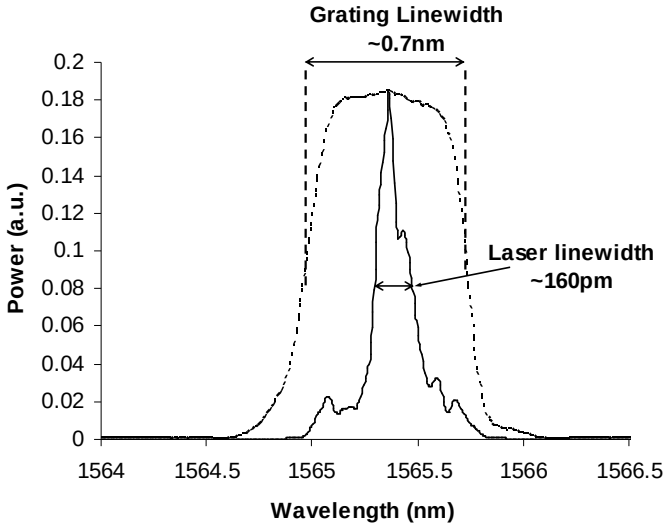

Figure 4.4: Comparison of the bandwidth of the grating and the laser linewidth

The fibre Bragg grating was fabricated for a wavelength of 1566 nm in its unstrained state and compression-tuned by as much as 33 nm, down to a wavelength of 1533 nm. Figure 4.5 shows the laser spectra for the different grating wavelengths at an output power of around 20 W, measured using an OSA with a resolution bandwidth (RBW) of 0.5 nm. The short-wavelength tuning range is limited to 1533 nm by the reduction in the Er:Yb gain at shorter wavelengths [3, 4]. For shorter tuning wavelengths, the Er excitation level required for lasing is so high that the gain at the gain peak becomes excessive, to the point where ASE at the gain peak starts to dominate the emission and the laser becomes unstable and prone to self-pulsing. This would damage the laser. It can be observed in figure 4.5 that already at 1533 nm the ASE build-up is quite significant. The limitation of operating the laser at wavelengths longer than 1566 nm is only due to the grating fabrication wavelength in this case. As the Er:Yb gain spectrum of this fibre extends up to almost 1580 nm, I would expect that the laser would be able to be tuned up to that wavelength. The laser tuning range would be about 45 nm. Similarly as for short-wavelength tuning, a low gain relative to the peak gain would ultimately limit the long-wavelength tuning. Nevertheless, already the results shown in figure 4.5 illustrate the wide tuning capability of this laser configuration.

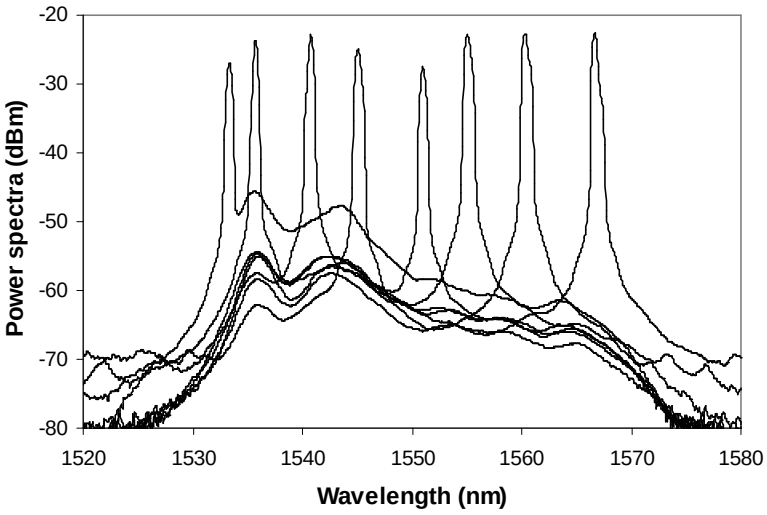

Figure 4.5: Spectrum of the tuneable C-band laser for different grating wavelengths

The laser slope efficiency and threshold at a wavelength of 1550 nm were measured to be ~30% and ~3.3 W, respectively. Figure 4.6 shows the laser output power for different launched pump powers. As most of the power is absorbed, the difference between absorbed and launched pump power can be neglected. Although not as high as that achieved in free-running, non-tuneable lasers, the laser efficiency is good, considering that the quantum defect limited efficiency for the laser is around 63% and that some power is lost in the taper (about 1 dB of the power launched into the taper), the fibre background loss, the imperfect transfer of energy from the Yb ions to the Er ions, and the ASE at 1 μm. Emission at 1 μm in EYDF can occur from excited Yb ions which do not transfer their energies to the Er ions. The most likely explanation is that a fraction of the Yb ions are too remote for energy transfer to any erbium ions. These Yb ions will produce some parasitic emission at ~1.1 μm. In this laser, this emission is relatively low (< 2 W) at the output, even at the highest output level. Still, most of the 1.1 μm emission is expected to be lost in the taper and therefore its power could not be reliably determined.

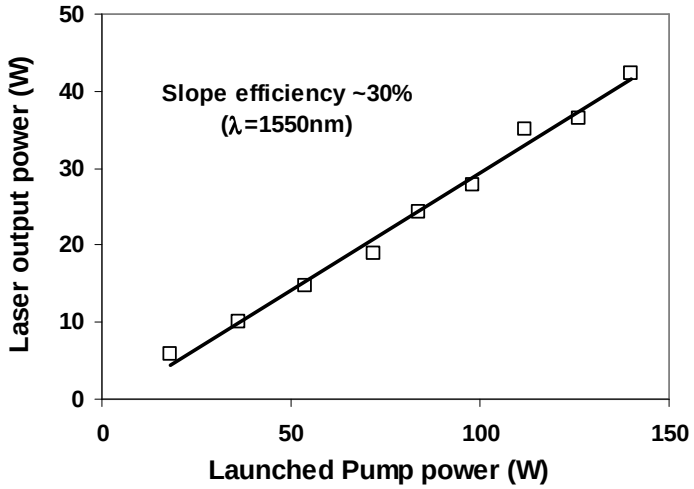

Figure 4.6: Slope efficiency of the laser for a wavelength of 1550 nm

Finally, the output power of the laser is measured for different wavelengths and pump powers. These results are shown in figure 4.7. It is observed that the laser output power is very flat across the wavelength range from 1533 nm to 1566 nm. Output powers in excess of 39 W were obtained over the whole tuning range with a maximum of 43 W at 1545 nm. The output beam quality is measured to be 1.7 times diffraction-limited, although the core with a V number of 15.6 can support a large number of modes. An M^2-value of ~ 8 would be expected if all supported modes were equally excited.

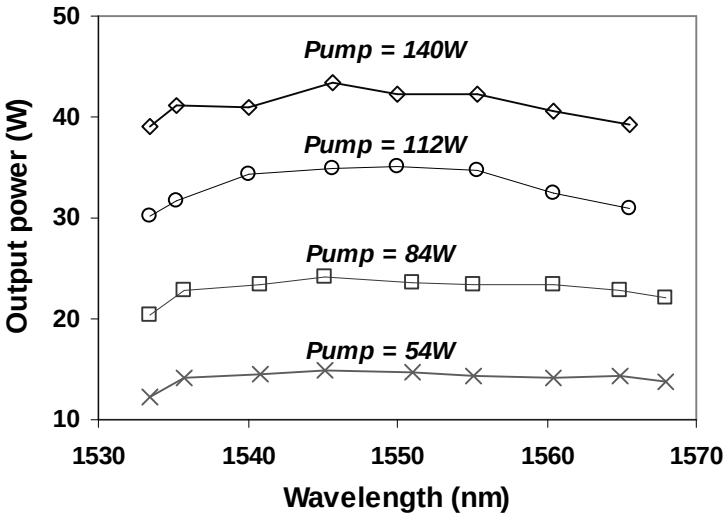

Figure 4.7: Measured output power of the laser as function of the wavelength for different pump power levels

The pump power was not increased further for fear of potential damage to the large-core – SMF splice region. Nonetheless, this experiment shows a significant capacity for power-scaling of complex all-fibre laser cavities, which in this case incorporates a tapered splice and a single-mode fibre with a FBG for improvement of spatial and spectral brightness as well as broadband tuning.

4.4.2 L-band laser

Figure 4.8 shows the laser output characteristics at the wavelengths of 1560 and 1590 nm for the L-band laser. Figure 4.9 shows tuning data. The output power increases linearly with the pump power at 1560 nm with a slope efficiency of 30%. A similar behaviour is observed in the wavelength range of 1550 - 1570 nm. By contrast, in the 1585 - 1602 nm wavelength range, a roll-off in the output power is observed at high pump power.

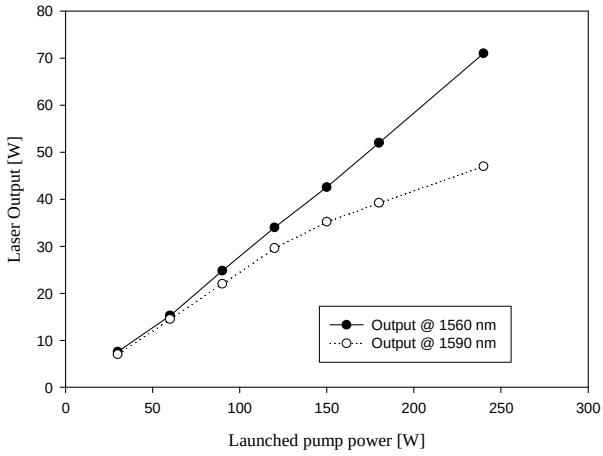

Figure 4.8: L-band EYDF laser output at 1560 and 1590 nm.

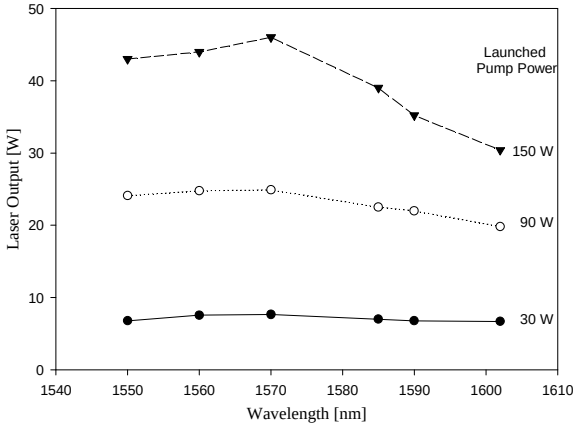

Figure 4.9: L-band EYDF laser tuning characteristics.

Similar behaviour has previously been observed in a low power experiment [24] and in simulation [25]. In the simulation, the roll-off is induced by the lasing or strong ASE from Yb-ions at 1.1 μm. From the laser configuration, one expects that this power is lost in the taper. Thus it is difficult in this case to experimentally determine how much power is lost through this process. The emission from the ytterbium ions can have different causes. Firstly, the energy transfer from Yb to Er ions can become less efficient when the signal at 1550 nm does not saturate the erbium ions, for example, near the edge of the core. In this case, the energy transfer saturates, which results in the growth of the gain at 1.1 μm. Secondly, there can be Yb ions which are isolated from any Er-ions and so cannot transfer any energy to them. Such Yb-ions

are readily excited and generate gain and ultimately emit through ASE at 1.1 μm. In addition, it has been experimentally [26] verified that in some of our EYDF the composition varies significantly along the length of a fibre preform. Therefore, a fibre from the same preform can exhibit a different concentration ratio at different fibre ends. In particular low concentrations tend to lead to poor energy transfer and thus a higher fraction of excited Yb-ions.

The roll-off can also be exacerbated by the large amounts of heat deposited in the fibre core [27, 28]. Indeed, even in efficient EYDFs, over 60% of the pump power is lost in the wavelength conversion process, mostly in the form of heat. Canat et al. [29] have shown that EYDF have a higher gain in the 1560 nm range thanks to the thermal effect on the population of the Stark energy sublevels. Their modeling also indicates that from 1580 to 1600 nm the ground state absorption increases as the fibre heats up. This would increase the threshold in a fictitious fibre laser in which the temperature is kept constant. In the real fibre with a varying temperature, this results in a roll-off, although it is unclear if the heating can account for the observed size of the roll-off. Nonetheless a maximum output power of 70 W at 1560 nm is obtained for 240 W of launched pump power (slope efficiency ~ 30%). Although the beam quality was not measured in this case, $M^2 = 2$ was obtained with this fibre in a slightly different configuration [30].

The laser could be tuned from 1550 to 1602 nm, as shown in figure 4.10. The short end of the tuning range is limited by the tuneability of the FBG. The linewidth was ~ 0.2 nm.

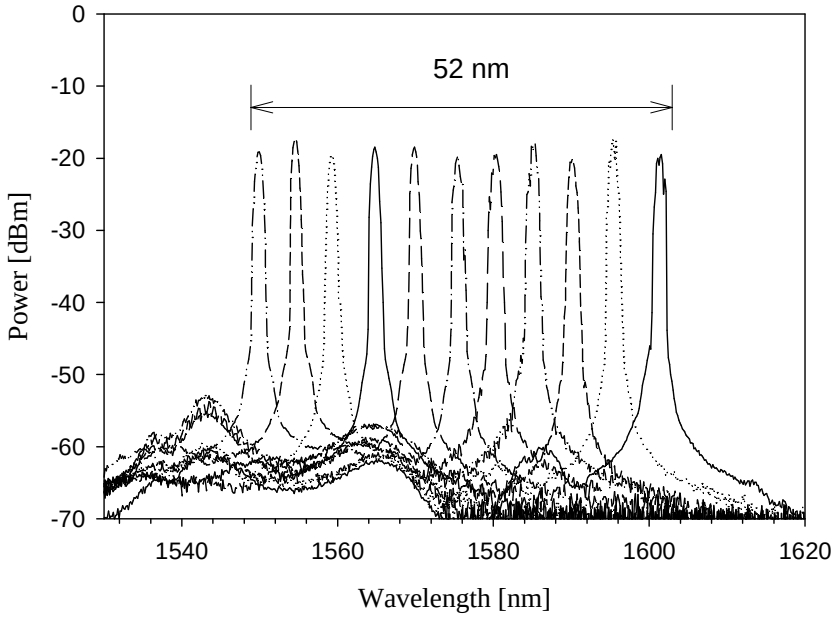

Figure 4.10: Normalized tuning spectra at 200 W of nominal pump power

4.5 Summary

In this chapter, the power-scaling of large core double-clad Er:Yb doped fibre is presented. The requirements for single-mode operation of large core fibres are reviewed, these being the fundamental mode excitation and the discrimination of the higher order modes. In order to achieve this, a tapered fibre section is used in all-fibre Fabry-Perot laser cavity. This leads to the construction of a short and a long wavelength range, tuneable, continuous-wave fibre laser. High output power with good beam quality is thus achieved. Such lasers are constructed using large-core EYDFs and a tapered fibre section connected to a compression-tuneable fibre Bragg grating. The EYDF are 3.5 m long for the C-band and 10 m for the L-band laser, but their dopant concentrations are also different. The lasers could be continuously tuned between 1533 – 1565 nm and 1550 – 1602 nm with a narrow linewidth of 0.16 and 0.2 nm, respectively. The laser slope efficiency is 30% in both cases. The output beam is good with a typical M^2 value of 1.7 – 2, thanks to the mode selection by the fibre taper. The output power is about 40 W over the tuning range except at the longest wavelengths where competing emission directly from the Yb ions reduces the laser efficiency. In the short wavelength range strong ASE reduces the gain available for the laser signal, while the parasitic emission from Yb ions remains quite low. The laser output powers are limited by the fibre preparation, i.e. fibre cooling, protection of the taper and fibre end-facet quality, which could easily be improved.

These results demonstrate that with a simple configuration, a larger core EYDF can be turned into a high-power, high-brightness and broadly tuneable laser source. However, different device configurations, in particular fibre lengths, need to be used for operation in the long and short wavelengths of the eye-safe spectral range.

4.6 References

[1] Z. Shu-Min, L. Fu-Yun, W. Jian, D. Fa-Jie, W. Hongjie, D. Xiaoyi, "High-efficiency generation of cladding pumped Erbium-ytterbium co-doped double clad fiber ring laser operating in L-band", Microw. Opt. Technol. Lett. **43**(3), 213 - 215 (2004).

[2] M. Laroche, W. A. Clarkson, J. K. Sahu, J. Nilsson, Y. Jeong, "High power cladding-pumped tunable Er-Yb fiber laser", in *Proc. Conference on Lasers and Electro-Optics (CLEO)*, Baltimore, US, 2003, paper CWO5.

[3] J. Nilsson, S. -U. Alam, J. A. Alvarez-Chavez, P. W. Turner, W. A. Clarkson, A. B. Grudinin, "High-power and tunable operation of erbium-ytterbium Co-doped cladding-pumped fiber lasers", IEEE J. Quantum Electron. **39**(8), 987-994 (2003).

[4] A. Usov, F. Shcherbina, and Y. Brannikov, "100W average power, tunable erbium fiber laser", in Proc. 2nd International Symposium on High-Power Fiber Lasers and Their Applications, (St. Petersburg, Russia, 2003), paper 4.5.

[5] N. S. Platonov, D. V. Gapontsev, V. P. Gapontsev, and V. Shumilin., "135W CW fiber laser with perfect single mode output", in *Proc. Conference on Lasers and Electro-Optics (CLEO)*, Long Beach, USA, 2002, paper CPDC3.

[6] N. G. R. Broderick, H. L. Offerhaus, D. J. Richardson, R. A. Sammut, J. Caplen, L. Dong, "Large mode area fibres for high power applications", Opt. Fiber Technol. **5**(2), 185-196 (1999).

[7] J. Limpert, A. Liem, T. Schreiber, S. Nolte, H. Zellmer, A. Tünnermann, J. Broeng, A. Petersson, Ch. Jacobsen, H. Simonsen, N. A. Mortensen, "Extended large-mode-area single mode microstructured fiber laser", in *Proc. Conference on Lasers and Electro-Optics (CLEO)*, San Francisco, US, 2004.

[8] Y. Jeong, J. K. Sahu, S. Baek, C. Alegria, D. B. S. Soh, C. Codemard, V. Philippov, D. J. Richardson, D. N. Payne, and J. Nilsson, "Ytterbium-doped double-clad large-core fiber lasers with kW-level continuous-wave output power", in *Proc. Conference on Lasers and Electro-Optics (CLEO)*, San Francisco, US, 2004.

[9] J. P. Koplow, D. A. V. Kliner, and L. Goldberg, "Single-mode operation of a coiled multimode fiber amplifier", Opt. Lett. **25**(7), 442 (2000).

[10] J. A. Alvarez-Chavez, H. L. Offerhaus, J. Nilsson, P. W. Turner, W. A. Clarkson, D. J. Richardson, "High-energy, high-power ytterbium-doped Q-switched fiber laser", Opt. Lett. **25**, 37 (2000).

[11] M. E. Fermann, "Single-mode excitation of multimode fibres with ultrashort pulses", Opt. Lett. **23**(1), 52 (1998).

[12] M. -Y. Cheng, Y. -C. Chang, A. Galvanauskas, P. Mamidipudi, R. Changkakoti, and P. Gatchell, "High-energy and high-peak-power nanosecond pulse generation with beam quality control in 200-µm core highly multimode Yb-doped fiber amplifiers", Opt. Lett. **30**(4), 358-360 (2005).

[13] D. Marcuse, "Curvature loss formula for optical fibers", J. Opt. Soc. Am. **66**(3), 216–220 (1976).

[14] J. -I. Sakai and T. Kimura, "Bending los of propagation modes in arbitrary-index profile optical fiber", Appl. Opt. **17**(10), 1499 (1978).

[15] D. Marcuse, *Theory of dielectric optical waveguides*, (2nd Ed., Academic Press, 1991).

[16] C. Headley, A. D. Yablon, M. J. Andrejco, M. D. Mermelstein, K. Brar, M. Fishteyn, ; J. Jasapara, D. J. DiGiovanni, "High-pulse energy MOPA using all-fiber components", Proc. SPIE **5709**, 343 (2005).

[17] J. Limpert, N. Deguil-Robin, I. Manek-Hönninger, F. Salin, F. Röser, A. Liem, T. Schreiber, S. Nolte, H. Zellmer, A. Tünnermann, J. Broeng, A. Petersson, and C. Jakobsen, "High-power rod-type photonic crystal fiber laser", Opt. Express **13**, 1055-1058 (2005).

[18] T. A. Birks, Y. W. Li, "The shape of fiber tapers", J. Lightwave Technol. **18**(4), 432 (1992).

[19] D. Marcuse, "Gaussian approximation of the fundamentals modes of graded-index fibers", J. Opt. Soc. Amer. **68**(1), 103-109 (1979).

[20] I. Yokohama, K. Okamoto, and J. Noda, "Fiber coupler fabrication with automatic fusion-elongation process for low excess loss and high coupling ratio accuracy", J. Lightwave Technol. **5**(7), 910 (1987).

[21] J. A. Alvarez-Chavez, A. B. Grudinin, J. Nilsson, P. W. Turner, and W. A. Clarkson, "Mode selection in high power cladding pumped fibre lasers with tapered section", in *Proc. Conference on Lasers and Electro-Optics (CLEO)*, Baltimore, USA, 1999, paper CWE7.

[22] A. Polynkin, P. Polynkin, A. Schulzgen, M. Mansuripur, and N. Peyghambarian, "Watts-level, short all-fiber laser at 1.5 μm with a large core and diffraction-limited output via intracavity spatial-mode filtering", Opt. Lett. **30**(4), 403 (2005).

[23] M. R. Mokhtar, C. S. Goh, S. A. Butler, S. Y. Set, K. Kikuchi, D. J. Richardson, M. Ibsen, "Fiber Bragg grating compression-tuned over 110 nm", Electron. Lett. **39**(6), 509 (2003).

[24] P. K. Cheo and G. G. King, "Clad-Pumped Yb:Er Codoped Fiber Lasers", IEEE Photon. Technol. Lett. **13**(3), 188 (2001).

[25] E. Yahel and A. Hardy, "Efficiency optimization of high-power, Er^{3+}–Yb^{3+}-codoped fiber amplifiers for wavelength-division-multiplexing applications", J. Opt. Soc. Am. B **20**(6), 1189 (2003).

[26] ORC internal report by V. Philippov.

[27] M. K. Davis, M. J. F. Digonnet, and R. H. Pantell, "Thermal effects in doped fibers", J. Lightwave Technol. **16**(6), 1013 (1998).

[28] D. C. Brown and H. J. Hoffman, "Thermal, Stress, and Thermo-Optics Effects in High Average Power Double-Clad Silica Fiber Lasers", IEEE J. Quantum Electron. **37**(2), 207 (2001).

[29] G. Canat, J. C. Mollier, Y. Jaouen, and B. Dussardier, "Evidence of thermal effects in a high-power Er^{3+}–Yb^{3+}fiber laser", Opt. Lett. **30**(22), 3030 (2005).

[30] J. K. Sahu, Y. Jeong, D. J. Richardson, J. Nilsson, "A 103 W erbium–ytterbium co-doped large-core fiber laser", Opt. Commun. **227**(1-3), 159 (2003).

Chapter 5 Pulsed erbium-ytterbium doped fibre MOPA

This chapter considers pulse energy scaling of EYDF. Firstly, section 5.1 introduces and reviews the performance of pulsed erbium and erbium-ytterbium co-doped fibre laser sources. Then, section 5.2 describes known challenges to energy scale pulsed narrow linewidth laser sources. Subsequently, in order to demonstrate a technique to overcome these issues, a fibre MOPA based on large core EYDFs is constructed. The experimental set-up is presented in section 5.3. The MOPA is capable of delivering high-peak power, high-energy pulses while maintaining a narrow linewidth. The detailed characteristics of each of the amplification stages are given in section 5.4. The performance of the MOPA is also discussed. Finally, section 3.6 summarises the results and findings of this chapter.

5.1 Introduction

High gain, high efficiency, and high average power can be obtained simultaneously in a rare-earth doped fibre. These properties make Master-Oscillator, Power-Amplifier (MOPA) configurations attractive for pulsed sources, in particular when a narrow-linewidth is required. In a MOPA, a low power seed from a Master Oscillator is amplified to a higher power by one or several Power Amplifiers. In multistage MOPAs, the signal gain can well exceed 50 dB. Furthermore, this configuration allows for excellent temporal (e.g. pulse shape, pulse duration and repetition rate) and spectral (e.g. linewidth and wavelength tuneability) control of the pulsed light. At the same time, high output power can be reached. Thus fibre MOPAs provide a unique and attractive combination of high power and flexibility, whilst still retaining the advantages of fibre based sources such as compactness and reasonable efficiency, which suit a number of applications.

Previously, several actively [1, 2] and passively [3] Q-switched erbium doped fibre lasers were constructed, and energy up to 0.5 mJ with several kW of peak power demonstrated. It is only recently that EYDFs have been used in a passively Q-switched laser [4]. In [4], the laser was tuneable from 1532 to 1563 nm with an output energy somewhat less than 100 μJ for a pulse duration as low as 3.5 ns. In a MOPA configuration, energy up to 0.5 mJ in an erbium-doped Yb-free fibre has been demonstrated as well [5].

The objective of this chapter is to demonstrate that power and energy scaling of narrow linewidth EYDF laser is possible by realization of a high energy pulsed MOPA. The simplest solution to reach high energy is to implement a similar approach to [6], with large core EYDF. However, the source has to have a narrow linewidth output and be more flexible than a Q-switched fibre laser.

5.2 Challenges

Ideally, higher energy pulses can be obtained when more energy is stored in the active medium. Therefore, fibres with large core and high concentrations are utilized [7] to increase the energy storage (see equation (1.1) and related text). However, in the 1.5 – 1.6 μm spectral range, it has always been more difficult to extract a lot of energy from erbium-ytterbium co-doped fibre than pure erbium doped fibres [8]. On the one hand, it is difficult to power-scale pure erbium-doped fibre [8] because the high-brightness pump sources required are limited to about the watt level. On the other hand, higher pump power can be used with EYDF, but the complex and various energy transfer processes which take place seems to limit the extractable energy.

Short duration, high energy pulses have high peak power. Therefore, non-linear effects can become significant inside the active or passive fibres that make up the laser source. Self-phase modulation, four-wave-mixing and stimulated Raman scattering deteriorate the temporal and spectral properties of the pulse. In order to mitigate the non-linear effects which scale with the intensity-length product [9], an arrangement of larger core and/or shorter fibre lengths are typically used in the laser source. When the source is narrow-linewith (e.g. one or several single-frequency lines), stimulated Brillouin scattering (SBS) becomes the major obstacle to high peak power output [10, 11]. Here, the high peak power, high energy pulsed fibre laser source presented in this section is based on a MOPA configuration, so that each amplification stage is optimised to avoid non-linear effect and still get the best performance. In this MOPA, non-linear effects are managed by using short length EYDF with high concentration and large cores.

The other challenge is that large-core step-index erbium-ytterbium doped fibres are multi-mode because of the phosphorous co-doping, required to enhance the energy transfer. This leads to a core with a large NA, typically ~ 0.2. Hence, fibres with core diameters of 30 μm are highly multi-moded with large V number (~ 12). If all their modes are equally excited the expected M^2 value is ~ 6. Still, large and multi-moded fibre cores can be made to operate on the fundamental

mode with the appropriate modal excitation and by suppressing higher-order mode coupling [12, 13].

Finally, amplified spontaneous emission (ASE) scales with the number of modes sustained by the core, and can become strong enough to limit further energy extraction. Therefore, the gain of the MOPA stages must be tailored for a given desired output energy.

Consequently, based on these considerations, a MOPA configuration and the use of the EYDF fibres seem like the best approach to reach high-energy, high peak power, narrow-linewidth output in the "eye-safe" wavelength range. For example, a high-coherence EYDF MOPA with energy of 0.4 mJ [14], and a millijoule single-stage MOPA with good beam quality and 575 ns long pulse [6] but with a large output linewidth (~7.3 nm) have been demonstrated. Other high-energy, narrow-linewidth results have been much more modest, i.e. [11].

5.3 Pulsed MOPA set-up

The fibre MOPA consists of a pulsed seed source followed by four fibre amplifiers (fig. 5.1). The master oscillator is a directly modulated, external-cavity tuneable laser (TLS) source (TUNICS-Plus) operating at 1535 nm. The seed laser can be tuned across the Er emission range in the 1.5 – 1.6 μm window. In this experiment, the choice of the wavelength is dictated by the short fibre length and the strong pumping of the cascaded amplifiers. As shown in figure 3.6, with a relative inversion above 60%, the wavelength with the highest gain is around 1535 nm. In order to avoid SBS, it is best to operate with the highest gain possible in the amplifier [15]. Therefore, monitoring taps have been introduced to monitor the spectral and temporal evolution of the pulse along the MOPA. The pulse duration is 250 ns and the repetition rate is set between 1 and 4 kHz. Though the precise linewidth is unknown, it is sufficiently narrow to generate SBS in the cascade. This indicates that some single-frequency lines are contained in the pulse. Direct measurements with an optical spectrum analyser show a linewidth of less than 0.05 nm (resolution-limited). Therefore, to avoid SBS, the overall length of the MOPA is kept to a minimum, < 12 m, including any passive fibres, and the power of the different amplifiers is adjusted to avoid both SBS and ASE saturation. The oscillator output is first amplified in a core-pumped erbium-doped fibre (EDF) amplifier (length ~ 3 m, core diameter ~12 μm), the output of which is time-gated with a synchronized acousto-optic modulator (AOM). The signal is then further amplified in a cladding-pumped Er:Yb co-doped fibre amplifier (length ~2.5 m, core diameter ~ 18 μm). Its output is spectrally filtered with a narrow-band FBG at the signal wavelength. Time-gating with a fibre-coupled AOM that I had available was not possible because the peak power leads to optical damage in the AOM. Time gating by the AOM and

spectral filtering with the FBG is necessary to reduce any forward propagating ASE between pulses, as this would otherwise limit the energy extraction in the amplifier cascade. The third amplifier consists of a 2.5 m long, double-clad EYDF with a core diameter of 50 µm (F260_LF35). The signal is injected through a taper (see figure 5.1 inset) and spliced to the previous stage with a single-mode fibre.

A polarisation controller (PC) is used to optimise the gain of the third amplification stage. Indeed, any doped fibres exhibit a degree of polarization dependent gain [16 - 19], either because of the pump polarization [17] (although this is unlikely here due to the nature of the pump source), or because of the anisotropy of the dopant ions [18]. In addition, polarization dependent gain (PDG) has been shown to be more important in multi-mode [19] than in single mode fibre lasers. Still, PDG is expected to be quite weak in rare-earth doped fibres, and polarization-dependent loss seems a more likely source of polarization-dependence, when this is observed.

The signal is then free space launched through coupling optics into the final 2 m-long large-core (core diameter ~ 90 µm) fibre (F546-LF218) amplifier. The two final stages are end-pumped with multi-mode pumps sources at 915 and 960 nm respectively, using dichroic mirrors to separate the signal and pump wavelengths. Beside the dichroic mirror and the lenses, there are no narrow-band filters or any other components between the last two stages, because of the power-level and the non-standard nature of the fibres.

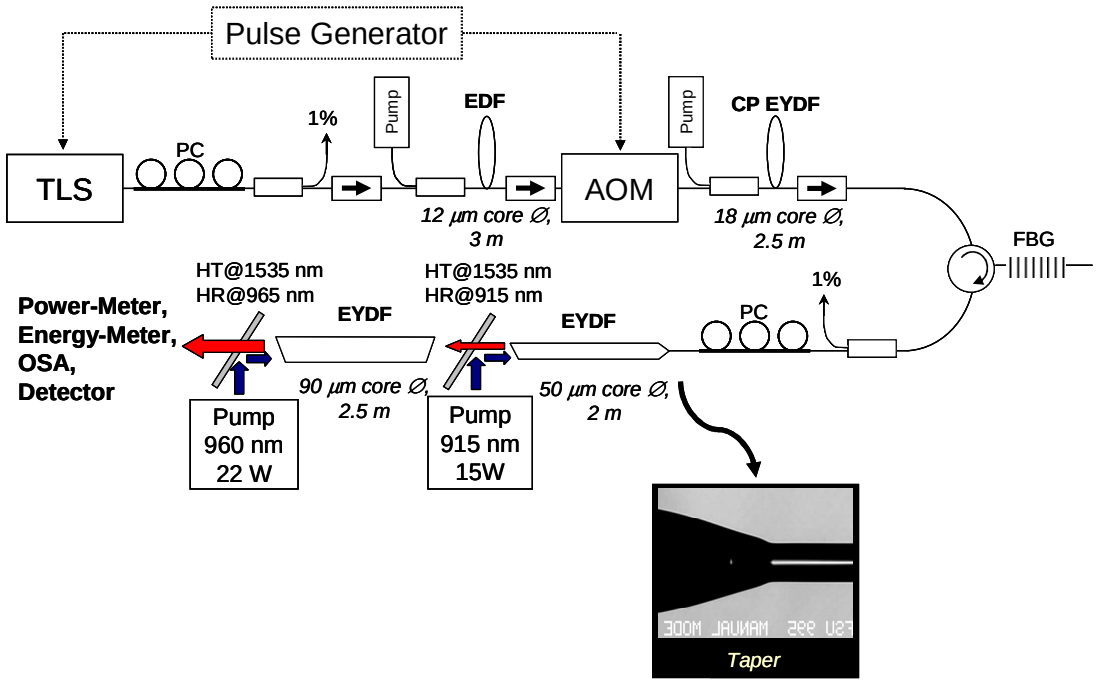

Figure 5.1: Experimental set-up of high-energy, narrow-linewidth erbium-ytterbium large-core fibre MOPA. Inset: large-core fibre taper.

Optical isolation between the amplifications stages, where possible, is used to prevent leakage of backward ASE and to protect upstream amplifiers from potential backward high-peak power pulses induced by SBS. The upstream amplifiers and components are particularly sensitive to damage, as the fibre cores are relatively small there and components such as AOMs have low damage thresholds. Nevertheless, thanks to the high-power fibre isolator between second and third stages, the MOPA can be operated with several orders of SBS in the third-stage amplifier without any damage. In addition, the fibre end facets of the third and fourth amplification stages are angle-polished with an angle greater than 12° to avoid any core back-reflection, which are known to reduce the performance of pulsed amplifiers by increasing ASE. Note that a relatively large end-angle is needed to suppress core-mode feedback in fibres with large core NAs.

Finally, the output pulses are characterised with a thermal power-meter, an energy-meter (Ophir), a fast detector (Thorlabs DT310) and an optical spectrum analyser (Ando AQ-6315E).

5.4 Amplification characteristics

5.4.1 Second amplification stage

The second-stage amplifier is first characterised by the amplification of short pulses (2.4 ns). For such short pulses, SBS can be avoided. The input pulse energy of the cladding pumped EYDF is about 50 nJ, after a 20 dB amplication from the first core pumped amplifier. The wavelength dependence of the energy obtained after the FBG at the maximum launched pump power is shown in figure 5.2.

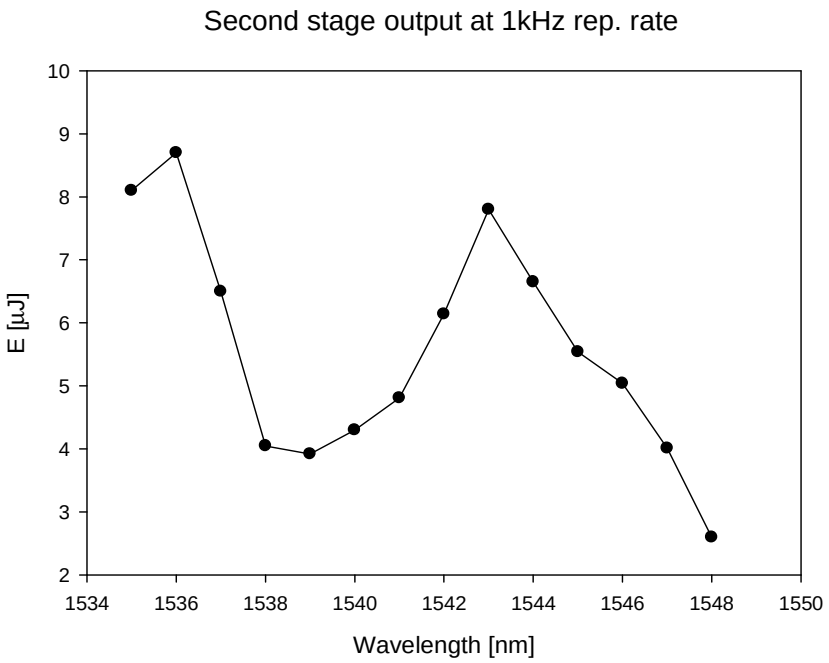

Figure 5.2: Energy dependence on the wavelength of the second amplification stage.

Clearly, the pulse energy follows the shape of the small-signal gain spectrum obtained with around 50 - 60% of the Er-ions excited. Thus in this condition, the maximum energy extraction is obtained at 1536 and 1543 nm although the maximum energy extractable from the excited erbium ions is always around 1600 nm, i.e., at the longest wavelength possible (but shorter than the ESA range). However, because of lower gain, in this case, higher input pulse energy would be required to actually extract this energy. Then the repetition rate is changed with the same initial pulse duration from 100 Hz to 4.5 kHz, which is the limit of the energy meter used. The energy and pulse peak power obtained in this frequency range, are shown in figure 5.3.

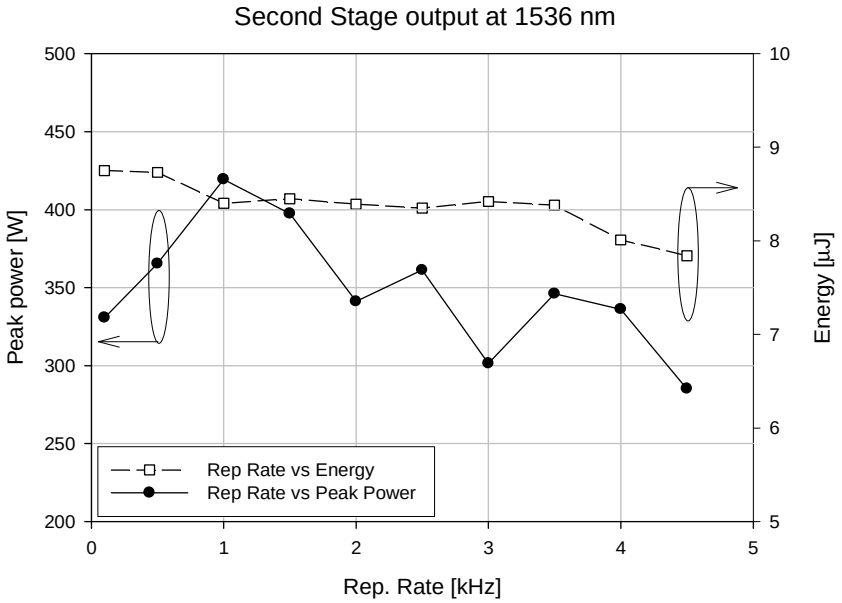

Figure 5.3: Peak power and energy at 1536 nm
for different repetition rate.

The energy measured is slightly higher at a very low repetition rate than near 5 kHz. Still the peak power is lower than expected if one considers the 2.4 ns output pulse. This is explained by the fraction of the energy which is contained in the tail of the pulse and measured by the energy meter. This power comes from a small fraction of ASE that is leaking through the AOM, between the amplification stages, and becomes pulsed. The highest peak power, i.e. the lowest power leak, is obtained at 1 kHz repetition rate.

This can be explained by the dynamics and interaction between the first and second amplifier. For example, the gain in the first amplifier may build up slower than that in the second stage because of the different amplifiers parameters, e.g. pumping rate, fibre length. As the first amplifier gain and ASE grows, the power leakage increases and then compresses the gain of the second amplifier. Thus, the pulse should be fired as soon as the first amplifier has enough gain, before it produces too much ASE. Therefore, the frequency of the source is fixed to 1 kHz and the operating wavelength is either 1536 or 1543 nm.

5.4.2 Third amplification stage

For the third amplification stage, EYDFs F402-LF122 and F260-LF35 were tested. When using a 2 m long piece of F402-LF122 pumped by a 962 nm laser diode, and 100 ns long pulses, the maximum energy obtained is 87 µJ before SBS appears and perturbs the output

pulse. Any pump power higher than this induces first and second order Brillouin Stokes waves and produces very narrow and unstable output pulses. As the energy extracted below SBS threshold is quite low, a fibre with a core twice the size is used in the third amplification stage, namely F260-LF35. Therefore, for the same gain and same absorption length, the energy extractable should be about 4 times (~350 μJ) before SBS sets in.

Indeed, with the same input pulse and a 2 m long fibre, more than 320 μJ are obtained at the maximum pump power. The output pulse duration (FWHM) decreases to between 90 ns and 80 ns due to the depletion of the EYDFA gain. This corresponds to a peak power of 2.5 kW. Here, the energy and output power are limited by the pump power available and the pump absorption at 962 nm. The output signal is SBS free, due to the large core [20, 21]. The output spectrum is measured using a single-mode fibre to collect the light and an OSA at highest resolution (0.01 nm). The output spectrum is very clean (see fig. 5.4), although some ASE leaks through the FBG. Still, the signal is 20 dB higher than the ASE pedestal in the immediate vicinity of the signal, as seen in the inset of figure 5.4, and the linewidth is resolution- limited. Still, in order to suppress any ASE in the final amplification stage, the signal is set at 1536 nm to reduce even further the ASE seen around that wavelength in figure 5.4.

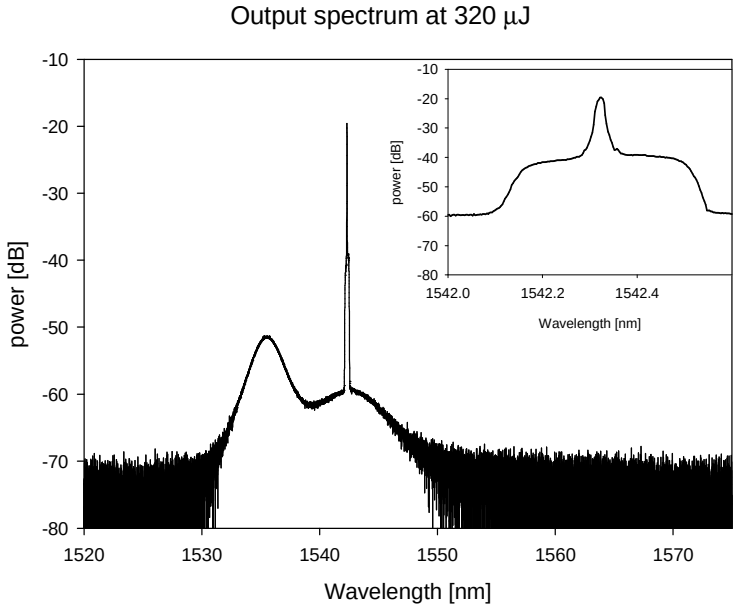

Figure 5.4: Output spectrum from the third stage amplifier, using fibre F260-F35, at the maximum energy of 320 μJ. The resolution is 0.01 nm. Inset: enlarged signal spectrum.

The same MOPA has been tested with even higher pump power using a 976 nm pump source from Laserline based on laser diode stacks. However, energy scaling is not possible beyond ~ 350 μJ because of fibre damage. A close inspection by I. Buffetov places this damage at the boundary between the core and cladding, which indicates multi-mode operation of the fibre at the moment of damage as shown in figure 5.5. Because the shape of the damage is different to the bullet shape that forms during the slow optical discharge [22], it may be due to the so-called fast optical discharge (FOD) [23]. FOD is characterised by a velocity of half the longitudinal sound velocity and only slightly lower than transverse sound velocity. Here, the damage happens over a short distance of about 3 cm. Further investigation is required to establish whether this is due to, for example, an enhancement of SBS or of the associated acoustic wave, because of back-reflection at the output end, which interacts with the incoming pulse. General estimates place the threshold of this damage around 20 – 30 W/μm^2, which is a greater intensity than that obtained in this fibre.

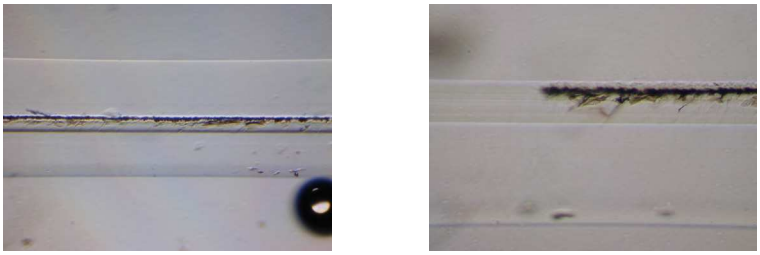

Figure 5.5: Two samples of core damages in F260-LF35 at 350 μJ (pictures by I. Buffetov [22]).

5.4.3 Fourth amplification stage

A fourth amplification stage consisting of a 2 m long piece of F546-LF218 is then added to the MOPA. The average input power to the final amplification stage is 233 mW at 1 kHz repetition rate. The input pulse energy is measured to be 179 μJ. Although this is not the maximum energy that one can extract from the first three amplifier stages, this is optimum for the final stage. This pulse is then amplified up to 1.011 mJ pulse at the maximum pump power (fig. 5.6).

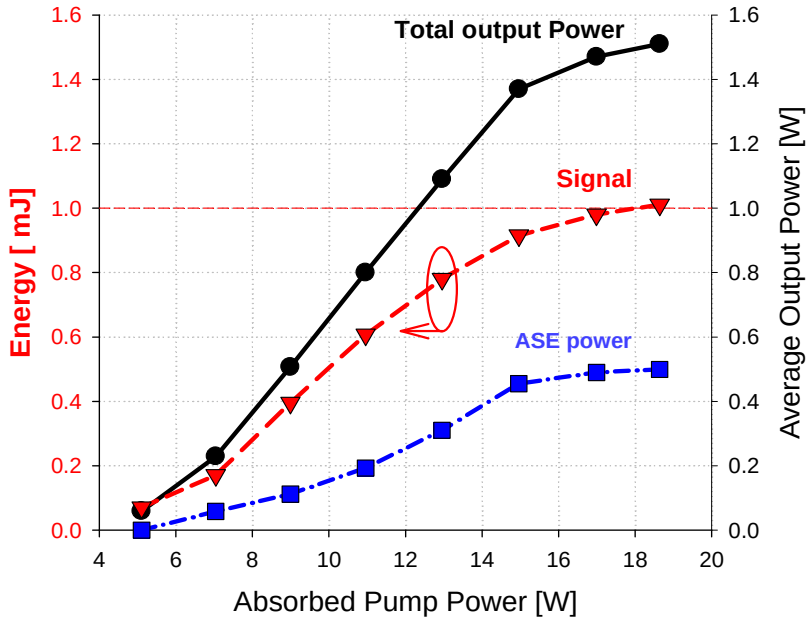

Figure 5.6: Signal output energy and average output power of the signal, ASE and total output from the final EYDFA.

The total average output power (ASE included) in the 1550 nm wavelength range is more than 1.5 W. It seems that the energy extraction is limited by ASE saturation, which represents about 30% of the total output power. However, at a high pump power level, even the ASE seems to roll off. Therefore, it appears that the pump energy is wasted in another process. One possibility is light generation at ~ 1 μm. The power and spectrum at 1 μm could not be directly measured because of the dichroic mirrors that were used. However, the same fibre was used in a cw laser configuration and the output spectrum is shown in figure 5.7.

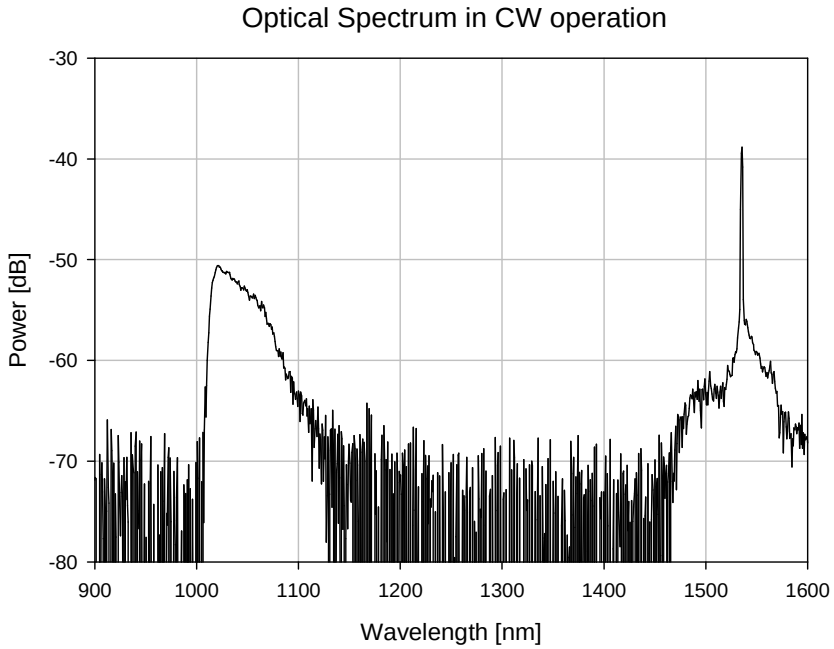

Figure 5.7: optical spectrum of F546-LF218 lasing in a 4% - 4% cavity configuration with 10 W of pump power absorbed.

In this configuration the ASE from the ytterbium is quite strong and represents about 50% of the total output power. Therefore, it is reasonable to assume that similarly when operating with a higher inversion in the final amplification stage ASE in the 1 μm Yb gain band starts to siphon off some of the pump energy. Indeed, it has been shown in [24] that the parasitic emission by Yb ions reduces the laser performance of EYDF. This is mainly due to a poor energy transfer from ytterbium to erbium ions, either because of a large fraction of Yb ions isolated from the Er-ions or because of a high fraction of excited Er-ions, as is the case here.

Still, the ASE at 1.5 and 1 μm can be reduced by increasing the repetition rate but this is at the expense of lower signal energy because of the shorter signal-gain build-up time between pulses. Alternatively, a better fibre end-facet with lower feedback could be prepared and additional time gating elements could be introduced between the amplification stages.

The pulse peak power at the maximum output energy is 6.6 kW for a pulse duration of 88 ns, as shown in figure 5.8.b. The pulse is compressed in the amplifier from the original 250 ns to 88 ns FWHM pulse duration due to the depletion-induced difference in gain between the leading and the trailing edge of the pulse. The evolution of the signal peak power and the average gain is shown in figure 5.8.a.

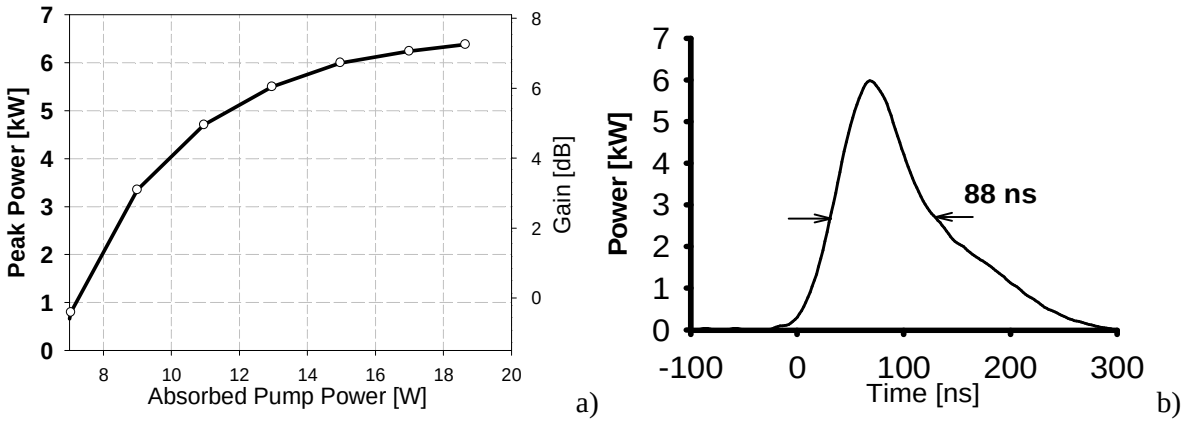

Figure 5.8: a) Peak power and average signal gain in F546-LF218,
b) Output pulse shape at 1 mJ.

Using the model of Frantz and Nodvik (equation (3.2)), at the maximum output energy the initial gain, G_0, is expected to be about 12 dB, although it is difficult to know exactly how much of the signal is launched into the fibre core. However, thanks to the large core dimension, it is expectred that practically all the power could be launched into the core.

A problem with the pulse compression, as observed in figure 5.8.b, that results from the high initial gain and with the subsequent gain depletion, is that the peak power grows accordingly and can induce SBS, in the case of single frequency laser lines. Shaping of the input pulses could allow the peak to be controlled so that the pulse peak remains below the non-linear threshold while the duration is sufficiently long for maximum energy extraction. In many cases, rectangular pulses would be ideal. With the textbook SBS gain coefficient being about 5×10^{-11} m/W for polarised light around 1550 nm, the SBS threshold becomes around 700 W peak power in a passive fibre of equivalent length and core size. However, no SBS is detected despite the peak power well exceeding the calculated threshold. In reality it is likely that pulse linewidth is larger than the SBS linewidth of ~ 20 MHz – possibly in the 100 – 1000 MHz range – which would reduce the Brillouin gain (equation (2.35)). Such broadening would not be measurable with our OSA. Furthermore, it is well known that a high quantum defect combined with a high concentration of active ions in Er:Yb doped fibres leads to large amounts of heat being deposited in the core. This leads to a strong thermal gradient in the fibre when end-pumped from only one end. The thermal gradient, in turn, broadens the SBS gain coefficient since the Brillouin gain shifts by around 1 MHz/K [25, 26]. Thus a temperature difference of 50°C between the input and output ends increases, in the case of a linear gradient, the SBS threshold by 2.5 dB [15]. In the large core fibre, a much larger amount of heat deposit is

expected near the pump injection point. Thanks to the combination of these effects, SBS is absent from this system.

The output optical spectrum at the maximum output energy is shown in in figure 5.9-a. The ASE level is 25 dB below the signal wavelength. However, a closer look at in figure 5.9-b shows a spectral pedestal due to the cw ASE leaked through the FBG filter and amplified in the amplifier cascade. A comparison with the seed spectrum shows that the output linewidth remains unchanged and is still resolution-limited, below 0.05 nm (fig. 5.9-b). Furthermore, the output spectrum is free from second order SBS or FWM, indicating the absence of non-linear effects.

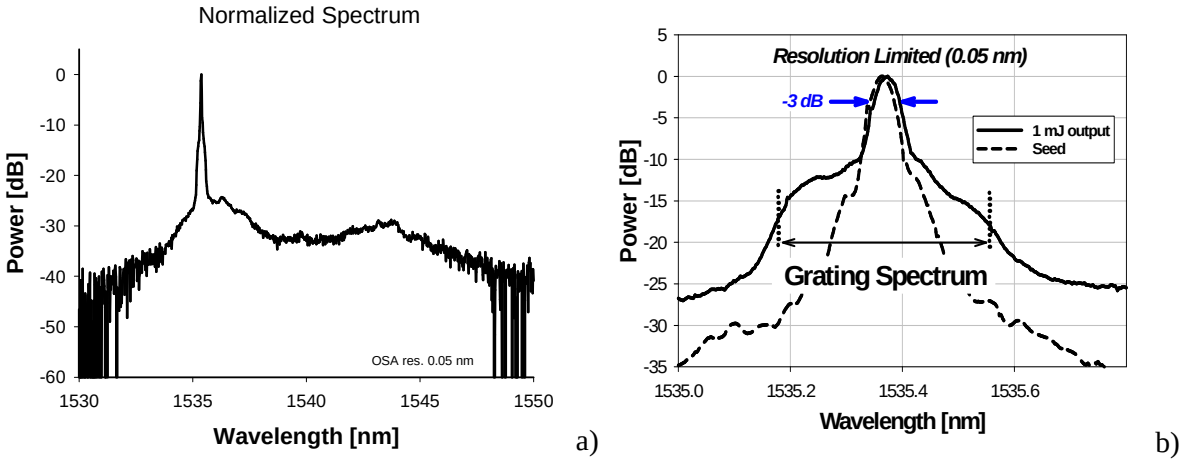

Figure 5.9: a) Normalized output optical spectrum (resolution 0.05 nm) at the maximum energy output, b) Enlarged spectra from: output (solid line), diode (dashed line)

Finally, experience with this fibre suggests that the beam is not diffraction-limited, but may have an M^2-value of 5. This value was measured in the cw regime. The direct measurement of the beam-quality of the pulses is difficult when there is a significant ASE-background. Whilst the launch of the signal pulses can be adjusted for best beam quality, the ASE cannot be controlled in this way and can therefore have a poorer beam quality. On the other hand, the population dynamics in the pulsed regime may degrade the beam quality relative to cw operation. A more advanced set-up that could have distinguished the beam quality of the pulses from the ASE was not available.

This result represents to the best of my knowledge; an unprecedented combination of high brightness, high energy, and high spectral density from an erbium-ytterbium doped fibre source.

5.5 Summary

In this chapter, the energy scaling of an EYDF is demonstrated. The challenges to reach high energy pulses while maintaining a narrow linewidth output are discussed. Using these design consideration, a fibre MOPA based on several large core EYDFs is implemented. The properties and performance of the various amplification stages are discussed. The final stage delivers up to 1 mJ, 6.6 kW peak power pulses of 88 ns duration, (FWHM) at 1 kHz repetition rate. The main limiting factor is thought to be ASE from the erbium and ytterbium ions. Thanks to the large core, the signal is free from deleterious non-linear effects such as stimulated Raman scattering and stimulated Brillouin scattering. This result indicates that even higher energy is possible with an improved fibre design and higher power pump sources. This example illustrates the energy-scaling capabilities of pulsed EYDF based laser sources which can be used as stand alone devices or, like in this thesis, as intermediate brightness converters for the generation of single-mode pulsed SRS laser light.

5.6 References

[1] D. J. Richardson, P. Britton, D. Taverner, "Diode pumped, high energy, single transverse mode Q-switch fibre laser", Electron. Lett. **33**(23), 1955-1956 (1997).

[2] H. L. Offerhaus, N. G. R. Broderick, D. J. Richardson, R. A. Sammut, J. Caplen, L. Dong, "0.5 mJ pulses from a single transverse-mode Q-switched erbium fibre laser", in *Proc. Conference on Lasers and Electro-Optics (CLEO/Europe)*, Glasgow, Scotland, 1998, paper CTuB3.

[3] R. Paschotta, R. Haring, E. Gini, H. Melchior, U. Keller, H. L. Offerhaus, D. J. Richardson, "Passively Q-switched 0.1 mJ fiber laser system at 1.53μm", Opt. Lett. **24**(6), 388-390 (1999).

[4] M. Laroche, A. M. Chardon, J. Nilsson, D. P. Shepherd, W. A. Clarkson, S. Girard, R. Moncorge, "Compact diode-pumped passively Q-switched tunable Er-Yb double-clad fiber laser", Opt. Lett. **27**(22), 1980-2 (2002).

[5] B. Desthieux, R. I. Laming, and D. N. Payne, "111 kw (0.5 mJ) Pulse Amplification at 1.5-μm Using a Gated Cascade of 3 Erbium-Doped Fiber Amplifiers", Appl. Phys. Lett. **63**(5), 586-588 (1993).

[6] V. N. Philippov, J. K. Sahu, C. A. Codemard, W. A. Clarkson, J. N. Jang, J. Nilsson, and G. N. Pearson, "All-fiber 1.15-mJ pulsed eye-safe optical source", Proc. SPIE **5335**, 1-7 (2004).

[7] C. C. Renaud, H. L. Offerhaus, J. A. Alvarez-Chavez, J. Nilsson, W. A. Clarkson, P. W. Turner, D. J. Richardson, and A. B. Grudinin, "Characteristics of Q-switched cladding-pumped ytterbium-doped fiber lasers with different high-energy fiber designs", IEEE J. Quantum Electron. **37**(2), 199 (2001).

[8] J. D. Minelly, V. Stasyuk, J. P. de Sandro, E. Gagnon, S. Chatigny, "Yb-free high energy double-clad Er fiber amplifier", in *Proc. Optical Amplifier and their Applications (OAA)*, San Francisco, USA, 2004, postdeadline paper PD4-1.

[9] G. P. Agrawal, *Nonlinear Fiber Optics*, (2nd Ed., Academic Press Inc, San Diego CA, 1995).

[10] N. A. Brilliant, "Stimulated Brillouin scattering in a dual-clad fiber amplifier", J. Opt. Soc. Am. B **19**(11), 2551 (2002).

[11] G. Canat, J. C. Mollier, J. -P. Bouzinac and Y. Aubry, G. Loas, Y. Jaouen, "100 μJ generation using a narrow linewidth Er^{3+}-Yb^{3+} doped fiber MOPA and its modelling", in *Proc. Conference on Lasers and Electro-Optics (CLEO)*, Munich, Germany, 2005, paper JWB67.

[12] M. E. Fermann, "Single-mode excitation of multimode fibres with ultrashort pulses", Opt. Lett. **23**(1), 52 (1998).

[13] J. P. Koplow, D. A. V. Kliner, and L. Goldberg, "Single-mode operation of a coiled multimode fiber amplifier", Opt. Lett. **25**(7), 442-444 (2000).

[14] V. Philippov, J. K. Sahu, C. A. Codemard, J. Nilsson, and G. N. Pearson, "All-fiber 0.4 mJ high-coherence eye-safe optical source", (International Society for Optical Engineering, Bellingham, WA 98227-0010, United States, London, United Kingdom, 2004), pp. 284-288.

[15] V. I. Kovalev, R. G. Harrison, J. Nilsson, Y. Jeong, V. Hernandes-Solis, and J. K. Sahu, "Analytic modeling of Brillouin gain in rare-earth doped fiber amplifiers with high-power single-frequency signals", Proc. SPIE **5709**, 142-146 (2005).

[16] P. Weßels, C. Fallnich, "Polarization dependent gain in saturated ytterbium and neodymium double-clad fiber amplifiers", in *Proc. Conference on Lasers and Electro-Optics (CLEO)*, Munich, Germany, 2003, paper CMK3.

[17] A. J. Poustie, "Polarization cross saturation in an Er^{3+}-doped fiber ring laser", Opt. Lett. **20**(18), 1868 (1995).

[18] J. K. Sahu, C. C. Renaud, J. Nilsson, W. A. Clarkson, S. U. Alam, A. B. Grudinin, "Single-polarization laser operation in polarization-maintaining single-polarization pumped erbium-doped Fiber", in *Proc. Conference on Lasers and Electro-Optics (CLEO)*, Baltimore, USA, 2001, paper CWC5.

[19] A. Saissy, B. Dussardier, G. Monnom, R. Jindal, "Modal contribution to the polarization dependent gain constant in Er^{3+}-doped Fiber", Opt. Commun. **185**(4-6), 407-412 (2000).

[20] A. Mocofanescu, L. Wang, R. Jain, K. D. Shaw, A. Gavrielides, P. Peterson, and M. P. Sharma, "SBS threshold for single mode and multimode GRIN fibers in an all fiber configuration", Opt. Express **13**(6), 2019-2024 (2005).

[21] M. Sjöberg, M. L. Quiroga-Teixeiro, S. Galt and S. Hård, "Dependence of stimulated Brillouin scattering in multimode fibers on beam quality, pulse duration, and coherence length", J. Opt. Soc. Am. B-Opt. Phys. **20**(3), 434-442 (2003).

[22] private communication with I. Buffetov.

[23] Y. Shuto, S. Yanagi, S. Asakawa, M. Kobayashi, R Nagase, "Fiber Fuse Phenomenon in Triangular-Profile Single-Mode Optical Fibers", J. Lightwave Technol. **24**(2), 846 (2006).

[24] J. K. Sahu, Y. Jeong, D. J. Richardson, J. Nilsson, "A 103 W erbium–ytterbium co-doped large-core fiber laser", Opt. Commun. **227**(1-3), 159 (2003).

[25] M. D. Mermelstein, A. D. Yablon, and C. Headley, "Suppression of stimulated Brillouin scattering in an Er-Yb fiber amplifier utilizing temperature-segmentation", in *Proc. Optical Amplifier and their Applications (OAA)*, Budapest, Hungary, 2005, paper TuD3.

[26] V. I. Kovalev and R. G. Harrison, "Suppression of stimulated Brillouin scattering in high-power single-frequency fiber amplifiers", Opt, Lett. **31**(2), 161 (2006).

PART III: CLADDING-PUMPED RAMAN FIBRE LASERS

Chapter 6 Principles of cladding-pumped Raman fibre lasers

This chapter describes stimulated Raman scattering in a multi-mode fibre which is then applied to the particular case of double-clad fibre. Section 6.1 introduces and reviews previous works on continuous-wave and pulsed multi-mode Raman fibre lasers. Section 6.2 presents the details and characteristics of the double-clad Ge-doped Raman fibre used in the experimental study presented in the next two chapters. Then, the theory of Raman scattering in multi-mode fibres is presented in section 6.3. Subsequently, a simple model for CW operation, which treats the multi-mode pump as an equivalent mode, is introduced to describe the general behaviour of a multi-mode Raman fibre in the continuous-wave regime. With this model the threshold of cladding-pumped Raman fibre laser action can be estimated. In addition, mode excitation, pump mode mixing and the generation of higher order Stokes radiation in the case of a double-clad fibre are discussed. Then section 6.4 treats the case of Raman lasers with pulsed pump and Stokes beams. Here, the walk-off length parameter, which defines a maximum length over which the pump and Stokes pulses are temporally overlapped, is introduced. In this regime, also called the quasi-CW regime, SRS can be treated with the CW Raman propagation equation which simplifies SRS modelling. Then, for various pump pulse durations and fibre refractive indexes, the calculated SRS small-signal gain and the pump critical power, are presented. Furthermore, the limitation by material damage threshold in the case of pulsed cladding-pumped Raman lasers is also briefly discussed. Finally, section 6.5 summarises the findings presented in this chapter.

6.1 Introduction

High-power Raman fibre lasers are much more wavelength-agile than rare-earth doped fibres which are restricted by their wavelength coverage (see fig. 1.2). Traditionally, these have been core-pumped single-mode devices with a relatively small core. Until recently, the lack of single-mode high-power pump sources had limited the power of Raman lasers to a few watts although this is now changing with the development of powerful single-mode fibre laser sources. An alternative to core-pumped fibre is to use multi-mode fibre which can be pumped with low-brightness sources. In the seventies, Raman scattering in multi-mode fibres has been

the subject of experimental [1] and theoretical [2] studies. However, it was only in the 1990s that Liu shows that multi-mode fibres could efficiently generate SRS [3]. In the same period of time, Chiang [4] experimentally demonstrated the beam clean-up properties of SRS in multi-mode fibre, i.e. brightness enhancement through SRS in a multi-mode fibre, and envisaged the single mode operation of such a fibre [5]. The SRS fibre laser was pumped by a high-peak power pulsed dye laser and low order mode operation was achieved by the appropriate modal excitation of the multi-mode fibre. The Raman beam clean-up properties were first investigated in a solid state "bulk" (non-waveguiding) laser [6, 7] and subsequently in a multi-mode fibre by Russell and co-workers [8]. Meanwhile Ilev presented a tuneable double-pass fibre Raman laser based on a multi-mode fibre [9], although the beam quality was not investigated. In conventional multi-mode fibre, the transverse pump distribution results in Raman gain which preferentially favours lower-order modes at the Stokes wavelength. Consequently, the output beam quality is improved with respect to the pump beam quality. Still, in a cladding-pumped fibre the power injected into the fundamental mode of the Stokes can be controlled more easily than in large multi-mode structures. Furthermore, determination of the Stokes output power is facilitated as the fibre modes are well discriminated. Therefore, the real performance of the beam clean up process can be evaluated more accurately. However, there has been little theoretical work on the understanding and modelling of the behaviour of cladding-pumped Raman fibre devices. Thus, some theoretical foundations specific to these fibres are required for cw and pulsed operation regimes.

6.2 Characteristics of the double-clad Raman fibre

6.2.1 Double clad fibre

The double-clad Raman fibre (DCRF) (F71-LF11), used in my experiments, was fabricated at the ORC using a standard modified chemical vapour deposition process. The DCRF is an all-glass fibre formed by a pure-silica outer-cladding and a germanosilicate inner-cladding and a germanosilicate core. The core is defined as the section with raised refractive index (with respect to the inner-cladding) of the fibre as shown in figure 6.1. Here, the core is formed by increased the germanium concentration. The inner cladding has a diameter of 21.6 µm and an NA of 0.22 with respect to the outer cladding. The core has a diameter of 9 µm and an average NA of 0.14 relative to the inner cladding. The outer cladding has an outside diameter comparable in size to that of a standard SMF fibre. The core has an estimated cut-off wavelength of 1630 nm.

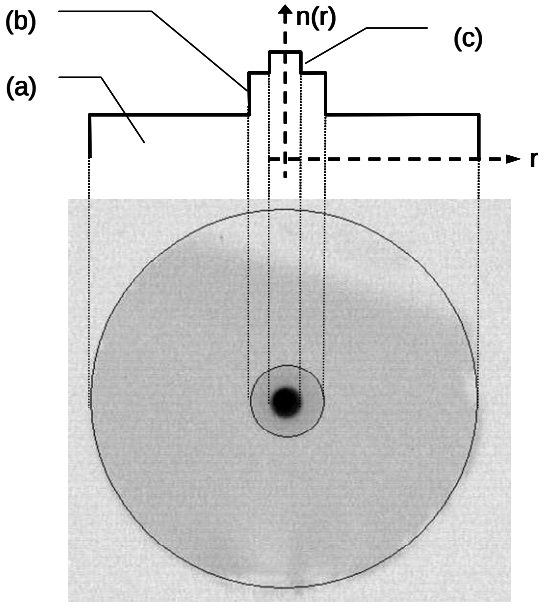

Figure 6.1: Double-clad Raman fibre with idealised refractive index profile and cross-section: (a) - outer silica cladding, (b) - germanium doped inner cladding and (c) - core.

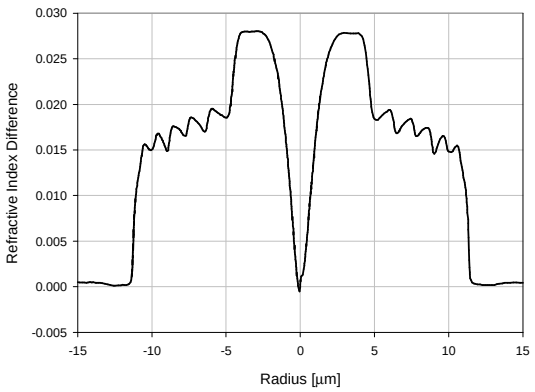

Figure 6.2: Measured refractive index profile of F71-LF11.

The measured refractive index profile of the fibre preform (F71-LF11) is shown in figure 6.2. A central dip is present in the fibre refractive index profile due to the evaporation of germanium during the preform collapse. The dip modifies the shape of the fundamental mode at the Stokes wavelength, but it does not affect the working principle of the Raman amplification process. The core section is still single-mode around 1660 nm.

6.2.2 Raman gain coefficient

The Raman gain coefficient, in the presence of germanium dopant, can be estimated [10 -12] from the difference of refractive index of the doped region with respect to fused silica. From the empirical formula given in [10 -12] for a wavelength at 1550 nm and from the refractive index profile shown in figure 6.2, the Raman gain coefficient is expected to be around $5.29\ 10^{-14}$ m/W in the inner-cladding whilst in the core it is estimated to be around $6.34\ 10^{-14}$ m/W because of the higher germanium concentration. Furthermore, the germanium concentration used in the fabrication "recipe" is estimated to be around 25 to 30% (mol.) which fits with a previous estimation of the Raman gain coefficient [11] of $5.5\ 10^{-14}$ m/W.

6.2.3 Raman Gain spectrum

The gain spectrum of the DCRF was measured using a white light source which was amplified with pulsed pump light. The pump power is kept low enough to avoid the presence of amplified spontaneous Raman scattering. The SRS gain coefficient spectrum obtained is shown in figure 6.3.

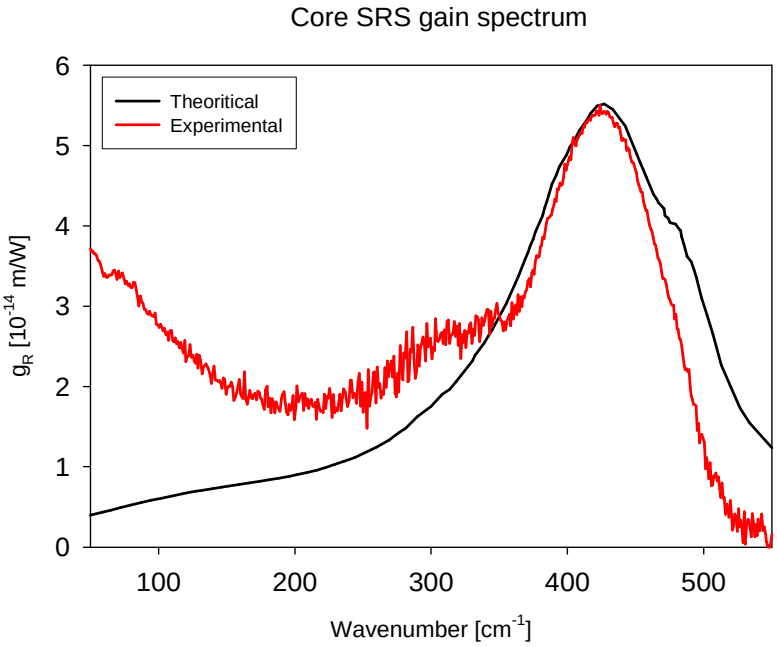

Figure 6.3: Core SRS gain coefficient, g_R : theoretical spectrum (black curve) from [13] and experimental measurement (red curve).

The measured core gain spectrum compares well with the spectrum calculated, from the core germanium concentration in the silica matrix, using the formula given by Kang [13]. At short wavelength shift (below 300 cm^{-1}) the SRS gain coefficient displayed is an artifact caused by the residual pump spectral content.

6.2.4 Background Loss

The high germanium concentration used in the design of F71-LF11 leads to scattering, which translates into background losses for the pump and signal. Originally, the fibre core background loss has been measured to be 3.1 dB/km whilst in the inner-cladding this loss was 2.3 dB/km. However, at a later stage of my study, using a high resolution optical time-domain reflectometer, several small sections of the DCRF were found to be defective (most likely because of the high-germanium concentration). Subsequently these sections were removed and the fibre respliced which reduced the overall background of the fibre. At that point, after

remeasuring the losses with a cut-back method, the core fibre loss became 2.3 dB/km and the inner-cladding loss 2.0 dB/km in the 1500 - 1700 nm wavelength range. Therefore, in the experimental work presented in the following chapters, the corresponding fibre background loss is given. The actual background loss value of the DCRF is slightly worse than the value given by Bubnov [14] and Dianov [15] of about 1.33 dB/km for a 30% (mol.) GeO_2 doped fibre at 1550 nm. This fibre was also manufactured using the standard MCVD process.

6.3 Raman scattering in cladding-pumped fibre

6.3.1 Theory of Raman scattering in multi-mode fibre

In a multi-mode fibre, stimulated Raman scattering arises from the non-linear response of the core material under the high intensity optical field that is propagating in the core. The light is transported in a number of excited modes which are supported by the waveguiding structure, i.e., the fibre core and inner cladding. The power of each of these modes, then, contributes to create an optical power distribution which generates a SRS gain proportional to the local intensity. It is essential that the description of SRS in a multi-mode fibre takes into account the contribution of all pump and Stokes modes in order to give an accurate description of the phenomenon [2]. Using the notion of effective area, equations (2.26) and (2.27) that describe SRS in a single mode fibre can be expanded to include the case of multi-mode fibres. Equation (6.1) shows the temporal and spatial evolution of the pump light while equation (6.2) and (6.3) represent the evolution of the first and second order Stokes:

$$\frac{\partial P_l^P(z,t)}{\partial z}+\frac{1}{v_l^P}\frac{\partial P_l^P(z,t)}{\partial t}=-\alpha_l^P P_l^P(z,t)-\frac{\lambda_{S_1}}{\lambda_P}\sum_{k=1}^{N_{S_1}}\frac{g_R\left(\left|\lambda_{S_1}-\lambda_P\right|\right)}{A_{l,l,k,k}^{eff}}P_l^P(z,t)P_k^{S_1}(z,t)$$
$$-\frac{\lambda_{S_2}}{\lambda_P}\sum_{k'=1}^{N_{S_2}}\frac{g_R\left(\left|\lambda_{S_2}-\lambda_P\right|\right)}{A_{l,l,k',k'}^{eff}}P_l^P(z,t)P_{k'}^{S_2}(z,t) \qquad (6.1)$$

$$\frac{\partial P_i^{S_1}(z,t)}{\partial z}+\frac{1}{v_i^{S_1}}\frac{\partial P_i^{S_1}(z,t)}{\partial t}=-\alpha_i^{S_1}P_i^{S_1}(z,t)+\sum_{k=1}^{N_P}\frac{g_R\left(\left|\lambda_{S_1}-\lambda_P\right|\right)}{A_{i,i,k,k}^{eff}}P_k^P(z,t)P_i^{S_1}(z,t)$$
$$-\frac{\lambda_{S_2}}{\lambda_{S_1}}\sum_{k'=1}^{N_{S_2}}\frac{g_R\left(\left|\lambda_{S_2}-\lambda_{S_1}\right|\right)}{A_{i,i,k',k'}^{eff}}P_i^{S_1}(z,t)P_{k'}^{S_2}(z,t) \qquad (6.2)$$

$$\frac{\partial P_j^{S_2}(z,t)}{\partial z}+\frac{1}{v_j^{S_2}}\frac{\partial P_j^{S_2}(z,t)}{\partial t}=-\alpha_j^{S_2}P_j^{S_2}(z,t)+\sum_{k=1}^{N_P}\frac{g_R\left(\left|\lambda_P-\lambda_{S_2}\right|\right)}{A_{j,j,k,k}^{eff}}P_k^{P}(z,t)P_j^{S_2}(z,t)$$
$$+\sum_{k'=1}^{N_{S_1}}\frac{g_R\left(\left|\lambda_{S_1}-\lambda_{S_2}\right|\right)}{A_{j,j,k',k'}^{eff}}P_{k'}^{S_1}(z,t)P_j^{S_2}(z,t) \tag{6.3}$$

Here, $P_{l,i,j}^{P,S_1,S_2}$ is the power in a specific mode *l*, *i*, or *j*, of either the pump (*P*), or first (S_1) or second (S_2) Stokes beams, $v_{l,i,j}^{P,S_1,S_2}$ is the group velocity, and $\alpha_{l,i,j}^{P,S_1,S_2}$ is the background loss (in Neper per metre) of the corresponding mode at the corresponding wavelength λ_{P,S_1,S_2}. The Raman gain coefficient g_R (in m/W) depends on the frequency difference between Stokes and pump waves and the phonon energy spectrum of the optical medium. Finally $A_{j,j,k,k}^{eff}$ is the effective area of the modes interacting in the Raman process as defined by equation (6.4) [16]:

$$\left(A_{i,i,j,j}^{eff}\right)^{-1}=\left\langle\psi_i,\psi_i,\psi_j,\psi_j\right\rangle=\frac{\int_0^{2\pi}\int_0^{\infty}\left|\psi_i(r,\theta)\right|^2\left|\psi_j(r,\theta)\right|^2 rdrd\theta}{\int_0^{2\pi}\int_0^{\infty}\left|\psi_i(r,\theta)\right|^2 rdrd\theta\int_0^{2\pi}\int_0^{\infty}\left|\psi_j(r,\theta)\right|^2 rdrd\theta} \tag{6.4}$$

where $\psi_{i,j}$ is the transverse electric distribution of the i, j modes considered in the fibre. The effective area represents an equivalent area which is the inverse of the mode overlap integrals over the waveguide. Depending on the modes involved, the effective area varies. Furthermore, higher-order modes can be degenerate, with a so-called sine and cosine mode. However, when those modes interact with the circularly symmetric LP_{0x} modes, like the LP_{01} mode, the overlap integrals are identical. Therefore, because the LP_{01} mode is the one of interest in the DCRF, I will assume that these degenerate modes are equally excited, so that the pump beam is independent of the angular coordinate.

In addition, pump mode beating is neglected. This may be justified by the fact that the SRS gain is small over a characteristic length given by the inverse of $k_{\max}-k_{\min}$, where $k_{\max}$ ($k_{\min}$) is the largest (smallest) wavevector of any pump mode at the pump wavelength. Assuming that $k_{\max}-k_{\min}\approx\frac{2\pi}{\lambda_p}\left(n_{core}-n_{outer\_cladding}\right)$, the "coherence length" of the pump light in different modes is of the order of 10^{-3} m. Very little happens over such distances in a Raman amplifier. Therefore, it is justified to neglect the interference of the pump modes

Furthermore, the mode beating between the Stokes waves can also be neglected. Garth and Sammut have demonstrated [17] that the impact of mode coupling of the Stokes waves depends on the modal gain. Here, the strong relative enhancement of the fundamental Stokes

when seeded or when selected by a grating or by an aperture (e.g. by a spliced single mode fibre), reduces the effect of modal interferences.

Moreover, the effect of pump mode coupling due to perturbations (see Chapter 2) can be reduced to the two extreme cases: weak and strong mode coupling [2]. In the absence of mode coupling effects, the pump modes are depleted at different rates. On the other hand, when strong mode mixing is present over a length where the SRS gain is small, the pump power becomes averaged over the number of modes and all the modes are depleted at the same rate. This case is discussed further in section 6.3.5.

In conclusion, the set of non-linear differential equations (6.1) - (6.3) can be integrated over the fibre length with the corresponding boundary conditions using, for example, a high-level language mathematical package like Matlab® and Mathematica®, to simulate cladding-pumped Raman fibre laser sources. An example of the model used in this thesis is given in Appendix I, where mode coupling is neglected. A more accurate model could be considered by taking into account the local intensities of the pump and signal modes which are then integrated over the transverse cross-section to obtain the modal power representation but this would be more complicated.

6.3.2 Averaged behaviour of multi-mode Raman fibre

In section 6.3.1 the simulation of the SRS phenomenon requires the knowledge of the initial boundary conditions which corresponds to the fibre modal power distribution and, in particular to the power distribution of the pump modes, which can be numerous in large multi-mode optical fibres. In order to simplify the propagation equation, the evolution of the total pump power can be considered independently of the number of pump modes or their power content. The total pump power launched, $P_T^P(0,t)$, at the instant t can be written as the sum of the power $P_l^P(0,t)$ of the fibre pump modes:

$$P_T^P(0,t) = \sum_l^{N_P} P_l^P(0,t) \tag{6.5}$$

where N_P is the total number of pump modes. Alternatively the power of each mode can be written as the fraction, k_l, of the total pump power:

$$P_l^P(0) = k_l P_T^P(0) \tag{6.6}$$

with $\sum_{l=1}^{N_P} k_l = 1$. By substituting in the differential equation (6.1) the term $P_l^P(z,t)$ with equation (6.6), and then summing the pump wavelength equations with respect to $P_T^P(z,t)$, the differential equations can be written as:

$$\frac{\partial P_T^P(z,t)}{\partial z} = -P_T^P(z,t)\sum_{l}^{N_P} k_l \alpha_l^P - \frac{\lambda_{S_1}}{\lambda_P} P_T^P(z,t)\sum_{k=1}^{N_{S_1}} P_k^{S_1}(z,t) g_R\left(\left|\lambda_{S_1} - \lambda_P\right|\right)\left(\sum_{l}^{N_P} \frac{k_l}{A_{l,l,k,k}^{eff}}\right) - \frac{\lambda_{S_2}}{\lambda_P} P_T^P(z,t)\sum_{k'=1}^{N_{S_2}} P_{k'}^{S_2}(z,t) g_R\left(\left|\lambda_{S_2} - \lambda_P\right|\right)\left(\sum_{l}^{N_P} \frac{k_l}{A_{l,l,k',k'}^{eff}}\right) \tag{6.7}$$

$$\frac{\partial P_i^{S_1}(z,t)}{\partial z} = -\alpha_i^{S_1} P_i^{S_1}(z,t) + P_i^{S_1}(z,t) P_T^P(z,t) g_R\left(\left|\lambda_{S_1} - \lambda_P\right|\right)\sum_{l=1}^{N_P} \frac{k_l}{A_{i,i,l,l}^{eff}} - \frac{\lambda_{S_2}}{\lambda_{S_1}} P_i^{S_1}(z,t)\sum_{k'=1}^{N_{S_2}} \frac{g_R\left(\left|\lambda_{S_2} - \lambda_{S_1}\right|\right)}{A_{i,i,k',k'}^{eff}} P_{k'}^{S_2}(z,t) \tag{6.8}$$

$$\frac{\partial P_j^{S_2}(z,t)}{\partial z} = -\alpha_j^{S_2} P_j^{S_2}(z,t) + P_T^P(z,t) P_j^{S_2}(z,t) g_R\left(\left|\lambda_P - \lambda_{S_2}\right|\right)\sum_{l=1}^{N_P} \frac{k_l}{A_{j,j,l,l}^{eff}} + \sum_{k'=1}^{N_{S_1}} \frac{g_R\left(\left|\lambda_{S_1} - \lambda_{S_2}\right|\right)}{A_{j,j,k',k'}^{eff}} P_{k'}^{S_1}(z,t) P_j^{S_2}(z,t) \tag{6.9}$$

Equation (6.7) represents the total power evolution while equations (6.8) and (6.9) still represent the evolution of the various modes of the first and second Stokes respectively.

Because it will be never possible to accurately represent the true multi-mode pump propagation, an "equivalent"effective area can be used to describe the propagation of the total pump power. This "equivalent" effective area which encompasses the various effects of the pump power distribution can be defined as:

$$\left(A_{i,pump}^{eff\_eq}\right)^{-1} = \sum_{l=1}^{N_P} \frac{k_l}{A_{i,i,l,l}^{eff}} \tag{6.10}$$

If the fundamental mode at the Stokes wavelength is only considered, the "equivalent" effective area, that I will call the joint effective area, is $A_{LP01,pump}^{eff\_eq}$. Then, the joint effective area can be used with the standard propagation equations and in some of the well-known equations introduced in section 2.4.2.

6.3.3 Cladding-pumped Raman fibre laser threshold

Thanks to the introduction of the joint effective effective area which takes into account the weight of each pump mode, it is possible to use the expression, already established, for the SRS gain (equation (2.30)) and for the threshold of a laser (equation (2.34)). These expressions are also valid for a multi-mode core. From [18], the SRS gain in a cladding pumped fibre becomes:

$$G_{linear}^{SRS} = \exp\left(\frac{g_R}{A_{LP01,pump}^{eff\_eq}} P_p L_{eff} \right) \tag{6.11}$$

The threshold of a Raman fibre laser [19] can be estimated using the modified expression of equation (2.34), and becomes:

$$P_{threshold}^{pump} = \frac{\alpha_p A_{LP01,pump}^{eff\_eq}}{g_R} \left[\frac{\alpha_s L - \frac{1}{2}\ln\left(R_1 R_2\right)}{1-\exp\left(-\alpha_p L\right)} \right] = \frac{A_{LP01,pump}^{eff\_eq}}{g_R L_{eff}} \left[\alpha_s L - \frac{1}{2}\ln\left(R_1 R_2\right) \right] \tag{6.12}$$

6.3.4 Modal excitations

It is clear from equations (6.1) - (6.3) that insofar as different pump modes have different effective areas for the interaction with the Stokes beams, the performance of a cladding-pumped Raman fibre laser source depends on the distribution of the pump power in the waveguide structure [20, 21]. In the absence of mode coupling between the pump modes, the modal distribution is determined by the modes excited at the pump injection point. In our case, where the fibre is free-space end-pumped, the excitation depends on the incident pump field shape (i.e., spot size in case of a gaussian beam), offset and angle with respect to the fibre optical axis. Using equation (2.11) and the knowledge of the properties of the pump field, it is possible to estimate the modal power distribution and therefore model such sources. It is worth pointing out, that the effective area according to (6.10), will not be equal to the spot area of the pump beam incident on the fibre.

The modal power distribution in a multi-mode Raman fibre laser determines the transverse SRS gain profile [4]. In a long multi-mode fibre, at equilibrium, the pump distribution tends to have a flat top or a gaussian shape [22] in the absence of pump modes depletion. Because the lowest-order modes have the largest overlap with a gaussian pump distribution, they mostly benefit from the Raman gain created by the pump. These modes are

closer to being diffraction-limited than the pump beam. Hence, the so-called, beam clean-up process, which converts the low-brigthness pump beam into a higher brightness laser output beam. The modelling of a single-pass cladding pumped Raman fibre amplifier brings out the behaviour of various pump modes (see fig. 6.4).

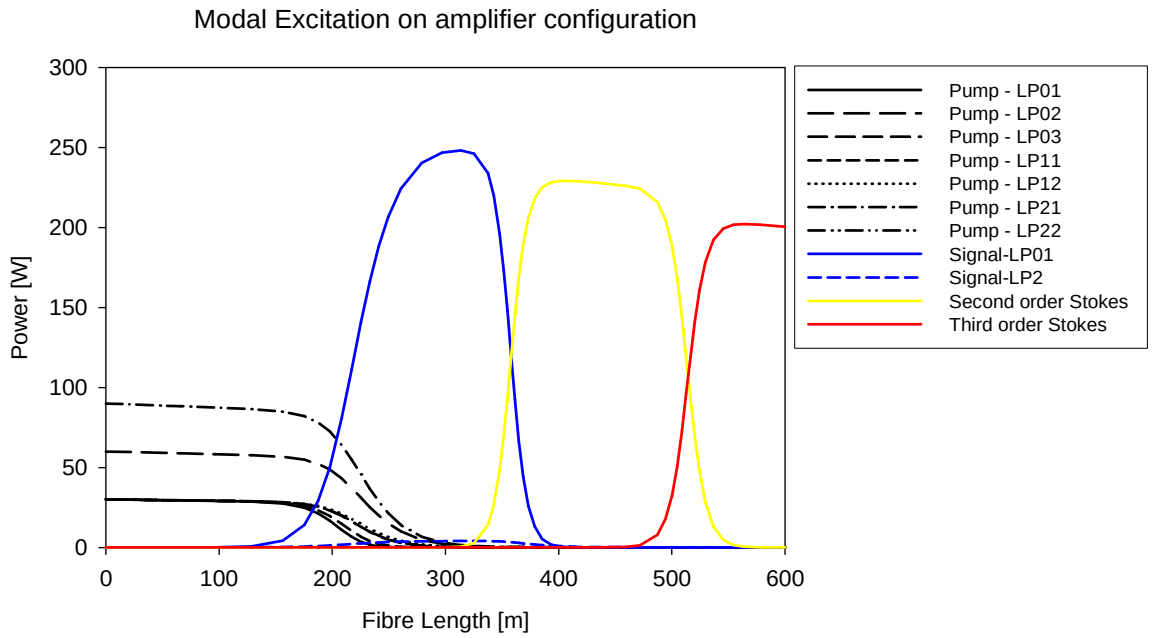

Figure 6.4: Simulation of a single-pass cladding-pumped Raman fibre amplifier.

In this example, the amplifier consists of a 500 m long cladding-pumped Raman fibre with the same physical properties as F71-LF11 given in section 6.2.1. Here the core background loss is 3.1 dB/km and the inner-cladding loss is 2.3 dB/km. I have considered a launched pump beam of 300 W, at 1545 nm, which is decomposed in various modes of the fibre. The pump modal decomposition is given in Table 6.1. Note that some of the modes are degenerate, and split into sine and cosine modes.

Pump Mode	LP_{01}	LP_{02}	LP_{03}	LP_{11}	LP_{12}	LP_{21}	LP_{22}
%	10	20	10	10	10	30	10

Table 6.1: Pump power distribution between the different modes.

Here, the pump and Stokes mode coupling mechanisms are neglected. Then, to demonstrate the effectiveness of the SRS beam clean-up properties, I have assumed that a signal at the Stokes

wavelength (around 1660 nm) is injected in the DCRF in co-propagation with the pump launch direction. The total signal power injected in the fibre is 1 mW of which 16% is in the LP_{01} mode whilst 84% is in the LP_{02} mode. For simplicity's sake, only the effective areas at the pump wavelength are considered because of the small difference in size between the modes at the pump and the Stokes wavelengths. Firstly, the mode field distributions have been calculated using a commercial fibre mode solver (FiberCAD® from Optiwave®) and the measured refractive index distribution (fig. 6.2) of the DCRF. Secondly, each effective area is calculated using equation (6.4). The effective areas of the different modes used for the modeling are shown in Table 6.2.

	LP_{01}	LP_{02}	LP_{03}	LP_{11}	LP_{12}	LP_{21}	LP_{22}
LP_{01}	64.97	233.19	171.42	93.56	208.25	223.12	175.01
LP_{02}		198.15	267.47	322.35	245.04	280.51	400.58
LP_{03}			168.01	274.51	390.4	362.14	359.25
LP_{11}				102.81	260.11	178.77	182.7
LP_{12}					218.43	312.33	269.98
LP_{21}						188.63	282.31
LP_{22}							205.86

Table 6.2: Effective Areas (in μm^2) of interacting modes.

These effective areas and initial conditions are subsequently used when the propagation equations (6.1) - (6.3) are integrated. For this, I used a modified Runge-Kutta method specially developed by X. Liu for SRS problems in [23] and other publications. An example of the implementation of this method is given in Appendix I.

Firstly, figure 6.4 shows that although the pump modes have very different overlaps (hence effective area) with the signal that propagates in the LP_{01} mode of the fibre, i.e. in the core, they are absorbed within a similar fibre length due to the non-linear pump absorption as the signal starts to grow. Secondly, in this simulation the Stoke power in the LP_{01} mode, which is much less than that of the LP_{02} mode, experiences a higher gain and dominates along the fibre length. The effective areas with respect to the LP_{01} mode are generally smaller than the effective areas respective to the LP_{02} mode. Therefore the joint effective area of the LP_{01} tends (depending upon the pump modal distribution) to be smaller than that of the other modes. As a result, the Raman gain of the LP_{01} mode is effectively larger than that of the other modes. In addition the LP_{01} mode benefits by its position in the core region from the higher SRS gain due to the higher germanium concentration. Even if higher order modes contains a fair fraction of power at the end facet of the fibre (i.e., following signal injection or reflection), the exponential dependence of the linear gain on pump intensity helps to select the mode with the highest gain

and power. Thus if the Stokes LP_{01} mode is seeded in a multi-mode Raman gain fibre, the output will principally be single-mode as verified in [10]. The difference in SRS gain between the Stokes modes forms the basis of the beam clean-up process.

6.3.5 Mode mixing

In double-clad rare-earth doped fibres, the pump absorption is improved by either a suitable fibre cladding geometry or by scrambling the cladding modes, for example, by bending the fibre [24]. This influences the optimum length and the spectral properties of doped fibres. However, in practice I found no significant changes of the Stokes output power in the double clad fibre lasers.

This might be explained by the fact that mode mixing does locally change the pump distribution and, therefore the pump absorption. However, in fibre with long interaction length, this effect is small because of the non-linear pump absorption by the Stoke wave. In the opposite case, e.g., for short fibre length, pump mixing helps into improving the number of pump modes participating in the SRS process. Otherwise, some pump modes would be depleted much faster than modes with larger effective area, reducing the device efficiency.

Capasso [2] showed that in the case of strong mode coupling, the pump power is distributed equally between the pump modes. Therefore the joint effective area becomes:

$$\left(A_{LP01,pump}^{eff\_eq}\right)^{-1} = \frac{1}{N_P}\sum_{l=1}^{N_P}\left(A_{LP01,l,l}^{eff}\right)^{-1} \tag{6.13}$$

The effective area is averaged over the number of pump modes sustained by the fibre. If the number of modes is significant and the modes are large, the efficiency of the cladding pumped Raman laser is reduced and must be compensated by longer fibre. Thus, in long fibre, it is more important to get the best modal excitation possible than to mix the pump modes in order to achieve the best performance

6.3.6 Higher order Stokes generation

When the Stokes signal power reaches a sufficiently high power level in the fibre core, it generates, in turn, a second Stokes wave at a wavelength determined by the SRS frequency shift. This process can be cascaded and used to generate wavelengths far away from the pump wavelength. However, my work focuses on generating a high power, high-brightness, first order Raman Stokes laser. Higher-order Raman scattering in cladding-pumped Raman lasers is interesting, but the lack of characterisation equipment and components such as fibre Bragg

gratings at long wavelengths would have hampered studies of this. In addition, above 1700 nm, silica glass starts to absorb because of the vibrational transitions of the Si-O bond. This effect can be somewhat mitigated in very high germanium concentration fibre [15] whose absorption curve is shifted towards longer wavelength. In the DCRF laser, the second order Stokes will arise in the core where the Stokes intensity is the highest. Any parasitic reflections will enhance the growth of the second order Stokes inside the lasing cavity and must be avoided, for example, by using angle cleaved fibre. In the DCRF, if the background loss is neglected, the second order Stoke small-signal gain in the fibre core is $G_{dB} = 4.34\frac{g_R}{A_{eff}} \approx 0.0037 dB/(m.W)$. Hence, if one assumes that around of 60 dB of gain is enough to notice the growth of the second order Stokes at the output of the laser, in a 1 km long DCRF (with no loss and a constant longitudinal power distribution), only 16 W of Stokes power is required.

6.4 Pulsed cladding-pumped Raman Amplification

6.4.1 Walk-off length in multi-mode fibre

In the previous section, the set of equations (6.1) - (6.3) describes the temporal and spatial evolution of the powers of the pump and Stokes modes under the Raman scattering process in a multi-mode fibre. These equations can also be used to describe the behaviour of double-clad Raman fibre amplifiers in the pulsed regime, with the knowledge of the power in the various modes involved in the process. In the case of a double-clad Raman fibre pumped by optical pulses co-propagating with Stokes beams, the pulse energy launched into different modes travel with different group velocities, v_g. This is known as modal dispersion. The signal travels with a different group velocity, as well. For sufficiently large differencies in group velocities, as determined by the pulse duration and the amplifier length, this will lead to (temporal) walk-off between signal and pump light. As a result, the energy transfer between different parts of the pump modes and the Stokes mode (or modes) can be concentrated to different locations along the fibre [25]. A DCRF with a large NA for the inner-cladding will have the pump modes more separated, i.e., with larger differences in v_g, than a low-NA fibre, even if the V-numbers, and therefore the numbers of modes, are the same. Pump modes with group velocities similar to the Stokes group velocity will, with the right timing, interact more strongly with the Stokes beam and will therefore transfer power more quickly. A second parameter which defines the energy transfer rate in the non-linear process is the power of the modes involved as discussed in section 6.3.4. A pump mode with a small joint effective area will transfer its power much faster to the Stokes mode than a mode with a larger joint effective

area. Thus, even when the walk-off is negligible, the power in different pump modes will be transferred to the Stokes beam with different relative rates, because of different effective areas. Furthermore, the SRS interaction will increase with higher intensity, i.e., with higher power as well as with tighter confinement. However, as the Stokes beam grows, it will in turn enhance the energy transfer from the pump mode with the largest joint effective area overlap to itself, so the presence of power in the pump modes with a small joint effective area helps with the conversion of pump power in modes with a larger effective area. For a constant V-number fibre, a low-NA inner-cladding will result in a lower intensity than a high NA design and the fibre length required for the SRS process will increase. Therefore, in pulsed SRS multi-mode fibre both the temporal overlap and the spatial intensity overlap are important parameters; both depend on the inner-cladding parameters and both will affect the temporal as well as the spatial evolution of the pump and Stokes beams.

The length for the maximum pump and Stokes pulse interaction is defined as the distance in which the Stokes signal passes through the pump pulse. This length is called the walk-off length and is defined as [18]:

$$L_{Walk-off} = \left| \frac{v_s v_p}{v_s - v_p} \right| \Delta T \tag{6.14}$$

where v_s and v_p are the group velocities of the signal and pump wave respectively and ΔT is the launched pump pulse duration. In the particular case of the double-clad fibre, the greatest velocity difference, i.e. the shortest interaction length, will correspond to the length involving a pump mode near the cut-off, i.e., with an effective index near the refractive index of the outer cladding, and the fundamental Stokes mode traveling in the core. Therefore, in the multi-mode case, when neglecting the wavelength dependence of the dispersion (in the 1500 - 1700 nm wavelength range the chromatic dispersion is about 20 ps/nm/km [18] in bulk silica) with respect to the material refractive index, the walk-off length becomes [26]:

$$L_{Walk-off} \approx c \left(\frac{n_{outer\_cladding}}{n_{core}} \right) \left(\frac{1}{n_{core} - n_{outer\_cladding}} \right) \Delta T \tag{6.15}$$

where n_{core} and $n_{outer\_cladding}$ are the refractive indexes of the core and outer cladding of the DCRF. This assumes a low-order signal mode and a high-order pump mode, with effective indices close to the refractive index of the core and outer cladding, respectively. Figure 6.5 illustrates the effect of the pulse duration and of the refractive index difference on the walk-off length.

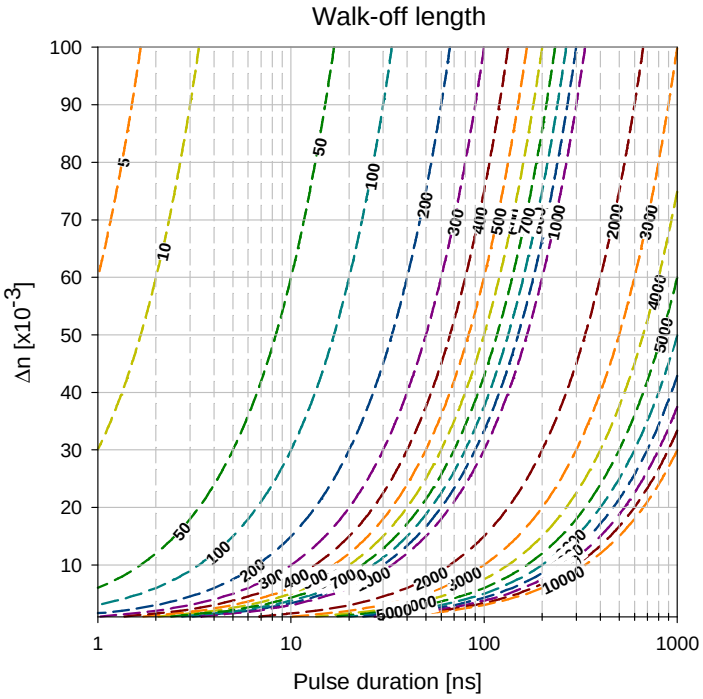

Figure 6.5: Walk-off length in meters for different pulse durations and (effective) index differences

In the double-clad Raman fibre (F71-LF11) the maximum refractive index difference (See fig. 6.2) is about 27×10^{-3}, therefore for a 100 ns pulse the expected walk-off distance is about 1.1 km. If the fibre length used is less than the walk-off length, the SRS gain is comparable to that obtained with continuous-wave operation during the pulse, which is the case in the experimental work presented later. This regime is called quasi-CW. However, in the case where the fibre length exceeds the walk-off length, the signal pulse duration can start to grow larger [25] depending on the SRS power transfer. As the pulse duration decreases, the walk-off length decreases accordingly which leads to a substantial increase in the pump intensity requirement for SRS generation.

6.4.2 Gain in pulsed regime

In the quasi-CW regime [18], neglecting the pump and signal background loss, the small-signal "averaged" pulsed SRS gain can be expressed for a gaussian shaped pulse as [25]:

$$G_{Stokes}^{dB} = 4.60358 \frac{P_{Launched}^{Pump} g_R}{A_{eff}} L_{Walk\_off} \tag{6.16}$$

where $P_{Launched}^{Pump}$ is the launched pump power, g_R is the SRS gain coefficient determined by the material and A_{eff} is the effective area defined by (6.4). This assumes that the interaction length is limited by walk-off rather than by loss or the actual fiber length. The term "averaged" gain is used to designate the gain over the pulse duration as opposed to the instantaneous gain at the pulse peak. Figure 6.6 shows the intensity required in order to reach 60 dB of small-signal gain according to the pulse duration and the difference between the refractive index of the guiding layers of the fibre.

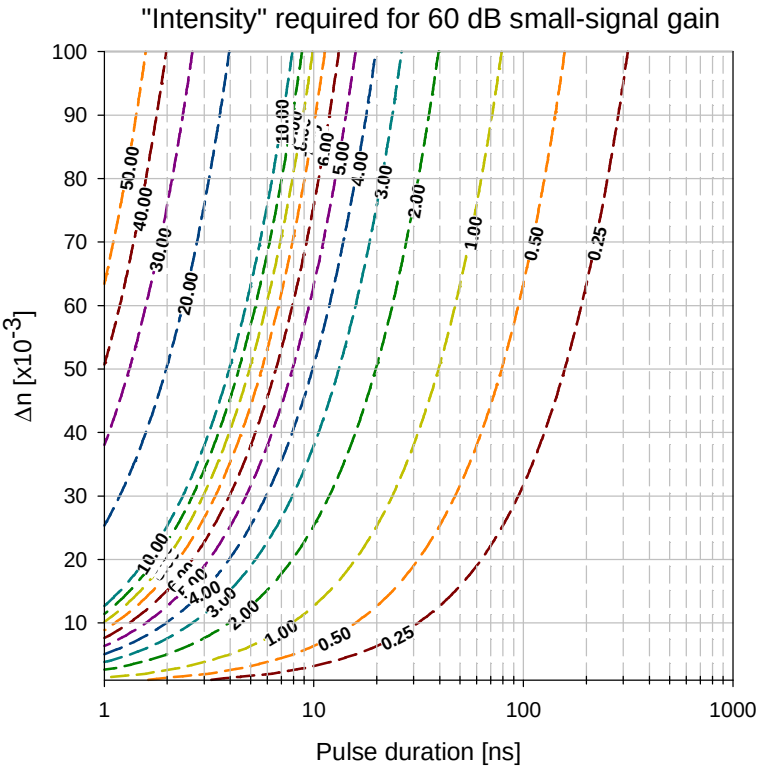

Figure 6.6: Pump intensity in [W/μm^2], relative to the joint effective area required for 60 dB of small-signal gain.

If the maximum pump effective diameter of the DCRF is about 20 μm and the cladding-core NA corresponds to a 27×10^{-3} refractive index difference, less than 78 W of peak power is required for a 100 ns pulse in order to reach a gain of 60 dB. It should be possible to reach an even higher gain using higher peak power pulse. Such a high gain from a single-stage amplifier is clearly an interesting feature worth investigating.

6.4.3 Critical pump power for first and second-order Stokes

The term pump critical power, defined in [27], is commonly used to determine the launched pump power required to obtain an equal amount of pump and Stokes output power, in an unseeded amplifier of a given fibre length, under the assumption of an undepleted pump. While this is an intrinsically inconsistent assumption, the critical power in the presence of pump depletion is only marginally different.

The critical pump power for the first Stokes line, as a function of the fibre core-cladding refractive index difference and the pulse duration is shown in figure 6.7. Here, for simplicity, the fibre length is fixed to the walk-off length.

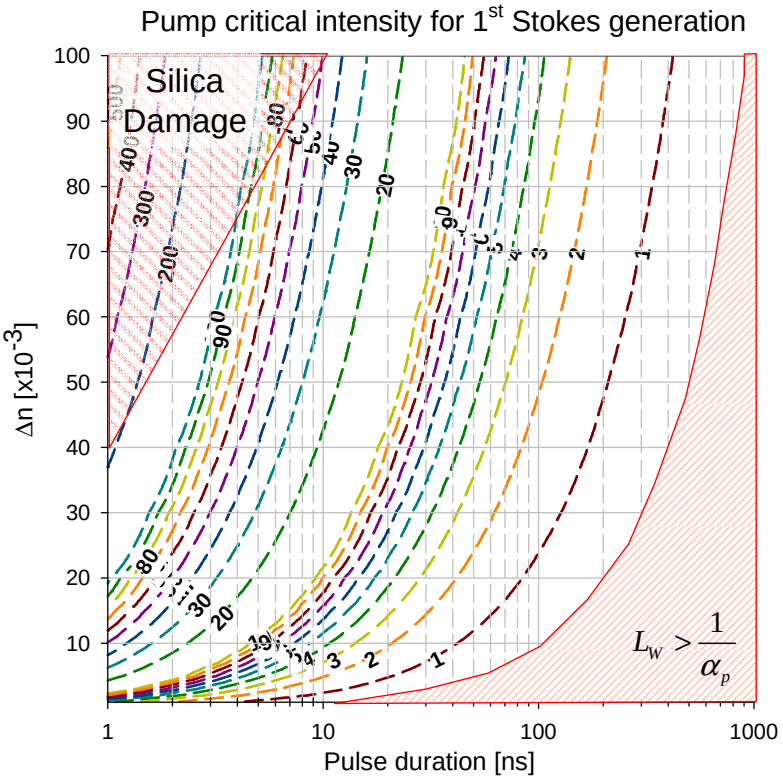

Figure 6.7: Pump critical intensity in [W/μm^2] for the first Stokes line generation in a cladding pumped Raman amplifier with a 1 mW seed.

The pump critical intensities are calculated by solving equations (6.7) - (6.9). The signal and pump background losses are also set to 2.3 dB/km as per the double-clad Raman fibre, F71-LF11. The amplifier Stokes seed is set to be 1 mW and the other modes modelled with an equivalent noiser input power. The general rule is to set the power of each mode to one photon per second per hertz per polarization mode within the equivalent bandwidth. As the number of modes increases with the fibre NA, so does the total equivalent input noise power.

The top left shaded area defines, approximately, the region where silica damage should occur for the pump intensity. This is mainly for indication purpose only, because the intensity of the Stokes could be higher than the pump intensity after amplification. The right hand side region indicates where the walk-off length is longer than the maximum effective length (the inverse of the pump background loss). In this region, an increase of the fibre length, made possible by longer pulse duration, no longer contributes to SRS because of the increased overall background loss.

Then, in the same configuration, with the same parameters, the pump intensity required for the output first Stokes power to be equal to the second Stokes power, is shown in fig. 6.8. Here, the second Stokes wave builds up from the thermal noise.

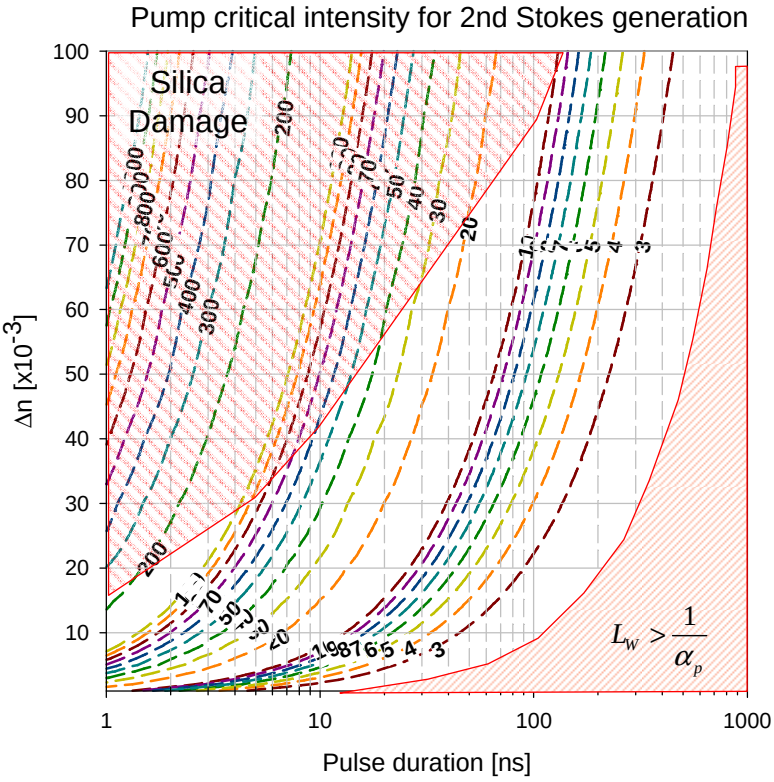

Figure 6.8: Pump critical intensity in [W/μm^2] for the second Stokes line generation in a Raman amplifier with a 1 mW seed at the first Stokes.

The operating region, in which the second Stokes line is obtained, is much narrower than that of the first Stokes, due to the increased demand on the pump power. In the case of a 100 ns long pulse, the minimum pump intensity is about 3 - 3.5 W/μm^2 in a 1.1 km long fibre. In a double-clad Raman fibre, this also depends on the pump and Stokes joint effective area so the critical

pump peak power will be typically between 100 and 300 W before the second Stokes becomes too important.

6.4.4 Pulse damage threshold

The maximum intensity that can be launched into a silica fibre is limited by the material damage [28]. This threshold intensity depends on the operating wavelength and the pulse duration. Typically, the damage threshold is taken to be proportional to the square root of the pulse duration [29]. Figure 6.9 shows that very high peak power pulses could be used to generate SRS in a multi-mode fibre, as calculated from [29]. However, because of the brightness enhancement process, the Stokes intensity could may well exceed that of the pump and then damage the fibre. Finally, the maximum energy (assuming square shaped pulses) that can be launched into a 20 μm diameter fibre is also shown to illustrate the potential of the DCRF to get higher energy pulses from a Raman amplifier. The damage threshold energy increases with the square root of the pulse duration, insofar as the (approximate) square-root law holds for the damage threshold intensity.

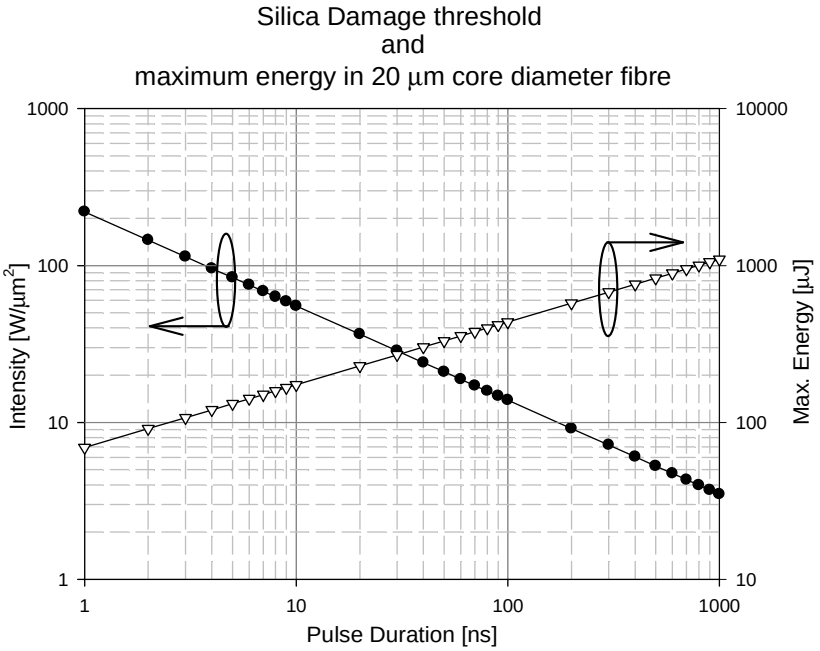

Figure 6.9: Silica damage threshold and maximum energy in a 20 μm diameter fibre for a range of pulses duration.

6.5 Summary

The characteristics of the double-clad Raman fibre used in this work, was presented early in this chapter. Around 1550 nm, the fibre has a Raman gain coefficient around 0.55 10^{-13} m/W and the background loss is around 2 dB/km for the inner-cladding, and 2.3 dB/km for the core. Then, the theory of SRS in multi-mode fibre was presented and was extended to form a theoretical framework which describes the behaviour of cladding-pumped Raman fibre, in the cw and the pulsed (quasi-cw) regime.

In the cw regime, an analysis of the propagation equations (6.1) - (6.3) of the various pump and signal modes revealed that pump modes can be collectively described by a power distribution which depends on the pump modal excitation and mode coupling mechanisms. This power distribution is represented by a joint effective area with the Stokes fundamental mode. From this joint effective area, the laser threshold can be derived and numerical simulation can be easily be implemented without exact knowledge of the pump power decomposition.

In the pulse regime, only the quasi-cw regime is studied because of the limitation on the available pump sources to perform experimental work. The quasi-cw regime is limited by the pump and Stokes pulse walk-off effect which causes pulses broadening and limits the conversion efficiency. The pulse walk-off effect depends on the numerical aperture of the double-clad fibre and on the pump pulse duration. It also defines a maximum permissible device length, called walk-off length, over which the pump and Stokes pulses are temporally coincident. In addition, the transverse dimension of the fibre leads to a minimum pump intensity required to reach SRS threshold. This intensity depends on the joint effective area which can be altered by the fibre design, i.e. core and cladding dimension and core numerical aperture. Still, as expected, the simulation indicates that short pulses require much higher peak power because of the shorter walk-off length. With high peak power, short pulses, the first Stokes in the low-order mode grows faster and the threshold for the second order Stokes can be reached quickly. Therefore the fibre length must be tailored for the pump properties in order to avoid, if undesired, the second order Stokes. Finally, additional consideration for pulse damage threshold was also discussed that let foresee potential for high energy output.

6.6 References

[1] R. H. Stolen, E. P. Ippen, and A. R. Tynes, "Raman oscillation in glass optical waveguide", Appl. Phys. Lett. **20**, 62 (1972).

[2] F. Capasso and P. Di Porto, "Coupled-mode theory of Raman amplification in lossless optical fibers", J. Appl. Phys., **47**(4), 1472 (1976).

[3] K. X. Liu and E. Garmire, "Role of stimulated four-photon mixing and efficient Stokes generation of stimulated Raman scattering in excimer-laser-pumped UV multimode fibers", Opt. Lett. **16**(3), 174-6 (1991).

[4] K. S. Chiang, "Stimulated Raman-Scattering in a Multimode Optical Fiber - Evolution of Modes in Stokes Waves", Opt. Lett. **17**(5), 352-354 (1992).

[5] K. S. Chiang, "Stimulated Raman scattering in a multimode optical fiber: self-focusing or mode competition?", Opt. Commun. **95**(4-6), 235 (1993).

[6] R. S. F. Chang, R. H. Lehmberg, M. T. Duignan and N. Djeu, "Raman Beam Cleanup of a Severely Aberrated Pump Laser", IEEE J. Quantum Electron. **QE-21** (5), 477 (1985).

[7] J. T. Murray, W. L Austin and R. C. Powell, "Intracavity Raman conversion and Raman beam clean up", Opt. Mater. **11**(4), 353-371 (1999).

[8] T. Russell, S. M. Willis, M. B. Crookston and W. B. Roh, "Stimulated Raman scattering in multimode fibers and its application to beam clean up and combining", J. Nonlinear Opt. Phys. Mater. **11**(3), 303 (2002).

[9] I. K. Ilev, H. Kumagai, and K. Toyoda, "Widely tunable (0.54-1.01μm) double-pass fiber Raman laser", Appl. Phys. Lett. **69**(13), 1846 (1996).

[10] S. T. Davey, D. L. Williams, B. J. Ainslie, W. J. M. Rothwell, and B. Wakefield, "Optical gain spectrum of GeO_2-SiO_2 Raman fiber amplifiers", Proc. Inst. Elect. Eng. **136**(6), 301–306 (1989).

[11] J. Bromage, K. Rottwitt, and M. E. Lines, "A Method to predict the Raman gain Spectra of germanosilicate fibers with arbitrary index profiles", IEEE Photon. Technol. Lett. **14**(1), 24 (2002).

[12] C. Fukai, K. Nakajima, J. Zhou, K. Tajima, K. Kurokawa, and I. Sankawa, "Effective Raman gain characteristics in germanium- and fluorine-doped optical fibers", Opt. Lett. **29**(6), 545 (2004).

[13] Y. Kang, Master Thesis, *Calculations and Measurements of Raman Gain*, (Virginia Polytechnic Institute and State University, 2002).

[14] M. M. Bubnov, S. L. Semjonov, M. E. Likhachev, E. M. Dianov, V. E. Khopin, M. Y. Salganskii, A. N. Guryanov, J. C. Fajardo, D. V. Kuksenkov, J. Koh, and P. Mazumder, "On the origin of excess loss in highly GeO_2-doped single-mode MCVD fibers", IEEE Photon. Technol. Lett. **16**(8), 1870 (2004).

[15] E. M. Dianov, "Advances in Raman fibers", J. Lightwave Technol. **20**(8), 1457 (2002).

[16] R. H. Stolen and J. E. Bjorkholm, "Parametric Amplification and Frequency Conversion in Optical Fibres", IEEE J. Quantum Electron. **18**(7), 1062 (1982).

[17] S. J. Garth and R. A. Sammut, "Theory of stimulated Raman scattering in two-mode optical fibers", J. Opt. Soc. Am. B **10**(11), 2040 (1993).

[18] G. P. Agrawal, *Nonlinear Fiber Optics*, (2nd Ed. Academic Press Inc, San Diego CA, 1995).

[19] J. Auyeung and A. Yariv, "Theory of a Cw Fiber Raman Oscillator", J. Opt. Soc. Am. **68**(10), 1383 (1978).

[20] C. A. Codemard, P. Dupriez, Y. Jeong, J. K. Sahu, M. Ibsen, and J. Nilsson, "High-power continuous-wave cladding-pumped Raman fiber laser", Opt. Lett. **31**(15), 2290-2292 (2006).

[21] M. B. Crookston, Master's Thesis, *Single-mode Raman fiber laser in a multimode fiber*, (Air Force Institute of Technology Wright-Patterson, March 2003).

[22] A. Kuhn, I. J. Blewett, D. P. Hand, and J. D. C. Jones, "Beam quality after propagation of Nd : YAG laser light through large-core optical fibers", Appl. Opt. **39**(36), 6754 (2000).

[23] X. Liu, H. Zhang and Y. Guo, "A Novel Method for Raman Amplifier Propagation Equations", IEEE Photon. Technol. Lett., **15** (3), 392 (2003).

[24] A. P. Liu and K. Ueda, "The absorption characteristics of rare earth doped circular double-clad fibres", Opt. Rev. **3**(4), 276-81 (1996).

[25] R. H. Stolen and A. M. Johnson, "The Effect of Pulse Walkoff on Stimulated Raman Scattering in Fibers", IEEE J. Quantum Electron. **QE-22** (11), 2154 (1986).

[26] A. W. Snyder and J. D. Love**,** *Optical Waveguide Theory*, (Chapman & Hall, London, 1983).

[27] R. G. Smith, "Optical power handling capacity of low-loss optical fibers as determined by stimulated Raman and Brillouin scattering", Appl. Opt. **11**(11), 2489–2494 (1972).

[28] A. -C. Tien, S. Backus, H. Kapteyn, M. Murnane, and G. Mourou, "Short-Pulse Laser Damage in Transparent Materials as a Function of Pulse Duration", Phys. Rev. Lett. **82**(19), 1999 (19).

[29] B. C. Stuart, M. D. Feit, S. Herman, A. M. Rubenchik, B. W. Shore, and M. D. Perry, "Nanosecond-to-femtosecond laser-induced breakdown in dielectrics", Phys. Rev. B **53**(4), 1749 (1996).

Chapter 7 High-power continuous-wave cladding-pumped Raman fibre lasers

This chapter contains my work on continuous-wave cladding-pumped Raman fibre laser sources. Firstly, section 7.1 reviews some previous work on multi-mode Raman fibre laser and recalls the motivations for this study. Then, section 7.2 and 7.3 present the experimental realisation and study of counter and co-pumped DCRF lasers. The lasers characteristics are presented and discussed. Subsequently, the properties and limitations of these lasers are discussed in section 7.4. Section 7.5 presents possible improvements to increase the output power and enhance the laser efficiency. Finally, section 7.6 summarises the findings of this chapter.

7.1 Introduction

Recently, Baek and Roh presented a low power single mode Raman fibre laser based on a multi-mode fibre [1] with a $M^2 \sim 1.66$. The laser consisted of a 40 m long, 50 μm core diameter fibre with two broadband FBGs written in the multi-mode fibre to form the laser cavity. The laser slope efficiency was quite low at only ~ 7.3%. At the same time, Nilsson and co-workers have proposed a cladding-pumped (i.e. multi-mode) Raman fibre [2]. By comparison to standard multi-mode fibre, in a double-clad fibre, the mode definition is greatly improved by the use of a single-mode core which is embedded inside the multi-mode waveguide structure which carries the pump power, similarly to rare-earth doped fibre lasers. As discussed in Chapter 1, cladding-pumped fibre lasers provide many advantages and are especially very good for power scaling purposes. However, a high power cladding-pumped Raman fibre laser had never been demonstrated, nor investigated. The critical parameters, for a good laser performance, still remain to be identified for this new class of fibre laser.

7.2 Counter-pumped DRCF laser

7.2.1 Experimental set-up

In this experiment, a cladding-pumped Raman fibre laser is realised with a counter-propagating pump (with respect to the laser output). The experimental set-up is shown in figure 7.1 and consists of a multi-mode Er:Yb co-doped fibre laser (EYDFL) pump source and a Raman fibre laser based on a DCRF. The fibre laser pump source consists of a 2.5 m long Er:Yb co-doped fibre (F196-LF59), fabricated at the ORC, which is cladding-pumped by a multi-mode laser diode stack source at 975 nm from Laserline GmbH. The EYDF has a 25 μm diameter, 0.22 NA core, and a 400 μm diameter D-shaped inner cladding, surrounded by a polymer outer cladding of low refractive index. With a V-number of 22, the fibre output is well multi-mode and the expected M^2 is 7.8 for a free-running laser. The EYDF laser output power was up to 26 W at 1545 nm. As there were no wavelength-selective elements in the EYDFL, the operating wavelength was determined by the Er-spectroscopy and the ion inversion (which depends on the Er-concentration, fibre length, and Er gain level). The fibre laser output is free-space coupled into a 1.42 km long double-clad Raman fibre via a dichroic mirror. The presence of defective regions in the length of fibre means that the average background loss of the core region is 3.1 dB/km whilst in the inner-cladding this loss is 2.3 dB /km, i.e., somewhat higher than the loss measured in defect-free regions.

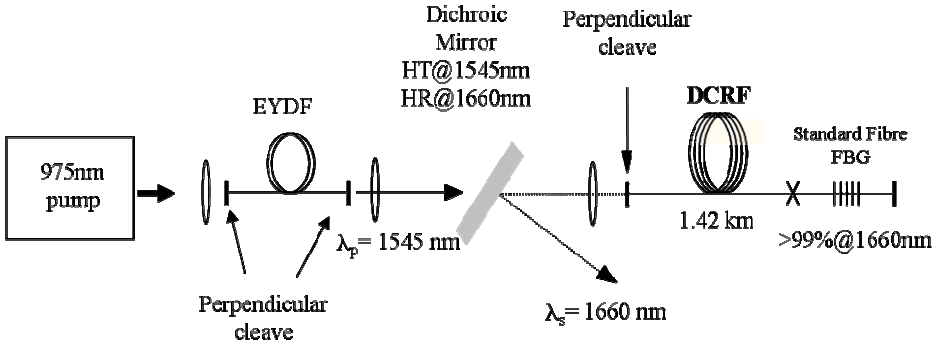

Figure 7.1: Experimental set-up of the counter-pumped DCRF laser.

A cutback measurement shows that up to 55% of the EYDFL's output power could be launched into the DCRF. Of the launched power, around 6.8% is the LP_{01} mode. This was evaluated by splicing a standard single-mode fibre to a short piece of DCRF. In the DCRF, the 1545 nm pump beam generates Raman gain with a peak at ~1658 nm. The Raman laser cavity is formed by a perpendicularly cleaved, 4% reflecting, facet at the pump launch end, and a fibre Bragg grating spliced to the DCRF, at the other end of the fibre. The reflectivity of the grating is

> 99% at 1660 nm with a bandwidth less than 0.2 nm. The transmission spectrum of two cascaded gratings in the same piece of DCRF is shown in figure 7.2.

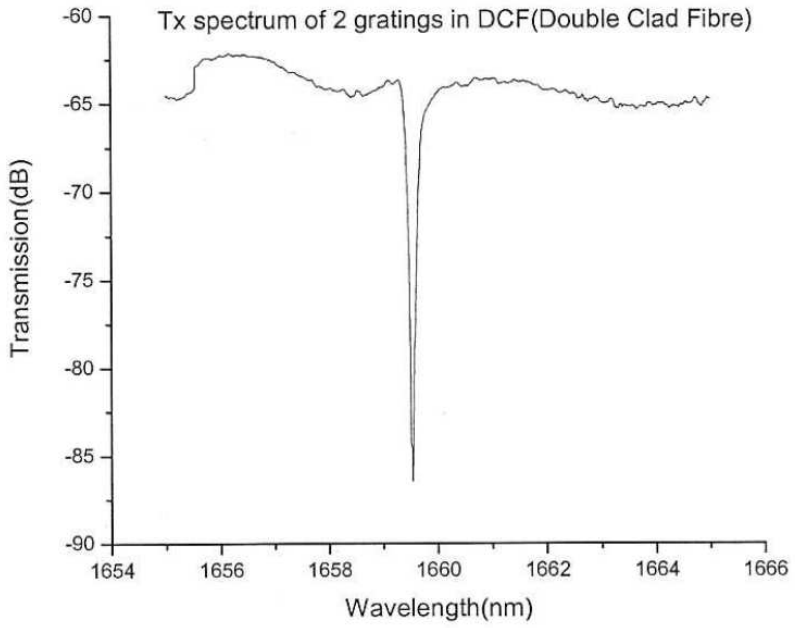

Figure 7.2: Transmission spectrum of two cascaded grating written in the DCRF.

Unlike in a conventional rare-earth doped double-clad fibre, Raman gain occurs both in the inner cladding and the core of the DCRF. Therefore, core-mode lasing must be promoted over any cladding-mode lasing. Here, a fibre Bragg grating selected the core mode in a similar way to [1]. However, because the inner-cladding is also germanium-doped and is photosensitive, a grating is quite likely to have been formed in it. Because the Bragg wavelength of the grating is proportional to the effective refractive index of the propagating mode [3], higher order modes, which have lower effective indices than the LP_{01} mode, are reflected at shorter wavelength. In the DCRF the number of modes is relatively small. Consequently, the modes are sufficiently spaced in refractive index for their Bragg wavelengths to be a few nanometres apart. Therefore, any reflections from higher order modes would be very distinct from the LP_{01} mode and easily identifiable from the output optical spectrum.

7.2.2 Laser characteristics

Figure 7.3 shows the Raman laser output power versus the launched pump power (at 1545 nm). The laser threshold is measured to be around 7.1 W and the slope efficiency is 67% which is quite remarkable taken into account the fibre background loss. The maximum output

power is 3.4 W at 1660 nm for a 27% power conversion of launched pump power. Here, the output power is limited by the pump power.

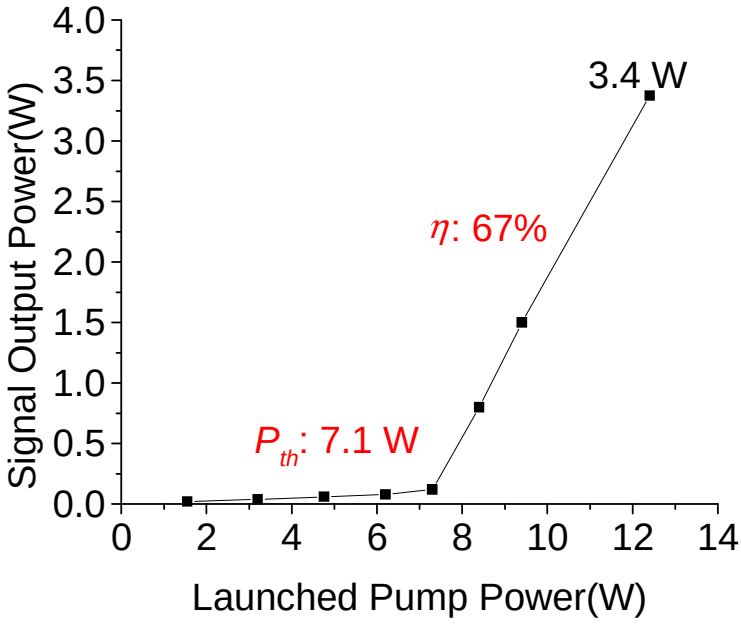

Figure 7.3: DRCF laser output power.

Using Eq. (6.12) with the experimental parameters given above and with the DCRF's Raman gain coefficient, the laser threshold becomes 7.2 W for a joint effective area of 150 μm^2. Note that the average value of a joint effective area is 184 μm^2 from Table 6.2. Thus this value of 150 μm^2 is quite reasonable because the modal excitation is not known exactly.

Figure 7.4 shows the output spectrum of the cladding-pumped CW Raman fibre laser at maximum output power. The signal spectrum is very clean and some pump is reflected from the end-facet. As discussed previously, the narrow laser linewidth indicates that no cladding modes are presents. The output beam quality was not measured in this experiment but single mode operation is expected. Furthermore, no second order Stokes is present in the laser. This agrees with the rough estimation given earlier, which places the threshold above 16 W of output power. Nonetheless, the laser fibre length must be tailored for the pump power and signal/pump background loss in order to achieve the best performance, and in particular to avoid higher second-order Raman scattering at high output powers.

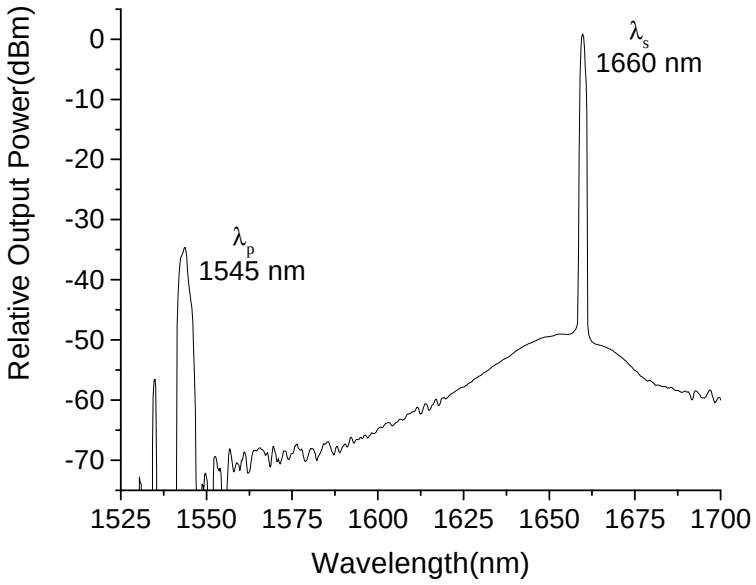

Figure 7.4: DRCF laser output spectrum (resolution 1 nm).

7.3 Co-pumped DCRF laser with true single-mode output

Compared to the laser presented in the previous section, here the DCRF laser is in a co-propagating pump configuration and provides a higher output power with an improved degree of brightness enhancement, from $M^2 \sim 8.5$ to a diffraction-limited beam, using an output port made of a standard single-mode fibre.

7.3.1 Experimental set-up

The experimental set-up, shown in figure 7.5, consists of a high-power continuous-wave pump source at 1552 nm and an all-fibre cladding-pumped Raman laser. The pump source is a two-stage fibre master-oscillator power-amplifier (MOPA) based on Er:Yb co-doped fibre amplifiers (EYDFAs). The seed source of the MOPA consists of a high-power tuneable fibre ring laser which uses a commercial 2 W EYDFA from Southampton Photonics, and a tuneable fibre Bragg grating made in-house, and attached to a circulator. The ring laser is set to an output power of 1.4 W at 1552 nm. The linewidth of the ring laser is large enough (0.2 nm) to avoid any stimulated Brillouin scattering in the relatively long Raman fibre laser. The seed from the ring-laser is then, free-space launched into a 4 m long large-core high-power EYDFA. The Er:Yb doped fibre in the power amplifier (F196-LF59) has a core diameter of 35 µm and a NA of 0.2. The inner-cladding is D-shaped. The diameter is 650 µm and the NA of the pump waveguide is 0.48, as determined by a low-index polymer coating. This diameter and NA allows

for a good pump coupling of our diode pump source. The high-power EYDFA is end-pumped by a high-power diode stack source at 972 nm (Laserline GmbH), launched through the signal input end. Both end-facets of the large-core EYDF are angle-polished to suppress any back-reflections into the amplifier.

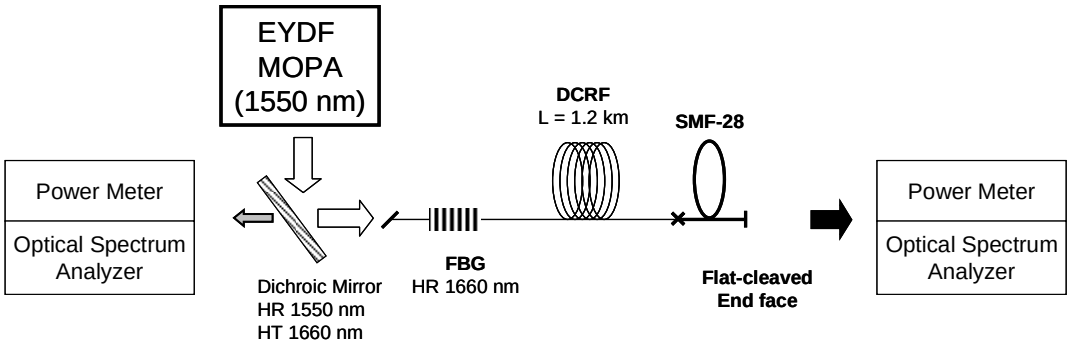

Figure 7.5: Experimental set-up of the co-pumped cladding-pumped Raman fibre laser.

An output power in excess of 35 W is obtained from the MOPA, as shown in figure 7.6, with a clean spectrum (fig. 7.6 inset). The EYDF must be relatively short to obtain the 1552 nm emission wavelength required in this experiment. The slope efficiency of the high-power EYDFA is somewhat low, 21%. It may be because of higher then expected background losses in the EYDF.

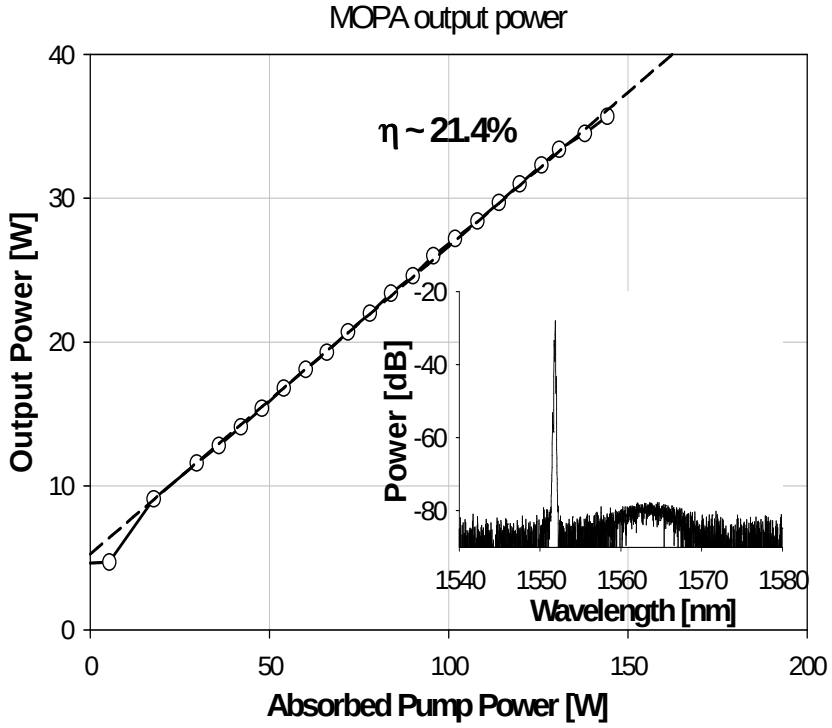

Figure 7.6: Multi-mode fibre MOPA output power and optical spectrum (inset).

The output beam quality of the MOPA corresponds to an M^2 of ~ 8.5, because of the multi-mode nature of the EYDF. The output beam is free-spaced launched into the DCRF via a set of lenses. It would also be possible to splice the EYDF directly to the DCRF, but because of the core size mismatch this was not attempted. The remaining unabsorbed pump power at 972 nm is removed by a dichroic mirror, so it is not launched into the DCRF. The 1552 nm pump beam is reflected by a dichroic mirror which transmits wavelengths longer than 1650 nm, before being launched into the inner cladding of the DCRF, through an angle-cleaved end. About 60% of the 1552 nm pump is launched into the DCRF.

The Raman gain medium consists of a 1.2 km long piece of the same DCRF as before, but with lower loss. Now, the inner-cladding loss is 2 dB/km and the core loss is 2.3 dB/km[4]. The DCRF output end is spliced to a 1 metre long piece of SMF-28. A high-index gel is used to strip all the unwanted modes and also to protect the high-index coating of the single-mode fibre. The splice loss for the core mode is evaluated to be less than 0.5 dB from equation (2.12), while all other modes are lost at this point to un-guided radiation modes. The Raman laser cavity is formed with a narrowband (~0.4 nm) highly-reflective FBG at 1660 nm, written in the core of the DCRF, placed at the 1552 nm pump launch end, and a laser output coupler formed by a flat cleave in the SMF-28 fibre. The highly reflective FBG has a reflection of 80% at 1660 nm. Thus, some leakage from the Raman laser in the backward direction is expected. Therefore, a protective dichroic mirror is used to prevent the 1660 nm radiation from being fed upstreams into the MOPA. The transmission spectrum of the grating is shown in figure 7.7. It was measured with an OSA by injecting a broad linewidth signal into the core of the DCRF.

[4] In this experiment (alone), the background of the DCRF is lower than previously. Indeed, using a high resolution optical time-domain reflectometer, several small sections of the DCRF were found to be defective (most likely because of the high-germanium concentration). Subsequently these sections were removed and the fibre re-spliced which reduced the overall background of the fibre after re-measurement.

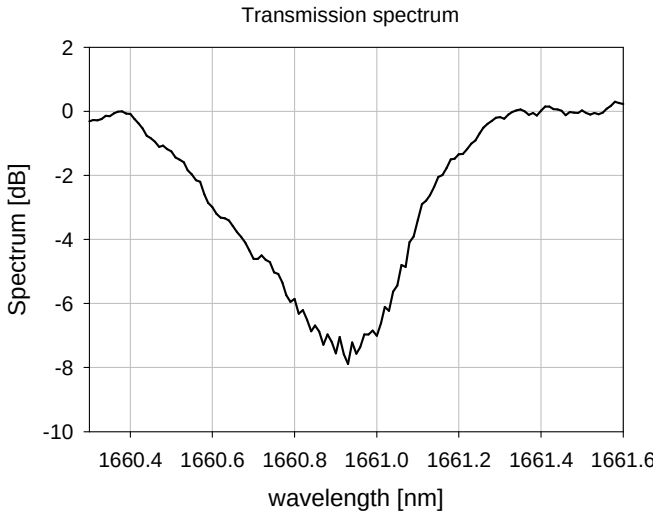

Figure 7.7: Transmission spectrum of the FBG written in the core of the DCRF.

7.3.2 Laser characteristics

7.3.2.1 Single-ended output power

The output power from the cladding-pumped Raman fibre laser through the SMF-28 output end is shown in figure 7.8 for a 1.2 km, 1 km and 0.85 km long cavity. The general performance is similar to the earlier work for the 1.2 km long fibre. The laser slope efficiency is 67% and the conversion efficiency is close to 48% at the maximum power About 10.2 W of output power is obtained for 21.4 W of launched pump power. Here, the thermal loading of the DCRF launch end can cause some misalignment of the launch optics and, therefore, limits the launched pump power.

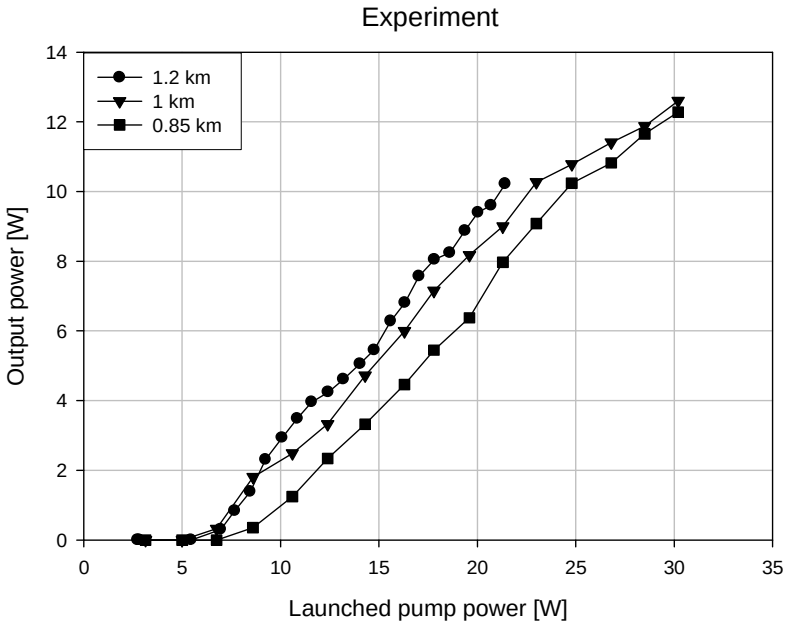

Figure 7.8: Experimental results – single-mode, DCRF laser output power for 1.2, 1.0 and 0.85 km lengths of fibre.

A roll-off is observed at high powers in figure 7.8 for the shorter fibre length. It could have been induced by the generation of a second-order Stokes wave. However, none could be detected when using a monochromator and a photodiode. Further investigation, using the modelling of the DCRF laser shows, that the roll-off can be explained by the the non-linear pump absorption. A simple simulation of a 1 km long DCRF laser, shown in figure 7.9, exhibits the same behaviour when the output power is plotted versus the launched pump power. In the experiment it is not possible to measure the absorbed pump power because of the single-mode fibre attached at the end of the laser cavity. Because of the non-linear absorption, the absorbed pump power can increase quicker than the launched pump power over a limited range of pump powers (near the laser threshold). As a result, the output power of the laser seems to roll-off.

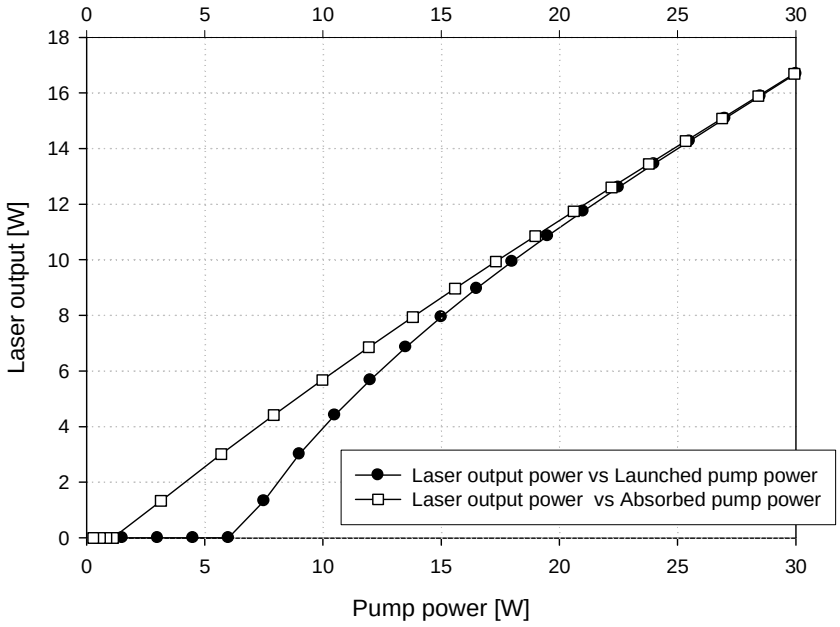

Figure 7.9: Comparison, by simulation, of a single-mode DCRF laser output power with respect to the launched (●) and absorbed (□) pump power. The fibre is 1 km long.

The non-linear pump absorption also occurs in the laser with shorter cavity length. The laser threshold and slope efficiency of the different cavity lengths are shown in Table 7.1.

DCRF Length [m]	Laser slope efficiency [%]	Laser threshold [W]	Calculated threshold for the 2nd Stokes [W]
1200	67	6.1	20.9
1000	60.8	6.4	23.9
850	61.7	8.73	27.2

Table 7.1: DCRF laser threshold and slope efficiency

Clearly the threshold is behaving as expected, it increases as the fibre length decreases as there is more SRS gain for a given pump power. However, the experimental measurement of the slope efficiency is not clear because of the non-linear pump absorption. Indeed, as the cavity becomes shorter, there are less intrinsic losses insides the cavity, i.e., background loss, thus the slope efficiency should increase. This is confirmed by the numerical simulation of the single-mode DCRF laser shown in figure 7.10.

The simulation assumes a cladding loss of 2 dB/km at the pump wavelength and a core background loss of 2.3 dB/km at the Stokes wavelength. The laser cavity is formed by an 84% and a 4% reflective grating. The cavity is co-pumped with 20% of pump power in the core while the rest of the pump power is in the cladding with a corresponding average effective area of about 184 μm^2. Here the slope efficiency increases as the fibre becomes shorter.

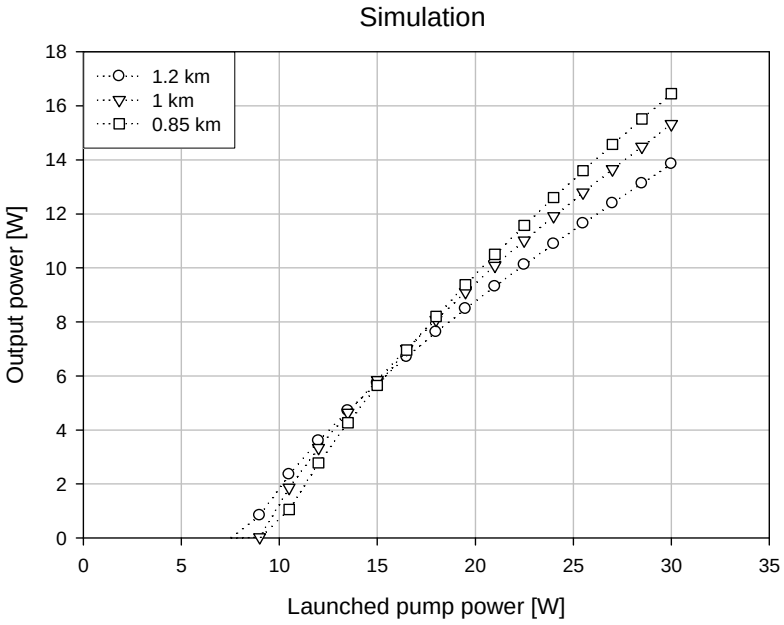

Figure 7.10: Simulation – single-mode, DCRF laser output power for 1.2, 1.0 and 0.85 km lengths of fibre.

This discrepancy is attributed to some experimental errors which might have been caused by some feedback from the DCRF laser into the final EYDFA, which can perturbed the pump power effectively launched in the double-clad fibre.

7.3.2.2 Dual-ended output power

The limited reflectivity of the FBG at the pump launch end leads to a significant amount of output power being lost at this point. Including this lost power, the total slope efficiency of the laser is in fact 84% with a conversion efficiency of 60% in a 1200 m long DCRF laser as shown in figure 7.11.

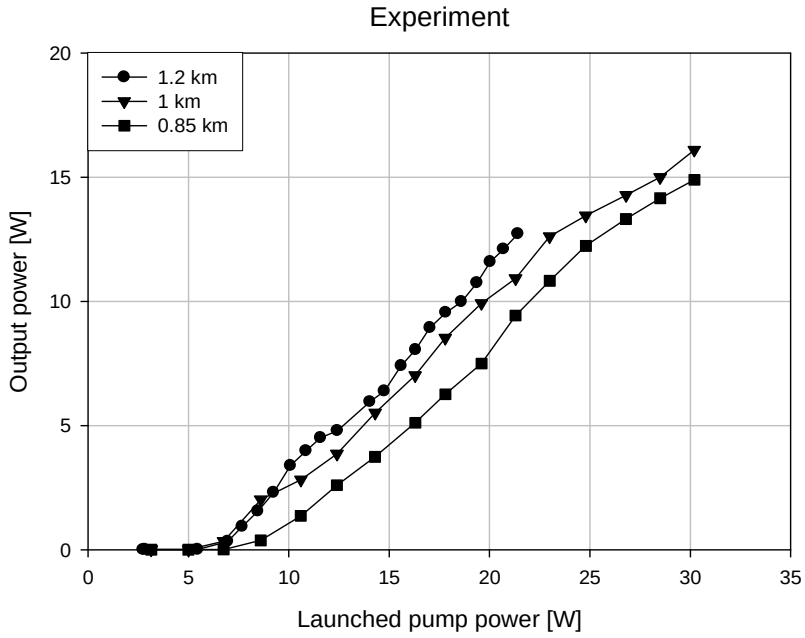

Figure 7.11: Experimental results – Total output power from the DCRF laser for 1.2, 1 and 0.85 km lengths of fibre.

The details of the dual-ended laser performance are presented in Table 7.2.

DCRF Length [m]	Laser slope efficiency [%]	Laser threshold [W]
1200	84	6
1000	70	6.54
850	72	8.65

Table 7.2: Dual ended DCRF laser threshold and slope efficiency

As expected, the thresholds measured are, within error margins, the same for single-ended and dual-ended output.

In figure 7.12, the simulation of the combined power from the single-mode end and from the pump launched end is presented for the three fibre lengths used in the experiment. Again, it is worth noticing that in this laser configuration the laser exhibits two slope efficiencies: one directly above the threshold which is about 91% for the 1.2 km fibre while it drops to around 54% for high powers. This is because of the non-linear pump absorption discussed previously.

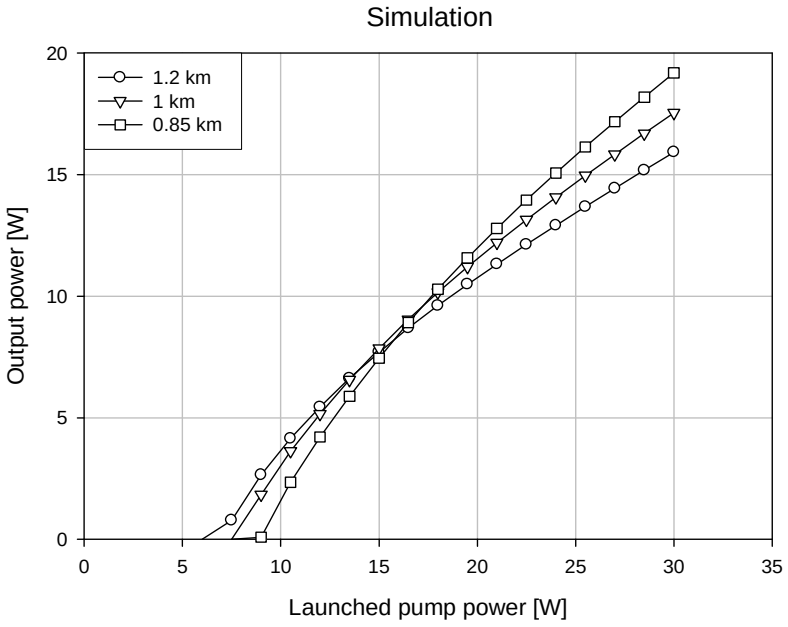

Figure 7.12: Simulation – Total output power from the DCRF laser for 1.2, 1 and 0.85 km lengths of fibre.

In fact, when the total power of the DCRF considered, clearly the laser is highly efficient and considering the background loss, the double-ended slope efficiency is very close to the quantum limit. This demonstrates that cladding-pumped Raman fibre lasers can be exceptionally efficient with a lower background loss and that with a stronger grating in the DCRF, a higher single-ended output power is expected.

7.3.2.3 Brightness enhancement

A main attraction of a cladding-pumped device is the increase in brightness of the signal laser compared to that of the pump. In order to measure the effectiveness of the brightness conversion, a brightness enhancement factor η_B can be defined simply as the ratio of the signal (here Stokes) brightness over the pump brightness:

$$\eta_B = \frac{B_{signal\_out}}{B_{pump\_in}} = \frac{P_{signal\_out}}{P_{pump\_in}} \left(\frac{M^2_{pump\_in}.\lambda_{pump\_in}}{M^2_{signal\_out}.\lambda_{signal\_out}} \right)^2 \tag{7.1}$$

In the case of the DCRF, the maximum power is about 12.5 W at 1660 nm ($M^2 = 1$) for 30 W of launched pump at 1545 nm ($M^2 \sim 8.5$), so the brightness is improved by 26 times. The brightness enhancement depends on the power conversion efficiency and the refractive index profile. The refractive index profile, by and large, determines the improvement in beam quality.

However, the refractive index profile is also intrinsically linked to the efficiency, as this depends on the overlap (the geometry of the refractive index distribution) and signal background loss, which depends on the value of the refractive index. By comparison a single-mode fibre will have $\eta_B < 1$ because of various system losses and because of the conversion to longer wavelengths. Thus a single-mode SRS source sees a reduction of brightness of the signal with respect to the pump of at least, $\left(\frac{\lambda_p}{\lambda_s}\right)^3$. At the other end of the spectrum, rare-earth doped fibres are excellent brightness converters because of high signal gain per unit length (or energy transfer), even when a large cladding is used. For example in [4], Jeong and co-workers have demonstrated a 1.36 kW single mode output from a cladding-pumped fibre laser whose inner-cladding had diameter of 650 μm for a numerical aperture of 0.48. If one assumes that the fibre cladding is completely filled and taking into account the power conversion of 83%, the brightness enhancement factor is roughly ~ 1.5 10^5.

7.3.2.4 Spectral characteristics

The forward optical spectra, emitted from the single-mode fibre end, are measured at each power level. The spectra, corresponding to the maximum output power and close to the laser threshold, are shown in figure 7.13 with a 1 nm resolution. When the output power increases, the remaining pump power in the single-mode core of the SMF is 18 dB lower than the laser output at 1660 nm whilst most of the un-depleted pump power in higher-order modes is lost at the splice point.

The high intensity in the fibre core can lead to the generation of a second order Stokes at the Raman gain peak at 1793 nm. However, using a monochromator, no second-order Stokes can be found. Its absence can be explained by the low reflection level from the angle-cleaved DCRF end, although at higher powers, significant second Stokes power would build up even without any feedback.

A broadening of the Raman fibre laser linewidth at the full-width half-maximum from 0.5 nm (near the threshold) to 2.5 nm (at the maximum output) is observed. This is caused by the combination of the high intensity in the core mode and SRS and four-wave mixing (FWM) in the Raman fibre laser [5, 6].

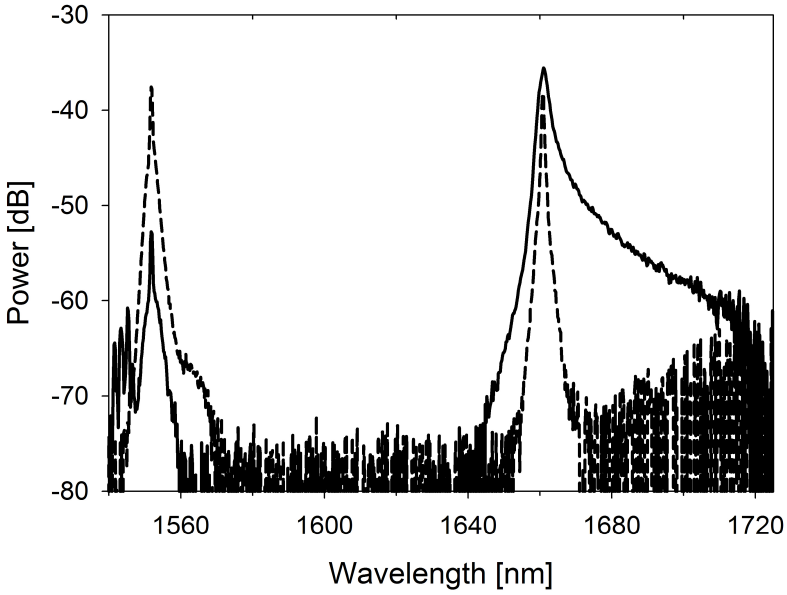

Figure 7.13: Optical spectra from the single mode fibre output at the maximum output power (solid line) and near the laser threshold (dashed line) at 1 nm resolution.s

It is well-known that because of the long interaction length and/or high intensity that is required to initiate the Raman process, especially with cladding-pumping, other non-linear effects such as FWM can also be expected [7], especially when the conversion efficiency is high. In some cases, the competition between both phenomena can lead to a bandwidth reduction of a continuous wave Raman fibre laser [8] if the FWM is induced by the SRS pump, and if the FWM gain bandwidth is larger, then the SRS shift. Here, the FWM only concerns the Stokes wave because of its higher intensity inside the laser cavity. Based on [9, 10], the broadening of the laser linewidth can be approximated by the bandwidth of the FWM parametric gain.

In the anomalous dispersion regime of an optical fibre, the FWM is phase-matched, i.e., at its maximum when the linear phase mismatch is compensated by a power-dependant non-linear contribution [11]. The phase-matching condition is:

$$2\gamma P_s = -\Delta\beta \tag{7.2}$$

Here, γ is the non-linear parameter, P_s is the Stokes power and $\Delta\beta$ the linear phase mismatch due to the waveguide and material dispersion. Furthermore, γ is defined as $\gamma = \frac{n_2^{'}\omega_P}{c.A_{eff}}$, where $n_2^{'}$ is the non-linear refractive index (typically between 2 and 2.2 10^{-20} m^2/W), ω_P is the optical

angular frequency of the Stokes beam, A_{eff} is the Stokes modal effective area and c is the speed of light in vacuum.

After a Taylor expansion of the dispersion, the linear phase mismatch can be expressed as a function of the dispersion [9]. Equation (7.2) becomes:

$$2\gamma P_s = \frac{2\pi c}{\lambda_0^2}\frac{dD}{d\lambda}(\lambda_s - \lambda_0)(\lambda_s - \lambda_{FWM})^2 = \frac{2\pi c}{\lambda_0^2}\frac{dD}{d\lambda}(\lambda_s - \lambda_0)\left(\frac{\Delta\lambda}{2}\right)^2 \tag{7.3}$$

where λ_0 is the zero dispersion wavelength of the waveguide, $\frac{dD}{d\lambda}$ is its dispersion and λ_{FWM} is the peak wavelength of the FWM process. $\Delta\lambda$ is the wavelength difference between the SRS Stokes and the FWM maximum. Because of the symmetry of the FWM, $\Delta\lambda = 2\left|\lambda_s - \lambda_{FWM}\right|$. Thus (7.3) can be rewritten such that $\Delta\lambda$ becomes:

$$\Delta\lambda = 2\sqrt{\frac{\gamma P_s}{\frac{\pi c}{\lambda_0^2}\frac{dD}{d\lambda}(\lambda_s - \lambda_0)}} \tag{7.4}$$

Now, the laser linewidth broadening under FWM can be roughly expressed as:

$$\Delta\lambda_{laser} = \begin{cases} \Delta\lambda_{laser\_no\_FWM} & if\ \Delta\lambda < \Delta\lambda_{laser\_no\_FWM} \\ 2\sqrt{\frac{\gamma P_s}{\frac{\pi c}{\lambda_0^2}\frac{dD}{d\lambda}(\lambda_p - \lambda_0)}} & if\ \Delta\lambda > \Delta\lambda_{laser\_no\_FWM} \end{cases} \tag{7.5}$$

where $\Delta\lambda_{laser\_no\_FWM}$ indicates the laser linewidth without any FWM and $\Delta\lambda_{laser}$ is the laser linewidth. Note that here the Stokes power, P_s is assumed to be constant along the fibre which is a rough approximation. Still, the experimental and theoretical linewidth, using equation (7.5), agree in a remarkable way for this power range, as shown in figure 7.14.

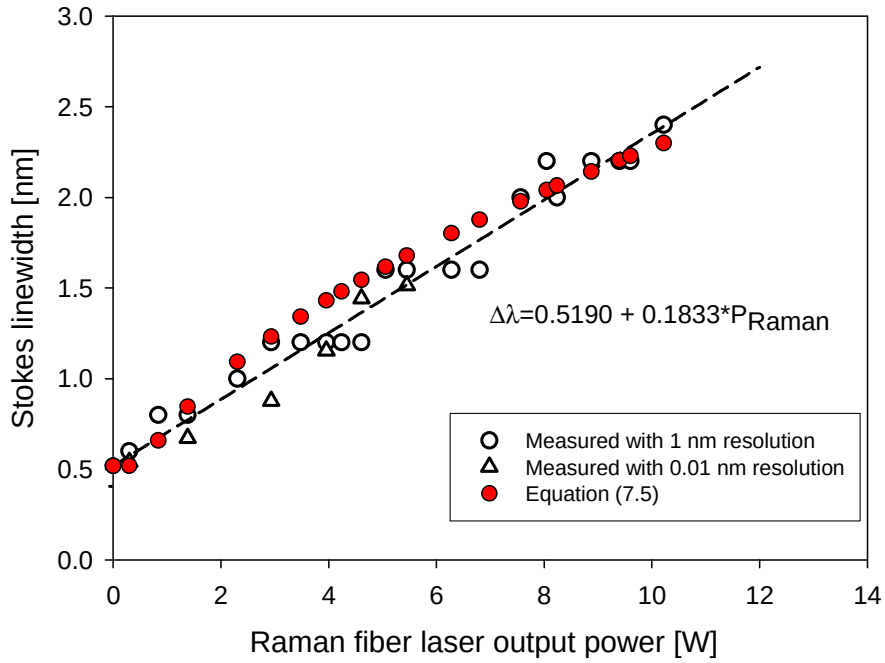

Figure 7.14: Raman linewidth vs Raman laser output power. The open symbols represent the FWHM linewidth measured with 1 nm (○) and 0.01 nm (△) resolutions, while the red circles (●) represent the estimated linewidth using eq. (7.5). The dotted line is the linear fit whose equation is shown on the graph.

In some applications, the broadening of the linewidth can be problematic. Nevertheless, FWM can be mitigated by using adequate dispersion-management, for example, with varying core parameters to disrupt the phase matching condition required.

7.3.2.5 Temporal characteristics

Although the steady-state properties of Raman fibre lasers are well-known, it is only recently that the temporal behaviour of such laser sources has been studied [12, 13]. For example, in telecom system, the transfer of the relative intensity noise from the pump to the Stokes signal degrades the signal quality by the resulting added noise [14].

In order to measure the temporal fluctuation of the output of the cladding-pumped Raman fibre laser, the signal output is fed into a fast photodiode (Thorlabs - DT210) with about 1 GHz bandwidth which is in turn connected to a RF spectrum analyser. Figure 7.15 shows the DCRF laser output, the pump (output from the EYDF MOPA) and the pump seed (EYDF ring laser) measured at several watts of output power from the DCRF laser. Clearly, the pump beam exhibits a periodic temporal fluctuation with a fundamental frequency of 7.6 MHz. This noise

comes from the longitudinal mode beating; corresponding to a round trip in the EYDF ring laser with a cavity length of 30.7 m. As expected from [14] the pump noise is transferred to the Raman laser output as shown in figure 7.15.

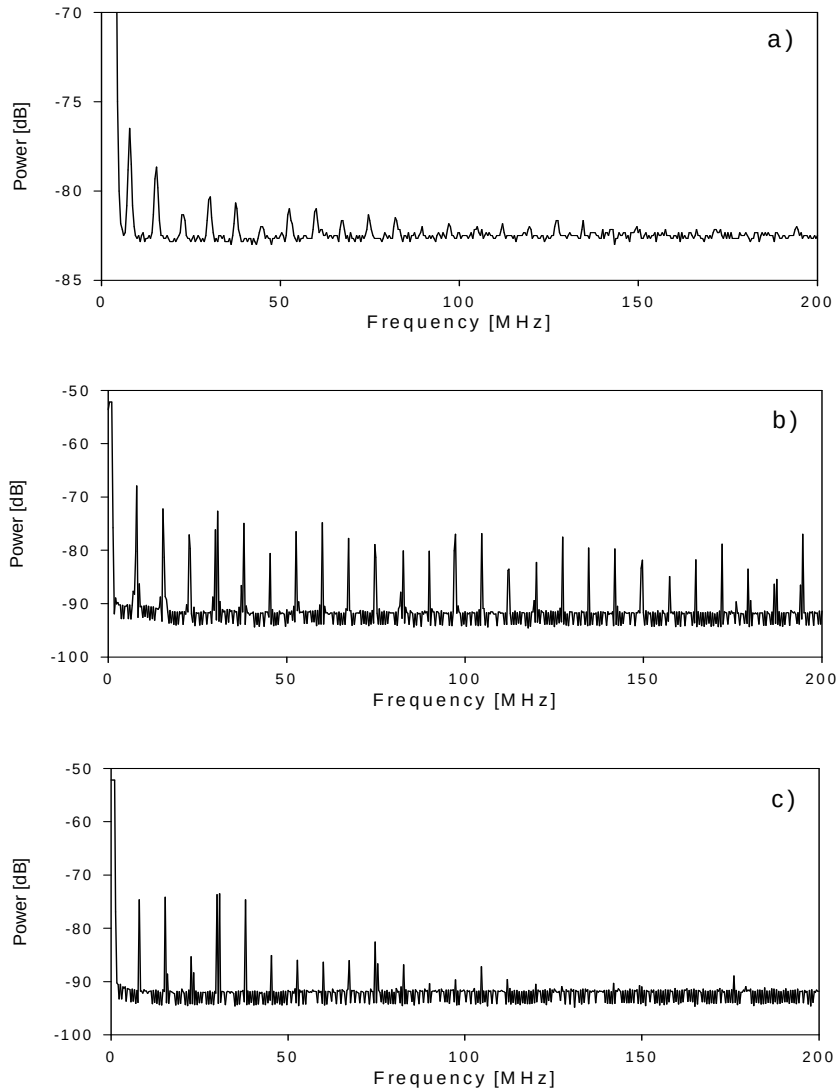

Figure 7.15: Temporal spectrum of the outputs from: a) EYDF ring laser, b) EYDF MOPA and c) DCRFL output.

In theory, it is possible to reduce the intensity noise of the pump using a less noisy laser source; however, in practice, this is not so easy. For example, a semiconductor DFB laser (like a ILX Lightwave 79800) could be used in a MOPA configuration instead of the ring laser. The narrow linewidth of a semiconductor means that SBS will arise, probably in the MOPA chain or otherwise in the DCRF. Therefore, the laser needs to be phase modulated to reach a linewidth of the order of 1 GHz. To avoid noise in the Raman laser output one would also have to avoid frequency modulation to amplitude modulation conversion effects.

If the DCRF is assumed to be relatively homogenous so that SBS linewidth has the typical value of 20 MHz, the critical pump power for SBS can be estimated using:

$$P_{Critical} = \frac{21}{L_{eff}}\left(1+\frac{\Delta\nu}{\Delta\nu_B}\right)\frac{A_{eff}}{g_B} \tag{7.6}$$

Taking the background loss to be 2dB/km for the pump, the effective length L_{eff} is then 920 m for a 1200 m long fibre, the core mode effective area A_{eff} is about 70 μm^2 in the DCRF, the SBS gain g_B has a typical value of 5.10^{-11} m/W, the SBS linewidth $\Delta\nu_B$ is about 20 MHz, while the laser linewidth $\Delta\nu$ is 1 GHz; the critical pump power $P_{Critical}$ is 1.6 W. With 40 W of pump power being launched into the DCRF and typically lower order modes containing 20% of the pump, SBS becomes a serious issue. SBS cannot be tolerated in the present set-up due to the absence of isolation between the pump fibre source and the Raman fibre laser. An alternative to semiconductor DFB lasers is to use for example a fibre laser in a linear cavity whose photon lifetime is long enough so that fluctuations is minimised [15]. However, in many cases the temporal fluctuations measured with the current set-up would be acceptable.

7.4 Limitations

7.4.1 Signal FWM

As shown in figure 7.13, the Raman fibre laser output can suffer from four-wave mixing which enlarges the spectral linewidth. In some applications this feature might not be desirable, e.g., for wavelength multiplexing or spectroscopy. The four-wave mixing process depends on the non-linear refractive index of the fibre, the waveguide dispersion and the signal intensity-length product. The non-linear refractive index n_2 is generally correlated with g_R because both are linked to material. Hence, the only practical route for reducing the FWM effect in the Raman fibre is to operate in the normal dispersion regime of the core; either by changing the operating wavelength to less than 1.3 μm, typically, or by shifting the fibre core zero-dispersion wavelength as in dispersion shifted fibre [16]. When operating at shorter wavelength, standard single mode fibre tends to have a small core diameter. In this case, in a DCRF structure a lower overall efficiency is expected because the overlap between the core mode and the pump modes of the inner cladding is reduced (unless the inner cladding is smaller, too).

7.4.2 Second-order Stoke generation

Because the signal core mode is smaller than the area of the inner-cladding, the intensity obtainable in the core can exceed that of the pump. As a result, the fibre length must be matched to the pump powers and the desired signal power level, in order to suppress the second-order or higher order Stokes from cascaded SRS in the core. Alternatively, it is possible to increase the threshold of the second-order Stokes by inserting a wavelength specific loss element in the laser cavity. For example, longer wavelengths are more sensitive to bend loss in step index fibre [17] and SRS filtering by bending can be enhanced with a W-type fibre [18]. Such an effective approach can easily be implemented in a DCRF format, as long as the Stokes – pump overlap remains unaffected.

7.4.3 Single mode operation

Single mode operation of the Stokes can be achieved through either a mode selective element such as specific waveguiding structure or by a controlled modal excitation in the case of an amplifier. For example, in some configurations it was found necessary to include a mode-selecting single-mode fibre in the cavity. When the DCRF is not spliced to a single-mode fibre at one end of the laser cavity, Stokes cladding-modes started to lase even at low output power as shown in fig. 7.16.

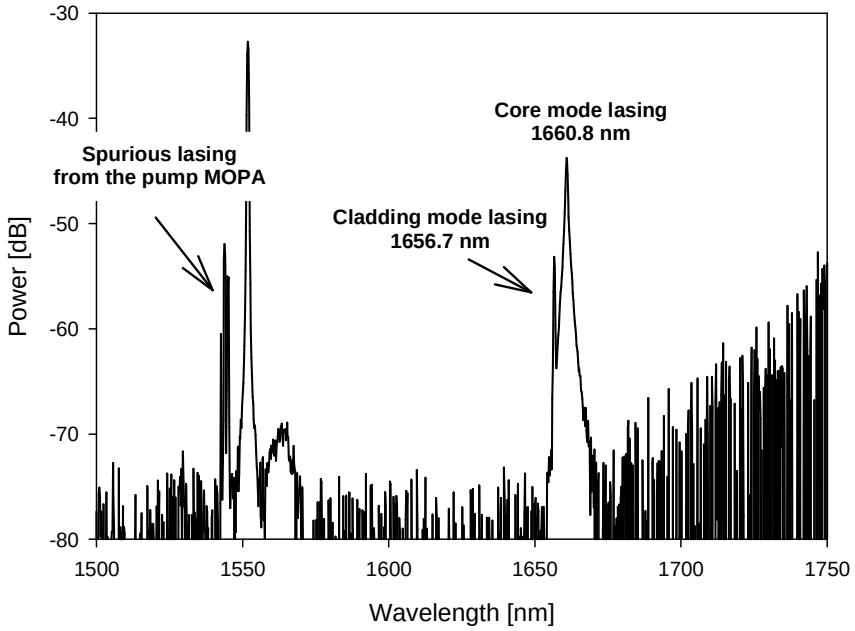

Figure 7.16: Spectrum at 1.6 W of output power at 1660.8 nm in a 1.2 km long DCRF fibre (Res.0.5 nm).

The grating is also expected to reflect the cladding modes. A laser cavity is then formed with a flat cleave at the opposite end of the DCRF which reflects indiscriminately. This clearly suggests that the Raman gain in the cladding is important when no modal selection is present. Note that in figure 7.16, the cladding mode lases at shorter wavelength as discussed in earlier in this chapter. In addition, the lack of isolation between the pump and the Raman laser makes the pump fibre laser more susceptible to any unwanted feedback which can lead to spurious lasing of the EYDFA.

7.5 Output power scaling

In order to improve the output power from a cladding-pumped Raman fibre a number of parameters must be adjusted for best performance.

7.5.1 Signal background loss

The first and main limiting parameter for a Raman fibre laser which consists generally of long fibre is the signal background loss. Figure 7.17 illustrates the effect of background loss on the laser threshold and the slope efficiency in a counter-pumped configuration, from simulation and using (6.12).

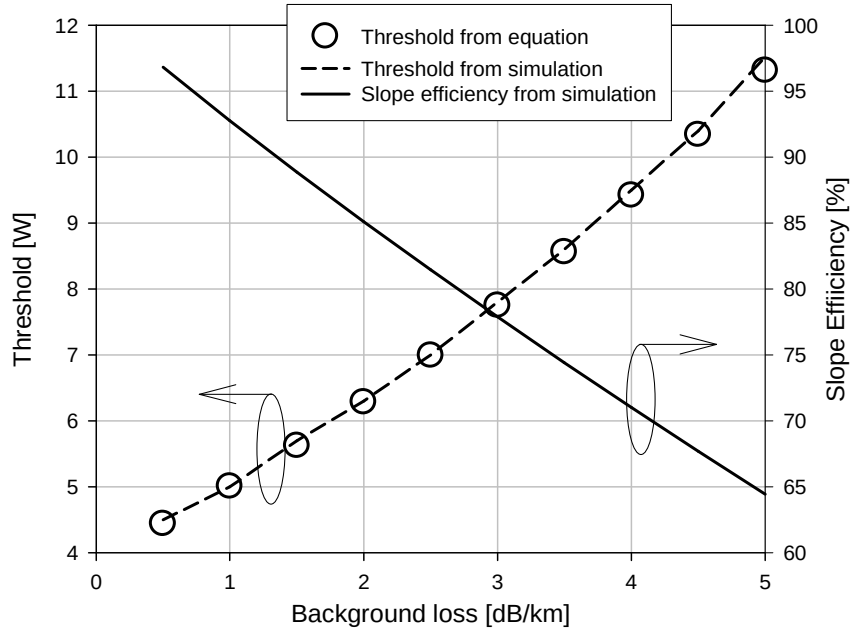

Figure 7.17: Effect of the signal/pump background loss on the DCRF laser threshold and slope efficiency, assuming a 1 km long piece of F71-LF11.

Here, the DCRF laser consists of a 1 km long fibre with a 100% – 4% cavity in a counter-pumped configuration. The fibre background loss of 2 dB/km, identical for pump and signal in this case, degrades both the laser threshold and the slope efficiency. A 1 dB variation or 20% on the background loss translate into a 7% change in the slope efficiency which is not negligible. As expected, the threshold evaluated using Eq. (6.12) is identical to that obtained from solving the complete propagation equations (6.7) - (6.9). To reduce the impact of the background loss one can either use low background loss fibres or short fibres. The Raman conversion occurs over shorter lengths at high powers, allowing shorter fibres with lower total loss to be used.

7.5.2 Laser configuration

The modelled DCRF laser performance with co- and counter-propagating pumping schemes is shown in figure 7.18. Here, the DCRF fibre possesses the same properties described earlier in the experimental work, and the cavity length is 1250 m. The cavity is formed by a 99% and a 4% reflective grating; both gratings selecting only the core mode.

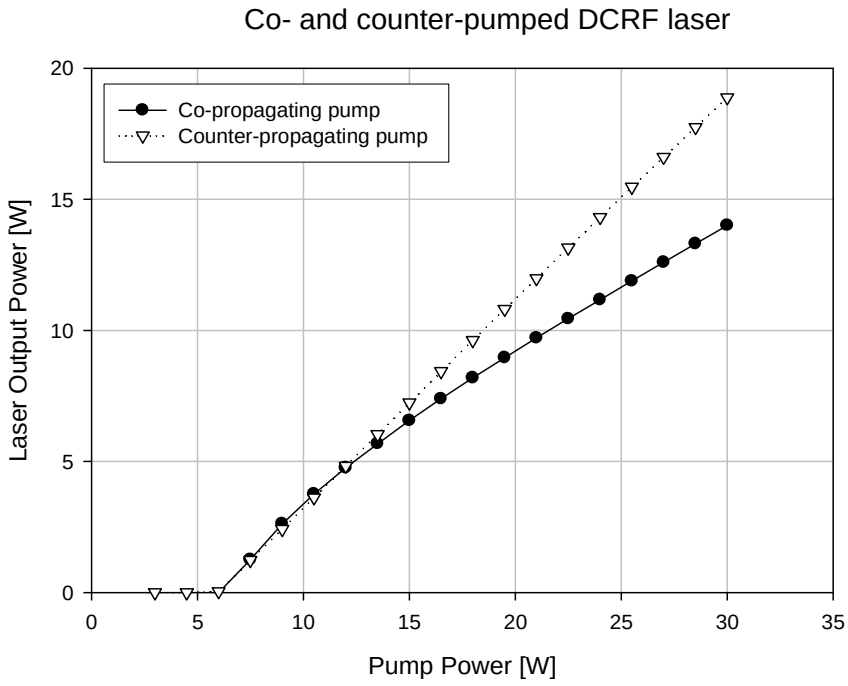

Figure 7.18: Comparison co- and counter-propagating DCRF laser.

The counter-pumped Raman fibre laser shows quite a linear dependence on the launched pump power while in the case of the co-propagating pump scheme the laser slope efficiency is lower.

The different slope efficiencies can be explained by the different background loss experienced by Stokes light during a round-trip inside the laser cavity. In the counter-pumped configuration the Stokes waves experiences a lower loss than the co-pumped configuration, before exiting the laser cavity as in most fibre lasers. In addition, both cases have an identical threshold as expected from the theory.

7.5.3 Higher pump power

In order to improve the output power of a cladding-pumped Raman fibre laser, one can try to increase the pump power launched into the inner-cladding of a DCRF. However, as the power of laser sources increases their brightness tends to decrease, especially if semiconductor laser sources are used. The obvious choice is to scale the dimension of the inner-cladding, however, this reduces the pump intensity and longer fibre lengths are required. Alternatively, the numerical aperture of the inner-cladding can be increased so that smaller inner cladding and therefore shorter fibres are used. Practically, this can be realised either with a fluorine doped all-glass fibre [19] or with an air-clad fibre [20]. Still, such fibres can have a relatively high loss but because the SRS gain is quite high at high powers, short fibre lengths can be used. Alternatively, one can use high peak power pulses to pump the fibre.

7.6 Summary

In this chapter, two Raman fibre lasers in co- and counter-pumped configurations are presented and characterised. Both lasers operate at around 1660 nm. The fibre laser slope efficiency reaches 67% and the threshold can be as low as 6 W. In the co-propagation scheme the output is made truly single-mode with a standard single-mode fibre. This is the first demonstration of a high power diffraction-limited Raman laser from a multi-mode fibre. In the single-mode single-ended configuration, up to 12.5 W of output power for 30 W of launched power are obtained. This represents a power conversion efficiency of 41% and a brightness enhancement of 26 times with respect to the brightness of the pump. In the dual-ended configuration, i.e. considering the Stokes power leaking through the highly reflective grating, up to 16 W of output power is obtained for 30 W of launched pump power. In that case the power conversion is 53%. Numerical simulations agree with the power characteristics of the co- and counter-pumped DCRF laser and explain the origin of the roll-off observed. The roll-off is induced by the non-linear pump absorption near the laser threshold. Still, the DCRF laser performance is near quantum limited considering the background loss of the fibre. These results are quite remarkable. The temporal behaviour and the spectral characteristics are also presented.

The laser output suffers from a linewidth broadening due to four-wave mixing as most Raman fibre lasers do at this wavelength. Then, some solutions are being proposed to mitigate or avoid the signal FWM, the generation of second order Stokes wave and the effects of Stokes light in higher order modes, encountered in this kind of laser.

These results are actual very promising and even higher output powers are foreseeable with more powerful pump sources. This novel concept has recently attracted attention and there are now some other research groups involved in the development of similar laser sources [21].

7.7 References

[1] S. H. Baek, and W. B. Roh, "Single-mode Raman fiber laser based on a multimode fiber", Opt. Lett. **29**(2), 153-155 (2004).

[2] J. Nilsson, J. K. Sahu, J. N. Jang, R. Selvas, D. C. Hanna, and A. B. Grudinin, "Cladding-pumped Raman fiber amplifier", in *Proc. Topical Meeting on Optical Amplifiers and Their Applications*, post-deadline paper PDP2, Vancouver, Canada, July 14 – 17, 2002.

[3] K. O. Hill, "Fiber Bragg grating technology fundamentals and overview", J. Lightwave Technol. **15**(8), 1263-1276 (1997).

[4] Y. Jeong, J. K. Sahu, D. N. Payne, and J. Nilsson "Ytterbium-doped large-core fiber laser with 1.36 kW continuous-wave output power", Opt. Express **12**(25), 6088 (2004).

[5] J. C. Bouteiller, "Spectral modeling of Raman fiber lasers", IEEE Photon. Technol. Lett. **15**(12), 1698-1700 (2003).

[6] M. Krause and H. Renner, "Numerical calculation of the linewidth of Raman fiber lasers due to spontaneous Raman scattering", Int. J. Electron. Commun. **59**(8), 502 (2005).

[7] K. X. Liu and E. Garmire, "Role of stimulated four-photon mixing and efficient Stokes generation of stimulated Raman scattering in excimer-laser-pumped UV multimode fibers", Opt. Lett. **16**(3), 174-6 (1991).

[8] A. Sharma, M. Dokhanian, Z. Wu, A. Williams, and P. Venkateswarlu, "Four-photon-mixing-mediated stimulated Raman scattering in a mu ltimode optical fiber", Opt. Lett., **19**(15), 1122-4 (1994).

[9] J. Hansryd, P. A. Andrekson, M. Westlund, J. Li and P. -O. Hedekvist, "Fiber-based Optical Parametric Amplifiers and their applications", IEEE J. Sel. Top. Quant. **8** (3), 506-520 (2002).

[10] K. Inoue, "Four-wave mixing in an optical fiber in the zero-dispersion wavelength region", J. Lightwave Technol. **10**(11), 1553-1561 (1992).

[11] R. H. Stolen and J. E. Bjorkholm, "Parametric Amplification and Frequency Conversion in Optical Fibres", IEEE J. Quantum Electron. **18**(7), 1062 (1982).

[12] M. Kraus, R. Stanslovaityte, S. Cierullies, H. Renner, E. Brinkmeyer, "Double-cavity Raman fiber laser with improved tolerance against high-Rin pump laser", in *Proc. European Conference on Optical Communication (ECOC)* 2005.

[13] F. Leplingrad, C. Martinelli, S. Borne, L. Lorcy, D. Montgardien, D. Bayart, "Up to 22 dB Reduction of the relatie intensity noise of a Raman fiber laser", in *Proc. European Conference on Optical Communication (ECOC)* 2005.

[14] M. D. Mermelstain, C. Headley and J.-C. Bouteiller, "RIN transfer analysis in pump depletion regime for Raman fibre Amplifiers", Electron.Lett. **38**(9), 403-405 (2002).

[15] M. Ding and P. K. Cheo, "Analysis of Er-Doped Fibre Laser Stability by Suppressing Relaxation Oscillation", IEEE Photon. Technol. Lett. **8**(9), 1151 (1996).

[16] T. Sakamoto, J. Kani, M. Jinno, S. Aisawa, M. Fukui, M. Yamada and K. Oguchi, "Wide wavelength band (1535-1560 nm and 1574-1600 nm), 28 x 10Gbit/s WDM transmission over 320km dispersion-shifted fibre", Electron. Lett. **34**(4), 392 (1998).

[17] A. Sharma, M. Dokhanian, Z. Q. Wu, R. Posey, A. Williams, and P. Venkateswarlu, "Stimulated Raman scattering in a multimode optical fiber with bend-induced loss", Opt. Commun. **111**(1-2), 127-131 (1994).

[18] E. A. Kuzin, G. Beltran-Perez, M. A. Basurto-Pensado, R. Rojas-Laguna, J. A. Andrade-Lucio, M. Torres-Cisneros, and E. Alvarado-Mendez, "Stimulated Raman scattering in a fiber with bending loss", Opt. Commun. **169**(1), 87-91 (1999).

[19] J. Wang, W. Zenteno, "All-glass high NA Yb-doped double-clad laser fibres made by outside-vapour deposition", Electron. Lett. **40**(10), 590-2 (2004).

[20] V. A. Kozlov, J. Hernandez-Cordero, R. L. Shubochkin, A. L. G. Carter, and T. F. Morse, "Silica-air double-clad optical fiber", IEEE Photon. Technol. Lett. **12**(8), 1007 (2000).

[21] R. Rice, "Multimode Raman fibre device with mode discrimination", patent application WO 2005/086300 A2 (2005).

Chapter 8 Pulsed cladding-pumped Raman fibre laser sources

This chapter contains six sections which cover my work on pulsed cladding-pumped Raman fibre laser sources. Section 8.1 reviews the motivations for the study of Raman scattering for pulse amplification. The theory of pulsed Raman scattering is introduced in section 8.2. Section 8.3 presents experimental results in a high gain pulsed SRS amplifier and the demonstration of the potential for high energy pulses amplification. Then section 8.4 deals with the competition of the parametric process called four-wave mixing (FWM) with the Raman scattering process. This competition can limit the performance of the SRS and some solutions are presented to prevent the growth of the FWM process. Section 8.5 reports studies on the potential for direct diode pumping of cladding pumped Raman fibres, which could be implemented in the future. Finally, section 8.6 summarises the findings of this chapter.

8.1 Introduction

For Raman amplification with pulses, the signal and pump pulses must temporally coincide in the fibre to achieve the maximum energy transfer, because the SRS gain is only available to the signal during the pump pulse. This is referred to as synchronous pumping. The gain disappears as soon as the pump pulse has passed. In comparison, in a RE-doped fibre, the pump energy is transferred to the gain medium, and the gain remains as long as the gain medium remains excited. The gain created in a Raman amplifier by a pump pulse automatically forms its own short time-gate, which negates the effects of spurious feedback and amplified spontaneous emission (ASE) build-up. There is no ASE generated between the pulses. Moreover, the SRS gain becomes biased co-directionally with the pump propagation because forward- and backward-propagating signal light have different temporal overlap with the pump [1]. The gain is higher in the forward direction (for light temporally synchronised with the pump pulses).

In a DCRF, the situation is more complicated because the pump is multi-mode while the Stokes is preferably in the fundamental mode. However, because the pump is multi-mode, one expects that higher energy pump pulses should be available and that, therefore, higher energy

output Stokes pulses could be obtained. Hence, the first aspect to investigate is the gain that can be achieve in the DCRF and then try to improve the output energy.

8.2 High gain single stage amplification

8.2.1 Experimental set-up

The experimental set-up consists of a multi-stage pulsed pump source, a continuous-wave (CW) seed signal and a DCRF as shown in figure 8.1.

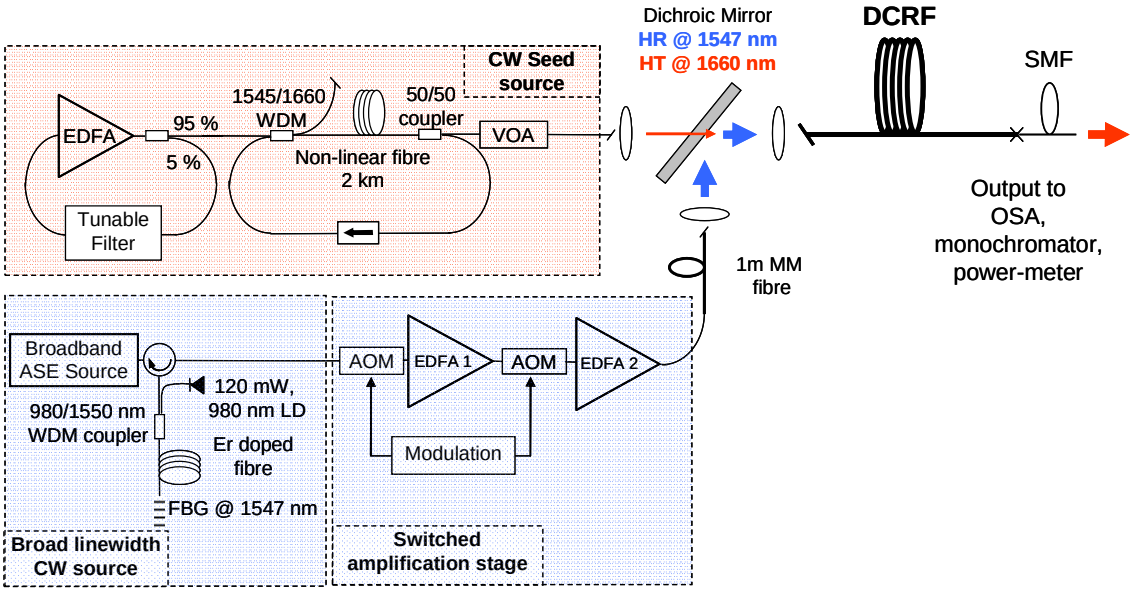

Figure 8.1: Experimental set-up of the pulsed DCRF amplifier.

The pump source is a MOPA incorporating a master oscillator (MO) emitting at 1547 nm. The MO output is then time gated and amplified in an amplifier cascade. In order to avoid any stimulated Brillouin scattering (SBS) in the long DCRF, the source has an output linewidth of about 20-50 pm. This is much larger than the Brillouin gain bandwidth of approximately 0.2 pm. An incoherent source is used because all (conventional) laser sources, including fibre laser or semiconductor laser, present one or, typcially, several single-frequency components (i.e., longitudinal modes) under a spectral envelope. However, even when there are a large number of modes participating in the laser process, it is difficult to rule out the occasional concentration of the output power into a single longitudinal mode. When that happens for a sufficient time, SBS will result. Here, a mode-free amplified stimulated emission (ASE) seed source is used. This is amplified in a core-pumped double-passed EDFA that incorporates a fibre Bragg grating at 1547 nm. The grating acts as a reflective filter for control of the spectral

content. The source delivers 34 mW of output power without any spurious lasing. If the ASE source is switched off, the EDFA starts to lase because of the high small-signal gain in conjunction with various reflections that create a cavity with the FBG in one end. The amplified pump is then modulated and further amplified by a consecutive set of acousto-optic modulators (AOM) and optical amplifiers. The first amplifier is a commercial core-pumed EDFA (Nortel). The final amplification stage consists of a high-power EYDFA delivering up 700 mW of average power in the present pulse regime. Both AOMs are modulated by electrical pulses of 100 ns duration at 100 kHz repetition rate, to avoid any self-Q-switching in the amplifiers resulting from a high MOPA gain between pulses and thus to avoid damaging any components. Also, the commercial EDFA has a restricted input power range which does not allow for low repetition rate operation because the average input power becomes too low. Furthermore, the peak power is limited by the temporal stability and the noise of the ASE pulse.

The pump source output spectrum is shown in figure 8.2. In order to simulate a multi-mode output, the pump brightness is reduced by splicing, with an offset, the single-mode output fibre into a 1 m long multi-mode fibre which is coiled in such way it provides good mode scrambling. The output M^2 is measured around 4.5.

By design, the cladding-pumped fibre Raman amplifier must be operated above 1640 nm, in order to provide a single-mode output. With the pump source used, the Raman gain peaks at ~ 1663 nm, so fulfills this condition. However, because there is no readily available conventional source at the operation wavelength of 1663 nm, a rather complex set-up of a Raman ring laser is used as a seed source. A high-power, tuneable fibre ring laser operating at 1547 nm, consisting of an EYDFA and a filter, pumps a Raman fibre ring laser. The Raman ring laser consists of a 2 km long, highly non-linear fibre (Sumitomo HNRAC-2), an output coupler with a large feedback, to slightly broaden the spectrum, as shown in figure 8.3, and of a WDM coupler to inject the pump co-directionally into the ring laser. An L-band isolator is inserted into the feedback loop, after the output coupler and before the WDM coupler to ensure uni-directionality of the lasing. Finally, a variable-optical attenuator is placed in front of the laser, outside the laser cavity, so that the output power can be varied up to a maximum power of 58 mW, without modifying the spectral content at 1663 nm.

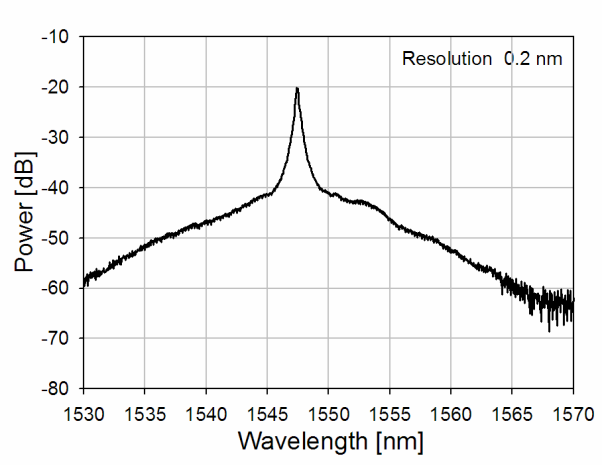

Figure 8.2: Spectrum of the MM pump at 1547 nm, (rep. rate 100 kHz, pulse duration ~ 100 ns)

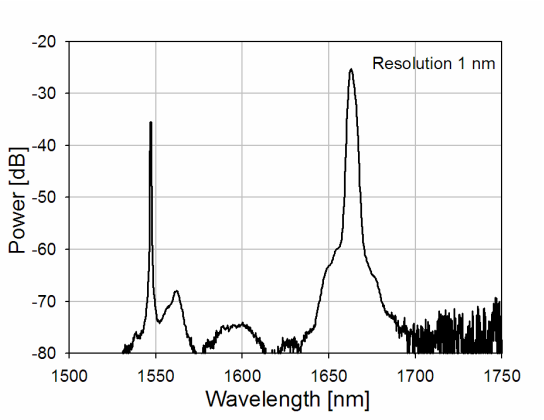

Figure 8.3: SRS CW seed output of the ring laser at 1660 nm

The final element of the set-up is the DCRF amplifier, which mainly consists of a long length of fibre F71-LF11. Its output end is spliced to a piece of standard single mode fibre (SMF) (NA 0.12, core diameter 8 μm). The splice loss between the SMF and DCRF is ~0.5 dB for the signal travelling in the core mode. By contrast, also in these experiments essentially all the pump light is lost here, since the cladding in the SMF does not guide light. In this experiment, the core loss is 3.1 dB/km and the inner cladding loss is 2.3 dB/km, both at 1550 nm.

The pulse pump and CW seed signal are free-space coupled into the DCRF inner-cladding and the core respectively, via a dichroic mirror highly reflective at 1547 nm and highly transmittive at 1663 nm. The pump launch efficiency is 65%, of which 15% is coupled into the DCRF core. Therefore, up to 500 mW of average power or 50 W peak power is launched into the DCRF. By contrast, the CW seed launch efficiency is 80%, of which 75% or about 31 mW of average power is in the core.

Since the Raman gain is essentially instantaneous and since the pump pulse is much shorter than the length of DCRF, the pump pulse creates Raman gain that travels with it through the fibre [1]. This makes the Raman gain essentially uni-directional, and even though a cw input signal is used, the signal at the output end of the DCRF will be pulsed, temporally coincident with the pump pulse.

8.2.2 Results and discussion

8.2.2.1 Amplifier characteristics

The average output and launched powers, and the corresponding peak powers, are shown in figure 8.4 for 450 m and 1100 m long DCRFs. At low launched pump powers, the average signal output power is dominated by the unamplifed part of the cw seed signal, between pump pulses. Insofar as the gain is low, the average power will be equal to the peak power in this regime. For higher pump powers, the energy in the amplified pulses dominates the average output power.

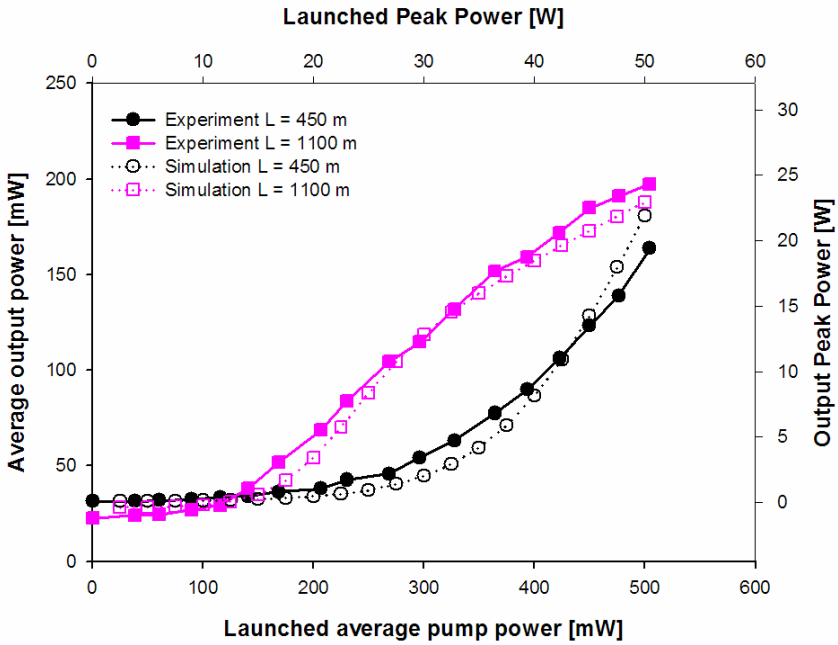

Figure 8.4: Average power and output peak power of the DCRF amplifier versus launched pump power for 450 and 1100 m long fibre (input seed power: 30 mW in the core)

The measurements were taken using a calibrated power meter and a monochromator with a fast detector to detect the output power and the shape and duration of the pulse at the pump and Stokes wavelength. In figure 8.4, the Stokes power in the 450 m long DCRF is growing exponentially up to 160 mW, while in the 1100 m long fibre, it is rolling off at the maximum pump power, with an average output of 200 mW. Both experiments agree with the amplifier simulation based on a joint effective area of 184 μm^2. The average power in the long DCRF rolls off because some second order Raman Stokes at 1800 nm is generated in the DCRF core. The second Stokes line limits the power obtainable from the single mode core if the fibre length is not adjusted to the pump and signal powers. The signal output spectrum and pulse shape are shown in figure 8.5.

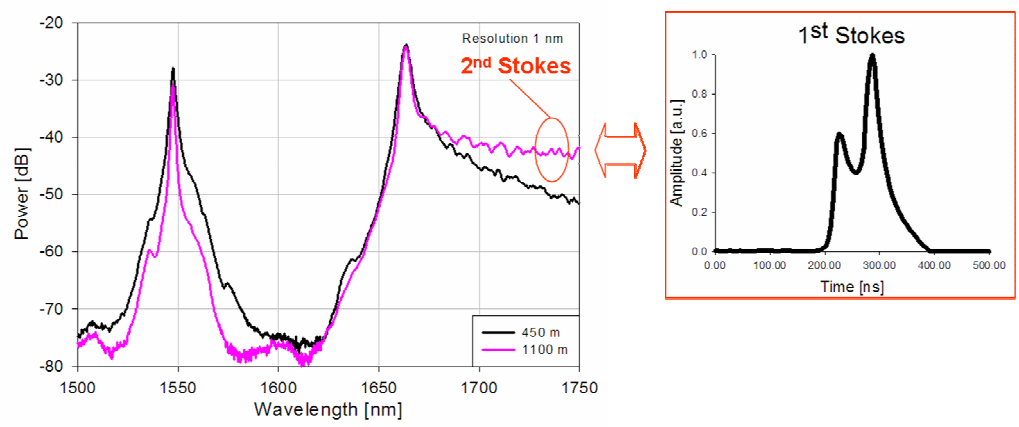

Figure 8.5: Left: Output spectra at maximum pump power for 450 and 1100 m long DCRFs. Right: Pulse shape of the signal output pulse for the 1100 m long DCRF.

Additionally, the different group velocities of the pump modes and the Stokes mode slightly increases the signal pulse duration, and therefore reduces its peak power as shown in figure 8.6, for the maximum input signal (31 mW) and pump peak power (51 W) for the 450 m long DCRF. This was confirmed by simulations, using the method of lines, in fig. 8.6. This method consists as discretizing the partial differential equations (6.1) - (6.3) in the z-dimension. Then, the semi discrete equations can be integrated as a system of ordinary differential equations. Here, the simulations agree reasonably well with experimental data. The difference in the remaining pump power can be explained by the inaccuracy of the modal power decomposition in the parameters used.

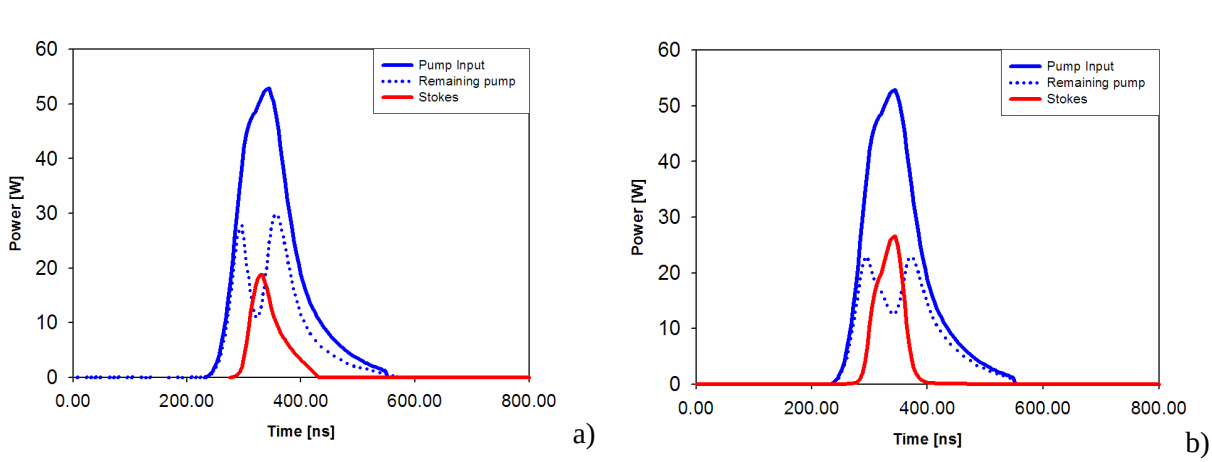

Figure 8.6: Pulse shapes for the incident and pump through signals and for the output Stokes signal: a) experimental, b) simulation.

As expected, only the region of the pump pulse with sufficiently high peak power contributes to the SRS process, whereas the wings of the pump pulse do not contribute. Therefore, it is obvious that a square-shaped pulse will have a better average power or energy conversion than a gaussian pulse. In addition, only the light synchronised with the pump pulse benefits from the SRS gain. Since a cw signal seed source was used, there was some signal light present between the pulses, but this was not amplified by the pump pulses.

8.2.2.2 Definitions of gain

In order to fully comprehend amplification in the pulse-pumped DCRF, two types of gain have to be considered: the peak gain and the energy gain. Firstly, there is what is called the peak gain, which represents the gain of the signal peak. Therefore the peak gain is defined as:

$$G_{dB}^{Peak} = 10Log_{10}\left(\frac{P_{peak}^{out}}{P_{peak}^{in}}\right) \tag{8.1}$$

where P_{peak}^{out} and P_{peak}^{in} are the output and the input peak power of the Stokes. Because the peak gain represents the gain that would be seen in the case of square pump pulses, when dispersion is negligible, i.e. the DCRF length is less than the walk-off length; it is generally higher than the energy gain.

The energy gain is the ratio between signal pulse output and input energies. In this case, when a cw input signal is used, the input signal energy corresponds to the energy of an "imaginary" input pulse of the same duration as the pump pulse. The pulse energy gain is defined as:

$$G_{Energy} = 10Log_{10}\left(\frac{P_{avg}^{out} - P_{CW}^{out}\left(\frac{T-\Delta T}{T}\right)}{P_{CW}^{in}\left(\frac{\Delta T}{T}\right)}\right) \tag{8.2}$$

where P_{CW}^{in}, P_{CW}^{out} and P_{avg}^{out} represent the launched seed power, the continuous part of the Stokes and the average Stokes power at the output of the DCRFA, respectively. T is the pulse periode and ΔT is the (pump or Stokes) pulse of duration.

The average power at the output consists of the pulse and a CW part, as shown in equation (8.3).

$$P_{avg}^{out} = P_{peak}^{out} \frac{1}{T} \int_0^{\Delta T} s(t) dt + P_{CW}^{out} \left(\frac{T - \Delta T}{T} \right) \tag{8.3}$$

where P_{peak} is the peak power of the Stokes pulse, T is the period of the in-between pulse and $s(t)$ is the Stokes pulse shape scaled to unity peak during the pulse duration ΔT. After inserting (8.3) into (8.2), the expression for the energy gain becomes:

$$G_{Energy} = 10Log_{10} \left(\frac{P_{peak}^{out}}{P_{CW}^{in}} \frac{\int_0^{\Delta T} s(t)\, dt}{\Delta T} \right) = G_{dB}^{Peak} - 10Log_{10} \left(\frac{\Delta T}{\int_0^{\Delta T} s(t)\, dt} \right) \tag{8.4}$$

Equation (8.4) confirms that the pulse energy gain is lower than the peak gain because of the output signal pulse shape. Thus, the energy gain is maximised for square-shape pump pulse, i.e. $\int_0^{\Delta T} s(t)\, dt = \Delta T$.

Another feature of interest is the power conversion efficiency (PCE) which indicates the performance of the process. Again, two power conversion efficiencies are defined to encompass the effect of the pulse. Firstly, the peak power PCE is defined as:

$$PCE_{peak} = \frac{P_{peak}^{signal\_out} - P_{peak}^{signal\_in}}{P_{peak}^{pump\_in}} \tag{8.5}$$

where $P_{peak}^{signal\_out}$, $P_{peak}^{signal\_in}$ and $P_{peak}^{pump\_in}$ are the peak power of the output signal, the input signal and the launched pump, respectively, within the duration of the pulse. Secondly, the energy PCE is defined as:

$$PCE_{energy} = \frac{E_{energy}^{signal\_out} - E_{energy}^{signal\_in}}{E_{energy}^{pump\_in}} \tag{8.6}$$

where $E_{energy}^{signal\_out}$, $E_{energy}^{signal\_in}$ and $E_{energy}^{pump\_in}$ are the energy of the signal output, of the signal input and of the launched pump pulse, respectively.

8.2.2.3 High-gain results

Measured signal peak gain and peak power conversion efficiency (defined in equation (8.5)) are shown in figure 8.7.

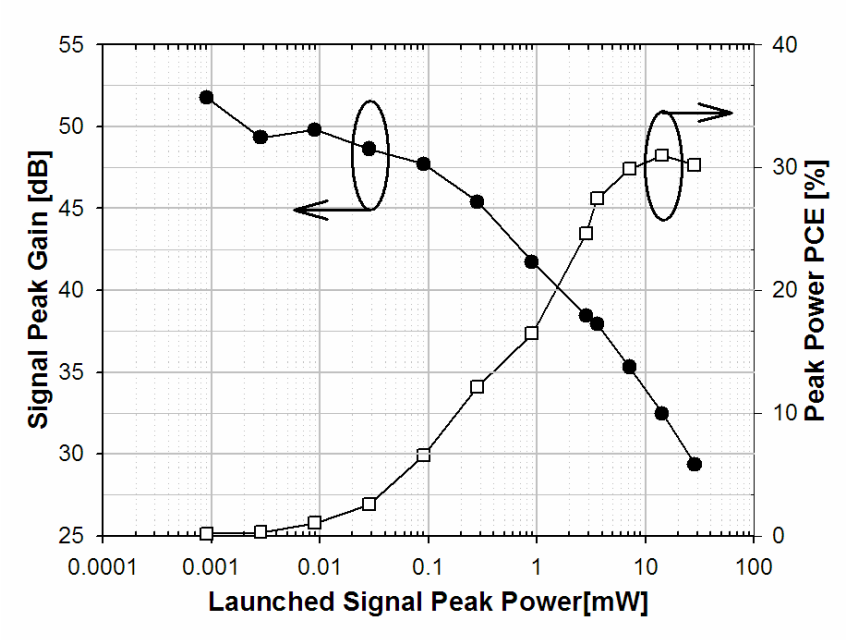

Figure 8.7: Signal peak gain and conversion efficiency of the peak power versus the amplifier signal input power for a 450 m long DCRF at the maximum pump power.

At low input seed power, the gain reaches about 50 dB in the 450 m long DCRF for a pump peak power of 50 W. As the signal peak power increases, the power conversion efficiency of the peak gain reaches 30% and stalls there. The conversion efficiency does not increase any further because the fibre is too short for the pump peak power. Still, the small-signal gain of the pulsed Raman amplifier is much higher than with rare-earth doped fibres because the amplification process only occurs when the pump pulse is present in the Raman fibre. Thus there is far less ASE to saturate the gain available to the signal

In order to investigate further the effect of the fibre length and of the pump peak power, the set-up is modified. The uncertainty in the signal launch power is removed by using a direct core splice for the injection of the seed light. In order to have the pump and signal co-propagating together for maximum efficiency in the fibre case, the signal is launched at the opposite end of the pump injection point and then it is reflected on a grating to travel alongside the pump. In addition, the pump source is replaced with the first three stages of the MOPA described in Chapter 5. However the peak power is limited to 100 W by SBS in the DCRF because the pump seed is a directly modulated tuneable external-cavity laser diode.

Figure 8.8 shows the average gain obtained for three fibre lengths: 465 m, 850 m and 1100 m and at different pump peak power. In Figure 8.8.a) the fibre length is 465 m, which is too short for the lowest pump power to generate an efficient Raman conversion. Therefore, only

the small fraction of the pump pulse corresponding to the highest peak power is depleted and used to create gain at the Stokes wavelength. By increasing the pump power, Raman amplification starts and the small-signal peak gain reaches 50 dB for a 1 μW seed power level. Then the DCRF length is increased to 850 m, which results in a higher gain, as shown in Figure 8.8.b), thanks to the longer pump-signal interaction length. In this case the greatest small-signal gain is achieved for a pump power of 70 W. However, at higher pump power, i.e., 105 W, the Stokes beam itself is depleted to generate a spontaneous second order Stokes beam. The generation of second Stokes power strengthens with the increase in the input seed power. Thus with high pump power, some of this is lost to the second Stokes with higher seed power. It is clear that pump peak power and fibre length must be adjusted to reach the optimum gain. Finally, with the longest fibre (Figure 8.8.c), the overall performance is the worst, except for the small-signal gain of the lower pump power. The performance decline is due to the higher background loss in the long fibre on the one hand and the second Stokes generation on the other.

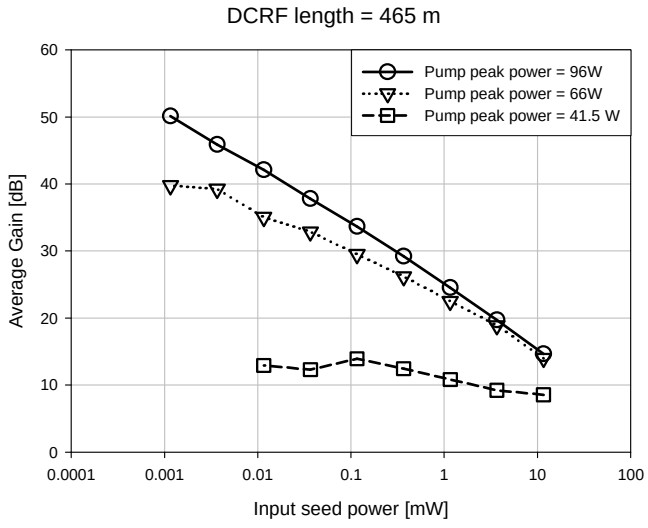

a)

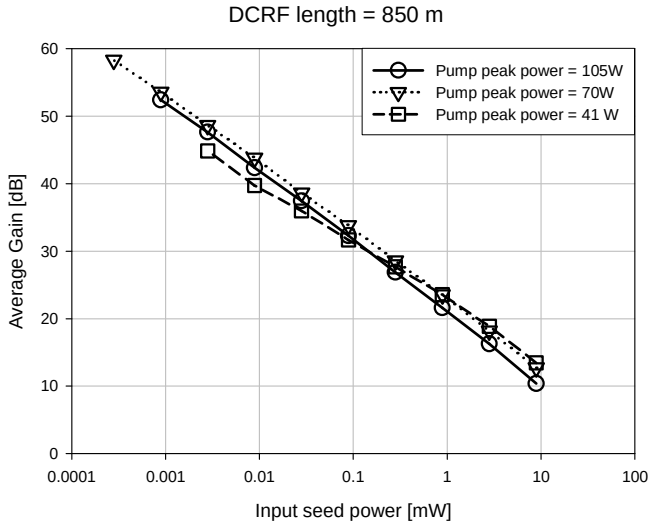

b)

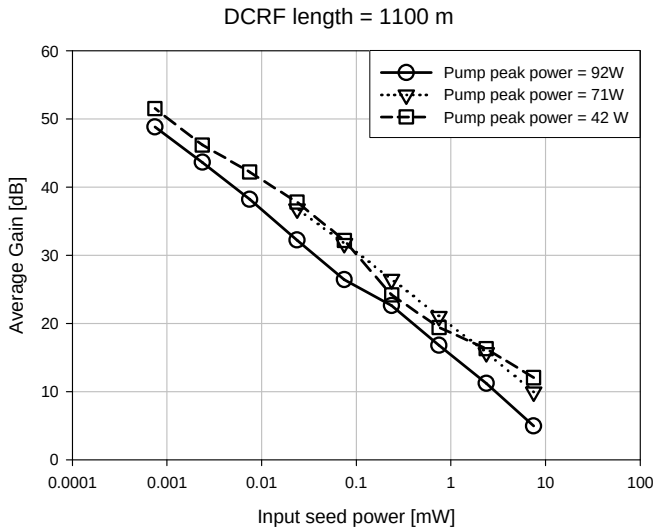

c)

Figure 8.8: Gain vs input power for a) 465 m, b) 850 m and c) 1100 m long DCRF, respectively

The experimental energy and peak power PCE of the DCRF amplifier are shown in figure 8.9.

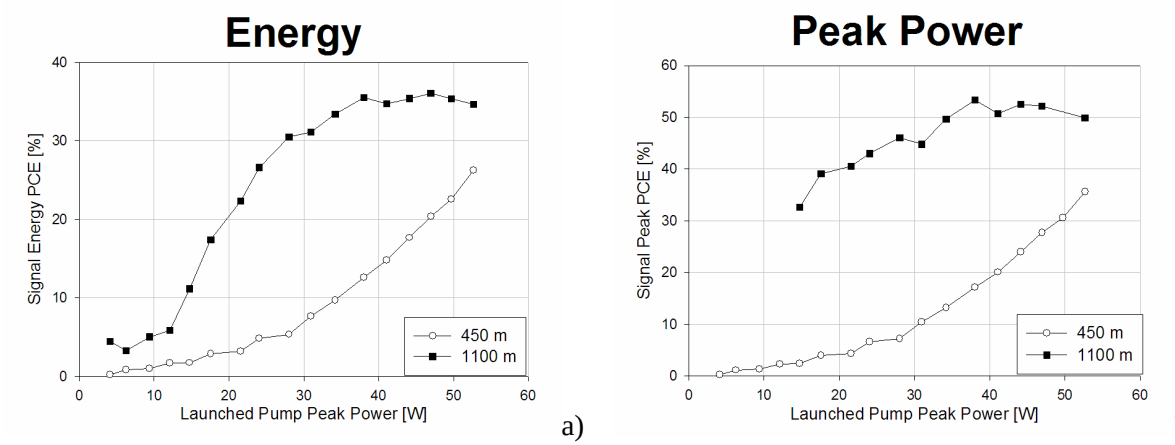

a) b)

Figure 8.9: power conversion efficiency according to the launched pump peak power for: a) the energy, b) the peak power.

In figure 8.9, the seed power is set at its maximum value of 30 mW, while the pump peak power is varied. The energy power conversion efficiency reaches 35% and rolls off in the long fibre length. This is explained by the pulse shape, the increased background loss and the generation of second order Stokes. The behaviour is much different in the case of the short fibre length and more pump power should yield to an even higher PCE. However, in this experiment the peak power was limited by the pump pulse temporal stability. The signal peak power PCE is also behaving in similar fashion, but this time the maximum efficiency is around 50%. This indicates that potentially in the long fibre length, up to 50% of the energy could be converted into the Stokes. Furthermore, if the background loss is taken into account, the PCE is near the quantum limit. Hence, with lower background loss fibre and shorter fibre, higher conversion efficiency could be expected.

The advantage of the cladding-pumped Raman laser source is that the multi-mode pump light is converted into a diffraction limited beam at the first Stokes wavelength. The maximum brightness enhancement (Equation (7.1)) that can be expected with this fibre in case of a peak power PCE of 50% is a factor of 7.3.

8.3 High-energy amplification

8.3.1 Experimental set-up

In this experiment, a diode-seeded MOPA pump source is used, and by controlling the initial pulse shape and the inversion of each amplification stage, high-energy rectangular shaped

pump pulses are generated. The aim is to show that with appropriate pulse shaping, most of the pump energy can be transferred into the signal.

The experimental set-up shown in figure 8.10 consists of three sections: a DCRF amplifier, a seed source at the Stokes wavelength, and a high peak power, high-energy, pulsed pump source at 1545 nm.

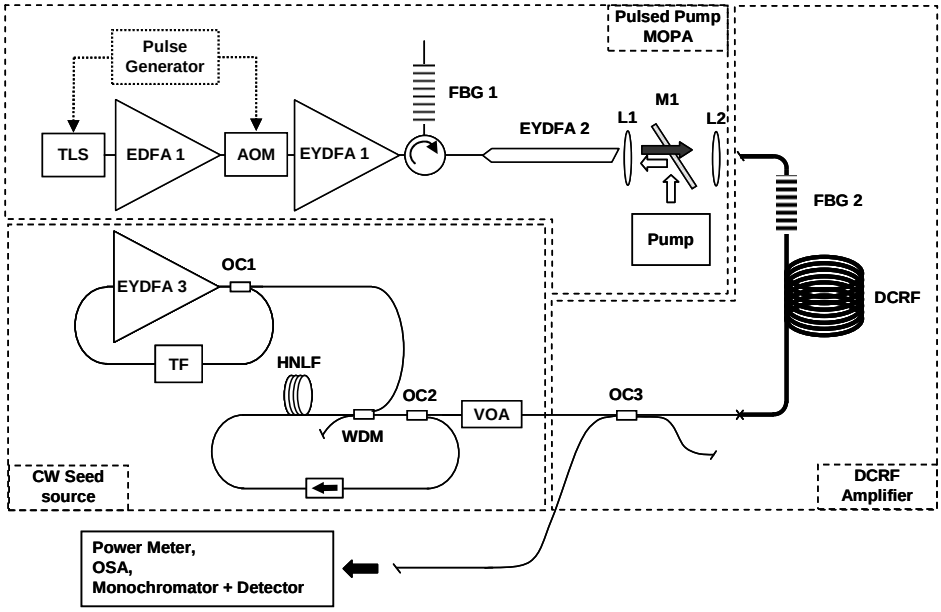

Figure 8.10: Experimental set-up of the double-clad Raman fibre amplifier.

The double-clad Raman fibre used in this experiment is the same as before, i.e., F71-LF11. The pump pulse is free-space launched into the DCRF through a set of lenses L1 and L2 of focal lengths 8 mm and 4.5 mm respectively. The pump launch efficiency is typically 70%. Less than 30% of the launched pump power is into the core mode. The DCRF end face is angle cleaved to avoid any back reflection into the pump source, as no free-space isolator was available. To use the DCRF in a pulsed amplifier configuration, for maximum gain, pump and signal should be co-propagating so that the temporal pump-signal overlap is maximized. As before, in order to ensure a proper seeding of the core mode and a robust set-up, the seed is core launched in a counter propagation scheme using a broadband 50/50 coupler (OC3). The seed is then reflected at the pump launch end by a fibre grating (FBG 2), written in the core of the DCRF and highly reflective for the core mode. The grating is identical to that used in Chapter 7 with a reflection of 83% at 1661 nm. Thus, following reflection, the seed signal and pump are co-propagating along the DCRF, with the seed in the core only. The pump pulse, through SRS, modulates and amplifies the seed signal similarly to the previous experiment. This ensemble forms the double-clad Raman fibre amplifier (DCRFA). The output of the DCRFA through OC3 is then analysed using a thermal power-meter (GENTEC PS-310-V3), an optical spectrum analyser (ANDO

AQ6315-E) and a monochromator, in combination with a fast detector (Agilent 83440D). The monochromator resolution is set at 2 nm.

The Raman seed laser consists of a CW Raman ring laser similar to the one described in the high gain experiment section of this chapter. The main difference is that the Raman ring laser is counter-pumped with respect to the lasing output direction to avoid any back reflection, from the DCRF amplifier, into EYDFA 3. Inherently, some powers at 1545 nm and 1660 nm are fed back into the ring laser from the DCRF fibre. However, there are no consequences, insofar as some of the reflected power is lost in the VOA, depending on the attenuation, and an additional 50% is lost in OC3 and again in OC2, protecting the ring laser from pertubations. The launched power, from the Raman ring laser, into the DCRF, varied from 0.016 mW to 16 mW.

The final element of the set-up is the pulsed pump source. It is the same cascade of amplifiers as in Chapter 5. The final amplifier (EYDFA2) consists of a 27 μm core diameter fibre (F402-LF122) which delivers pulses with a beam propagation factor (M^2) of 4. In this experiment, the seed for the 1545 nm MOPA is generated by a directly modulated tunable external cavity diode laser, a Photonetics Tunics-Plus tuneable laser source (TLS). The TLS is directly modulated by an electrical pulse shaped such that the optical signal shape compensates the changes in the gain that occurs during the pulse, as the pulse extracts energy from the amplifiers. A triggered arbitrary waveform generator (Agilent 33120A) is used as a generator for shaped pulses. The pulse shape from the generator is carefully adjusted to make the MOPA output pulses rectangularly shaped. Figure 8.11.a shows the shape of the pump pulse launched into the DCRF inner cladding through the grating's end. The multiple peaks present within the pump pulse are caused by the shape of the pulse from arbitrary waveform generator.

This complex system forms the experimental set-up. The length of the pulse is mostly imposed by the speed of arbitrary waveform generator. Thus, the pump pulses launched into the DCRF are 700 ns long. The repetition rate is fixed at a 25 kHz which corresponds to a launched peak power of 40 W or an energy of 28 μJ, and a pulse of square shape.

Finally, The DCRF length is set at 850 m because, from the previous experiment (see fig. 8.8), it presents the best performance for the pump peak power settings and the fibre background loss.

8.3.2 Output characteristics

The incident pump pulse, the output Stokes pulse and the residual pump are shown in figure 8.11. These pulses were taken at the maximum output power from the single mode output fibre.

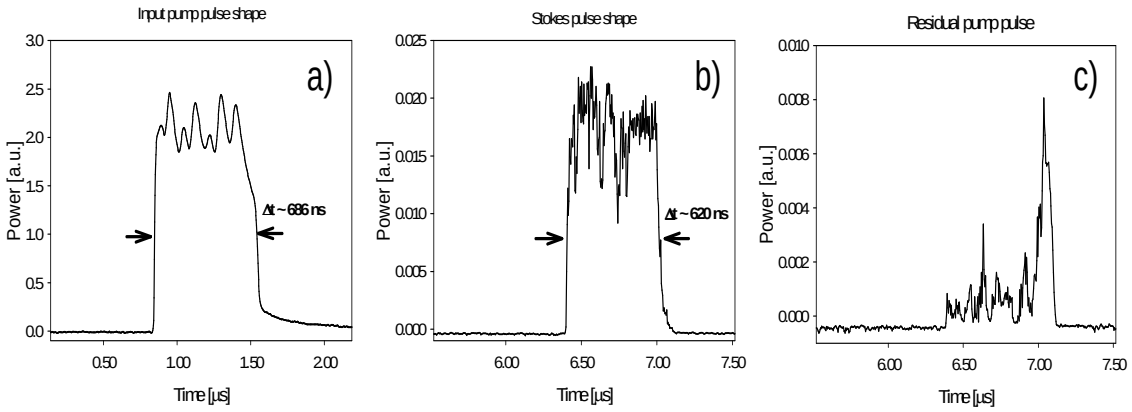

Figure 8.11: a) Input pump pulse shape after the fibre MOPA, b) Stokes pump pulse, c) Residual pump pulse at the pump wavelength in the SM fibre.

In figure 8.11.c, the residual pump in the core is strongly, but not completely, depleted. A fraction of the pump pulse seems to not have experienced SRS most likely because of pulse walk-off. In addition, the output pulses are much noisier than the input pump pulse and present many sharp and fast peaks. At first, it was believed that because of the narrow linewidth nature of the pump pulse, some pump light was reflected by SBS. Thus the backward light from the double-clad fibre was monitored in order to check for backward SBS pulses. Virtually no pump was reflected at the pump power level used in this experiment, which indicates that no SBS was taking place.

A more plausible explanation is that the noise might be induced by modulation instabilities [3 - 7] because the pump and the signal are operating in the anomalous dispersion regime of the fibre. Furthermore, similar effect has been already observed by Ilev [8] in a double pass Raman amplifier. Still further measurements would be required to precisely identify the origin of this noise.

In the output spectrum, shown in figure 8.12, as expected, the pump through is nearly completely depleted, with nearly all of the pump power converted to the Stoke wavelength. The Stokes linewidth is about 1.85 nm, which is larger than the grating transmission FWHM (~ 0.4 nm). The broadening exceeds that expected from SPM, which therefore seems to confirm that the signal might experience additional broadening through modulation instability [3].

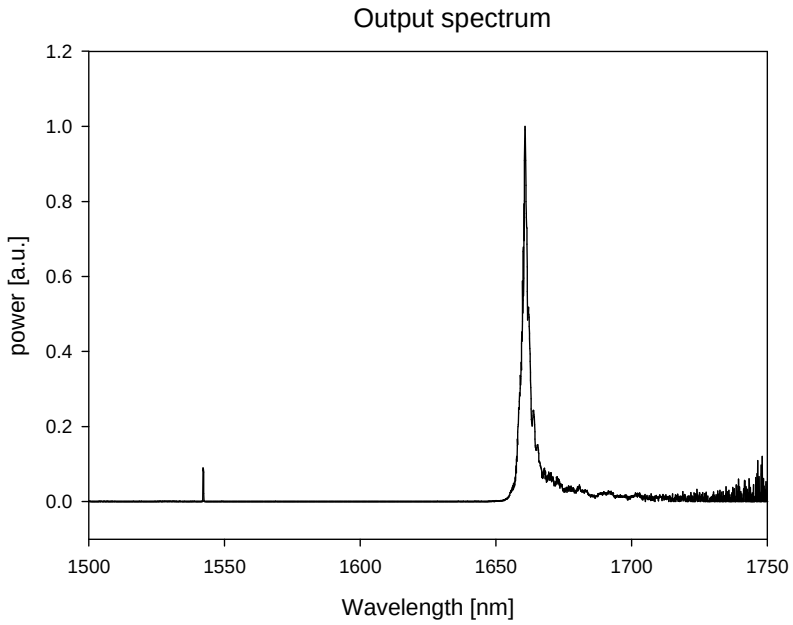

Figure 8.12: Output spectrum of high-energy Stokes pulse (optical resolution 0.5 nm)

Finally, figure 8.13 shows the signal energy for various input seed powers and energy.

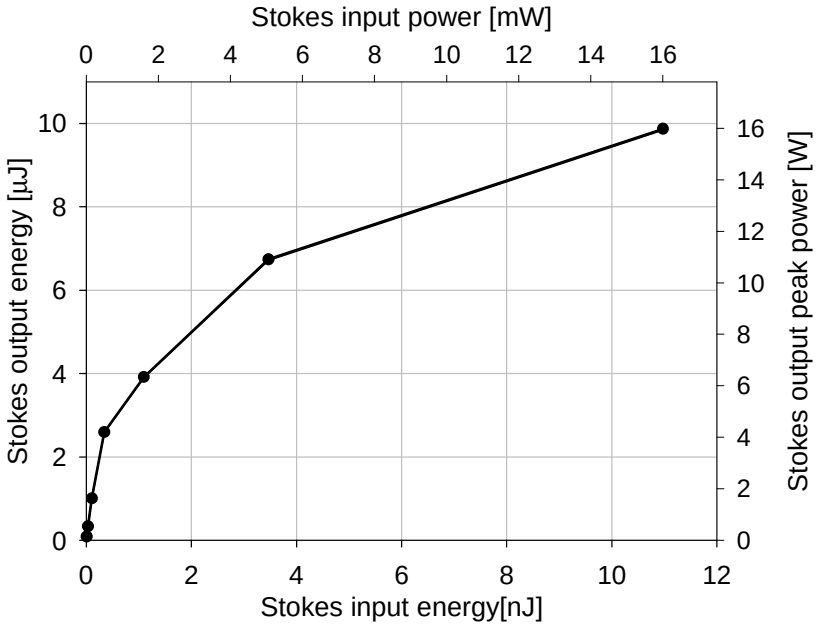

Figure 8.13: Stokes output energy versus seed input energy. The seed input power and the Stokes peak power are also given.

In figure 8.13, the Stokes pulse energy reaches the level of 9.9 µJ in a 620 ns pulse, at the maximum input power (or energy). The Stokes peak power is estimated to about 16 W. As

the Stokes input energy is increased, more power is transferred from the pump into the signal until the output energy saturates. This indicates that nearly all the pump power is transferred into the single mode. Thus, even if the input Stokes energy increases no more energy can be extracted from the pump pulse. In fact, the output energy should decreases because of the excess loss from the background loss. For higher input energy, the fibre length should be shortened. Indeed as discussed previsously the SRS gain is strongly depends on the Stokes seed power, and stronger seed power "accelerate" the pump to Stokes energy transfer.

It is worth noting, that, here, no higher-order Raman Stokes was detected. Obviously, if the fibre was longer or if the pump power was higher, most likely higher order Stokes lines would have been produced.

The energy conversion efficiency is quite low at 36% but considering the background loss of the fibre, this is a quite remarkable result which represents the first tentative and demonstration energy pulse generation from a cladding-pumped Raman fibre device.

8.4 Pump induced four-wave mixing in cladding pumped Raman fibre

8.4.1 Introduction

As the cladding-pumped Raman fibre becomes shorter or the inner-cladding becomes larger, higher and higher pump peak powers are required to obtain SRS amplification. However, at higher power, in multi-mode and double-clad fibres, spontaneous SRS can take place in the cladding and other non-linear processes start to become significant, especially four-wave mixing (FWM). For example, in [9], FWM was observed at 600 MW/cm^2 (or 6 W/μm^2) in a 200 m long fibre using 8 ns long pulses. FWM gives rise to gain which can be outside the Raman gain bandwidth. The photons created by the FWM process can be lost to the SRS. The mutual influence of SRS and FWM in optical fibres has been thoroughly studied in single-mode Raman fibre lasers, e.g., [10], and amplifiers, e.g., [11, 12], as well as in multi-mode fibres, e.g., [13 - 15] over the last three decades. In case of cladding-pumped Raman fibre, the multi-mode structure favours four-wave mixing because of the multitude of possible phase-matched interactions. In a Raman amplifier, FWM should, preferably, be avoided, but this is not always the case. Therefore, it is necessary to compare the gain of both processes in the case of multi-mode fibre.

8.4.2 Comparison between FWM and SRS

The comparison of FWM and SRS can be quite difficult because FWM is a phase-matched process which can have a multitude of interactions (although not all these interactions are efficient) while SRS is not phase matched and therefore only depends on the pump intensity distribution. In order to simplify this analysis, let us consider the following scenario where a pump light propagates in a multi-mode fibre. Let us assume that the pump and Stokes modes have a nearly identical effective area. Let P_1 and P_2 be the incident pump powers of two distinct modes. The four-wave mixing parametric gain g becomes [3]:

$$g = \sqrt{4\gamma^2 P_1 P_2 - \left(\frac{\kappa}{2}\right)^2} \tag{8.7}$$

where γ is the fibre non-linear parameter [3 - 15] and κ is the net phase mismatch [3 - 15]. To simplify the expression in the case of a multi-mode fibre, γ is an averaged value for the different modes considered. The non-linear parameter γ is defined by:

$$\gamma = \frac{2\pi n_2}{\lambda A_{eff}} \tag{8.8}$$

where λ is the pump wavelength, n_2 is the non-linear refractive index of the medium and A_{eff} is the mode effective area for the interaction. Based on the germanium concentration, n_2 can be estimated [17] to about 3.15 10^{-20} m^2/W for the core of F71-LF11 and to 2.7 10^{-20} m^2/W for the inner cladding. Thus in F71-LF11 assuming a 300 μm^2 effective area at 1550 nm, γ becomes ~0.36 10^{-3} m/W.

The net phase mismatch κ can be expressed as:

$$\kappa = \Delta\kappa + \gamma\left(P_1 + P_2\right) \tag{8.9}$$

where $\Delta\kappa$ is the phase mismatch due to the material and waveguide dispersion, while the term $\gamma\left(P_1 + P_2\right)$ represents a non-linear contribution to the net phase mismatch.

The phase mismatch $\Delta\kappa$ is defined as [18]:

$$\Delta k = n_a^{eff}\omega_a + n_s^{eff}\omega_s - n_{p1}^{eff}\omega_{p1} - n_{p2}^{eff}\omega_{p2} \tag{8.10}$$

where n^{eff} is the modal effective index and ω is the optical frequency of the anti-Stokes, the Stokes and the pump power in the first and second mode, as indicated by subscripts $a, s, p1$ and $p2$, respectively. Here, I consider the case of a single pump wavelength in different modes.

The calculated effective indices for L71-LF11 modes are shown in figure 8.14 as functions of the frequency offset from a 1550 nm pump.

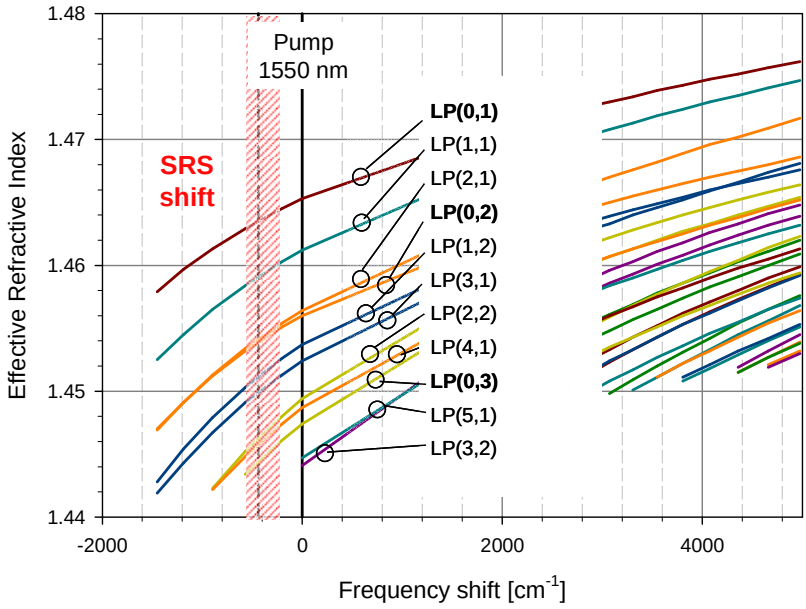

Figure 8.14: Calculated effective refractive index for various modes of L71-LF11 at the pump wavelength 1550 nm.

In figure 8.14 , the red shaded region, at ~500 cm^{-1}, denotes the frequency shift corresponding to the SRS process. The modal phase matching is achieved when the sum of the effective index of an anti-Stokes and Stokes component of identical frequency difference with the pump (i.e., of equal distance on opposite sides of the pump frequency) is equal to the sum of the effective indices of the two pump modes (see eq. (8.10)). If the frequency difference is such that it corresponds to the SRS shift then both processes interact. Then, the SRS process and the FWM process start to "amplify" each other [13].

When phase matching is realised, the maximum gain coefficient for the FWM process is given by [19 - 38]:

$$g_{FWM\_\max} = \frac{2\pi n_2}{\lambda_p} \tag{8.11}$$

Assuming the previous value of n_2 ~ 2.7 10^{-20} m^2/W for the inner-cladding of F71-LF11, the gain coefficient becomes 1.09 10^{-13} m/W or about twice the value of the SRS gain coefficient (~ 0.55 10^{-13} m/W).

The Stokes gain over a length L for which the process remains phase matched, is given by:

$$G_{FWM} = 1 + \left(\frac{2\gamma (P_1 P_2)^{1/2}}{g} \right)^2 \sinh^2 (gL) \tag{8.12}$$

Equation (8.12) can be approximated by [3]:

$$G_{FWM} \approx \frac{1}{4} \exp\left(2\gamma P_p L\right) = \exp\left(2\gamma P_p L - \ln(4)\right) = \exp\left(2 \frac{g_{FWM\_\max}}{A_{eff}} P_p L - \ln(4) \right) \tag{8.13}$$

where $P_p = P_1 + P_2$, is the total pump power, L is the interaction length and γ is the fibre non-linear parameter. For comparison, recall that the SRS gain in the multi-mode fibre is given by: $G_{linear}^{SRS} = \exp\left(\frac{g_R}{A_{LP01,pump}^{eff\_eq}} P_p L_{eff} \right)$.

In order to compare FWM and SRS, let us assume a double-clad fibre with similar properties to F71-LF11, i.e. with a FWM gain coefficient of 1.09 10^{-13} m/W and a SRS gain coefficient of 0.55 10^{-13} m/W, supporting 15 modes equally excited by 1 kW pump power, with a core effective area of 64 μm^2 and an effective area of 300 μm^2 for some cladding modes. The calculated SRS gain and FWM gain (under perfect phase matched condition) for a core mode and some cladding modes are shown in figure 8.15.

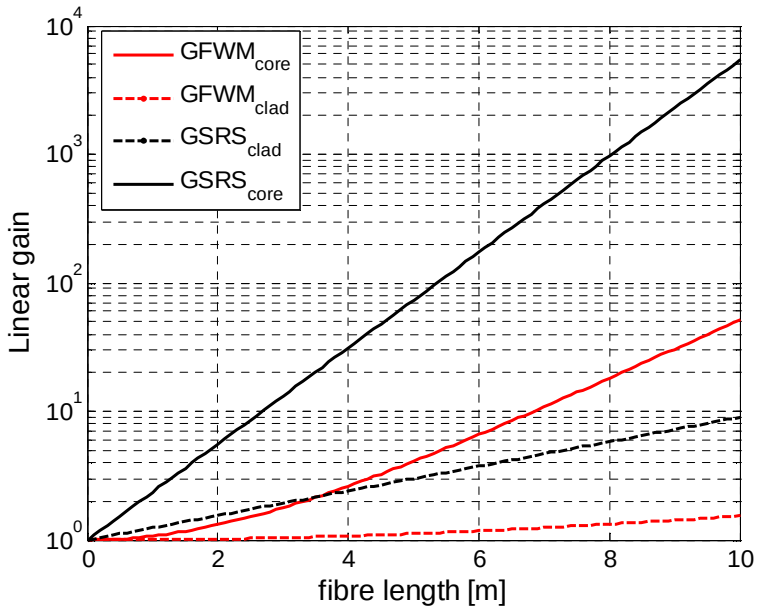

Figure 8.15: Comparison of the Four-Wave Mixing and Raman gain in the core and the cladding of LF71-LF11.

Figure 8.15 shows that the SRS gain is much more important than the FWM gain in the cladding and in the core. As the fibre length increases the gain of the FWM in the core overtakes the SRS gain in the cladding. This figure illustrates the predominance of the SRS process over FWM in the multi-mode fibre. However, because of the approximations assumed and because it is possible and likely that for some modes have a smaller effective area, and also because of the pump power modal distribution, that the FWM gain becomes higher than the SRS gain. Nonetheless Ilev remarks [8] that in multi-mode fibre: "…, the influence of four-photon mixing is also relatively small, due to the use of the highly multi-mode optical fibre and the fact that these parametric processes appear within the framework of separate transverse modes, while the Raman components comprise the energy of many modes.". Furthermore, in my experiment the SRS process is seeded which further increases the SRS gain and reduces the effect of other the non-linear processes. Still, the SRS process with or without any seed is more important for low-order modes because of the bean clean-up properties. Furthermore, FWM is more likely to occur in higher order mode, as noticed by Sharma [14]. In fact, under a 1 kW peak power pump pulse, LF71-L11 exhibits some third harmonic of the pump (a degenerate form of FWM) as shown in figure 8.16.

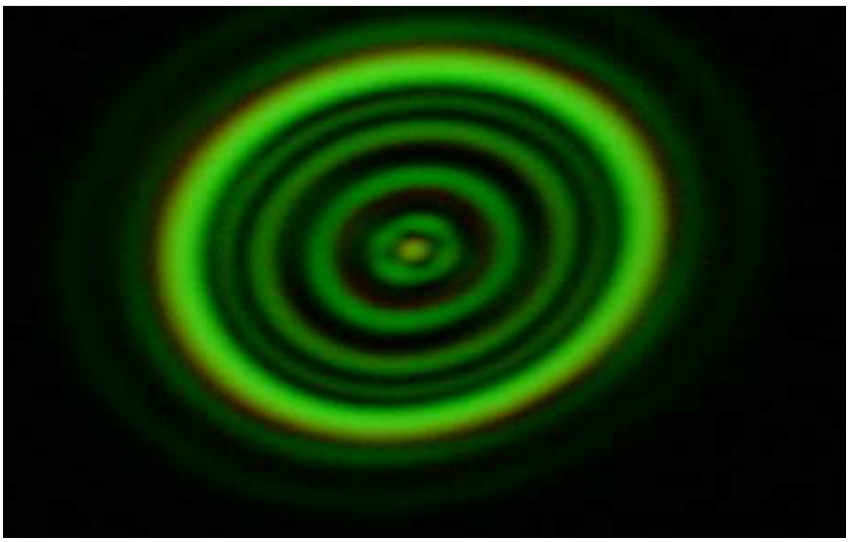

Figure 8.16: Third harmonic generation by modal phase matching in a 20 m length of F71-LF11 with 1kW pump pulses (2 ns long).

In figure 8.16, a clear ring structure is visible, that indicates that the modes, involved in the FWM process, seem to belong to the circularly symmetric modes of the LP_{0x} family. Still, even at 1 kW peak pump power, only a small fraction of pump power estimated to less than 1% is converted into the visible spectrum by the FWM process.

However, in order to avoid any detrimental pump loss through FWM, several solutions exist. Firstly, the Raman Stokes wave can be seeded with a low power signal alongside the

pump wave to reduce the threshold for Raman scattering, as demonstrated in [13]. Once the SRS process is started, the energy of the pump will be transferred to the Stokes wave. The seed power for the Stokes wave at the desired mode should significantly exceed the equivalent input power of all the other modes. Thus, the seed input power requirement scales with the NA and cladding dimension of the fibre. Still it does not suppress FWM, which can occur in the fibre core as we have seen in Chapter 7. Secondly, the coherence length can be reduced by perturbing the effective indices of the modes over a short length [18]. Typically, the fibre cladding can be perturbed periodically or tapered to reduce building up the phase matching process. However, in some cases, some of phased-matched processes can be, at the first order, insensitive to the fluctuation of the fibre diameter [15].

8.4.3 Conclusions

A study of the competition between FWM and the SRS is presented. The FWM process occurs between modes that are phase-matched while the SRS process only depends on the intensity overlap between the pump and the Stokes modes. Consequently, the power of the modes involved in a FWM process is much less than in the SRS process. Thus, the gain of the FWM becomes less than that of the SRS. Furthermore, in a long multi-mode fibre, SRS is the dominant non-linear process. It is only when high peak power pulses are used, that FWM can transfer some of the pump photon energy to a frequency shift larger than the SRS shift. In that case, these photons are lost. However, solutions exist that mitigate the effects of FWM on the SRS process, for example, by reducing the SRS threshold or by reducing the FWM coherence length.

8.5 Laser diode pumped pulsed double-clad Raman fibre

In this section, semiconductor laser diodes are proposed as laser sources to directly pump a cladding-pumped Raman fibre transformer. Thanks to the recent progress in semiconductor technology, laser diodes have seen a dramatic increase of their output power and an improvement of their output brightness [19]. Usually they are used to pump rare-earth doped fibres, which in turn can be used as pump sources for a SRS laser. The use of an intermediate brightness transformer makes the SRS laser more complex and reduces the electrical to optical efficiency. Furthermore, the wavelength range of the rare-earth fibre laser is limited (see Chapter 1), while the operation range of laser diodes is much broader. Laser diodes can easily be operated in continuous-wave and pulsed mode, even with diode stacks. In addition, the pump power can be increased by multiplexing diodes spatially, in polarization, and spectrally. Finally,

diodes can be controlled electrically and do not suffer from pulse distortion like in the pulse amplification process in RE fibre. Thus laser diodes should be an excellent candidate to replace RE-doped fibre lasers as pump sources for cladding-pumped fibre Raman devices. Obviously, laser diodes can be operated with a short pulse duration in the order of of nanoseconds to a much longer duration. Still, the short pulses generation can be difficult due to of the large amount of current needed to be rapidly switched.

In order to verify that laser diodes can generate enough intensity, so that SRS can take place in the multi-mode fibre, the SRS gain per unit length must be expressed in terms of the fibre brightness. The SRS gain in decibels, in the un-depleted regime, in a multi-mode fibre can be written as:

$$G_{SRS}^{dB} = 4.34 g_R L_{eff} \frac{P_P}{A_{eff}} - \alpha_s L \tag{8.14}$$

where P_P is the launched pump power into a fibre of length L which has an effective area A_{eff} and exhibits a SRS gain coefficient g_R. L_{eff} is the fibre effective length and α_s is the Stokes background loss.

Using the definition of the brightness, equation (8.15) becomes:

$$G_{SRS}^{dB} / L = 4.34 g_R \frac{L_{eff}}{L} B \pi N A_{clad}^2 - \alpha_s \tag{8.15}$$

where B is the fibre brightness and NA_{clad} is the inner-cladding numerical aperture. From equation (8.15), the SRS gain per unit length can be plotted according to the pump brightness, as shown in figure 8.17. Here, it is assumed the optical system conserves the pump brightness in the fibre. Also the pump and signal background loss is set at 1 dB/km to give a more realistic view.

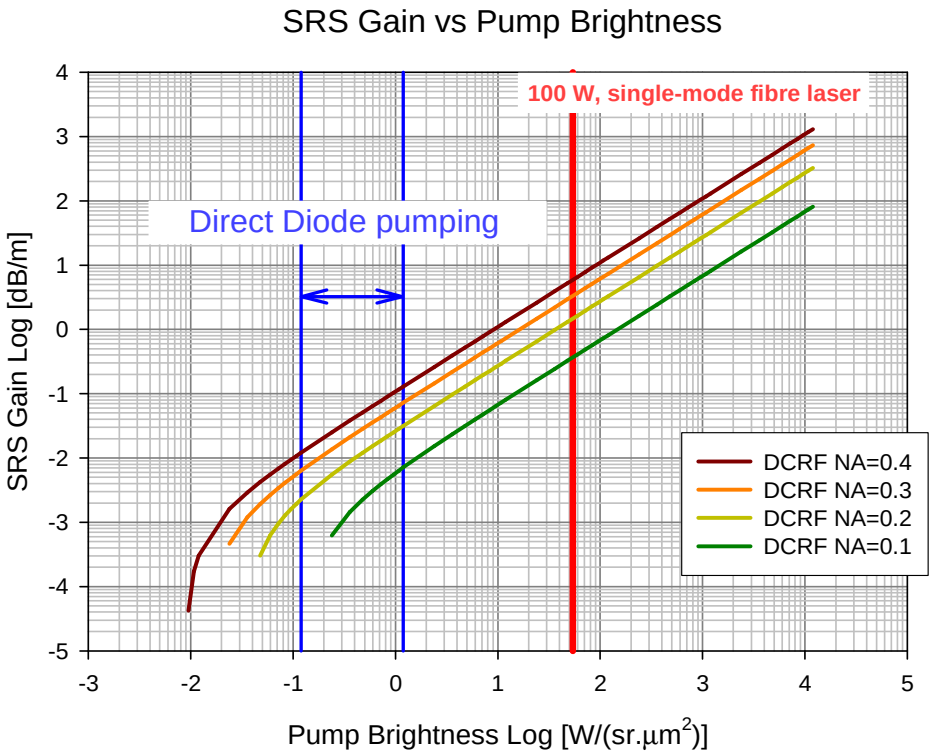

Figure 8.17: SRS small-signal gain vs pump brightness for cladding-pumped Raman fibre with NA=0.1, 0.2, 0.3 and 0.4 respectively.

Figure 8.17 highlights the effect of the cladding NA on the SRS performance. It has been demonstrated recently that all-glass fibre structure can be made with high NA [20]. Alternatively, an inner-cladding with a higher NA is also possible using an air-clad structure but so far these fibres have exhibited a higher background loss [21] than all-silica fibre.

In Figure 8.17, the area in-between the blue lines indicates where state of the art multi-mode laser diodes operate from cw to quasi-cw. A red line indicates, for comparison, the brightness of a 100 W single mode laser. This graph indicates that it should be possible to reach a SRS gain of 0.1 dB/m in a high NA fibre pumped by semiconductor laser diodes. To reach this regime, the operation of the laser diodes in the quasi-CW regime is recommended because the peak power is then higher than the average power that the diodes can deliver. It is also worth mentioning that lower background loss fibre would help in reducing the requirement on the laser diodes. This approach to directly transform the light from a multi-mode semiconductor laser diodes source into a single mode laser output is interesting and certainly worth pursuing further.

8.6 Summary

In conclusion, a pulsed DCRF has been studied for high gain amplification and for the generation of high energy pulse has been investigated. A gain in excess of 50 dB has been demonstrated experimentally in a pulsed single-stage cladding-pumped Raman fibre amplifier using 100 ns long pulses. The peak power conversion efficiency was 50%. The experimental temporal shape and output power of the Stokes beam highlight the influence of pump pulse shape and of the fibre length. In order to obtain maximum energy transfer from the pump to the signal, the pump pulse should be rectangular. Furthermore, as expected from Chapter 6, the fibre length must be tailored to the pump peak powers in order to avoid any second order Stokes generation. Then, using an 850 m long DCRF and pump pulses with the best achievable shape, a Raman amplifier delivering nearly 10 μJ pulses, 620 ns long, has been demonstrated experimentally. Here, the output energy was limited by the characteristics of the pump source (pulse shape and energy) and by the pump temporal stability at higher power. The interaction of FWM and SRS is discussed, as both non-linear effects can compete for pump photons and, therefore reduce the SRS efficiency. However, it was found that in seeded amplifiers SRS should dominate.

Finally, thanks to recent development of pump laser diode, laser diode drivers and fibre manufacturing, I show that in theory, laser diodes could potentially be used as pulsed pump sources. Using high-power, high-brightness, multi-mode laser diodes sources, a SRS gain of 0.1 dB/m should be achievable in high-NA double-clad fibres. The DCRF would be then a direct brightness converter which would produce single mode pulses. The combination of high power laser diodes and double-clad Raman fibre would provide a simple and elegant solution to a high brightness laser source.

8.7 References

[1] R. H. Stolen and A. M. Johnson, "The Effect of Pulse Walkoff on Stimulated Raman Scattering in Fibers", IEEE J. Quantum Electron. **QE-22** (11), 2154 (1986).

[2] C. Codemard, C. Farrell, P. Dupriez, V. Philippov, J. K. Sahu, J. Nilsson, "Millijoule high-peak power narrow-linewidth sub-hundred nanosecond pulsed fibre master-oscillator power-amplifier at 1.55 microns", C.R. Physique **7**, 170-176 (2006).

[3] G. P. Agrawal, *Nonlinear Fiber Optics*, (2nd Ed., Academic Press Inc, San Diego CA, 1995).

[4] E. A. Golovchenko and A. N. Pilipetskii, "Unified analysis of four-photon mixing, modulational instability, and stimulated Raman scattering under various polarization conditions in fibers", J. Opt. Soc. Am. B. **11**(1), 92 (1994).

[5] O. L. Antipov. O. Mehi and H. J. Eichler, "Modulation instabilities and stimulated Raman scattering in Nd^{3+} and Er^{3+} doped fibers by picosecond laser pulses", Proc. SPIE **3928**, 245 (2000).

[6] S. Pitois, G. Millot, and P. Tchofo Dinda, "Influence of parametric four-wave mixing effects on stimulated Raman scattering in bimodal optical fibers", Opt. Lett. **23**(18), 1456 (1998).

[7] G. Millot, P. Tchofo Dinda, E. Seve, and S. Wabnitz, "Modulational Instability and Stimulated Raman Scattering in Normally Dispersive Highly Birefringent Fibers", Opt. Fiber Technol. **7**(3), 170 (2001).

[8] I. K. Ilev, H. Kumagai, and K. Toyoda, "A widely tunable (0.54-1.01 μm) double-pass fiber Raman laser", Appl. Phys. Lett. **69**(13), 1846 (1996).

[9] K. X. Liu and E. Garmire, "Role of stimulated four-photon mixing and efficient Stokes generation of stimulated Raman scattering in excimer-laser-pumped UV multimode fibers", Opt. Lett. **16**(3), 174-176 (1991).

[10] M. Krause and H. Renner, "Numerical calculation of the linewidth of Raman fiber lasers due to spontaneous Raman scattering", Int. J. Electron. Commun. **59**, 502 – 509 (2005).

[11] T. -T. Kung, C. -T. Chang, J. -C. Dung and S. Chi, "Four-Wave mixing between pump and signal in a distributed Raman amplifier", J. Lightwave Technol. **21**(5), 1164 (2003).

[12] W. S. Wong, C. -J. Chen, M. -C. Ho, and H. K. Lee, "Phase-Matched Four-Wave Mixing between pumps and signals in a co-pumped Raman amplifier", IEEE Photon. Technol. Lett. **15**(2), 209 (2003).

[13] Y. Chen, "Combined processes of stimulated Raman scattering and four-wave mixing in optical fibers", J. Opt. Soc. Am. B **7**(1), 43 (1990).

[14] A. Sharma, M. Dokhanian, Z. Wu, A. Williams, and P. Venkateswarlu, "Four-photon-mixing-mediated stimulated Ramn scattering in a multimode optical fiber", Opt. Lett. **19**(15), 1122 (1994).

[15] Y. P. Yatsenko, A. D. Pryamikov, V. M. Mashinsky, M. E. Likhachev, A. O. Mavritsky, E. M. Dianov, A. N. Guryanov, V. F. Khopin, and M. Yu. Salgansky, "Four-wave mixing with large Stokes shifts in heavily Ge-doped silica fibers", Opt. Lett. **30**(15), 1932 (2005).

[16] R. H. Stolen and J. E. Bjorkholm, "Parametric Amplification and Frequency-Conversion in Optical Fibers", IEEE J. Quantum Electron. **18**(7), 1062-1072 (1982).

[17] A. Boskovic, S. V. Chernikov, J. R. Taylor L. Gruner-Nielsen and O. A. Levring "Direct continuous-wave measurement of n_2 in various types of telecommunication fiber at 1.55 μm", Opt. Lett. **21**(24), 1966 (1996).

[18] R. H. Stolen, "Phase Matched-Stimulated Four-Photon Mixing in Silica-Fiber Waveguides", IEEE J. Quantum Electron. **QE-11**(3), 100 (1975).

[19] Information available from various laser diodes manufacturers, e.g. Alfalight: www.alfalight.com and Bookham: www.bookham.com.

[20] J. Wang, W. Zenteno, "All-glass high NA Yb-doped double-clad laser fibres made by outside-vapour deposition", Electron. Lett. **40**, 590-2 (2004).

[21] T. A. Birks, "Reducing losses in photonic crystal fibres", in *Proc. Optical Fiber Communication Conference (OFC)*, (Anaheim, CA, USA, 2006), paper OFC7.

Chapter 9 Summary and future work

This final chapter summarises the work and results presented throughout this thesis on the advancement of Raman and erbium-ytterbium doped, cladding-pumped fibre device, and presents possible future directions of research and investigations.

9.1 Cladding-pumped Raman fibre laser sources

9.1.1 Summary

Cladding-pumping is a well established approach to power-scaling of high power fibre lasers. In this thesis, this approach generally reserved to rare-earth doped fibre, is extended to stimulated Raman scattering. Optical amplification through stimulated Raman scattering enables cladding-pumped high-power fibre lasers to operate at any wavelength. However, the power of Raman lasers was until recently relatively modest, typically up to ~10 W [1], because of the lack of high power single mode sources. Since cladding-pumping allows for higher pump power to be launched into the fibre, it seems natural to investigate the potential and properties of a cladding-pumped Raman fibre, fabricated at the ORC. Raman scattering in multi-mode fibres has been the subject of early studies [2, 3], and more recently SRS beam-clean up properties have been the subject of further investigations [4 - 6].

In this thesis, the experimental and theoretical works on continuous-wave cladding-pumped Raman fibre laser sources are presented in Chapter 7. The brightness conversion process due to the so called “beam clean-up” from Raman scattering in a multi-mode fibre is explained considering the various fibre modes. The waveguide brightness and the pump modal excitation determine the efficiency of SRS process. However, I show that when the Stokes wave is seeded or preferentially selected, for example, with a grating for the core mode, pump mode mixing is not critical and that the multi-mode SRS process can be modelled by an equivalent effective area that encompass the pump mode distribution. An all-glass germanium doped double-clad Raman fibre has been fabricated at the ORC. The fibre is single-mode above 1640 nm and the inner-cladding is 20 μm wide. The fibre Raman gain coefficient has been evaluated to be around 0.55 10^{-13} m/W due to the high germanium concentration while the background loss is around 2 dB/km. Using this fibre, I experimentally demonstrated high-power operation of a co- and a counter-pumped Raman fibre laser. Both lasers were operated at around

1660 nm and pumped by high power erbium-ytterbium doped fibre lasers fabricated in-house. The single-mode fibre laser slope efficiency can reach up to 67% and the threshold can be as low as 6 W. In the co-propagation scheme the output is truly single-mode and compatible with a standard single-mode fibre. However, the performance of the counter-pumped laser is slightly better because the signal experience a lower loss inside the laser cavity with respect to the gain distribution. Nonetheless, this is the first demonstration of a diffraction-limited Raman laser using a multi-mode fibre. Then the spectral characteristics and temporal behaviour of the laser are discussed. The laser suffers from a linewidth broadening of the signal due some four-wave mixing in the fibre core.

In Chapter 8, the amplification of single mode pulse in the DCRF is studied. The theory of pulsed Raman scattering in a multi-mode fibre is presented with a detailed description of the influence of the fibre parameters, such as the numerical aperture and the fibre length, and also the pump pulse temporal and peak power requirement to amplify a signal at the Stokes wavelength. From the theory, high gain is expected in the pulse regime. This is then experimentally demonstrated with gain in excess of 50 dB in a single-stage of DCRF. The pulses used were 100 ns long and the peak power up 90 W. The peak power conversion is 50% and is mostly limited by the background loss of the fibre while the energy conversion is lower at 30 - 35%. These results highlight the influence of pump pulse shape and of the fibre length (for the background loss and for second Stoke generation). Therefore, using a 850 m long DCRF and pump pulses with the best achievable shape, a Raman amplifier delivering nearly 10 μJ, 620 ns long pulses, is demonstrated experimentally, for the first time. This approach could be used to generate high energy pulse. In pulsed SRS, there is no energy stored in the gain medium but the energy is contained in the pump pulse itself. Then the interaction of FWM and SRS are discussed. SRS is expected to dominate in an amplifier configuration where the Stokes wave is seeded. Nonetheless, experimentally it has not been possible to use peak powers above 200 W, because of the pulse stability. The novel approach of cladding-pumped Raman fibre laser sources seems very promising and definitely requires future investigations.

9.1.2 Future work and directions

In my experiments, the efficiency and the power scaling of the DCRF is mainly limited by the current fibre design which limits the output power and the efficiency because of the relatively high signal background loss and because the inner-cladding dimension restrains the maximum launched pump power. Furthermore, very often, the germanium doping of silica glass leads to an increased background loss which restricts the useable fibre length and, therefore, accentuates the requirement for high pump power. Nonetheless, with the recent advances in

fibre fabrication [7], a new way could be found to incorporate more germanium into the glass while maintaining a low background loss to improve the device performance and to reach higher efficiency and lower threshold in laser configuration. Then, new material with a higher Raman gain or with a different Raman gain shift like phosphate-doped silica could be interesting to use. For example, Dianov [7] has proposed, recently, to use multi-component glasses, including heavy-metal oxides-doped glasses which can exhibits large Raman gain bandwidth in novel Raman fibres.

Secondly, the waveguide design could be altered to increase the numerical aperture of the inner cladding. This will enable more pump power to be launched and therefore, increase the pump intensity. This can be realised either with a fluorine doped all-glass fibre [8] or with an air-clad fibre [9]. If such fibres can be realised with low-background loss and an optimised inner-cladding design then it is possible to envisage using multi-mode semiconductor lasers source as pump sources. In Chapter 8, I show that it might be possible to reach a SRS gain of 0.1 dB/m in a high NA fibre pumped by a high-brightness semiconductor source. Furthermore, in order to increase the pump power several sources could be combined spectrally, spatially and polarisation-wise. In addition, semiconductor laser can be operated in the quasi-cw regime which nearly doubles the peak power. Therefore the direct brightness conversion in a Raman double-clad fibre could be a unique and straightforward process to produce single-mode laser output either cw or pulsed. Obviously the alternative is use highly efficient multi-mode fibre laser sources as intermediate brightness converter before using the DCRF to obtain single-mode output.

Finally, this work and approach could be extended and developed for the SBS process which is also known for its beam clean-up properties in a multi-mode fibre [10, 11]. For example, SBS which has a gain about 100 times larger than SRS, has been used in the past for the incoherent beam combination in a multi-mode fibre [12]. In that case, the output intensity distribution is identical to that of the fundamental mode. Still, by using a double-clad fibre, the fundamental mode can be seeded [13], very easily, while the output is diffraction limited by the design of the core.

9.2 High-power erbium-ytterbium doped fibre laser source.

9.2.1 Summary

In Chapter 4 and Chapter 5, the power scaling of double-clad erbium-ytterbium co-doped fibre in the continuous-wave and in the pulsed regime is experimentally demonstrated and some of the limitations encountered are discussed.

Firstly, continuous-wave tuneable fibre lasers, based on large-core EYDF, are realised using a tapered fibre section connected to a tuneable fibre Bragg grating. The FBG tuning is achieved by the compression-tuning technique. Thus, the output of two different lasers could be tuned between 1533 – 1565 nm and 1550 – 1602 nm with a narrow linewidth of around 0.2 nm. The laser slope efficiency is 30% in both cases. The output power is about 40 W over the tuning range except at long wavelengths where a competition with Yb ions takes place and reduces the laser efficiency. At 1560 nm, more than 70 W is obtained, indicating that further power scaling is possible with higher pump power and better cooling of the EYDF. Indeed the large amount of heat generated in the erbium-ytterbium doped fibre makes the fibre more susceptible to optical damage like fuse effect [14].

Secondly, the details of high peak power, high energy, large-core EYDF MOPA are presented. Up to 1 mJ energy and 6.6 kW peak power pulses with a 88 ns FWHM, are obtained at 1 kHz repetition rate. This result is the highest energy reported for sub-hundred nanosecond pulses from a rare-earth doped fibre in the 1550 nm wavelength range. Here, the main limiting factor is thought to be ASE from the erbium and ytterbium ions which, reduces extractable energy and the average power. However, thanks to the large core neither SBS, nor any other non-linear effects, has been observed which indicates that even higher energies should be possible with improved fibre design.

Finally, both examples shows the capability for further power-scaling of cw and pulsed EYDF based laser sources that can be used as standalone devices or, like in this work, as intermediate brightness converter for the generation of single-mode cw or pulsed SRS laser lights in a cladding-pumped Raman fibre.

9.2.2 Future work and directions

Although, erbium-ytterbium fibres have been studied in the past, a number of aspects still remain to be investigated. First, the ultimate power scaling of EYDF can be explored theoretically with a model which includes the effect of the ions concentrations and takes into account the thermally induced change of the spectroscopic properties in the fibre [15]. There is a limit to how much power can be obtained from a given EYDF before the ytterbium ions starts emitting ASE or start lasing because of reflections. This work could be completed by some experimental work using fibre fabricated in-house. Recently, some of the highest powers from an EYDF have been reported [16, 17] but the power level is still marginal compared to that of ytterbium doped fibre.

The second axis, of research is to gain insight in the energy exchange process in erbium-ytterbium co-doped fibre with in particular, the determination of the energy transfer rates between ytterbium and erbium ions. Currently, a new set-up for that purpose is being fabricated at the ORC based on a Q-switched 920 nm fibre laser source. This work is important to understand the behaviour of erbium-ytterbium in the pulsed regime with a particular attention to energy storage.

9.3 References

[1] Z. Xiong, , N. Moore, Z. G. Li, and G. C. Lim, "10-W Raman Fiber Lasers at 1248 nm Using Phosphosilicate Fibers", J. Lightwave Technol., **21**(10), 2377 (2003).

[2] K. X. Liu, and E. Garmire, "Role of Stimulated four-Photon Mixing and Efficient Stokes Generation of Stimulated Raman-Scattering in Excimer-Laser-Pumped UV Multimode Fibers", Opt. Lett. **16**(3), 174-176 (1991).

[3] K. S. Chiang, "Stimulated Raman scattering in a multimode optical fiber: evolution of modes in Stokes waves", Opt. Lett. **17**(5), 352-354 (1992).

[4] R. S. F. Chang, R. H. Lehmberg, M. T. Duignan, and N. Djeu, "Raman Beam Cleanup of a Severely Aberrated Pump Laser", IEEE J. Quantum Electron. **21**(5), 477-487 (1985).

[5] J. Reintjes, R. H. Lehmberg, R. S. F. Chang, M. T. Duignan, and G. Calame, "Beam Cleanup with Stimulated Raman-Scattering in the Intensity-Averaging Regime", J. Opt. Soc. Am. B-Opt. Phys. **3**(10), 1408-1427 (1986).

[6] J. T. Murray, W. L. Austin, and R. C. Powell, "Intracavity Raman conversion and Raman beam cleanup", Opt. Mater. **11**(4), 353-371 (1999).

[7] E. M. Dianov, "Advances in Raman fibers", J. Lightwave Technol. **20**(8), 1457 (2002).

[8] J. Wang, W. Zenteno, "All-glass high NA Yb-doped double-clad laser fibres made by outside-vapour deposition", Electron. Lett. **40**(10), 590-2 (2004).

[9] V. A. Kozlov, J. Hernandez-Cordero, R. L. Shubochkin, A. L. G. Carter, and T. F. Morse, "Silica-air double-clad optical fiber", IEEE Photon. Technol. Lett. **12**(8), 1007 (2000).

[10] B. C. Rodgers, T. H. Russell, and W. B. Roh, "Laser beam combining and cleanup by stimulated Brillouin scattering in a multimode optical fiber", Opt. Lett. **24**(16), 1124-1126 (1999).

[11] T. H. Russell, S. M. Willis, M. B. Crookston, and W. B. Roh, "Stimulated Raman scattering in multi-mode fibers and its application to beam cleanup and combining", J. Nonlinear Opt. Phys. Mater. **11**(3), 303-316 (2002).

[12] T. H. Russell, and W. B. Roh, "Incoherent beam combining using stimulated Brillouin scattering in multimode fibers", Opt. Express **8**(4), 246-254 (2001).

[13] G. T. Moore, "A Model for Diffraction-Limited High-Power Multimode Fiber Amplifiers Using Seeded Stimulated Brillouin Scattering Phase Conjugation", IEEE J. Quantum Electron. **37**(6), 781 (2001).

[14] D. P. Hand, T. A. Birks, "Single-mode tapers as “fibre fuse’’ damage circuit breakers", Electron. Lett. **25** (1), 33 (1989).

[15] G. Canat, J. C. Mollier, Y. Jaouen, and B. Dussardier, "Evidence of thermal effects in a high-power Er^{3+}–Yb^{3+} fiber laser", Opt. Lett. **30**(22), 3030 (2005).

[16] Y. Jeong, J. K. Sahu, D. B. S. Soh, C. A. Codemard, and J. Nilsson, "Tunable single-frequency ytterbium-sensitized erbium-doped fiber MOPA source with 150 W (51.8 dBm) of output power at 1563 nm", in *Proc. Optical Fiber Communication Conference (OFC)*, (Anaheim, CA, USA, 2006), paper PDP1.

[17] D. Y .Shen, J. K. Sahu, and W. A. Clarkson, "Highly efficient Er,Yb-doped fiber laser with 188W free-running and >100W tunable output power", Opt. Express, **13**(13), 4916-4921 (2005).

Appendix I: Modelling stimulated Raman scattering in optical fibre

This appendix contains the listing of the Matlab® programme that I wrote to model the cladding-pumped Raman fibre. Here, the programme only simulates the Raman scattering in an amplifier configuration. It can easily be modified for laser configuration using standard numerical methods for boundary value problem [A1]. The integration is performed using a modified Runge-Kutta type integrator given by Lui [A2, A3]. This method requires much less points to integrate the typical laser and amplifier differential equations, than the Runge-Kutta method of the same order and for the same precision. This is especially beneficial when, for example, large number of the equations must be integrated.

In this example, a double-clad fibre with the same parameters as L71-LF11 is modelled considering 7 modes, a pump and several Stokes orders. The propagations equations (6.1) - (6.3) are integrated for a 1 km long fibre. No mode coupling effects are considered.

```
%=====================================================================
function [T,Y]=MM_Raman

close all;

h=6.62618e-34;    %Planck Constant

%---- variable type definition

waveguide=struct('radius',[],'index',[],'loss',[]);
modes=struct('n',[],'LP',[]);
fiber=struct('core',[],'cladding',[],'length',[],'n_modes',[],'n_wl_bi
ns',[],'npump',[],'nsignals',[],'nASE',[],'s',[],'wavelength',[],'freq
uency',[]);

disp('START ....');

%---- fibre data

core=waveguide;
core.radius=4.5;
core.loss=dBkm_to_m(3);

cladding=waveguide;
cladding.radius=10;
cladding.loss=dBkm_to_m(2.3);
```

```
fiber.core=core;
fiber.cladding=cladding;
fiber.length=600;

%---- definition of the modes considered (pump, signal and ASE)

modes_max=7;
fiber.n_modes=modes;
fiber.n_modes.n=modes_max;
fiber.n_modes.LP=[1;2;3;4;5;6;7];
modes_name=[[0,1];[0,2];[0,3];[1,1];[1,2];[2,1];[2,2]];

%---- initialisation of the pump/signals/ASE wavelengths

fiber.npump=1;    %number of pump wavelength

fiber.nsignal=1;  %number of signal wavelength

fiber.nASE=2;     %number of ASE wavelength

fiber.n_wl_bins=fiber.npump+fiber.nASE+fiber.nsignal;

%---- initialization of the pump/signals/ASE power

%     initialisation of the powers of all the modes of all the
%     wavelengths to zero

fiber.s=zeros(fiber.n_modes.n,fiber.n_wl_bins);
fiber.wavelength=zeros(fiber.n_wl_bins,1);
fiber.frequency=fiber.wavelength;

%     initialization of the pump data (wavelength and power)
fiber.wavelength(fiber.npump)=1555e-9;
fiber.frequency(fiber.npump)=LtoV(fiber.wavelength(fiber.npump));

launched_pump=300;      % total launched pump power
k=[0.1 0.2 0.1 0.1 0.1 0.3 0.1];    % pump modal power distribution

for i=1:1:modes_max
      fiber.s(i,fiber.npump)=launched_pump*k(i);
end

%--- initialization of the signal data (wavelength and power)
fiber.wavelength(fiber.npump+1)=1661e-9;
fiber.frequency(fiber.npump+1)=LtoV(fiber.wavelength(fiber.npump+1));

launched_signal=1e-3;   % total launched signal power
kk=zeros(modes_max,1);  % signal modal power distribution
kk(1)=0.1;
kk(2)=0.9;


for i=1:1:modes_max
      fiber.s(i,fiber.npump+1)=launched_signal*kk(i);
end

%--- initialization of the ASE data (wavelength and power)
wavelength_step=20e-9;
```

```
fiber.wavelength(fiber.npump+fiber.nsignal+1)=1791e-9;
fiber.wavelength(fiber.npump+fiber.nsignal+2)=1944e-9;
fiber.frequency=LtoV(fiber.wavelength);

% here 2 photons (polarisation) per mode for the ASE
for i=1:1:modes_max
      fiber.s(i,fiber.npump+fiber.nsignal+1:1:fiber.n_wl_bins)=2*h*fib
      er.frequency(fiber.npump+fiber.nsignal+1:1:fiber.n_wl_bins).^2*w
      avelength_step./fiber.wavelength(fiber.npump+fiber.nsignal+1:1:f
      iber.n_wl_bins);
end

%---- shaping and sorting of the variable prior to integrations

P=reshape(fiber.s,fiber.n_modes.n*fiber.n_wl_bins,1);

%---- Mode vector
Modes=fiber.n_modes.LP;
for i=1:1:fiber.n_wl_bins-1
      Modes=[Modes;fiber.n_modes.LP];
end

%---- Frequency vector
F=ones(fiber.n_modes.n,1)*fiber.frequency(1);
for i=2:1:fiber.n_wl_bins
      F=[F;ones(fiber.n_modes.n,1)*fiber.frequency(i)];
end

%---- Wavelength vector
W=ones(fiber.n_modes.n,1)*fiber.wavelength(1);
for i=2:1:fiber.n_wl_bins
      W=[W;ones(fiber.n_modes.n,1)*fiber.wavelength(i)];
end

%---- Sorting of the variables according to their frequencies

[W_sorted sorting_index]=sort(W);
F_sorted=F(sorting_index(:),1);
Modes_sorted=Modes(sorting_index(:),:);
P_sorted=P(sorting_index(:),1);
[temp_s sorting_back]=sort(sorting_index);

%---------------------------------------
% ODEs integrations
%---------------------------------------
disp('INTEGRATION STARTING ...');
cpustart=cputime;

      %---- Integration parameters
      odesetRHK=struct('RelTol',[],'AbsTol',[],'Order',[]);
      odesetRHK.RelTol=1e-3;
      odesetRHK.AbsTol=1e-4*1:1:fiber.n_modes.n*fiber.n_wl_bins;
      odesetRHK.Order=5;

      %---- Integration
      [Z,PP]=RHK(@derivs,[0
      fiber.length],P_sorted,odesetRHK,fiber.n_modes.n*fiber.n_wl_bins
      ,F_sorted,Modes_sorted,fiber.core.loss);
```

```
disp(sprintf('DONE in %f second',cputime-cpustart));

%---- Sorting back the powers
P_final=PP(:,sorting_back(:)); %sorting back such as Pump,signal,ASE
plot(Z,P_final(:,1));


%=== END OF MAIN FUNCTION ========================================

%--- function which calculates the differential equations
function dy=derivs(t,y,varargin)

n=varargin{1};
frequency=varargin{2};
modes=varargin{3};
loss=varargin{4};

dy=rand(n,1);     %allocate memory for the output vector prior to any
                  %calculations

for i=1:1:n
      S1=0;
      S2=0;
      if i~=1
            for j=1:1:i-1
                  S1=S1+(frequency(j)~=frequency(i))*GrV(frequency(j),
                  frequency(i))./frequency(i).*y(j)'./AEFF(modes(j,:),
                  modes(i,:));
            end
      end

      for j=i+1:1:n
            S2=S2+(frequency(j)~=frequency(i))*(GrV(frequency(i),frequ
            ency(j))./frequency(j).*y(j)'./AEFF(modes(j,:),modes(i,:))
            );
      end

      dy(i)=(-1).*loss+frequency(i).*(S1-S2);
end

%--- function which returns the effective area of two modes of DCRF
function rt=AEFF(n1,n2)
persistent A_eff;

if isempty(A_eff)
      A_eff=[[64.97   233.19  171.42  93.56   208.25  223.12  175.01];
      [233.19 198.15  267.47  322.35  245.04  280.51  400.58];
      [171.42 267.47  168.01  274.51  390.4   362.14  359.25];
      [93.56  322.35  274.51  102.81  260.11  178.77  182.7];
      [208.25 245.04  390.4   260.11  218.43  312.33  269.98];
      [223.12 280.51  362.14  178.77  312.33  188.63  282.31];
      [175.01 400.58  359.25  182.7   269.98  282.31  205.86]].*1e-12;
end

rt=A_eff(n1,n2);

%--- function which converts wavelength to frequency and vice-
%--- versa
function rt=LtoV(x)
```

```
rt=2.998e8./x;

%--- function which converst frequency to wavenumber
function rt=VtoV(x)
rt=x./(2.998)*1e-10;

%--- function which returns the Raman gain for the frequence
difference
%--- abs(x-y)
function rt=GrV(x,y)
rt=1.8180e-014.*raman(abs(VtoV(x) - VtoV(y

%--- function which returns the Raman gain for the wavelength
%--- difference (x-y)
function rt=GrL(x,y)
rt=GrV(LtoV(x), LtoV(y));                                    % Raman
gain for the wavelength


%--- function which converts loss or gain from dB/km to neper (inverse
%--- meter)
function rt=dBkm_to_m(x)
rt=-log10(10^(-x./10000));

%--- function that returns the Raman gain for silica glass
function rt=raman(x)

      persistent a;
      persistent b;

      if isempty(b)
          a=[0 0.165845 0.169813 0.173848 0.177948 0.182115 0.186346
      0.190643 0.195004 0.199428 0.203916 0.208466 0.213077 0.217748
      0.222479 0.227268 0.232113 0.237015 0.241971 0.246979 0.252039
      0.257148 0.262306 0.267509 0.272757 0.278048 0.283379 0.288748
      0.294155 0.299595 0.305068 0.31057 0.316101 0.321657 0.327236
      0.332836 0.338455 0.34409 0.349739 0.3554 0.36107 0.366747
      0.37243 0.378114 0.383799 0.389483 0.395162 0.400835 0.406501
      0.412156 0.417799 0.423429 0.429043 0.43464 0.440217 0.445774
      0.45131 0.456821 0.462308 0.467769 0.473202 0.478607 0.483983
      0.489328 0.494642 0.499924 0.505174 0.51039 0.515572 0.52072
      0.525832 0.53091 0.535952 0.540958 0.545928 0.550862 0.55576
      0.560621 0.565446 0.570235 0.574988 0.579704 0.584384 0.589028
      0.593637 0.59821 0.602747 0.607249 0.611716 0.616148 0.620546
      0.624909 0.629238 0.633533 0.637794 0.642022 0.646216 0.650377
      0.654506 0.658601 0.662664 0.666694 0.670692 0.674659 0.678593
      0.682495 0.686366 0.690205 0.694013 0.69779 0.701536 0.705252
      0.708936 0.71259 0.716214 0.719808 0.723372 0.726907 0.730412
      0.733888 0.737336 0.740755 0.744145 0.747508 0.750844 0.754153
      0.757434 0.76069 0.76392 0.767125 0.770306 0.773462 0.776595
      0.779704 0.782792 0.785858 0.788904 0.791929 0.794935 0.797923
      0.800892 0.803846 0.806783 0.809705 0.812613 0.815507 0.81839
      0.821261 0.824122 0.826974 0.829818 0.832654 0.835485 0.838311
      0.841132 0.843951 0.846769 0.849585 0.852403 0.855222 0.858043
      0.860869 0.8637 0.866536 0.86938 0.872233 0.875094 0.877967
      0.880851 0.883747 0.886657 0.889582 0.892522 0.89548 0.898455
      0.901448 0.904461 0.907495 0.91055 0.913627 0.916728 0.919852
      0.923002 0.926176 0.929377 0.932605 0.935861 0.939145 0.942459
      0.945802 0.949175 0.952579 0.956014 0.959481 0.96298 0.966512
      0.970078 0.973677 0.977309 0.980977 0.984678 0.988415 0.992186
```

```
0.995993 0.999835 1.00371 1.00763 1.01158 1.01556 1.01958
1.02364 1.02774 1.03187 1.03603 1.04023 1.04447 1.04874 1.05305
1.0574 1.06178 1.0662 1.07065 1.07513 1.07965 1.08421 1.08879
1.09342 1.09807 1.10276 1.10748 1.11224 1.11702 1.12184 1.12669
1.13157 1.13648 1.14143 1.1464 1.1514 1.15643 1.16149 1.16658
1.17169 1.17683 1.182 1.1872 1.19242 1.19767 1.20294 1.20824
1.21356 1.21891 1.22428 1.22967 1.23508 1.24052 1.24598 1.25146
1.25696 1.26248 1.26802 1.27358 1.27916 1.28475 1.29037 1.296
1.30165 1.30731 1.313 1.3187 1.32441 1.33014 1.33588 1.34164
1.34741 1.3532 1.35899 1.36481 1.37063 1.37646 1.38231 1.38817
1.39404 1.39991 1.4058 1.4117 1.41761 1.42352 1.42945 1.43538
1.44132 1.44727 1.45322 1.45918 1.46515 1.47112 1.4771 1.48308
1.48906 1.49505 1.50105 1.50704 1.51304 1.51904 1.52505 1.53105
1.53706 1.54306 1.54907 1.55507 1.56108 1.56708 1.57308 1.57908
1.58507 1.59106 1.59705 1.60303 1.60901 1.61498 1.62094 1.62689
1.63284 1.63878 1.64471 1.65063 1.65653 1.66243 1.66831 1.67418
1.68004 1.68588 1.69171 1.69751 1.70331 1.70908 1.71483 1.72057
1.72628 1.73197 1.73763 1.74328 1.74889 1.75449 1.76005 1.76558
1.77109 1.77656 1.78201 1.78742 1.79279 1.79813 1.80343 1.80869
1.81392 1.8191 1.82424 1.82934 1.83439 1.8394 1.84435 1.84926
1.85412 1.85892 1.86367 1.86837 1.87301 1.87759 1.88211 1.88657
1.89096 1.89529 1.89956 1.90375 1.90788 1.91193 1.91591 1.91982
1.92365 1.9274 1.93107 1.93466 1.93816 1.94158 1.94492 1.94816
1.95131 1.95438 1.95734 1.96021 1.96299 1.96566 1.96824 1.97071
1.97308 1.97534 1.97749 1.97953 1.98146 1.98328 1.98499 1.98658
1.98805 1.9894 1.99063 1.99173 1.99272 1.99357 1.9943 1.9949
1.99537 1.99571 1.99592 1.99599 1.99592 1.99572 1.99538 1.9949
1.99428 1.99352 1.99262 1.99157 1.99037 1.98903 1.98754 1.98591
1.98413 1.98219 1.98011 1.97788 1.9755 1.97297 1.97029 1.96746
1.96448 1.96136 1.95809 1.95468 1.95114 1.94746 1.94365 1.93972
1.93567 1.93152 1.92727 1.92295 1.91856 1.91412 1.90966 1.90519
1.90075 1.89637 1.89208 1.88792 1.88394 1.88018 1.87669 1.87352
1.87074 1.86841 1.86658 1.86533 1.86472 1.8648 1.86566 1.86733
1.86988 1.87335 1.87777 1.88318 1.88958 1.89697 1.90534 1.91464
1.92482 1.9358 1.94749 1.95976 1.97247 1.98548 1.99859 2.01161
2.02433 2.03654 2.048 2.05848 2.06776 2.07559 2.08178 2.0861
2.08838 2.08844 2.08615 2.0814 2.0741 2.0642 2.0517 2.03661
2.01898 1.9989 1.97649 1.9519 1.9253 1.89687 1.86683 1.83541
1.80284 1.76934 1.73517 1.70056 1.66573 1.63089 1.59625 1.56199
1.52828 1.49526 1.46307 1.43179 1.40151 1.37231 1.34422 1.31726
1.29145 1.26677 1.24322 1.22076 1.19936 1.17896 1.15951 1.14097
1.12328 1.10637 1.0902 1.0747 1.05983 1.04553 1.03176 1.01848
1.00564 0.993224 0.981189 0.969514 0.958175 0.947157 0.936443
0.926023 0.915889 0.906033 0.896454 0.887149 0.878119 0.869364
0.860888 0.852695 0.844788 0.837172 0.829853 0.822835 0.816124
0.809725 0.803642 0.79788 0.792442 0.78733 0.782547 0.778094
0.773971 0.770176 0.766708 0.763563 0.760737 0.758223 0.756014
0.754101 0.752474 0.751121 0.75003 0.749185 0.74857 0.748168
0.747961 0.747929 0.748049 0.7483 0.748657 0.749098 0.749595
0.750123 0.750655 0.751164 0.751622 0.752002 0.752274 0.752411
0.752386 0.752172 0.751741 0.751069 0.750129 0.748899 0.747355
0.745476 0.743242 0.740636 0.737641 0.734241 0.730426 0.726184
0.721507 0.716388 0.710825 0.704814 0.698356 0.691455 0.684114
0.676342 0.668148 0.659542 0.650538 0.641152 0.631399 0.621299
0.610873 0.60014 0.589125 0.577851 0.566342 0.554625 0.542725
0.530669 0.518484 0.506196 0.493834 0.481424 0.468991 0.456563
0.444164 0.431819 0.419552 0.407386 0.395343 0.383443 0.371706
0.36015 0.348792 0.337648 0.326731 0.316055 0.305631 0.295469
0.285578 0.275965 0.266635 0.257594 0.248845 0.240389 0.232228
0.224362 0.21679 0.209509 0.202517 0.19581 0.189383 0.183231
0.177348 0.171728 0.166364 0.161248 0.156374 0.151733 0.147318
```

```
0.14312 0.13913 0.135342 0.131745 0.128333 0.125097 0.122028
0.11912 0.116364 0.113752 0.111279 0.108935 0.106716 0.104615
0.102624 0.100739 0.0989547 0.0972648 0.0956648 0.0941502
0.0927167 0.0913604 0.0900777 0.0888652 0.0877199 0.086639
0.0856202 0.0846611 0.08376 0.0829151 0.0821251 0.0813887
0.0807052 0.0800737 0.0794937 0.0789651 0.0784877 0.0780615
0.077687 0.0773646 0.0770948 0.0768785 0.0767166 0.0766101
0.0765602 0.0765682 0.0766356 0.0767638 0.0769545 0.0772094
0.0775302 0.0779188 0.0783771 0.0789069 0.0795104 0.0801894
0.080946 0.0817822 0.0827 0.0837014 0.0847884 0.0859629
0.0872267 0.0885817 0.0900295 0.0915717 0.09321 0.0949456
0.0967799 0.0987139 0.100749 0.102885 0.105123 0.107464 0.109908
0.112455 0.115104 0.117855 0.120708 0.123661 0.126714 0.129864
0.13311 0.136451 0.139882 0.143403 0.147011 0.150701 0.15447
0.158316 0.162233 0.166218 0.170265 0.174371 0.178529 0.182735
0.186983 0.191267 0.19558 0.199918 0.204273 0.208639 0.213009
0.217376 0.221734 0.226074 0.23039 0.234675 0.238921 0.243122
0.247269 0.251356 0.255376 0.25932 0.263183 0.266958 0.270637
0.274214 0.277683 0.281037 0.28427 0.287377 0.290352 0.293189
0.295884 0.298432 0.300828 0.303068 0.305149 0.307067 0.308818
0.310401 0.311812 0.31305 0.314112 0.314998 0.315706 0.316235
0.316586 0.316758 0.316752 0.316568 0.316207 0.315671 0.314962
0.314081 0.31303 0.311813 0.310431 0.308889 0.307189 0.305336
0.303332 0.301183 0.298891 0.296462 0.293901 0.291212 0.2884
0.28547 0.282427 0.279277 0.276025 0.272676 0.269237 0.265712
0.262108 0.258429 0.254682 0.250873 0.247007 0.243089 0.239126
0.235122 0.231085 0.227018 0.222927 0.218818 0.214695 0.210565
0.206432 0.2023 0.198174 0.19406 0.189961 0.185882 0.181827
0.1778 0.173804 0.169843 0.165922 0.162042 0.158207 0.15442
0.150683 0.147 0.143371 0.139801 0.136289 0.132839 0.129451
0.126127 0.122868 0.119675 0.116549 0.113491 0.1105 0.107577
0.104723 0.101937 0.0992185 0.0965681 0.0939849 0.0914683
0.0890176 0.086632 0.0843105 0.0820523 0.079856 0.0777205
0.0756446 0.073627 0.0716662 0.0697608 0.0679094 0.0661104
0.0643623 0.0626636 0.0610128 0.0594082 0.0578484 0.0563319
0.054857 0.0534223 0.0520263 0.0506677 0.049345 0.0480568
0.046802 0.0455792 0.0443871 0.0432248 0.0420911 0.0409849
0.0399053 0.0388515 0.0378225 0.0368176 0.035836 0.0348772
0.0339405 0.0330253 0.0321314 0.0312581 0.0304052 0.0295724
0.0287594 0.027966 0.0271922 0.0264377 0.0257026 0.0249869
0.0242905 0.0236135 0.0229561 0.0223184 0.0217005 0.0211027
0.020525 0.0199679 0.0194314 0.018916 0.0184218 0.0179493
0.0174985 0.01707 0.016664 0.0162808 0.0159208 0.0155842
0.0152715 0.0149828 0.0147186 0.0144792 0.0142648 0.0140757
0.0139123 0.0137749 0.0136636 0.0135787 0.0135206 0.0134893
0.0134852 0.0135085 0.0135592 0.0136377 0.013744 0.0138783
0.0140408 0.0142314 0.0144504 0.0146976 0.0149733 0.0152774
0.0156099 0.0159708 0.0163601 0.0167776 0.0172232 0.0176969
0.0181985 0.0187278 0.0192846 0.0198687 0.0204797 0.0211175
0.0217816 0.0224717 0.0231874 0.0239284 0.024694 0.0254839
0.0262974 0.0271341 0.0279932 0.0288742 0.0297764 0.0306991
0.0316414 0.0326026 0.0335819 0.0345784 0.0355912 0.0366193
0.0376617 0.0387175 0.0397855 0.0408647 0.041954 0.0430521
0.0441579 0.0452703 0.0463878 0.0475094 0.0486336 0.0497592
0.0508848 0.052009 0.0531306 0.054248 0.05536 0.0564651
0.0575619 0.058649 0.059725 0.0607884 0.061838 0.0628723
0.0638899 0.0648895 0.0658697 0.0668293 0.0677669 0.0686813
0.0695714 0.0704358 0.0712734 0.0720832 0.0728641 0.0736151
0.0743353 0.0750236 0.0756793 0.0763016 0.0768898 0.0774432
0.0779611 0.0784432 0.0788888 0.0792977 0.0796694 0.0800037
0.0803005 0.0805597 0.0807811 0.080965 0.0811112 0.0812201
```

```
      0.081292 0.0813271 0.0813258 0.0812886 0.0812161 0.0811089
      0.0809676 0.0807929 0.0805858 0.0803469 0.0800774 0.079778
      0.0794498 0.079094 0.0787115 0.0783036 0.0778714 0.0774162
      0.0769393 0.0764418 0.0759252 0.0753907 0.0748397 0.0742737
      0.0736938 0.0731016 0.0724984 0.0718856 0.0712646 0.0706368
      0.0700034 0.069366 0.0687257 0.0680839 0.067442 0.0668011
      0.0661625 0.0655274 0.064897 0.0642723 0.0636546 0.0630448
      0.0624439 0.0618529 0.0612728 0.0607043 0.0601484 0.0596057
      0.059077 0.0585631 0.0580644 0.0575815 0.057115 0.0566653
      0.0562328 0.0558179 0.0554209 0.0550419 0.0546813 0.0543391
      0.0540154 0.0537103 0.0534237 0.0531557 0.052906 0.0526747
      0.0524613 0.0522659 0.052088 0.0519274 0.0517837 0.0516565
      0.0515455 0.0514502 0.05137 0.0513046 0.0512534 0.0512157
      0.0511912 0.0511791 0.0511788 0.0511898 0.0512113 0.0512428
      0.0512835 0.0513327 0.0513899 0.0514543 0.0515252 0.0516019
      0.0516837 0.0517699 0.0518598 0.0519528 0.0520482 0.0521452
      0.0522432 0.0523415 0.0524396 0.0525367 0.0526322 0.0527254
      0.0528159 0.052903 0.0529861 0.0530647 0.0531383 0.0532062
      0.0532681 0.0533234 0.0533717 0.0534125 0.0534453 0.0534699
      0.0534858 0.0534926 0.0534899 0.0534776 0.0534552 0.0534226
      0.0533793 0.0533252 0.0532601 0.0531838 0.0530961 0.0529968
      0.0528859 0.0527631 0.0526285 0.0524818 0.0523232 0.0521524
      0.0519696 0.0517747 0.0515677 0.0513488 0.0511178 0.0508749
      0.0506202 0.0503538 0.0500758 0.0497863];
      b=0;

end

if x>=1200
      rt=0;
else
      rt=a(ceil(x)+1);
end
```

Here, the implementation of the 5th order modify Runge-kutta described by X. Liu [REF] and used for the integration of the differential equations is listed below. The function returns an array `PP` which contains the results of the integration of the initial boundary vector `y0` along `tspan`. The vector `Z` is the position of the integration.

```
function [Z,PP]=RHK(odeFcn,tspan,y0,optionsRHK,varargin)

  epsilon=optionsRHK.RelTol;  %relative tolerance for the integration
  if epsilon>0.1              %check the relative tolerance
   epsilson=1e-3;
  end

  P=y0;                       % initial boundary vector
  n=length(y0);               % size of boundary vector

  %Memory pre-allocation for increased speed
  MEM_MAX=1000;
  PP=zeros(MEM_MAX,n);        % variable array
  Z=zeros(MEM_MAX,1);         % position array

  nstep=0;                    % counter for monitoring purpose
  index=1;                    % counter of the index
```

```
z=tspan(1);                 % initial position

PPP(index,:)=P;             % initial position
ZZ(index)=z;                % initial position

FLAG=1;                     % a flag is used to exit loop

switch optionsRHK.Order
 case 5                     % only the 5th order is considered here

  % coefficients
  A=[0 1/4 3/8 12/13 1 1/2 ];
  B=[0 0 0 0 0 0,
  1/4 0 0 0 0 0,
  3/32 9/32 0 0 0 0,
  1932/2197 -7200/2197 7296/2197 0 0 0,
  439/216 -8 3680/513 -845/4104 0 0,
  -8/27 2 -3544/2565 1859/4104 -11/40 0];
  C=[(25/216) 0 (1408/2565) (2197/4104) (-1/5)]';
  D=[(16/135) 0 (6656/12825) (28561/56430) (-9/50) (2/55)]';

  ZMAX=tspan(2);
  dzmin=tspan(2)/1e4;
  dzmax=tspan(2)/5;
  dz=dzmax;


  k1=feval(odeFcn,z,P,varargin{:});
  f=zeros(n,6);

  while FLAG==1
    hA=dz*A;
    f(:,1)=k1*dz;
    f(:,2)=dz*feval(odeFcn,z+hA(2),P.*exp(f*B(2,:)'),varargin{:});
    f(:,3)=dz*feval(odeFcn,z+hA(3),P.*exp(f*B(3,:)'),varargin{:});
    f(:,4)=dz*feval(odeFcn,z+hA(4),P.*exp(f*B(4,:)'),varargin{:});
    f(:,5)=dz*feval(odeFcn,z+hA(5),P.*exp(f*B(5,:)'),varargin{:});
    f(:,6)=dz*feval(odeFcn,z+hA(6),P.*exp(f*B(6,:)'),varargin{:});

    P_5=P.*exp(f*[C;0]);
    P_6=P.*exp(f*D);

    Error=norm(P_6-P_5);          % error of the integration

    if Error<1e-10
      Error=1e-10;
    end

    delta=0.8*(epsilon/Error)^(1/5);
    nstep=nstep+1;

    if Error<=epsilon       %find the appropriate value for the next
                            %integration step
      k1=f(:,5)/dz;

      %Resize the pre-allocated vector if more than 1000 integration
      points are requiried
      if index==MEM_MAX
       P_new=zeros(MEM_MAX*2,n);
```

```
          P_new(1:1:MEM_MAX,:)=PPP;
          PPP=P_new;
          Z_new=zeros(MEM_MAX*2,1);
          Z_new(1:1:MEM_MAX,1)=ZZ;
          ZZ=Z_new;
        End

        P=P_5;
        index=index+1;
        PPP(index,:)=P;
        z=z+dz;
        ZZ(index,1)=z;
      end

      % calculate the next step size
      if delta<=0.1
        dz=0.5*dz;
      else if delta>=10
        dz=10*dz;
        else
         dz=delta*dz;
        end
      end

      if dz>dzmax
        dz=dzmax;
      end

      % check the current position and adjust the step size
      % accordingly
      if z>=ZMAX
        FLAG=0;
      elseif z+dz>ZMAX
        dz=ZMAX-z;
      elseif dz<dzmin
        disp(sprintf('COMPUTATION TERMINATED - low step size after :
%f step',index));
        FLAG=0;
        break;
      end

    end %end while

    Z=ZZ(1:index,1); % we copy only what as been calculated...
    PP=PPP(1:index,:);


   otherwise
      disp('Unrecongnized RHK order -- calling ODE45 instead...');
      options =
      odeset('RelTol',optionsRHK.RelTol,'AbsTol',optionsRHK.AbsTol);
      [Z,PP] = ode45(odeFcn,tspan,y0,options,varargin{:});

  end
```

[A1] W. H. Press, S. A. Teukolsky, W. T. Vetterling, and B. P. Plannery, *Numercical Recipes in C*, (2nd Ed., Cambridge Univ. Press, 1992).

[A2] X. Liu, H. Zhang and Y. Guo, "A Novel Method for Raman Amplifier Propagation Equations", IEEE Photon. Technol. Lett., **15** (3), 392 (2003).

[A3] X. Liu, "Effective numerical algorithm for fiber amplifiers", Opt. Eng. **44**(3), 2220 (2005).

Appendix II: List of publications

This appendix contains the list of published work during my PhD time at the ORC.

Journals publications

- C. Codemard, P. Dupriez, Y. Jeong, J. K. Sahu, M. Ibsen, J. Nilsson, "High-power continuous-wave cladding-pumped Raman fibre laser", Opt. Lett. **31**(15), (2006).
- C. Codemard, C. Farrell, P. Dupriez, V. Philippov, J. K. Sahu, J. Nilsson, "Millijoule high-peak power narrow-linewidth sub-hundred nanosecond pulsed fibre master-oscillator power-amplifier at 1.55 microns", C.R. Physique **7**, 170-176 (2006).
- K. Gallo, C. Codemard, C. B. E. Gawith, J. Nilsson, P. G. R. Smith, N. G. R. Broderick, and D. J. Richardson, "Guided-wave second-harmonic generation in a LiNbO3 nonlinear photonic crystal", Opt. Lett. **31**, 1232-1234 (2006).
- Y. Jeong, J. K. Sahu, D. B. S. Soh, C. A. Codemard, and J. Nilsson, "High-power tunable single-frequency single-mode erbium:ytterbium codoped large-core fiber master-oscillator power amplifier source", Opt. Lett. **30**, 2997-2999 (2005).
- Y. Jeong, J. Nilsson, J. K. Sahu, D. B. S. Soh, P. Dupriez, C. A. Codemard, S. Baek, D. N. Payne, R. Horley, J. A. Alvarez-Chavez, and P. W. Turner, "Single-mode plane-polarized ytterbium-doped large-core fiber laser with 633-W continuous-wave output power", Opt. Lett. **30**, 955-957 (2005).
- Y. Jeong, J. Nilsson, J. K. Sahu, D. B. S. Soh, C. Alegria, P. Dupriez, C. A. Codemard, D. N. Payne, R. Horley, L. M. B. Hickey, L. Wanzcyk, C. E. Chryssou, J. A. Alvarez-Chavez, and P. W. Turner, "Single-frequency, single-mode, plane-polarized ytterbium-doped fiber master oscillator power amplifier source With 264 W of output power", Opt. Lett. **30**, 459-461 (2005).
- V. Philippov, C. Codemard, Y. Jeong, C. Alegria, J. K. Sahu, J. Nilsson, and G. N. Pearson, "High-energy in-fiber pulse amplification for coherent lidar applications", Opt. Lett. **29**, 2590-2592 (2004).
- D. B. S. Soh, S. Yoo, J. Nilsson, J. K. Sahu, K. Oh, S. Baek, Y. Jeong, C. Codemard, P. Dupriez, J. Kim, and V. Philippov, "Neodymium-doped cladding-pumped

aluminosilicate fiber laser tunable in the 0.9 μm wavelength range", IEEE J. Quantum Electron. **40**, 1275-1282 (2004).

- C. Alegria, Y. Jeong, C. Codemard, J. K. Sahu, J. A. Alvarez-Chavez, L. Fu, M. Ibsen, and J. Nilsson, "83-W single-frequency narrow-linewidth MOPA using large-core erbium-ytterbium co-doped fiber", IEEE Photon. Technol. Lett. **16**, 1825-1827 (2004).
- Y. Jeong, J. K. Sahu, S. Baek, C. Alegria, D. B. S. Soh, C. Codemard, and J. Nilsson, "Cladding-pumped ytterbium-doped large-core fiber laser with 610 W of output power", Opt. Commun. **234**, 315-319 (2004).
- Y. Jeong, C. Alegria, J. K. Sahu, L. Fu, M. Ibsen, C. Codemard, M. R. Mokhtar, and J. Nilsson, "A 43-W C-band tunable narrow-linewidth erbium-ytterbium codoped large-core fiber laser", IEEE Photon. Technol. Lett. **16**, 756-758 (2004).
- D. B. S. Soh, C. Codemard, S. Wang, J. Nilsson, J. K. Sahu, F. Laurell, V. Philippov, Y. Jeong, C. Alegria, and S. Baek, "A 980-nm Yb-doped fiber MOPA source and its frequency doubling", IEEE Photon. Technol. Lett. **16**, 1032-1034 (2004).
- D. B. S. Soh, J. Nilsson, S. Baek, C. Codemard, Y. Jeong, and V. Philippov, "Modal power decomposition of beam intensity profiles into linearly polarized modes of multimode optical fibers", J. Opt. Soc. Am. A-Opt. Image Sci. Vis. **21**, 1241-1250 (2004).
- K. H. Yla-Jarkko, C. Codemard, J. Singleton, P. W. Turner, I. Godfrey, S. U. Alam, J. Nilsson, J. K. Sahu, and A. B. Grudinin, "Low-noise intelligent cladding-pumped L-band EDFA", IEEE Photon. Technol. Lett. **15**, 909-911 (2003).
- L. B. Fu, R. Selvas, M. Ibsen, J. K. Sahu, J. N. Jang, S. -U. Alam, J. Nilsson, D. J. Richardson, D. N. Payne, C. Codemard, S. Goncharov, I. Zalevsky, and A. B. Grudinin, "Fiber-DFB laser array pumped with a single 1-W CW Yb-fiber laser", IEEE Photon. Technol. Lett. **15**, 655-657 (2003).

Conferences

- J. Kim, P. Dupriez, D. B. S. Soh, C. Codemard, S. Yoo, Y. Jeong, J. Nilsson, J. K. Sahu, "Depressed clad hollow optical fiber with the fundamental LP01 mode cut-off", Proc. SPIE **6102**, 113-119 (2006).
- C. A. Codemard, P. Dupriez, Y. Jeong, J.K. Sahu, M. Ibsen, J. Nilsson, "High power cladding-pumped Raman fiber laser with true single-mode output at 1660 nm", in *Proc.*

Optical Fiber Communication Conference (OFC), Anaheim, CA, USA, 2006, paper OThJ2.

- P. Dupriez, C. Farrell, M. Ibsen, J. K. Sahu, J. Kim, C. Codemard, Y. Jeong, D. J. Richardson, J. Nilsson, "1W average power at 589 nm from a frequency doubled pulsed Raman fiber MOPA system", Proc. SPIE **6102**, 348-353 (2006).
- J. K. Sahu, P. Dupriez, J. Kim, C. Codemard, J. Nilsson, D. N. Payne, "Suppression of stimulated Raman scattering in a high-peak-power pulsed 1060 nm fiber MOPA source with purely single-mode output using W-type fiber", in *Proc. Optical Fiber Communication Conference (OFC)*, Anaheim, CA, USA, 2006, paper OWD5.
- Y. Jeong, J. Nilsson, D. B. S. Soh, C. A. Codemard, P. Dupriez, C. Farrell, J. K. Sahu, J. Kim, S. Yoo, D. J. Richardson, D. N. Payne, "High power single-frequency Yb doped fiber amplifiers" in *Proc. Optical Fiber Communication Conference (OFC)*, Anaheim, CA, USA, 2006, paper OThJ7.
- J. Nilsson, Y. Jeong, D. B. S. Soh, C. A. Codemard, P. Dupriez, C. Farell, J. K. Sahu, J. Kim, S. Yoo, D. N. Payne, "High-power fiber lasers: progress and opportunities", Proc. 14th International Laser Physics Workshop 2005 (LPHYS 2005) Kyoto 4-8 Jul 2005 PS5 (Plenary).
- P. Dupriez, J. Nilsson, Y. Jeong, J. K. Sahu, C. Codemard, D. B. S. Soh, C. Farrell, J. Kim, A. Piper, A. Malinowski, D. J. Richardson, "Current progress in high-power fiber lasers and amplifiers", in *Proc. Optical Amplifier and their Applications (OAA)*, Budapest, Hungary, 2005, invited paper.
- K. Gallo, C. Codemard, C. B. E. Gawith, N. G. R. Broderick, P. G. R. Smith, J. Nilsson, D. J. Richardson, "Buried slab waveguides in LiNbO3 nonlinear photonic crystals", WFOPC 2005 Palermo 22-24 Jun 2005 pp.36-40.
- J. Kim, D. B. S. Soh, C. Codemard, S. Yoo, Y. Jeong, J. Nilsson, J. K. Sahu, "Yb:Al-doped depressed clad hollow optical fiber laser operating at 980nm", in *Proc. Conference on Lasers and Electro-Optics (CLEO/IQEC) Pacific Rim*, Tokyo, Japan, 2005, paper CTuI4-5.
- C. Codemard, C. Farrell, P. Dupriez, V. N. Philippov, J. K. Sahu, J. Nilsson, "Milijoule high-peak power narrow-linewidth sub-hundred nanosecond pulsed fibre MOPA at 1.55 microns", ONERA Scientific Day Paris 27-28 Jun 2005 (Invited).
- D. B. S. Soh, A. B. Grudinin, J. Nilsson, Y. Jeong, S. Yoo, J. Kim, C. Codemard, P. Dupriez, "Stimulated Raman scattering effect on femtosecond pulse generation using

a parabolic amplification and a pulse compressor", ONERA Scientific Day Paris 27-28 Jun 2005.

- Y. Jeong, J. Nilsson, J. K. Sahu, P. Dupriez, C. A. Codemard, D. B. S. Soh, C. Farrell, J. Kim, D. J. Richardson, D. N. Payne, "High power fiber lasers", in *Proc. Conference on Lasers and Electro-Optics (CLEO/IQEC) Pacific Rim,* Tokyo, Japan, 2005, paper CWI4.
- Y. Jeong, J. K. Sahu, D. B. S. Soh, C. A. Codemard, and J. Nilsson, "Tunable single-frequency ytterbium-sensitized erbium-doped fiber MOPA source with 150 W (51.8 dBm) of output power at 1563 nm" in *Proc. Optical Fiber Communication Conference (OFC)*, Anaheim, CA, USA, 2006, paper PDP1.
- Y. Jeong, J. Nilsson, J. K. Sahu, D. B. S. Soh, P. Dupriez, C. A. Codemard, C. Farrell, J. Kim, D. J. Richardson, D. N. Payne, "Beyond 1 kW, the rising power of fibre lasers", OECC Seoul 4-8 Jul 2005 8D1-1 (Invited).
- Y. Jeong, D. B. S. Soh, C. A. Codemard, P. Dupriez, C. Farrell, V. Philippov, J. K. Sahu, D. J. Richardson, J. Nilsson, D. N. Payne, "State of the art of cw fibre lasers", in *Proc. Conference on Lasers and Electro-Optics (CLEO)*, Munich, Germany, 2005, paper TFII1-1.
- J. K. Sahu, P. Dupriez, J. Kim, A. J. Boyland, C. A. Codemard, J. Nilsson, D. N. Payne, "New Yb:Hf-doped silica fiber for high-power fiber lasers", in *Proc. Conference on Lasers and Electro-Optics (CLEO)*, Baltimore, US, 2005, paper CTuK1.
- J. Nilsson, J. K. Sahu, Y. Jeong, V. N. Philippov, D. B. S. Soh, C. Codemard, P .Dupriez, J. Kim, D. J. Richardson, A. Malinowski, A. N. Piper, J. H. V. Price, K. Furusawa, W. A. Clarkson, D. N. Payne, "High power fiber lasers", in *Proc. Optical Fiber Communication Conference (OFC)*, Anaheim, CA, USA, 2005, paper OTuF1.
- C. Codemard, J. K. Sahu, and J. Nilsson, "Cladding-pumped Raman fiber amplifier for high-gain high-energy single-stage amplification", in *Proc. Optical Fiber Communication Conference (OFC)*, (Anaheim, CA, USA, 2005).
- C. Codemard, C. Farrell, V. N. Philippov, P. Dupriez, J. K. Sahu, and J. Nilsson, "1 mJ narrow-linewidth pulsed fiber MOPA source at 1535 nm", in *Proc. Conference on Lasers and Electro-Optics (CLEO)*, Munich, Germany, 2005, paper CJ3-3.
- K. A. Gallo, C. Codemard, C. B. E. Gawith, N. G. R. Broderick, P. G. R. Smith, J. Nilsson, D. J. Richardson, "Guided-wave second harmonic generation in hexagonally

poled RPE:LiNbO3", in *Proc. Conference on Lasers and Electro-Optics (CLEO)*, Munich, Germany, 2005.

- J. H. V. Price, A. Malinowski, A. Piper, F. He, W. Belardi, T. M. Monro, M. Ibsen, B. C. Thomsen, Y. Jeong, C. Codemard, M. A. F. Roelens, P. Dupriez, J. K. Sahu, J. Nilsson, and D. J. Richardson, "Advances in high power, short pulse, fiber laser systems and technology", (International Society for Optical Engineering, Bellingham, WA 98227-0010, United States, San Jose, CA, United States, 2005), pp. 184-192.
- C. Corbari, A. Canagasabey, M. Ibsen, F. Mezzapesa, C. Codemard, J. Nilsson, P. G. Kazansky, "All-fibre frequency conversion in long periodically poled silica fibres", in *Proc. Optical Fiber Communication Conference (OFC)*, Anaheim, CA, USA, 2005, paper OFB3.
- V. Philippov, J. K. Sahu, C. A. Codemard, J. Nilsson, and G. N. Pearson, "All-fiber 0.4 mJ high-coherence eye-safe optical source", (International Society for Optical Engineering, Bellingham, WA 98227-0010, United States, London, United Kingdom, 2004), pp. 284-288.
- Y. Jeong, J. Nilsson, J. K. Sahu, D. B. S. Soh, C. Alegria, P. Dupriez, C. A. Codemard, D. N. Payne, R. Horley, L. M. B. Hickey, L. Wanzcyk, C. E. Chryssou, J. Alvarez-Chavez, P. W. Turner, "Single-frequency polarized ytterbium-doped fiber MOPA source with 264W output power", in *Proc. Conference on Lasers and Electro-Optics (CLEO)*, San Francisco, US, 2004.
- C. Alegria, Y. Jeong, C. Codemard, J. K. Sahu, L. Fu, M. R. Mokhtar, M. Ibsen, S. Baek, D. B. S. Soh, V. Philippov, and J. Nilsson, "Wideband tunable high power narrow linewidth erbium-ytterbium doped fiber laser using compression-tunable fiber Bragg grating", (International Society for Optical Engineering, Bellingham, United States, San Jose, CA, United States, 2004), pp. 285-290.
- C. A. Codemard, L. M. B. Hickey, K. Yelen, D. B. S. Soh, R. Wixey, M. Coker, M. N. Zervas, and J. Nilsson, "400-mW 1060-nm ytterbium-doped fiber DFB laser", Proc. **5335**, 56-63 (2004).
- J. K. Sahu, Y. Jeong, C. Alegria, C. Codemard, D. B. S. Soh, S. Baek, V. Philippov, L. J. Cooper, J. Nilsson, R. B. Williams, M. Ibsen, W. A. Clarkson, D. J. Richardson, D. N. Payne, "Recent advances in high power fiber lasers", in *Proc. Advanced Solid-State Photonics (ASSP)*, New Mexico, US, 2004.
- Y. Jeong, J. K. Sahu, S. Baek, C.Alegria, D. B. S. Soh, C. Codemard, V. Philippov, D. J. Richardson, D. N. Payne, and J. Nilsson, "Ytterbium-doped double-clad large-core

fiber lasers with kW-level continuous-wave output power", in *Proc. Conference on Lasers and Electro-Optics (CLEO)*, San Francisco, US, 2004.

- V. N. Philippov, J. K. Sahu, C. A. Codemard, W. A. Clarkson, J. N. Jang, J. Nilsson, and G. N. Pearson, "All-fiber 1.15-mJ pulsed eye-safe optical source", Proc. **5335**, 1-7 (2004).

- J. K. Sahu, Y. Jeong, C. Codemard, J. Nilsson, M. R. Mokhtar, M. Ibsen, D. J. Richardson, and D. N. Payne, "Tunable narrow linewidth high power erbium:ytterbium co-doped fiber laser", in *Proc. Conference on Lasers and Electro-Optics (CLEO)*, San Francisco, US, 2004.

- J. K. Sahu, V. Philippov, J. Kim, C. Codemard, P. Dupriez, J. Nilsson, A. Abdolvand, and N. V. Kulshov, "Passively Q-switched thulium-doped silica fiber laser", in *Proc. Conference on Lasers and Electro-Optics (CLEO)*, San Francisco, US, 2004.

- D. B. S. Soh, S. W. Yoo, J. Nilsson, J. K. Sahu, S. Baek, Y. Jeong, L. J. Cooper, C. Codemard, P. Dupriez, C. Alegria, V. Philippov, and K. Oh, "Cladding pumped Nd-doped fiber laser tunable from 908 to 938 nm", in *Proc. Conference on Lasers and Electro-Optics (CLEO)*, San Francisco, US, 2004.

- D. B. S. Soh, S. W. Yoo, C. A. Codemard, S. Baek, J. K. Sahu, J. Nilsson, and K. Oh, "Tunable cladding pumped neodymium-doped three-level fiber laser", in *Proc. Advanced Solid-State Photonics (ASSP)*, Santa Fe, USA, 2004, pp. 113-117.

- B. C. Thomsen, J. Yoonchan, C. Codemard, M. A. F. Roelens, P. Dupriez, J. K. Sahu, J. Nilsson, and D. J. Richardson, "60 W, 10 GHz 4.5 ps pulse source at 1.5 μm", in *Proc. Conference on Lasers and Electro-Optics (CLEO)*, San Francisco, USA, 2004.

- D. B. S. Soh, C. Codemard, J. K. Sahu, J. Nilsson, V. N. Philippov, C. Alegria, Y. Jeong, "A 4.3W 977 nm ytterbium-doped jacketed-air-clad fiber amplifier", in *Proc. Advanced Solid-State Photonics (ASSP)*, Santa Fe, USA, 2004.

- D. B. S. Soh, C. A. Codemard, J. K. Sahu, J. Nilsson, B. Seungin, W. Shunhua, and F. Laurell, "An 18-mW 488.7-nm cw frequency-doubled fiber MOPA source", Proc. SPIE **5335**, 51-55 (2004).

- K. H. Yla-Jarkko, S. -U. Alam, P. W. Turner, J. Moore, J. Nilsson, R. Selvas, D. B. S. Soh, C. Codemard, J. K. Sahu, "Cladding pumping technology for next generation of fiber amplifiers and lasers", in *Proc. Optical Amplifier and their Applications (OAA)*, Otaru, Japan, 2003, paper TuC1.

- V. N. Philippov, J. Nilsson, Y. Jeong, C.Alegria, D. B. S. Soh, C. Codemard, S. Baek, J. K. Sahu, W. A. Clarkson, D. N. Payne, "Versatile and functional high power fiber sources", 2nd International Symposium on High-Power Fiber Lasers and Their Applications St Petersburg 1-3 Jul 2003 HPFL-2.4 (Invited).
- D. N. Payne, J. Nilsson, Y. Jeong, C. Alegria, V. N. Philippov, D. B. S. Soh, C. Codemard, S. Baek, J. K. Sahu, D. J. Richardson, W. A. Clarkson, "The revolution in high-power fiber lasers", 2nd International Symposium on High-Power Fiber Lasers and Their Applications St Petersburg 1-3 Jul 2003 HPFL-1.2 (Invited).
- Y. Jeong, J. K. Sahu, S. Baek, C. Alegria, C. A. Codemard, D. B. S. Soh, V. Philippov, R. B. Williams, K. Furusawa, D. J. Richardson, D. N. Payne, and J. Nilsson, "The rising power of fibre lasers", (Institute of Electrical and Electronics Engineers Inc., TUCSON, AZ, United States, 2003), pp. 792-793.
- J. K. Sahu, C. A. Codemard, R. Selvas, J. Nilsson, M. Laroche, W. A. Clarkson, "Tunable Tm-doped silica fibre laser", in *Proc. Conference on Lasers and Electro-Optics (CLEO)*, Munich, Germany, 2003, paper CL4-5.
- J. Nilsson, Y. Jeong, C.Alegria, V. N. Philippov, D. B. S. Soh, C. Codemard, S. Baek, J. K. Sahu, D. J. Richardson, W. A. Clarkson, D. N. Payne, "Fiber lasers: flexible and functional solutions for today and the future", Third International Symposium on Laser and Nonlinear Optical Materials (ISLNOM) Colorado 20-24 Jul 2003.
- K. H. Yla-Jarkko, R. Selvas, D. B. S. Soh, J. K. Sahu, C. A. Codemard, J. Nilsson, S. A. Alam, and A. B. Grudinin, "A 3.5 W 977 nm cladding-pumped jacketed air-clad ytterbium-doped fiber laser", (Optical Soc. of America, San Antonio, CA, USA, 2003), pp. 103-107.
- C. Codemard, D. B. S. Soh, K. Yla-Jarkko, J. K. Sahu, M. Laroche, J. Nilsson, "Cladding-pumped L-band phosphosilicate erbium-ytterbium co-doped fiber amplifier", in *Proc. Optical Amplifier and their Applications (OAA)*, Otaru, Japan, 2003, paper TuC2.
- J. N. Jang, Y. Jeong, J. K. Sahu, M. Ibsen, C. A. Codemard, R. Selvas, D. C. Hanna, and J. Nilsson, "Cladding-pumped continuous-wave Raman fiber laser", in *Proc. Conference on Lasers and Electro-Optics (CLEO)*, Baltimore, MD, United States, 2003), pp. 1286-1287.
- C. Codemard, K. Yla-Jarkko, J. Singleton, P. W. Turner, I. Godfrey, S. -U. Alam, J. Nilsson, J. K. Sahu, A. B. Grudinin, "Low noise intelligent cladding pumped L-band

EDFA", in *Proc. European Conference on Optical Communication (ECOC)*, Copenhagen, 2002, postdeadline paper.

- L. B. Fu, R. Selvas, M. Ibsen, J. K. Sahu, S. -U. Alam, J. Nilsson, D. J. Richardson, D. N. Payne, C. Codemard, S. Goncharev, I. Zalevsky, A. B. Grudinin, "An 8-channel fibre-DFB laser WDM-transmitter pumped with a single 1.2W Yb-fibre laser operated at 977nm", in *Proc. European Conference on Optical Communication (ECOC)*, Copenhagen, 2002.